

Durham E-Theses

Series-tuned cavity frequency multipliers

D.F. Oxford

How to cite:

Oxford, D.F. (1983) Series-tuned cavity frequency multipliers. Doctoral thesis, Durham University.

Use policy

The full-text may be used and/or reproduced, and given to third parties in any format or medium, without prior permission or charge, for personal research or study, educational, or not-for-profit purposes provided that:

- a full bibliographic reference is made to the original source
- a <https://etheses.durham.ac.uk/id/eprint/7175/> is made to the metadata record in Durham E-Theses
- the full-text is not changed in any way

The full-text must not be sold in any format or medium without the formal permission of the copyright holders.

Please consult the [full Durham E-Theses policy](#) for further details.

SERIES-TUNED CAVITY FREQUENCY MULTIPLIERS

by

D.F. Oxford

B.Sc(Eng), M.Sc., A.M.I.E.E.

A thesis submitted to the Faculty of Science,
University of Durham, for the degree of
Doctor of Philosophy

The copyright of this thesis rests with the author.
No quotation from it should be published without
his prior written consent and information derived
from it should be acknowledged.

Department of Applied Physics
and Electronics,
University of Durham, U.K.

December 1983



ABSTRACT

The project investigates the theory and design of varactor diode frequency multiplier circuits. Special consideration is given to multipliers which use series-tuned transmission-line cavities for filtering and impedance matching and an assessment is made of the merits of these cavities. Practical multiplier circuits are constructed in microstripline and are tested with the objective of verifying the analytical predictions.

The theory of the series-tuned cavity is given and its performance is predicted by computer plots of the insertion loss when it is used between a $50\text{-}\Omega$ source and a $50\text{-}\Omega$ load. These predicted results are verified on experimental series-tuned cavities in which the transmission lines are of two types, namely, coaxial lines and microstriplines, and the predictions are used in due course in the design of the multiplier circuits.

A new method of analysis for frequency multiplier circuits is introduced in which the device equation is written in terms of a Chebyshev expansion. The coefficients of the terms in the device equation are then given by the results of a spectrum test on the device and this has the considerable advantage that the device law will include the effects of parasitics caused by the test circuit which will be similar to those which occur when the device is used in a multiplier circuit. The method can be used to analyse both shunt mode and series mode multipliers and is used here on three particular circuits: the shunt-diode doubler, the shunt-diode tripler and the shunt-diode tripler with idler. Expressions are obtained for the power delivered to the load resistance and the input and output capacitances of the diode.



The main achievement of the analysis is that it produces a method for finding the conditions for matching a non-linear reactive diode to a source and a load so that the harmonic power delivered to the load at the required output frequency can be maximised. Measurements on practical shunt-diode doublers using microstrip technology are reported and they indicate that the predictions given by the analysis of doubler circuit operation are of the correct order. The foundations for the design of microstrip series-tuned cavity multipliers have been laid and further investigations, especially with regard to multipliers with idlers, would be of value.

ACKNOWLEDGEMENTS

I would like to express my thanks to my supervisor Dr. B.L.J. Kulesza for his guidance and help throughout this project. His great enthusiasm and scholarship were an invaluable stimulation.

My thanks are also extended to the Directorate of Newcastle Polytechnic for allowing and encouraging me to undertake the work and to Mr. A. Ritchey (Head of School of Electronics, Newcastle Polytechnic) and Professor G.C. Roberts (Department of Applied Physics and Electronics, University of Durham) for placing the facilities of their departments at my disposal and to Mrs. L. Bateson for typing the thesis.

I would also like to thank all my friends and colleagues at Newcastle Polytechnic who gave me considerable assistance, especially Dr. E. Korolkiewicz and Dr. R. Armstrong.

Finally I wish to thank my wife Jean, and my children Kate and John, for their encouragement and understanding during the considerable time taken by the project.

D.F. Oxford
December 1983

SERIES-TUNED CAVITY FREQUENCY MULTIPLIERS

| <u>CONTENTS</u> | <u>Page</u> |
|---|-------------|
| CHAPTER 1: THE DEVELOPMENT OF FREQUENCY MULTIPLICATION TECHNIQUES | 8 |
| 1.1 Introduction | 9 |
| 1.2 Historical Review | 12 |
| CHAPTER 2: ANALYSIS OF THE SERIES-TUNED CAVITY | 19 |
| 2.1 Introduction | 19 |
| 2.2 Analysis of the Series-Tuned Cavity | 21 |
| 2.3 Theoretical Results for the Series-Tuned Cavity | 27 |
| 2.3.1 Variation of cavity length | 27 |
| 2.3.2 Variation of probe position | 28 |
| 2.3.3 Design procedure | 28 |
| 2.4 The Coaxial Series-Tuned Cavity | 39 |
| 2.5 The Microstrip Series-Tuned Cavity | 44 |
| 2.6 Conclusion | 49 |
| CHAPTER 3: PERFORMANCE OF PRACTICAL SERIES-TUNED CAVITIES | |
| 3.1 Introduction | 51 |
| 3.2 A Practical Coaxial Cavity | 52 |
| 3.2.1 Design details | 52 |
| 3.2.2 Tests on Cavity C1 | 53 |
| 3.2.3 Summary | 54 |
| 3.3 A Practical Microstrip Cavity | 55 |
| 3.3.1 Design details | 55 |
| 3.3.2 Tests on Cavities M2 and M4 | 56 |
| 3.3.3 Tests on Cavity M1 | 57 |
| 3.3.4 Summary | 57 |
| 3.4 Conclusion | 58 |

| <u>CONTENTS</u> (Continued) | <u>Page</u> |
|---|-------------|
| CHAPTER 4: A METHOD OF ANALYSING DIODE MULTIPLIER CIRCUITS AND ITS APPLICATION TO THE SHUNG-DIODE DOUBLER | |
| 4.1 Introduction | 75 |
| 4.2 A Method of Analysis for Multiplier Circuits in Terms of Varactor Spectral Data | 76 |
| 4.3 Shunt-Diode Doubler Analysis | 84 |
| 4.3.1 Two-term approximation to the diode characteristic | 84 |
| 4.3.2 Three-term approximation to the diode characteristic | 95 |
| 4.3.3 Four-term approximation to the diode characteristic | 99 |
| 4.4 Conclusion | 104 |
| CHAPTER 5: ANALYSIS OF THE SHUNT-DIODE TRIPLER | |
| 5.1 Introduction | 108 |
| 5.2 Shunt-Diode Tripler without Idler | 109 |
| 5.2.1 Two-term approximation to the diode characteristic | 109 |
| 5.2.2 Three-term approximation to the diode characteristic | 111 |
| 5.2.3 Four-term approximation to the diode characteristic | 117 |
| 5.3 Shunt-Diode Tripler With Idler | 118 |
| 5.3.1 Two-term approximation to the diode characteristic | 118 |
| 5.3.2 Three-term approximation to the diode characteristic | 121 |
| 5.3.3 Four-term approximation to the diode characteristic | 127 |
| 5.4 Conclusion | 129 |
| CHAPTER 6: PERFORMANCE OF PRACTICAL MULTIPLIER CIRCUITS | |
| 6.1 Introduction | 132 |
| 6.2 General Test Procedure | 133 |
| 6.3 Microstrip Cavity Multipliers | 137 |
| 6.3.1 Design details | 137 |
| 6.3.2 Practical results | 138 |
| 6.3.3 Summary | 143 |

| <u>CONTENTS (Continued)</u> | <u>Page</u> |
|--|-------------|
| 6.4 Coaxial Cavity Multipliers | 144 |
| 6.4.1 Introduction | 144 |
| 6.4.2 Design details | 144 |
| 6.5 Conclusion | |
| CHAPTER 7: CONCLUSION | 158 |
| 7.1 The Analysis of the Multiplier Circuit | 159 |
| 7.2 Practical Multiplier Circuits | 164 |
| 7.3 Future Developments | 167 |
| REFERENCES | 169 |
| APPENDICES | |
| List of Appendices to Chapter 2 | A1 |
| 2(i) | A2 |
| List of Appendices to Chapter 4 | A9 |
| 4(i) | A10 |
| 4(ii) | A14 |
| 4(iii) | A15 |
| 4(iv) | A16 |
| 4(v) | A18 |
| 4(vi) | A21 |
| List of Appendices to Chapter 5 | A23 |
| 5(i) | A24 |
| 5(ii) | A25 |
| 5(iii) | A28 |
| 5(iv) | A31 |
| 5(v) | A32 |
| 5(vi) | A34 |
| 5(vii) | A37 |

CHAPTER 1

THE DEVELOPMENT OF FREQUENCY MULTIPLICATION TECHNIQUES

| | <u>Page</u> |
|-----------------------|-------------|
| 1.1 Introduction | 9 |
| 1.2 Historical Review | 12 |

1.1 Introduction

The investigation of the theory and the design of diode frequency-multiplier circuits were the main objectives of this project. Such circuits have been developed over many years because they provided stable sources at VHF, UHF, and microwave frequencies when driven by crystal-controlled oscillators in the 10 MHz to 100 MHz range. As a particular example there is a need for a stable 12-GHz microwave source which can be used as the local oscillator of an 11-GHz receiver. At the present time 11-GHz receivers are required for the reception of television signals from satellites and a receiver having a local oscillator driven from a crystal-controlled source would have advantages in terms of cost and performance over alternative systems. In the last five years there have been developments with crystal oscillators which utilize surface acoustic waves (SAW) at frequencies around 1 GHz and it is possible that one of these circuits could be used in the proposed 12-GHz source. A multiplier chain of two doublers and a tripler, for example, would then be required to multiply from 1 GHz up to 12 GHz.

Basically, multiplier circuits consist of a non-linear element which is energised at a particular frequency. As a result, harmonics of the input fundamental frequency are generated in the non-linear element and a particular component of the spectrum is then selected by a filter and delivered to the load. In order to obtain highly efficient multiplier circuits variable reactance diodes are normally used as the non-linear elements. Although transistor frequency multipliers are presently used extensively, especially in the UHF range, they will not be investigated here. A very important part of the multiplier circuit is the microwave filter necessary for extraction

of the required harmonic and the type selected for use in this project is the series-tuned transmission-line cavity. The analysis of this type of filter is dealt with in Chapter 2 and its performance is predicted by a number of computer-plotted graphs. The design and testing of practical series-tuned cavities is reported in Chapter 3 which also gives the comparison of the advantages of the two types of transmission line which were used, namely, the coaxial line and the microstrip line.

The analysis of frequency multipliers is usually based on the characteristic of the non-linear diode. The new approach presented here is to write the diode equation in terms of the harmonic spectrum generated within it under specified test conditions. This has the considerable advantage that the device law will then include the effects of parasitics which will be reflected in the harmonic spectrum. When the diode is embedded in a multiplier circuit it is to be ensured that the parasitic elements will be very similar to those in the test circuit. This method of analysis is developed in Chapter 4 and it is used to predict the performance of several multiplier circuits with the results as reported in Chapters 4 and 5.

It was initially thought that the coaxial cavity would be used in the construction of most of the multiplier circuits because it was easily-tuned by mechanical means. However, the fact that microstrip line multipliers could be produced much more easily, quickly and cheaply led to this type of circuit being used almost exclusively in the development of the practical multipliers. Microstrip lines are, of course, presently being used widely in commercial microwave integrated circuits for the same reasons. The problem of tuning the microstrip line cavity was satisfactorily solved as reported in Chapter 6 which gives details of the design and testing of the practical multiplier circuits.

In conclusion the objectives may be summarized as follows:

- (a) the analysis of the operation of the series-tuned cavity so that its performance as a filter may be predicted,
- (b) the design, construction and testing of practical series-tuned cavities to verify the predicted performance and to prepare for the use of these cavities in multiplier circuits,
- (c) the analysis of diode multiplier circuits where the device characteristic is written in terms of the harmonic spectrum generated by the diode under specified test conditions. The input and output impedances of the non-linear circuit are to be investigated to find the conditions for maximum power transfer,

and

- (d) the design, construction and testing of practical diode multiplier circuits using series-tuned cavities as input and output filters. The circuits will be tested to verify the results predicted by the theoretical analysis.

1.2 Historical Review

In the early nineteen fifties the semiconductor diode began to be used as a voltage-controlled capacitor in applications such as the automatic control of the resonant frequency of tuned circuits. As semiconductor technology improved a special type of diode was developed for this purpose and was given the name "varactor diode" which is a contraction of the words "variable" and "reactor". The varactor diode soon found many other applications in the microwave frequency range, for example, in parametric amplifiers, frequency converters, mixers, modulators, and frequency multipliers.

Interest in the use of the varactor as a frequency multiplier was stimulated by a paper by MANLEY and ROWE (Reference 20, 1956) which led to the prediction that a varactor with negligible parasitic resistance should be 100% efficient as a frequency multiplier. The performance of a varactor is degraded by a parasitic series resistance which was first investigated by UHLIR (Reference 41, 1958) who suggested a simple equivalent circuit consisting of a resistance in series with a non-linear capacitance. In another important paper PAGE (Reference 28, 1958) showed that the maximum efficiency obtainable when generating the n th harmonic in a non-linear resistance cannot exceed $1/n^2$.

Towards the end of the nineteen fifties varactor diode frequency multipliers were being extensively investigated and many circuit analyses have been presented since that time. A major contribution was contained in the book by PENFIELD and RAFUSE (Reference 29, 1962) who gave computed results for multipliers using abrupt-junction varactors with and without idlers. Their analyses assumed that the varactor was not over-driven, i.e. not driven into forward conduction. A similar treatment is given by LEESON and WEINREB (Reference 18, 1959) who

analysed frequency multiplier circuits for small signals by using a Taylor Series expansion about the operating point for the non-linear Q-V relationship. They extended the analysis to apply to large signals as the harmonics generated are of small amplitude relative to the fundamental drive. In 1965 SCANLAN and LAYBOURN (References 33, 34) analysed varactor multipliers with and without idlers and one of their conclusions was that a cascade of two doublers would be more efficient than a single times-four multiplier with idler. This result applied before it was realised that over-driving the varactor could produce higher output powers at higher efficiencies and for higher orders of multiplication.

A further development was the invention of the step-recovery diode which can conduct a large reverse current for a brief time immediately following forward conduction. The reverse current then ceases abruptly and the result is that considerable power can be generated at the harmonics of the input current frequency. The step-recovery diode has a doping profile which is not abrupt at the junction and some diodes of this type are known as "graded-junction varactors".

The extension of multiplier circuit analyses to cover the cases of graded-junction varactors and step-recovery diodes in circuits where the diodes were driven into the conducting state started with BURCKHARDT (Reference 04, 1965) with a complete numerical solution for a variety of circuits. A publication by SCANLAN and LAYBOURN (Reference 35, 1967) concluded that operation in the over-driven mode, especially when using the characteristic attributed to a step-recovery diode resulted in a much higher efficiency which is defined as the ratio of output power to power available from the source.

HAMILTON and HALL (Reference 09, 1967) published the first complete account of the operation of multipliers using step-recovery diodes (SRD) switching between forward conduction and the reverse-bias condition. The circuits used at that time were mainly of the coaxial cavity and waveguide cavity type but since then strip-line and microstrip filters have been increasingly used in multiplier circuits. The analysis of the SRD multiplier uses the equivalent circuit of KOTZEBUE (Reference 14, 1965) which is based upon the physical theory of the operation of the SRD given by MOLL, KRAKAUER and SHEN (Reference 24, 1962). An alternative approach by GARDINER and WAGIEALLA (Reference 08, 1973) represented the step recovery effect as a charge-controlled switch which allowed the device to be represented as a time-varying element thus permitting the application of linear circuit theory.

The design of step-recovery multipliers using coaxial cavities has been given in various application notes (References 10, 26). A multiplier using microstrip output filters is described by ACCATINO and ANGELUCCI (Reference 01, 1979) with an output power of about 20 dBm at a frequency of 12.948 GHz. It is expected that output powers of this order will be obtained from the circuits investigated in this project.

Recently avalanche diodes have been investigated in frequency multiplication circuits and high order multiplication has been achieved. Multiplication from 1 GHz to 35 GHz with an output power of 250 mW and conversion loss of 13 dB has been claimed by ROLLAND et al (Reference 31, 1973) using silicon avalanche diodes, and GaAs diodes were used by KRAMER et al (Reference 15, 1976) to achieve an output of 100 mW at 32 GHz from an input of 400 mW at 4 GHz. These circuits take power

from a d.c. bias supply but in some applications may well supersede other multiplier circuits.

A recent commercially-manufactured sweep oscillator uses two dual-gate field-effect transistors in a doubler circuit to give + 10 dBm at 26 GHz (Reference 11, 1982). This circuit, in common with most contemporary multipliers, uses microstripline technology.

There is a large amount of technical literature on the subject of resonant cavities as microwave circuit elements, one of the early contributions being by MONTGOMERY, RICKIE and PURCELL (Reference 25, 1948). Many of the transmission-line resonant filters which have been described have been with parallel coupling, for example, CRISTAL (Reference 05, 1964) described interdigital and comb-line filters which used coupled circular cylindrical rods, and MATTHAEI had described similar filters (References 21, 22, 1962). The series-tuned coaxial cavity has been used in experimental mixer circuits by EMMETT (Reference 06, 1974) and in frequency multiplier circuits by SAUL (Reference 32, 1974) and KULESZA (Reference 17, 1967) who obtained excellent results with capacitive transformers as matching circuits.

From about 1960 onwards the stripline (or tri-plate) type of transmission line began to be the subject of research and development in microwave filters and numerous publications appeared such as the book by MATTHAEI, YOUNG & JONES (Reference 23, 1964). The stripline is a balanced transmission line with a single strip conductor parallel to and mid-way between two parallel conducting planes which are the return path. All three conductors are separated by an insulating dielectric. If one of the conducting planes is removed the structure remaining is a copper strip separated from a ground plane by a thin dielectric plate and this unbalanced line is called a microstrip line.

The characteristic impedance and wavelength of signals in microstrip is a function of the geometry and various papers have derived formulae for the parameters (references 13, 36, 37, 38, 42).

The unbalanced nature of microstrip means that the travelling waves exist in the dielectric substrate and in the air above the strip conductor and it is convenient to introduce the concept of an effective dielectric constant which can be used in the formulae for characteristic impedance and wavelength. Very important contributions on this subject were made by WHEELER (Reference 42, 1965) and SCHNEIDER (Reference 36, 1969). Useful data on the mitreing of corners on microstrip lines to prevent reflections and attenuation is given by KELLEY et al (Reference 12, 1968). The series capacitance of a gap in a microstrip line has been investigated and reported by BENEDEK and SILVESTER (Reference 03, 1972) who also calculated the shunt capacitance at a step in the line. The latter occurs in the quarter-wavelength transformer configuration which is used for impedance matching in the circuits described in Chapter 6. Details of band-pass microstrip line filters are given by FLEMING (Reference 07, 1977) although no references have been found for the series-tuned microstripline cavities used in this project.

Finally, an important aspect of multiplier operation is the effect of the embedding of the non-linear device in a microwave circuit. Early analyses of frequency multipliers often ignored this effect and started from the mathematical law,

$$C_1 = C_0' (1 - V_a/\phi)^{-\gamma} \quad (1.1)$$

where C_i is the incremental capacitance of the varactor junction when V_a is the voltage applied across it. The other quantities in equation (1.1) are the contact potential ϕ , the constant γ which depends upon the doping profile and a constant C_0 which is the capacitance when zero voltage is applied across the junction. KULESZA (Reference 16, 1966) for example, computed the efficiencies of multipliers using varactors having various values of γ and showed that for $\gamma = \frac{1}{2}$ the second harmonic is the highest harmonic present. This conclusion, however, might be modified by the effect of parasitics upon the device law. The analysis used in this project (Chapters 4 and 5) employs a characteristic for the device which includes the effects of the parasitics present when the diode is embedded in a typical circuit. This method was suggested by ARMSTRONG (Reference 02, 1983) and is applied to several multiplier circuits in this report.

CHAPTER 2ANALYSIS OF THE SERIES-TUNED CAVITY

| | <u>Page</u> |
|---|-------------|
| 2.1 Introduction | 19 |
| 2.2 Analysis of the Series-Tuned Cavity | 21 |
| 2.3 Theoretical Results for Series-Tuned Cavity | 27 |
| 2.3.1 Variation of cavity length | 27 |
| 2.3.2 Variation of probe position | 28 |
| 2.3.3 Design procedure | 28 |
| 2.4 The Co-axial Series-Tuned Cavity | 39 |
| 2.5 The Microstrip Series-Tuned Cavity | 44 |
| 2.6 Conclusion | 49 |

2.1 Introduction

The series-tuned cavity is defined here as a length of short-circuited transmission line connected to a tuning capacitor to form a series resonant circuit. The transmission line is of length just less than a quarter wavelength so that its input impedance is an inductive reactance. It is normally required that the selectivity of the circuit should remain at a high value under load conditions. Power can be extracted from the cavity via a coupling loop, a capacitor probe or a probe which is directly coupled to the conductors as shown in the schematic diagrams of Figures 2.1, 2.2 and 2.3.

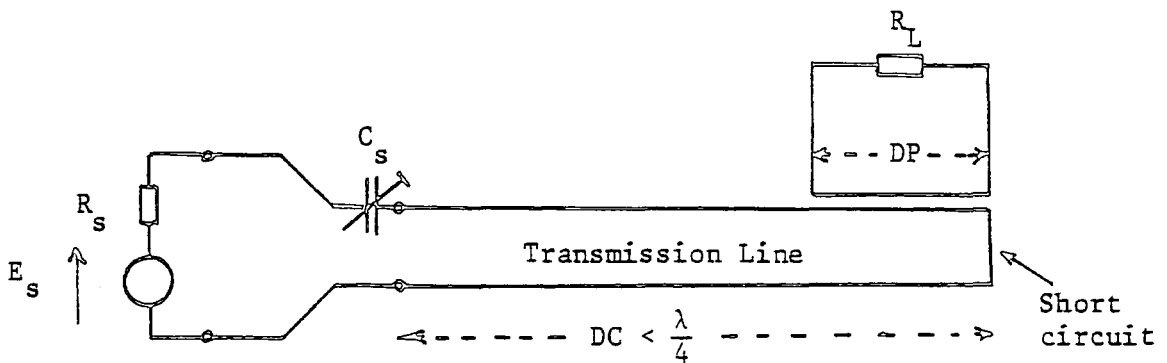


Figure 2.1
Mutual Inductive Coupling

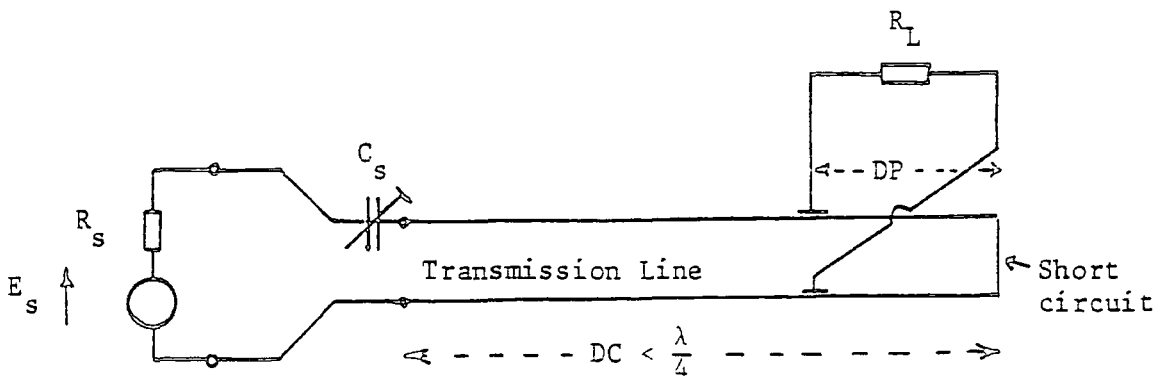


Figure 2.2
Capacitive Coupling

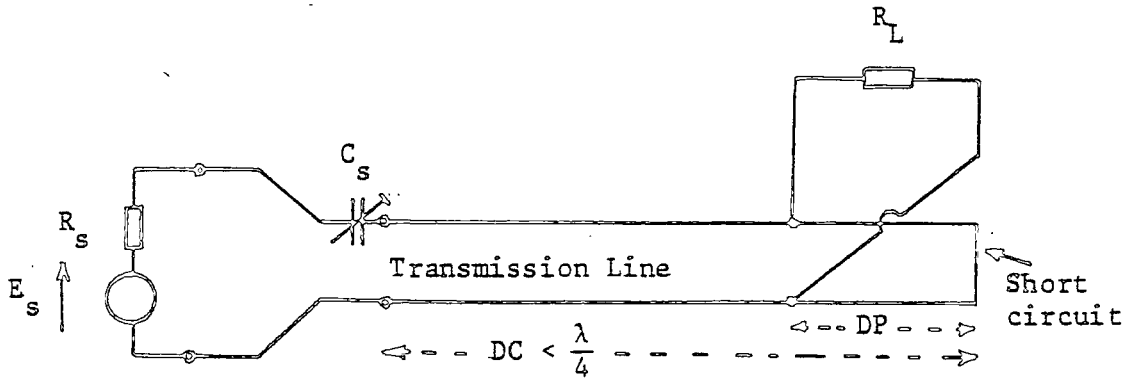


Figure 2.3
Direct Coupling

Two types of transmission line which are particularly useful in UHF and microwave circuits, namely the coaxial line and the microstrip line, will be used as cavities operating in the series-tuned mode. They will be required for use as filters and matching networks in the frequency multiplier circuits investigated in Chapter 6.

The analysis and predicted performance for the series-tuned cavity are presented in this chapter and practical results for some examples of coaxial and microstrip cavities are given in Chapter 3.

2.2 Analysis of the series-tuned cavity

In the first instance the transmission line is assumed to be lossless in order to simplify the analysis. Furthermore, the simplest type of coupling is used, namely, direct coupling and the primary objective is to obtain the variation of the frequency plot of the available power gain as various parameters of the cavity are changed. The parameters of importance are the length of the cavity DC, the position of the probe DP, the value of the tuning capacitance C_s and the characteristic impedance Z_o . The parameters of the circuit are the source resistance R_s and the load resistance R_L .

A normalised frequency variable f' is used so that the results may be generalised to design a cavity for any required frequency. The symbols employed are defined as the analysis is developed although a full list is also given in Appendix 2(i).

The input impedance Z_{in} of a length DC of a transmission line terminated in an impedance Z_T ohms is given by

$$Z_{in} = Z_o \frac{Z_T + jZ_o \tan \beta (DC)}{Z_o + jZ_T \tan \beta (DC)} \quad (2.1)$$

where β is the phase change constant per metre length of the transmission line which has zero attenuation per unit length.

When the transmission line is terminated in a short circuit the input impedance is reactive given by

$$Z_{sc} = jZ_o \tan \beta (DC) \quad (2.2)$$

The electrical length of the cavity measured in radians of phase change is

$$\theta = \beta (DC) \quad (2.3)$$

and β can be written in terms of the inductance and capacitance per unit length of line, L_m and C_m as

$$\beta = 2\pi f \sqrt{L_m C_m} \quad (2.4)$$

or for an air-dielectric line as

$$\beta = \frac{2\pi f}{c} \quad (2.5)$$

where c is the velocity of light in air.

The frequency at which the cavity is a quarter wavelength long will be called f_{cav} and hence

$$4 \text{ (DC)} = \frac{c}{f_{cav}} = \lambda \quad (2.6)$$

$$\therefore \text{ (DC)} = \frac{\lambda}{4}$$

and
$$\theta = \frac{\beta c}{4f_{cav}} = \frac{\pi f}{2f_{cav}} \quad (2.7)$$

If the frequency f is normalised by dividing by f_{cav} then

$$\theta = \frac{\pi}{2} f' \quad (2.8)$$

where

$$f' = \frac{f}{f_{cav}} \quad (2.9)$$

The series resonant frequency of the unloaded cavity (i.e. $R_L = \infty$) will be less than f_{cav} , denoted as f_o and given by the relation

$$\frac{1}{2\pi f_o C_{SN}} = Z_o \tan \frac{\pi}{2} \frac{f_o}{f_{cav}} \quad (2.10)$$

The unloaded series resonant frequency f_o may also be normalised and expressed as,

$$f'_o = \frac{f_o}{f_{cav}} \quad (2.11)$$

At the frequency f_o the value of θ can be called θ_o where

$$\theta_o = \frac{\pi}{2} \frac{f_o}{f_{cav}} \quad (2.12)$$

The cavity parameter DC and the tuning capacitance C_{SN} are included in the expressions for the variables θ and θ_o respectively (see equations (2.6), (2.7), (2.10) and (2.12)) and the position of the probe DP in the angle ϕ given by

$$\phi = \beta (DP) = \frac{2\pi f (DP)}{c} \quad (2.13)$$

The source resistance R_s will initially be assumed to equal Z_o and the load impedance Z_L will be normalised as

$$Z'_L = \frac{Z_L}{Z_o} \quad (2.14)$$

The input impedance of the loaded cavity at the terminals 1, 1' as shown in Figure 2.4 is $Z_{i/p}$, and using equations (2.1), (2.2), (2.3), (2.13) and (2.14) this can be expressed as

$$Z_{i/p} = Z_o \frac{\{-\tan(\theta-\phi) \tan \phi\} + j Z'_L \{\tan(\theta-\phi) + \tan \phi\}}{Z'_L \{1 - \tan \phi \tan(\theta-\phi)\} + j \tan \phi} \quad (2.15)$$

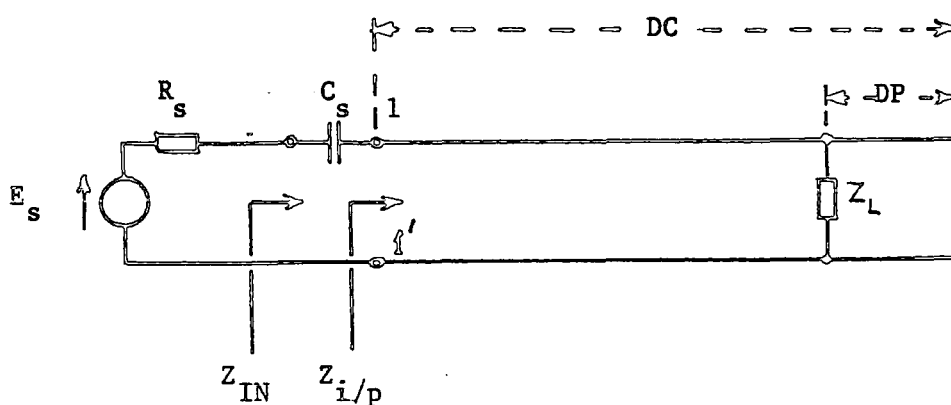


Figure 2.4

When the input capacitor C_s is included, the total input impedance Z_{IN} is given by

$$Z_{IN} = Z_{i/p} - j \frac{1}{2\pi f C_s} \quad (2.16)$$

or

$$Z_{IN} = R_{i/p} + jX_{i/p} - j \frac{1}{2\pi f C_s} \quad (2.17)$$

These resistances, reactances and impedances can be normalised by dividing by Z_o so that

$$Z_{IN}' = R_{i/p}' + j \left(X_{i/p}' - \frac{1}{Z_o 2\pi f C_s} \right) \quad (2.18)$$

The real and imaginary parts of equation (2.15) are plotted against f in Figures 2.9, 2.10 and the modulus of $Z_{i/p}'$ is shown in Figure 2.8.

The quantity measured during swept-frequency tests is the output voltage V_L and this is normally calibrated against the signal generator output into 50Ω , making the ratio V_L to $E_s/2$ a useful quantity to compute. The load power P_L and the maximum power available from the source P_A are related to the available power gain G by the following equations

$$G = \frac{P_L}{P_A} \quad (2.19)$$

$$P_L = \frac{|V_L|^2}{|Z_L' Z_o|^2} R_L \quad (2.20)$$

$$P_A = \frac{E_s^2}{4Z_o} \quad \text{where } R_s = Z_o \quad (2.21)$$

If Z_L' is real then,

$$\frac{V_L}{E_s/2} = \sqrt{\frac{(Z_L' Z_o P_L)}{(Z_o P_A)}} = \sqrt{Z_L' G} \quad (2.22)$$

$$G = \frac{1}{Z_L'} \left(\frac{V_L}{E_s/2} \right)^2 \quad (2.23)$$

The insertion loss L is the decrease in load power caused by connecting the 2-port network between the signal source and the load and is thus

$$L = 10 \log_{10} \frac{P_A}{P_L}$$

or

$$L = 10 \log_{10} Z_L' - 20 \log_{10} \left(\frac{V_L}{E_s/2} \right) \quad (2.24)$$

Expressions for P_L and P_A may be easily obtained using equation (2.17) when the cavity losses are assumed to be zero. Alternatively the load power may be deduced using the Thévenin Equivalent circuit for the cavity as shown in Figure 2.5, leading to

$$V_{OC}' = \frac{V_{OC}}{E_s} = \frac{j \cos(\theta - \phi) \{ \tan \theta - \tan(\theta - \phi) \}}{1 + j \left\{ \tan \theta - \frac{1}{2\pi f C_s Z_o} \right\}} \quad (2.25)$$

$$Z_{o/p}' = \frac{Z_{o/p}}{Z_o} = \frac{\tan \phi \{ X_c' - \tan(\theta - \phi) \} + j \tan \phi}{\text{Re} + j \text{Im}} \quad (2.26)$$

$$\text{where } \text{Re} = 1 - \tan \phi \tan(\theta - \phi) \quad (2.26a)$$

$$\text{and } \text{Im} = \tan \phi + \tan(\theta - \phi) + \frac{\{ \tan \phi \tan(\theta - \phi) - 1 \}}{2\pi f C_s Z_o} \quad (2.26b)$$

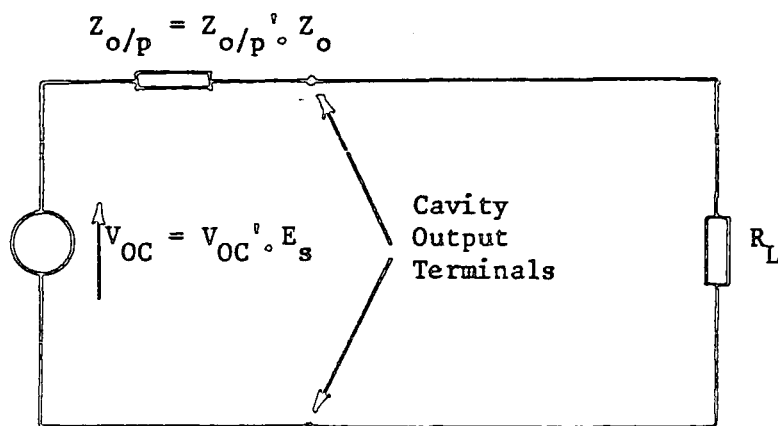


Figure 2.5

An expression for P_L is

$$P_L = \frac{E_s^2 R_{i/p}' Z_o}{Z_o^2 (1 + R_{i/p}')^2 + (Z_o X_{i/p}' - \frac{1}{2\pi f C_s})^2} \quad (2.27)$$

Some of the equations developed in this section are plotted in section 2.3.

2.3 Theoretical Results for Series-Tuned Cavity

The equations (2.15) to (2.27) can be used to plot the variation of G , L , $2V_L/E_s$ and Z_{IN}' with normalised frequency f' for various values of Z_L' , A and θ_0 . Graphs of some of these quantities are shown in Figures 2.6 to 2.13. A is the ratio of the distance of the probe from the short circuit to the length of the cavity.

2.3.1 Variation of cavity length

With reference to Figure 2.6 it can be seen that two series resonant frequencies occur, one just below the quarter wavelength and the other just below the three-quarter wavelength frequency where the cavity is again inductive. The available power gain G and insertion loss L curves in Figures 2.6 and 2.7 respectively, show that the length of the cavity must not be too near a quarter wavelength ($\theta_0 = \frac{\pi}{2}$), in fact, zero insertion loss occurs when $\theta_0 = 81^\circ$. This happens when the input impedance $Z_{i/p}$ is 50Ω resistive in series with an inductive reactance which can then be resonated with the tuning capacitor C_s .

The matching of the input impedance of the loaded cavity to the source can easily be obtained from the graphs in Figures 2.9 and 2.10. The frequency at which $R_{i/p}' = 1$ is noted and the value of $X_{i/p}'$ at this frequency is resonated by adjusting C_s . This occurs at $\theta_0 = 81^\circ$ and there are no other values of θ_0 which give this maximum power transfer.

The "selectivity" of the cavity may be measured from the graphs of output voltage versus frequency which are given in Chapter 3 where practical and theoretical graphs are compared. A 'Q-factor' of about 20 is obtained for the first resonance when $Z_L' = 1$, $A = 0.1$, and $\theta_0 = 81^\circ$.

2.3.2 Variation of probe position

The position of the probe or load coupling is given by the constant A which is usually of the order of 0.1. As the probe is moved towards the input end of the cavity the resonant peaks tend to broaden as shown in Figure 2.13. The value of G for the first resonance when $A = 0.2$ (see Figure 2.13) could be adjusted to the matched condition of unity if a different value of θ_0 were used. This could be obtained by plotting curves of $R_{i/p}$ and $X_{i/p}$ (similar to Figures 2.9 and 2.10), for various values of θ_0 for $A = 0.2$.

Further investigations show that the response for $A = 0.57$, for example, can be changed by making $\theta_0 = 88^\circ$ so that the first resonance disappears and the second resonance becomes more selective. This can be seen from the practical result shown in Figure 3, in Chapter 3.

2.3.3 Design procedure

Since the load impedance Z_L will normally be specified, Z_L' is known. Graphs of $R_{i/p}$ and $X_{i/p}$ can then be plotted using particular values of A (for example 0.1 and 0.2) for various values of θ_0 . This enables θ_0 to be determined which produces zero attenuation at the first resonance, and the graphs of G and L can then be plotted. A suitable pair of values of θ_0 and A can then be chosen to give the required selectivity. The normalised resonant frequency is obtained from the graph of L (in Figure 2.7) which gives f_s' of 0.8.

Then f_{cav} may be found from

$$f_{cav} = \frac{f_s}{f_s'} \quad (2.28)$$

and hence the required length of cavity DC may be determined from equation (2.6), i.e.

$$DC = \frac{3.10^8}{4 f_{cav}}$$

The value of θ_o is known and can be used to find the required C_{SN} which tunes the unloaded cavity. If equations (2.10) and (2.12) are combined the following expression for the capacitance may be obtained,

$$C_{SN} = \frac{1}{4 f_{cav} Z_o \theta_o \tan \theta_o} \quad (2.29)$$

Values of C_{SN} for any f_{cav} , $Z_o = 50\Omega$ and certain values of θ_o are shown in Figures 2.14 and 2.15. The actual value of C_s required when the cavity is loaded will be different from C_{SN} and will be needed to resonate with $X_{i/p}$, and therefore it will be slightly greater than C_{SN} .

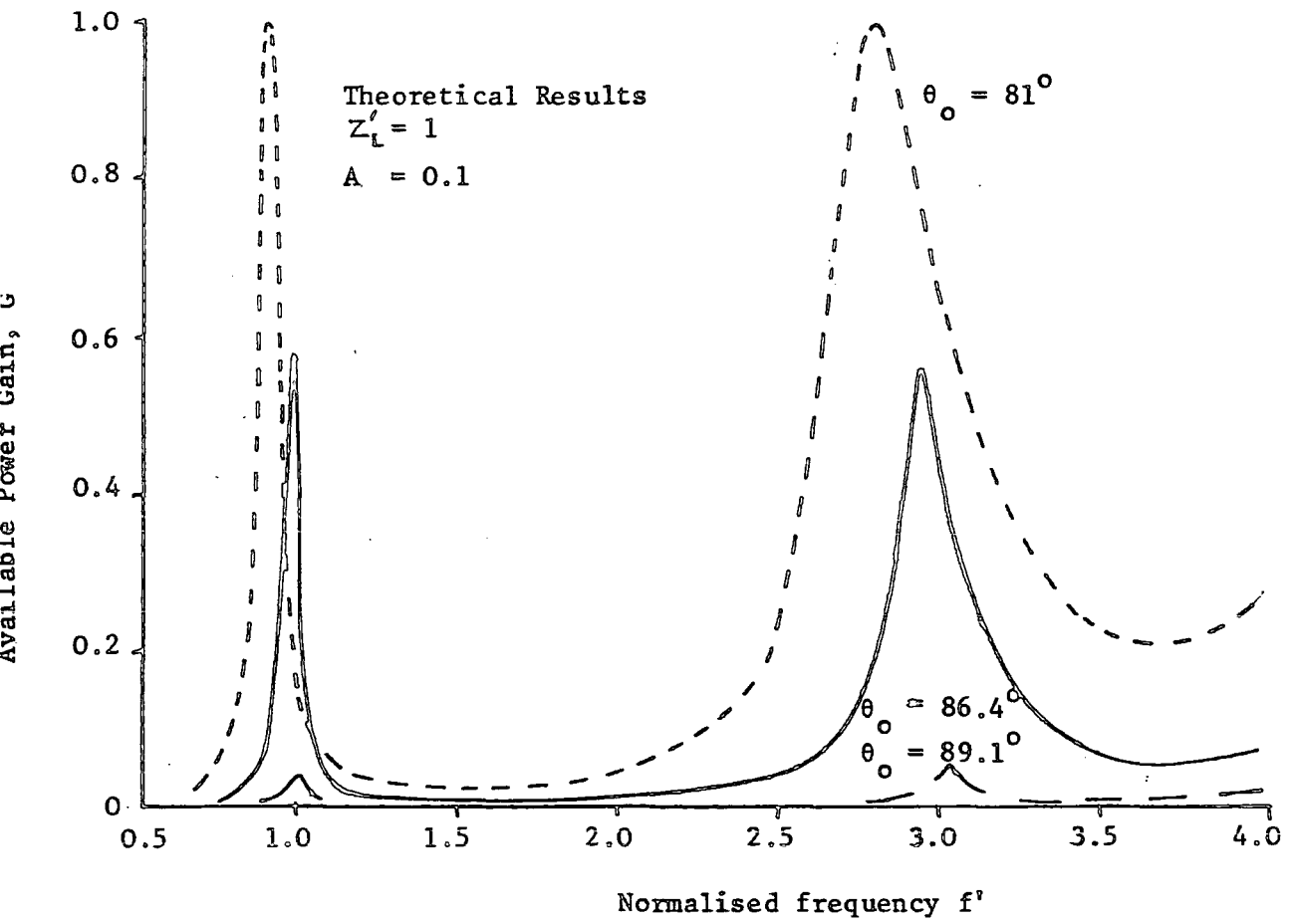


Figure 2.6

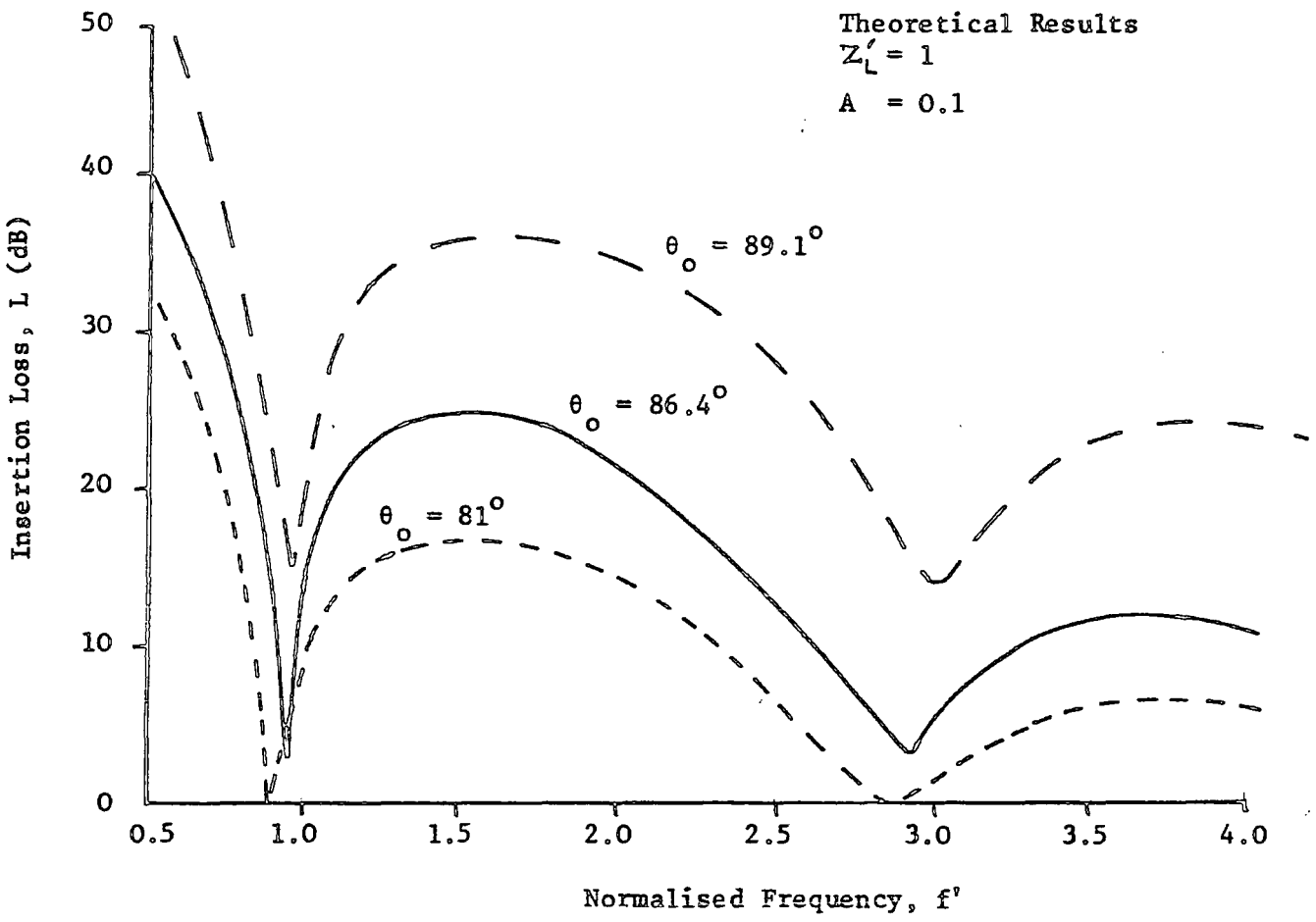


Figure 2.7

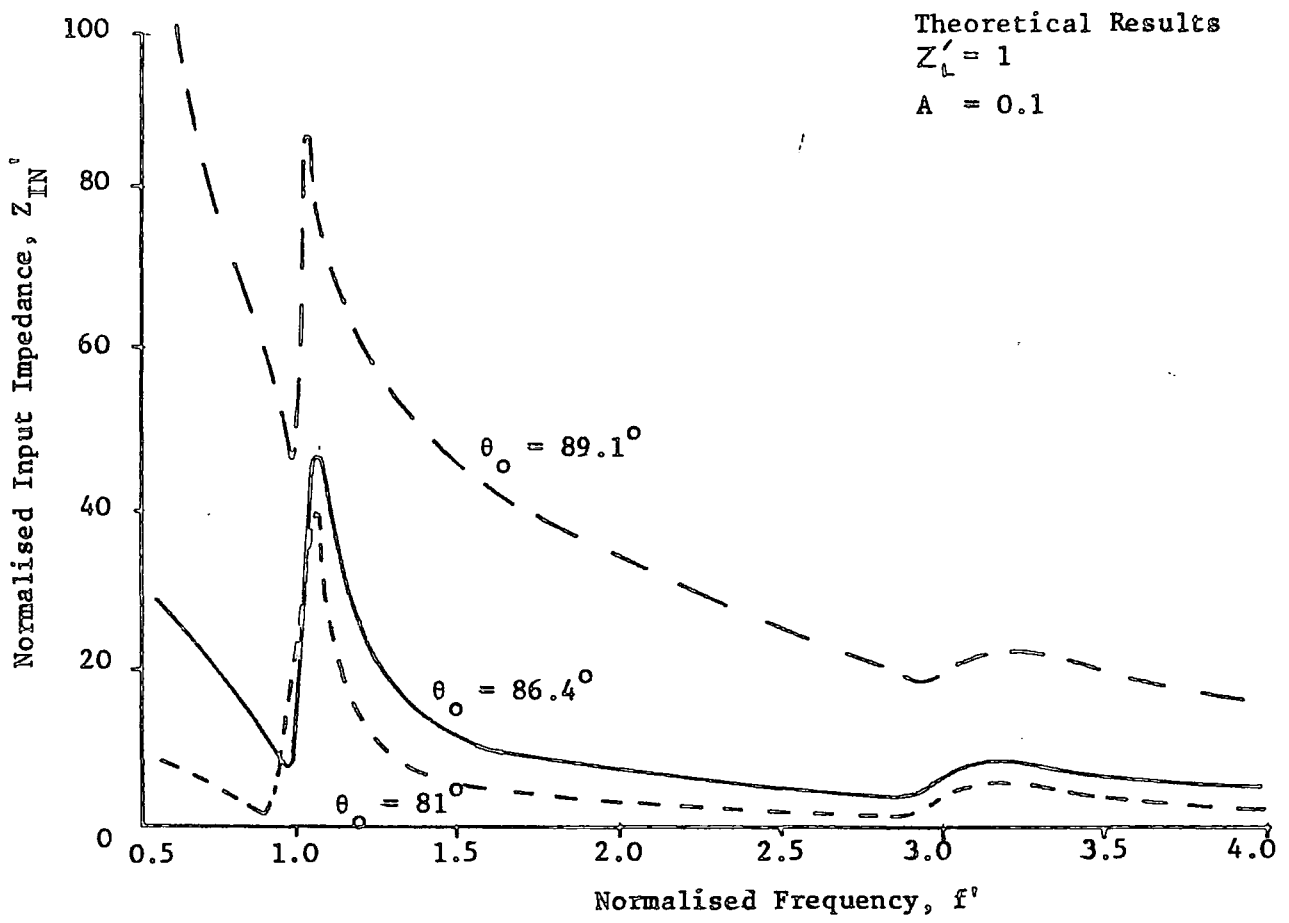


Figure 2.8

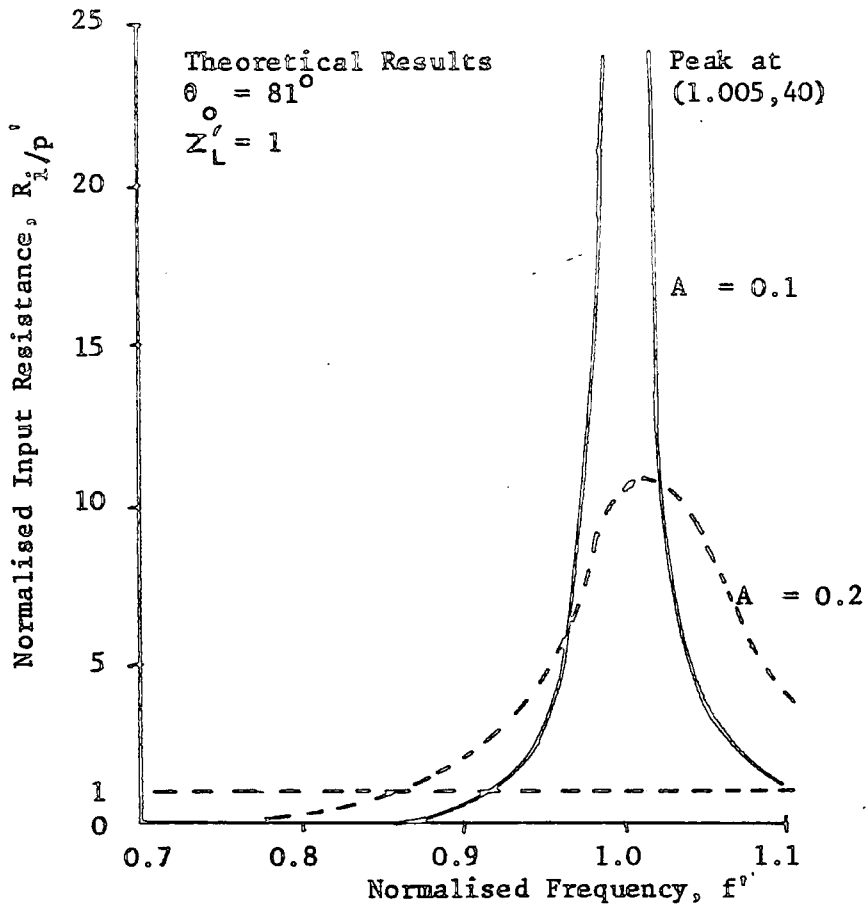


Figure 2.9

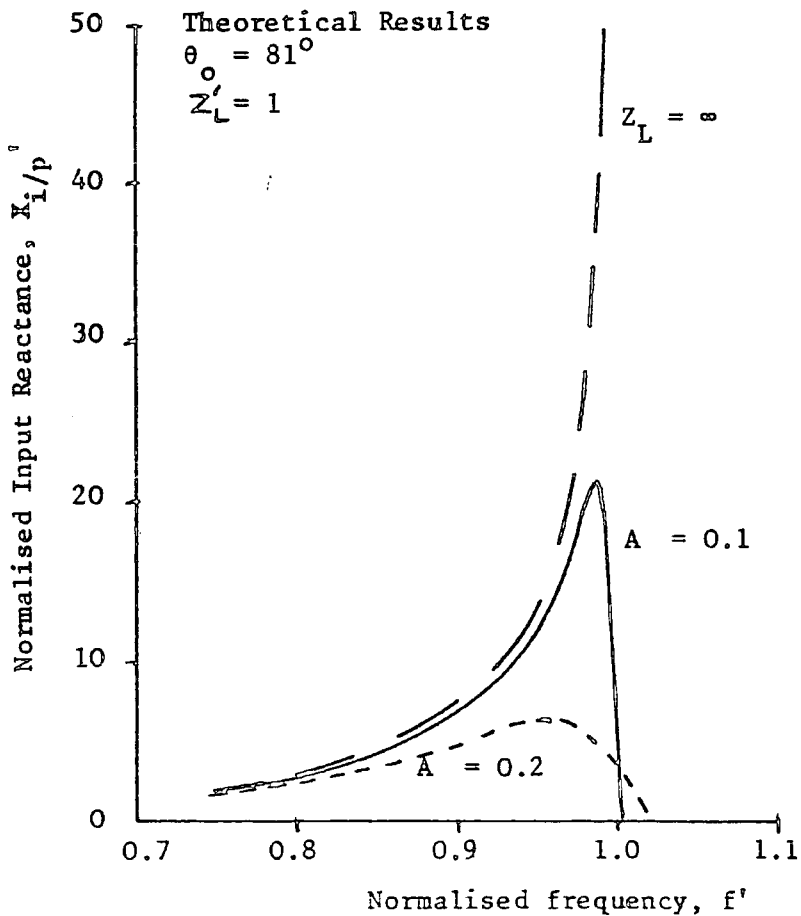


Figure 2.10

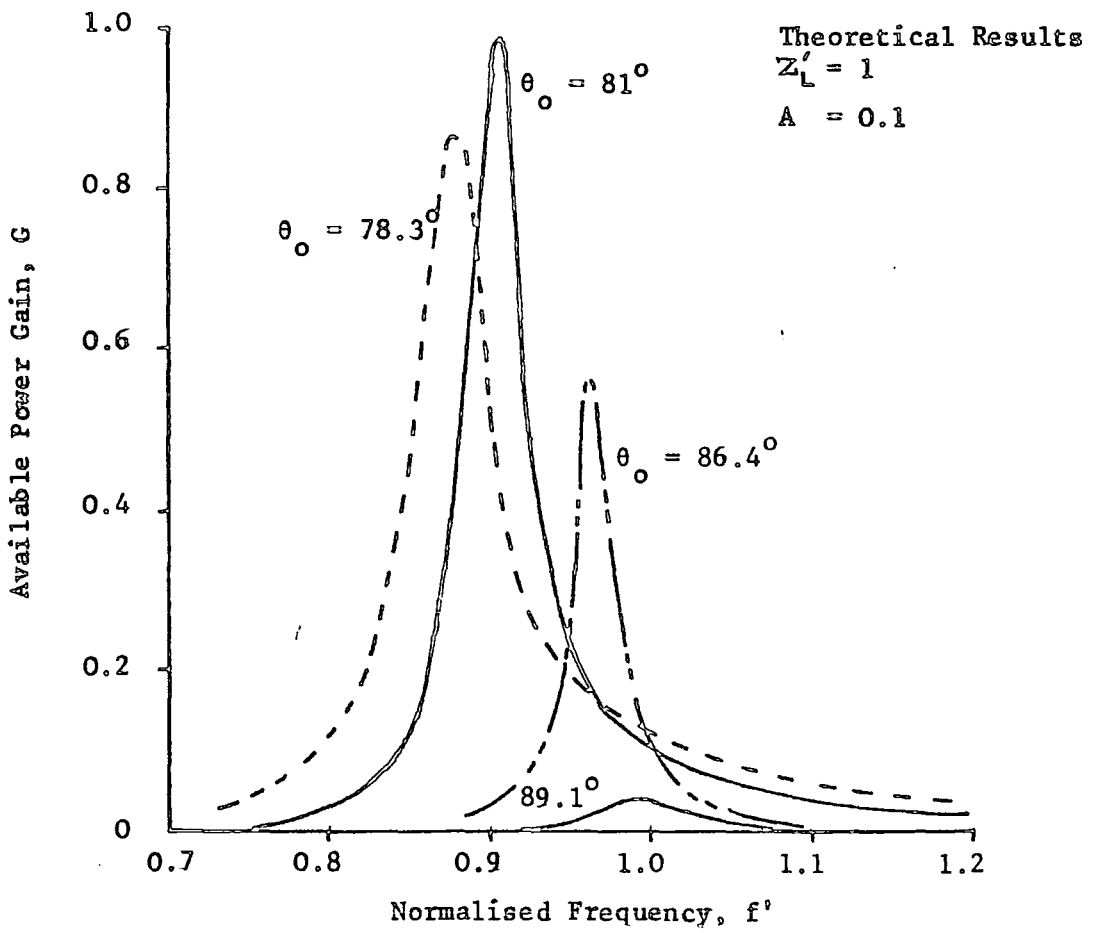


Figure 2.11

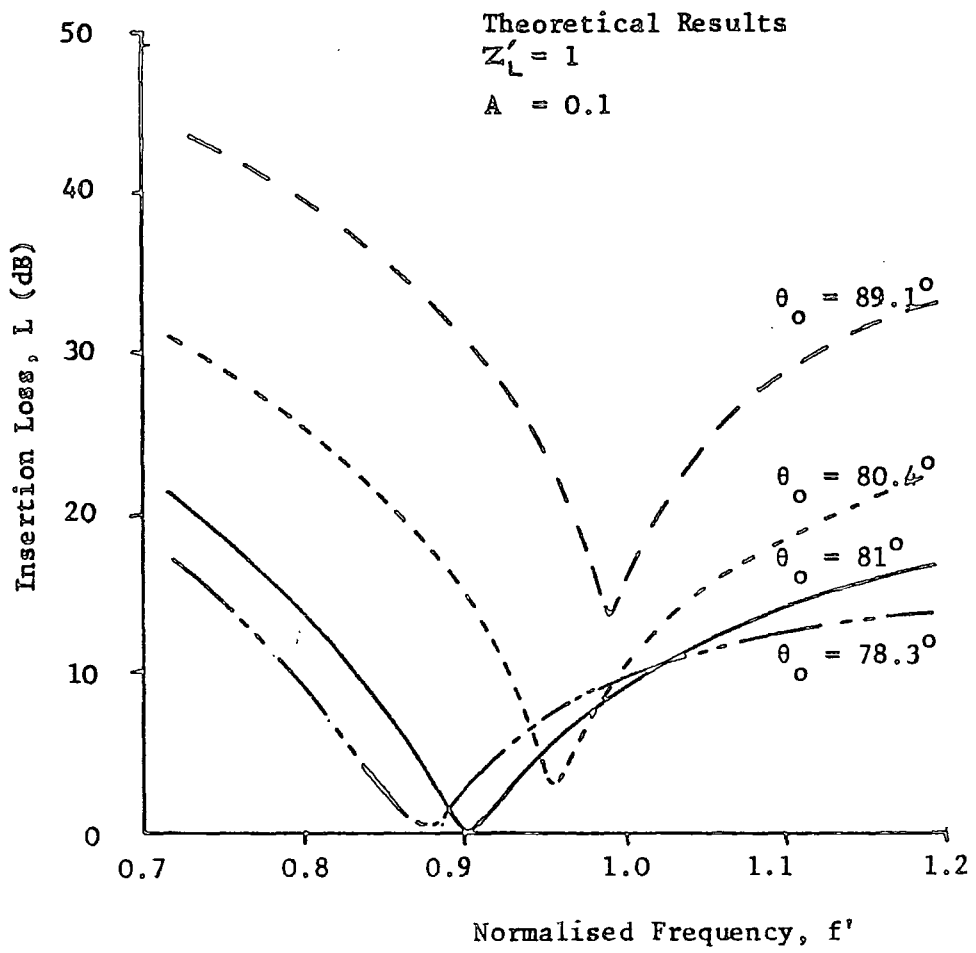


Figure 2.12

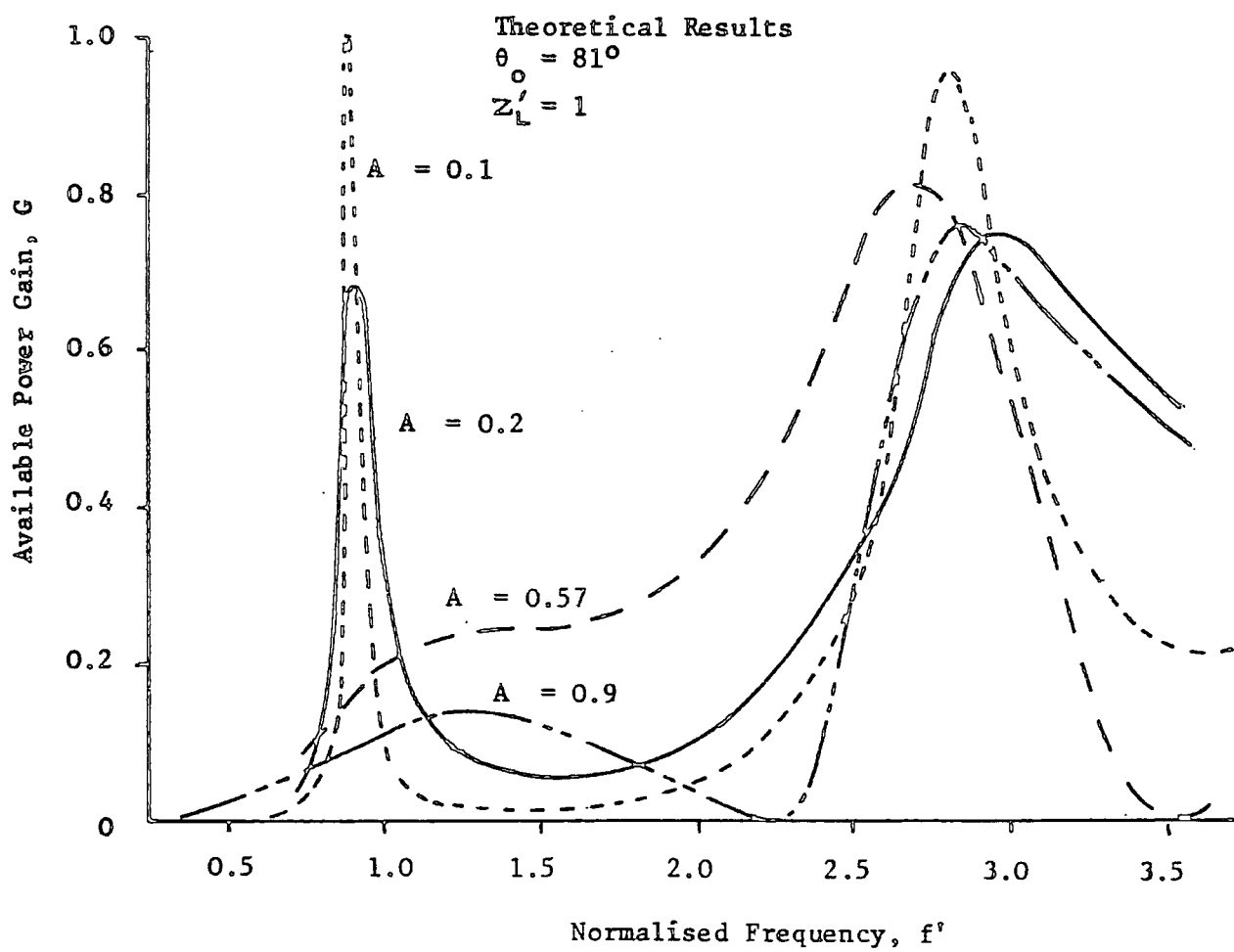


Figure 2.13

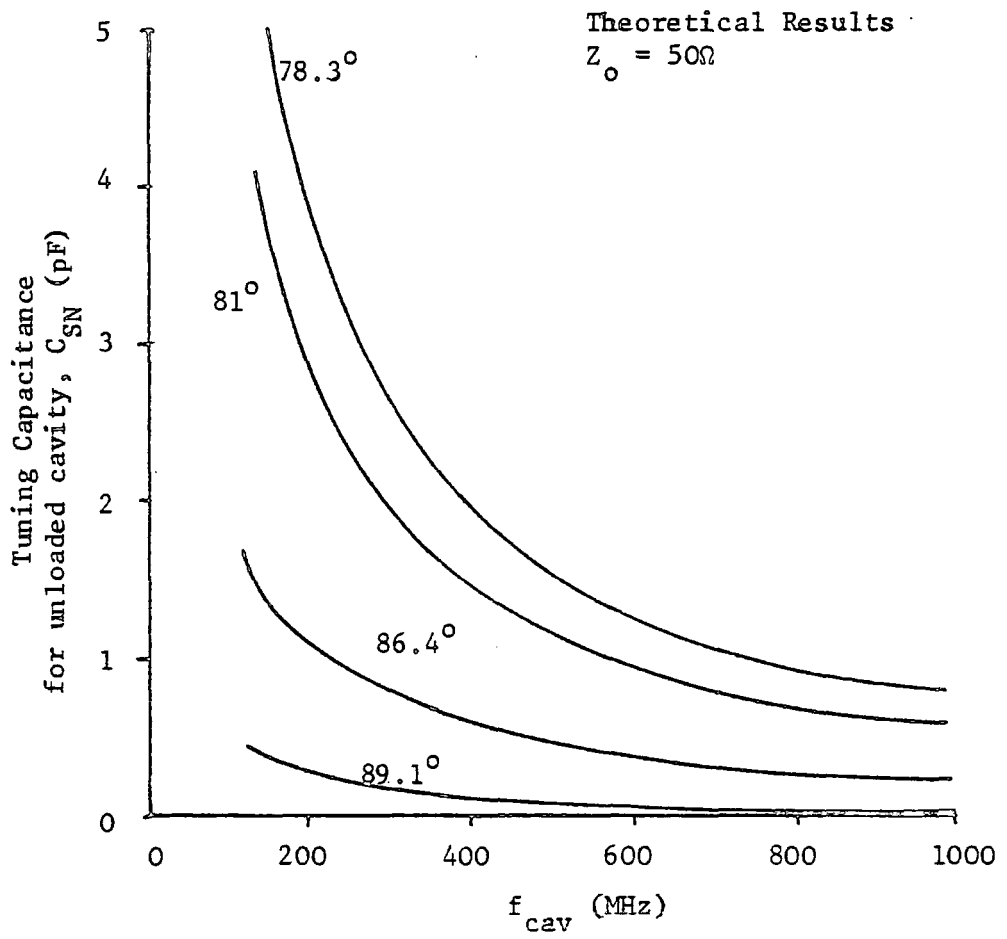


Figure 2.14

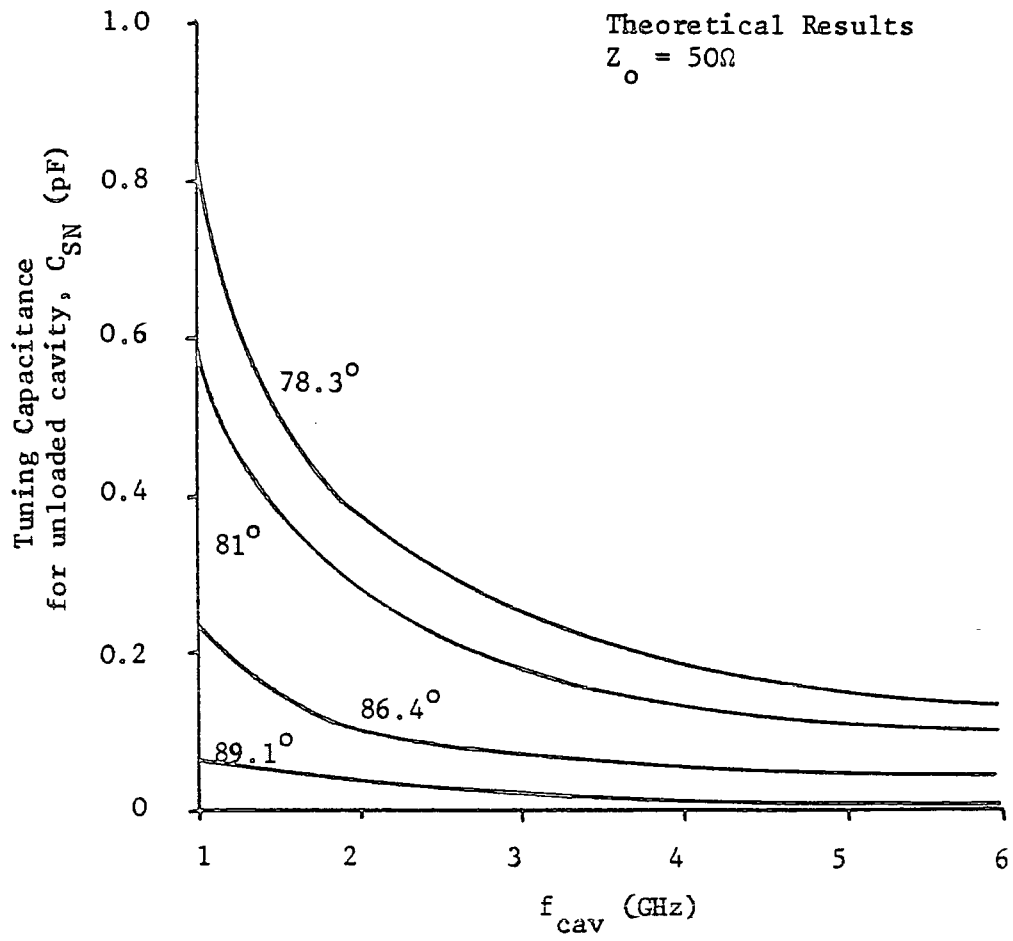


Figure 2.15

2.4 The Coaxial Series-Tuned Cavity

A coaxial series-tuned cavity with direct-coupled load is illustrated in Figure 2.16.

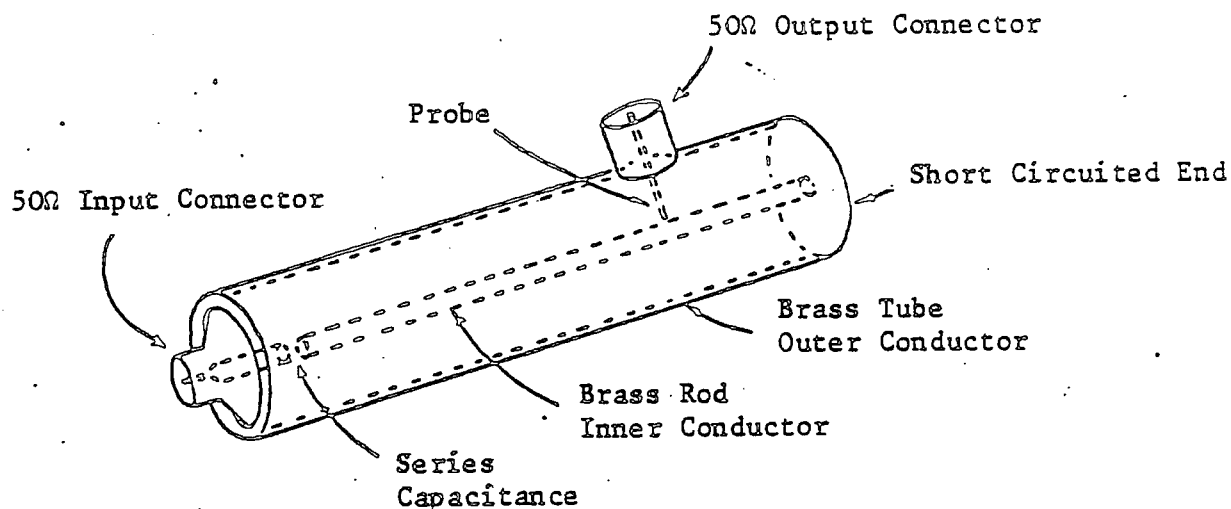


Figure 2.16

The dominant mode in coaxial transmission lines is the transverse electromagnetic (TEM) with the electric and magnetic field components always at right angles to each other and to the direction of propagation. Different modes occur when the frequency is high enough such that the wavelength becomes equal to the mean circumference of the coaxial system. Formulae for the parameters with TEM propagation on the coaxial line are well-known and are summarised below so that they may be used in design calculations. A schematic diagram is shown in Figure 2.17.

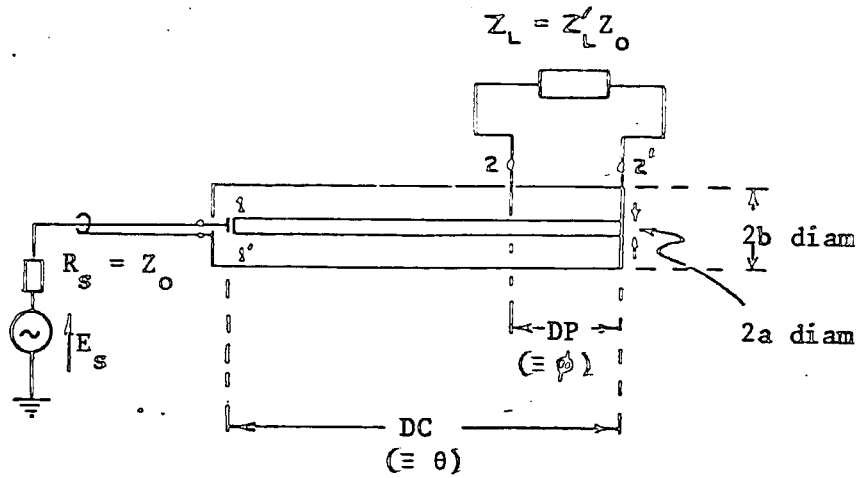


Figure 2.17
Schematic Diagram of Coaxial Cavity

The inductance per metre and the capacitance per metre are

$$L_m = \frac{\mu_0 \mu_r}{2\pi} \ln \left(\frac{b}{a} \right) \text{ henrys per metre} \quad (2.30)$$

$$C_m = \frac{2\pi \epsilon_0 \epsilon_r}{\ln \left(\frac{b}{a} \right)} \text{ farads per metre} \quad (2.31)$$

where $2b$ is the diameter of the outer conductor

$2a$ is the diameter of the inner conductor

μ_r is the relative permeability of the material between the two conductors

μ_0 is the permeability of free space, and

\ln is the natural logarithm

ϵ_r is the relative permittivity of the material between the two conductors, and

ϵ_0 is the permittivity of free space.

The characteristic impedance of any transmission line is

$$Z_o = \sqrt{\frac{R_m + j\omega L_m}{G_m + j\omega C_m}} \quad (2.32)$$

where R_m = series resistance of line per metre

G_m = shunt capacitance of line per metre

L_m = inductance of line per metre

C_m = capacitance of line per metre

If R_m and G_m are negligibly small then for a coaxial line,

$$Z_o = \sqrt{\frac{L_m}{C_m}}$$

from which

$$Z_o = 60 \sqrt{\frac{\mu_r}{\epsilon_r}} \ln \left(\frac{b}{a} \right) \quad (2.33)$$

and when $\mu_r = 1$ and $\epsilon_r = 1$ as for the air-dielectric line,

$$Z_o = 60 \ln \left(\frac{b}{a} \right) \quad (2.34)$$

or
$$Z_o = 138 \log \left(\frac{b}{a} \right) \quad (2.35)$$

where log is the logarithm to the base 10.

The wavelength λ for a signal of frequency f is given by equation (2.36)

$$\lambda = \frac{c}{f \sqrt{\mu_r \epsilon_r}} \quad (2.36)$$

where c is the velocity of electromagnetic waves in free space.

The variation of characteristic impedance with b and a is given by equation (2.35) which is shown as a graph in Figure 2.18. This shows that it is difficult to make a coaxial line with a value of Z_o much less than 20Ω as the ratio b/a becomes less than 1.4. A lower characteristic impedance can be produced by using a dielectric other than air but this will increase dielectric losses which are generally more significant than conductor losses at microwave frequencies.

The attenuation per metre of an air-dielectric coaxial line can be shown to be a minimum for $\frac{b}{a}$ of 3.6 which corresponds to a characteristic impedance of 77 ohms. However, the attenuation does not increase by more than 20% within the range $2 \leq \frac{b}{a} \leq 9.5$ which corresponds to the range of characteristic impedance 40 to 136 ohms. The graph of attenuation against $\frac{b}{a}$ is shown in Figure 2.19.

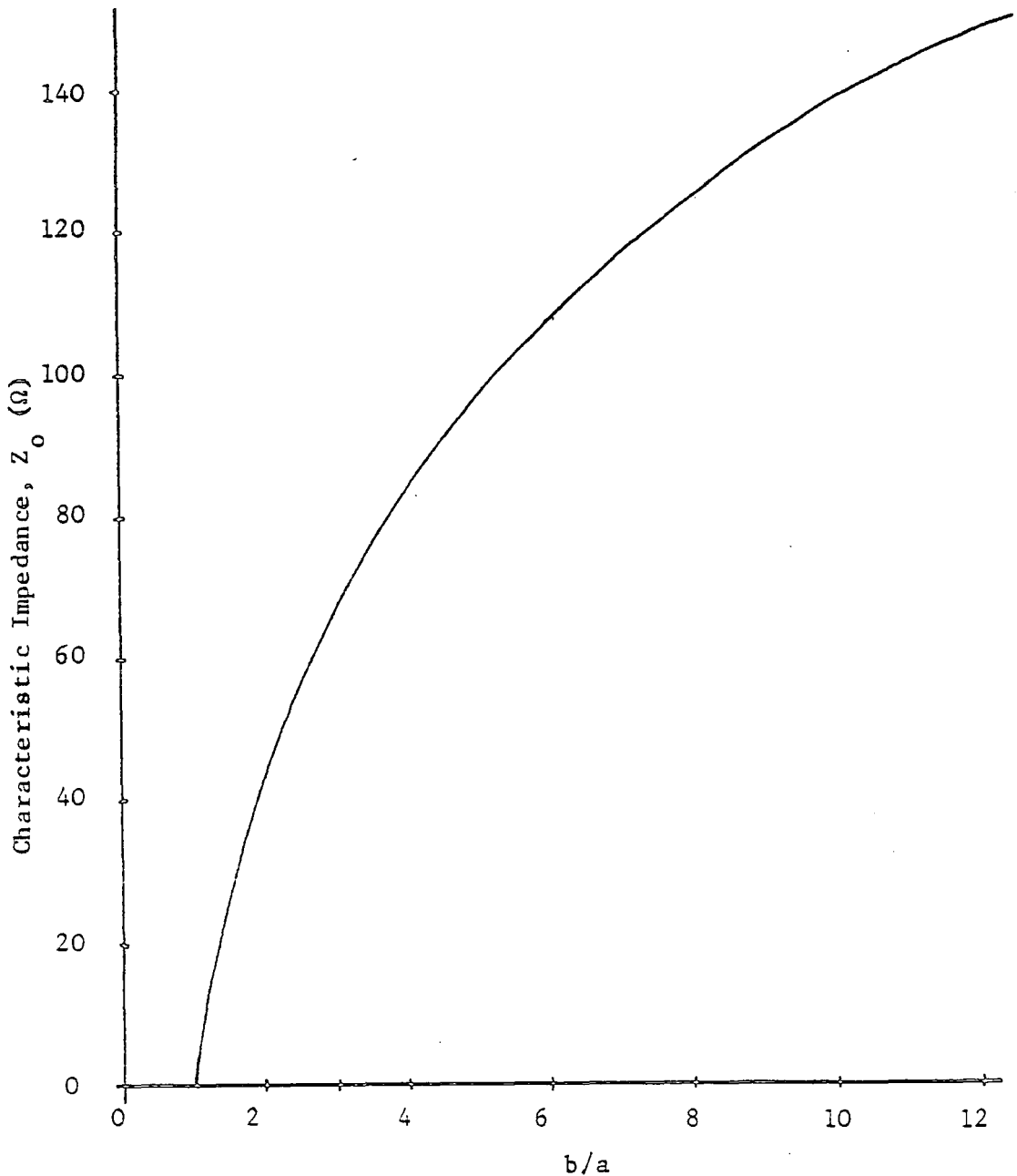


Figure 2.18 Z_0 versus b/a for a coaxial line

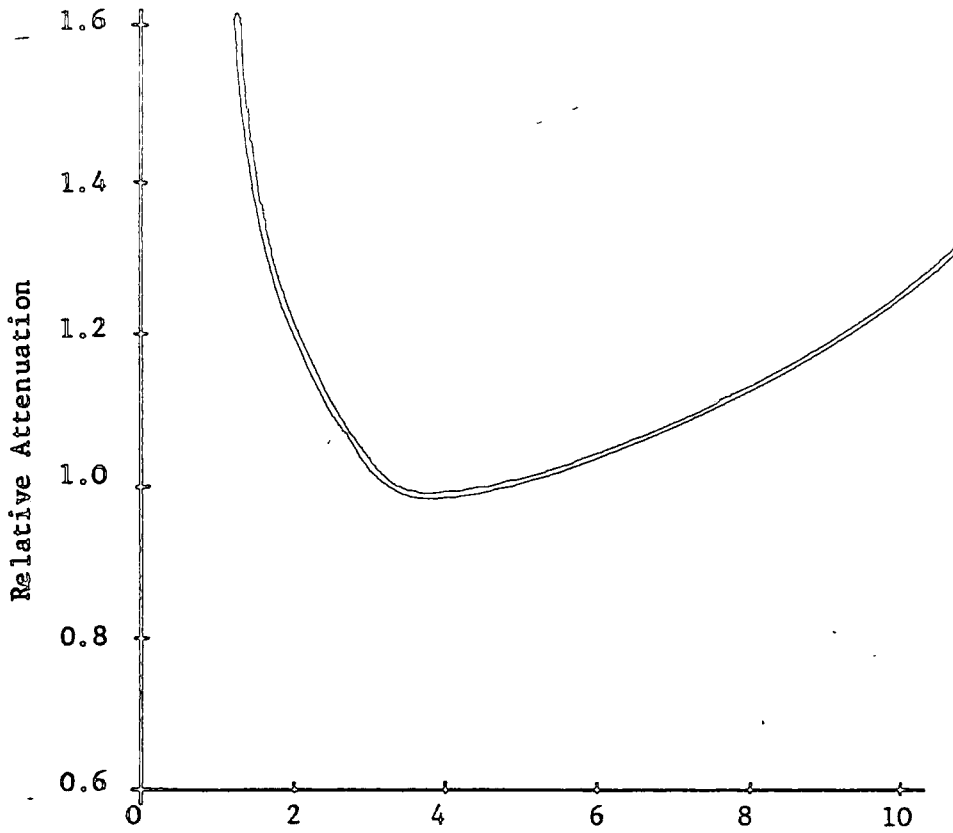


Figure 2.19 Attenuation versus b/a for a coaxial line

2.5 The microstrip series-tuned cavity

The microstrip transmission line has been the subject of extensive research and development in recent years because of its suitability for use in microwave integrated circuits. A microstrip circuit is normally produced using the techniques developed for printed-circuit board production, however, more accuracy is required with the conductor patterns. The reproducibility of the photolithographic process, the ease of production and the small size give the microstrip considerable advantages over the alternative waveguide and coaxial systems.

A microstrip transmission line is shown in Figure 2.20 and can be seen to consist of three parts: (i) a substrate which is initially fully clad with copper on both sides (ii) a ground plane of copper on one side of the substrate and (iii) a conductor pattern of strips of copper on the opposite side.

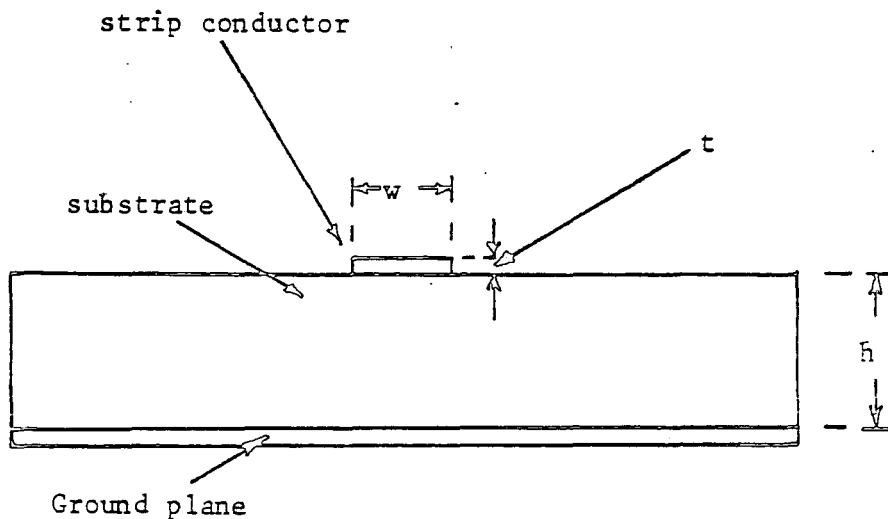


Figure 2.20
Cross-section of microstrip transmission line

The conducting strip is surrounded by two different materials, air and substrate, the latter consisting of any of the following: p.t.f.e.-impregnated glass fibre, alumina, sapphire or ferrite. Due to this lack of symmetry the propagation along the transmission line is not exactly TEM and exact computation of the velocity of propagation and characteristic impedance are difficult. An effective relative permittivity ϵ_{eff} has a value between the values of relative permittivity for air and the substrate. A useful formula for ϵ_{eff} is given by SCHNEIDER (reference 36) which shows that it depends upon the ratio w/h as well as the relative permittivity of the substrate, i.e.

$$\epsilon_{\text{eff}} = \frac{\epsilon_r + 1}{2} + \frac{\epsilon_r - 1}{2} \left(1 + \frac{10h}{w}\right)^{-\frac{1}{2}} \quad \text{for } \frac{w}{h} \geq 2 \quad (2.37)$$

$$\epsilon_{\text{eff}} = \frac{\epsilon_r + 1}{2} + \frac{\epsilon_r - 1}{2} \left(1 + \frac{10h}{w}\right)^{-\frac{1}{2}} + C \quad \text{for } \frac{w}{h} \leq 2 \quad (2.38)$$

where

$$C = 0.468 \frac{(\epsilon_r + 0.5)}{1.5} \left(\frac{t}{w}\right)^{\frac{1}{2}}$$

and ϵ_r is the relative permittivity of the substrate

h is the thickness of the substrate

w is the width of the transmission line

t is the thickness of the transmission line

The characteristic impedance of the microstrip is

$$Z_0 = \frac{Z_{0A}}{(\epsilon_{\text{eff}})^{\frac{1}{2}}} \quad (2.39)$$

where Z_{0A} is the characteristic impedance of a microstrip with a substrate having a relative permittivity ϵ_r of 1, and ϵ_{eff} is the effective relative permittivity given by equations (2.37) and (2.38).

Z_{OA} may be calculated from

$$Z_{OA} = 60 \ln \left(\frac{8h}{w} + \frac{w}{4h} \right) \text{ for } \frac{w}{h} \leq 1 \quad (2.40)$$

or

$$Z_{OA} = \frac{120\pi}{\frac{w}{h} + 2.42 - 0.44 \frac{h}{w} + \left(1 - \frac{h}{w}\right)^6} \text{ for } \frac{w}{h} \geq 1 \quad (2.41)$$

The wavelength of a signal of frequency f in the microstrip is

$$\lambda_m = \frac{\lambda_o}{(\epsilon_{eff})^{\frac{1}{2}}} \quad (2.42)$$

where λ_o is the wavelength in a microstrip with a substrate having a relative permittivity ϵ_r of 1. λ_o is also the free-space wavelength and for a signal of frequency f is

$$\lambda_o = \frac{3 \cdot 10^8}{f} \text{ metres} \quad (2.43)$$

The attenuation in the microstrip transmission line is due to conductor loss and dielectric loss, which are both dependent upon the characteristic impedance and frequency. An example of the typical parameters for a 50- Ω microstrip on a fibre-glass substrate is given in Table 2.1 below.

| | | |
|--|---|--|
| Substrate | : | epoxy fibre glass |
| h | : | 1.626 mm |
| w | : | 2.72 mm |
| t | : | 0.12 mm |
| ϵ_r | : | 5 |
| Dielectric loss tangent, $\tan \theta$ | : | 0.025 |
| f | : | 895 MHz |
| λ_o | : | 0.335 mm |
| ϵ_{eff} | : | 3.69 |
| λ_G | : | 0.175 m |
| Z_o | : | 50 Ω (Z_{OA} : 96 Ω) |
| conductor loss | : | 0.3 dB/m |
| dielectric loss | : | 3.56 dB/m |

Table 2.1
50- Ω microstrip on fibre-glass substrate

The variation of characteristic impedance with the width of conductor strip for the example given in table 2.1 is shown in Figure 2.21.

The microstrip transmission line can be used as a series-tuned cavity if a discrete variable capacitor or a fixed-value chip capacitor is used as the tuning capacitor as shown in Figure 2.22.

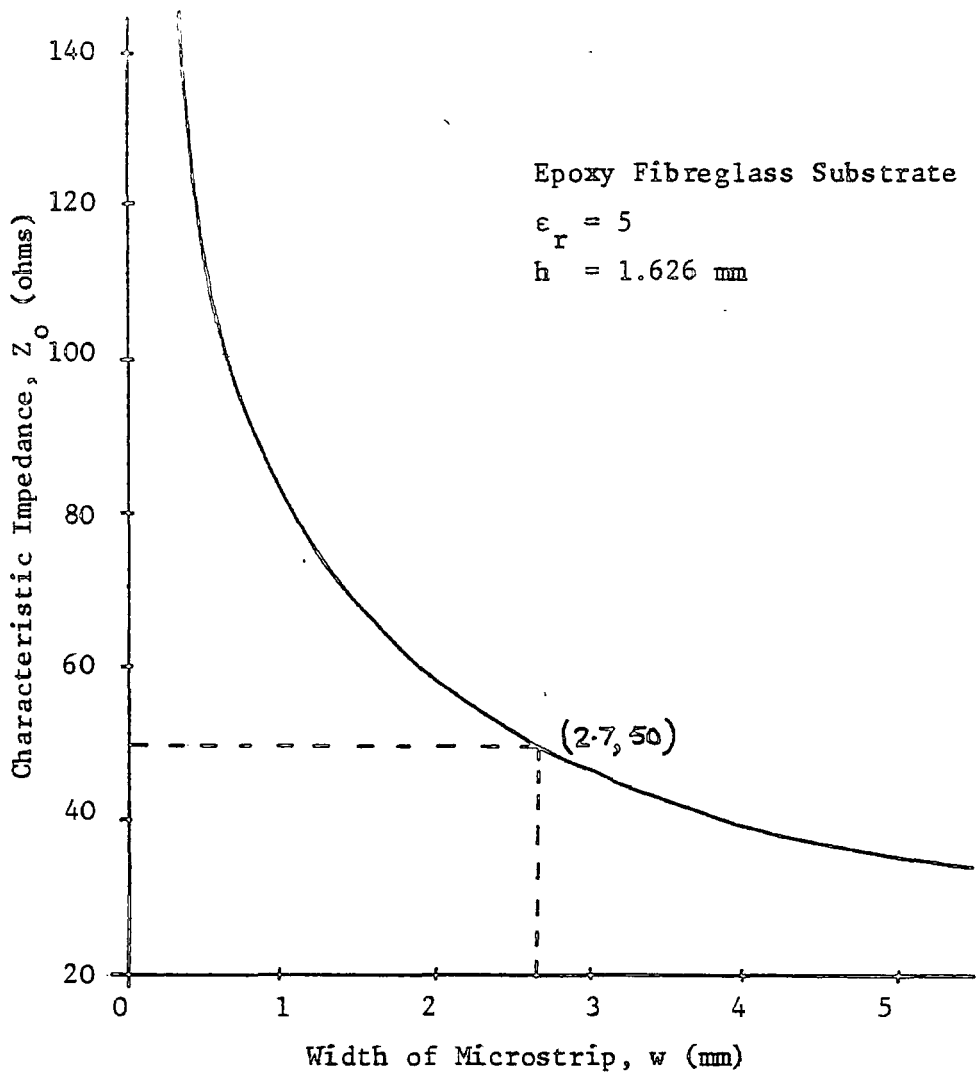
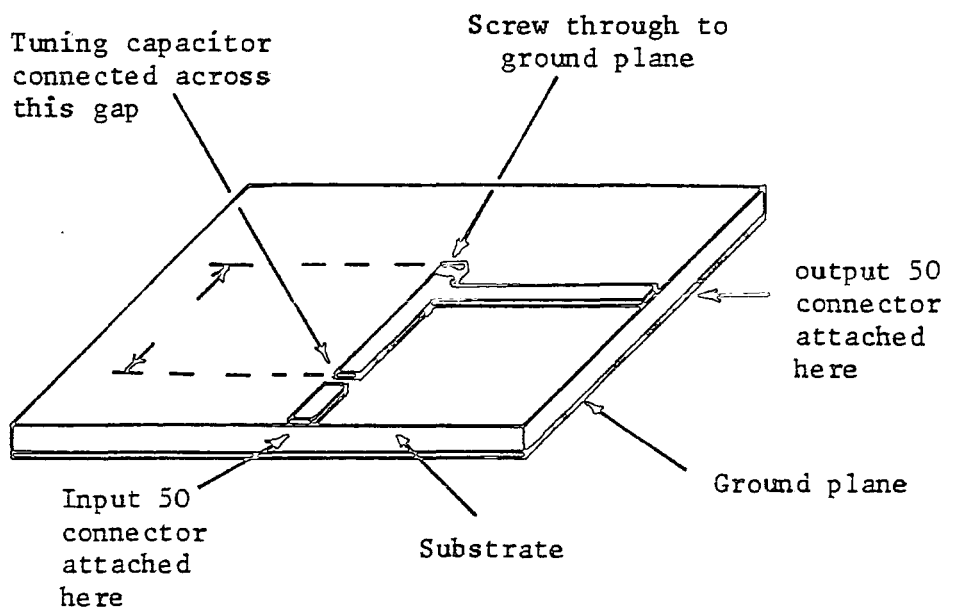


Figure 2.21



Microstrip series-tuned cavity

Figure 2.22

2.6 Conclusion

The theoretical results shown graphically in Figures 2.6 to 2.13 show that the selectivity of the cavity when feeding a $50\text{-}\Omega$ resistive load is a maximum when the probe is positioned near the short-circuited end. The Q-factor of 20 observed for the case when $A = 0.1$, $Z_L^0 = 1$ and $\theta_0 = 81^\circ$ is obtained with an effective series resistance of 100Ω . The unloaded Q of the cavity might be of the order of 20,000, or greater, but the cavity is loaded by the source resistance and load resistance each of which is 50Ω in the case considered. Higher values of loaded Q-factor can be obtained but at the expense of an increasing insertion loss due to mismatch.

A design procedure is given in section 2.3.3 so that the required cavity length, tapping point and series capacitance may be calculated for any case. Graphs of $R_{i/p}$ and $X_{i/p}$ are useful in choosing suitable values of θ_0 and A. There may be cases when Z_L is not equal to Z_0 and the cavity may then be used to provide impedance match at the required frequency.

Experimental results on two practical cavities are given in Chapter 3 and these show very little deviation from the theoretical results obtained in this chapter.

CHAPTER 3PERFORMANCE OF PRACTICAL SERIES-TUNED CAVITIES

| | <u>Page</u> |
|-----------------------------------|-------------|
| 3.1 Introduction | 51 |
| 3.2 A Practical Coaxial Cavity | 52 |
| 3.2.1 Design details | 52 |
| 3.2.2 Tests on cavity CI | 53 |
| 3.2.3 Summary | 54 |
| 3.3 A Practical Microstrip Cavity | 55 |
| 3.3.1 Design details | 55 |
| 3.3.2 Tests on cavities M2 and M4 | 56 |
| 3.3.3 Tests on cavity M1 | 57 |
| 3.3.4 Summary | 57 |
| 3.4 Conclusion | 58 |

3.1 Introduction

The theoretical results predicted in Chapter 2 apply to resonant cavities constructed with any type of transmission line. Coaxial transmission lines have been used for many years and have the important advantage, when compared with microstriplines, that the electromagnetic field is enclosed. A practical coaxial cavity was therefore designed and tested and the details are given in section 3.2.

Coaxial technology is now being replaced in many microwave applications by a planar technology because the latter produces smaller and more easily manufactured circuits. The resulting transmission lines are either striplines or microstrips as described in section 2.5. Three microstrip cavities were designed, produced and tested with results presented in section 3.3.

The coaxial cavity was called "cavity C1" and the microstrip cavities were given the titles "cavity M1", "cavity M2" and "cavity M4".

3.2 A Practical Coaxial Cavity

3.2.1 Design details

The cavity C1 was designed to have a characteristic impedance of 50Ω and a first resonance at 192 MHz. A $50\text{-}\Omega$ G.R. connector was used at the input and an adjustable air-gap in the centre conductor of the coaxial transmission line provided the required tuning capacitance C_s . The mechanical design of the mainly-brass cavity is illustrated in Figures 3.1, 3.2 and 3.3.

Dimensions of the cavity

Consider a value of θ_o of 81° , then from equation (2.12),

$$f_{\text{cav}} = 90 \times \frac{192 \text{ MHz}}{81^\circ} = 213.3 \text{ MHz} \quad (3.1)$$

The cavity length DC may then be found from equation (2.6) as,

$$DC = \frac{c}{4f_{\text{cav}}} = \frac{3.10^8}{4 \times 213.3 \times 10^6} = 35.1 \text{ cm} \quad (3.2)$$

Equation (2.35) can be used to determine the required ratio of B to A (see Figure 3.1). The values used for B and A were those of the $50\text{-}\Omega$ connector, namely,

$$A = 7 \text{ mm} \quad (3.3)$$

$$B = 16 \text{ mm} \quad (3.4)$$

The value of input capacitance required to resonate the unloaded cavity can be calculated from equation (2.10) as,

$$C_{\text{SN}} = \frac{1}{2\pi f_o Z_o \tan \theta_o} = \frac{1}{2\pi \times 192 \times 10^6 \times 50 \tan (81^\circ)} = 2.6 \text{ pF} \quad (3.5)$$

The parallel plate capacitor was produced with annular plates and the plate area A_c is given by the value in expression (3.6)

$$A_c = \frac{\pi}{4} \{ (7.10^{-3})^2 - (3.5 \cdot 10^{-3})^2 \} = 28.9 \cdot 10^{-6} \text{ m}^2 \quad (3.6)$$

It is useful to know the distance between the plates, d_c , when the parallel-plate capacitor has capacitance C_{SN} given by equation (3.5),

$$d_c = \frac{A_c \epsilon_0}{C_{SN}} = \frac{28.9 \cdot 10^{-6} \cdot 8.856 \cdot 10^{-12}}{2.6 \cdot 10^{-12}} = 0.098 \text{ mm} \quad (3.7)$$

This value of d_c is very small and it suggests that a very fine thread adjustment is required on part H of the cavity shown on Figure 3.3.

3.2.2 Tests on cavity C1

Swept frequency tests were carried out on the cavity with a probe consisting of the stiff inner conductor of a 50- Ω coaxial cable. The probe is shown on the photograph in Figure 3.4. The load resistor was the 50- Ω diode detector used with the sweep oscillator. Graphs of $2V_L/E_s$ versus frequency were plotted using an X-Y plotter.

Test 2A: The position of the probe was such that DP was 3.5 cm and thus it was one tenth of the length of the cavity. The practical results were plotted on the same axes as theoretical results from computer plots of the equations developed in Chapter 2, see Figures 3.5 and 3.6.

Test 2B: Variation of the tuning capacitor C_s produced responses as shown in Figure 3.7, the corresponding theoretical results being shown in Figure 3.8.

Test 2C: This test was conducted with DP of 20 cm so that $A = 0.57$ for which the theoretical results are plotted in Figure 2.13. The practical results are shown in Figure 3.9.

Test 2D: If the value of C_s is decreased to 0.5 pF the "third harmonic resonance" becomes sharper as the practical results of Figure 3.10 indicate. However, it should be noted that the available power gain G at this resonance is approximately 0.16.

3.2.3 Conclusion

The correlation between practical and theoretical results is very good as displayed in Figures 3.5 and 3.6. At the resonance the voltage response is about 10% below the theoretical voltage response; the practical response is thus less than 1dB below the theoretical. This difference is probably due to the losses in the cavity.

The construction of the cavity requires careful design of the input capacitance and of the probe connection.

3.3 A Practical Microstrip Cavity

3.3.1 Design details

A microstrip test board with layout as shown in Figure 3.11 was produced to obtain practical results which could be compared with the theoretical results of Chapter 2. The board consisted of a fibreglass substrate with conductor strips of width 2.7 mm, previous tests having shown that these transmission lines have characteristic impedance of 50Ω and effective relative permittivity of 3.17.

In fact three cavities, numbered M1, M2 and M4, were included on the board with dimensions and data as given in Table 3.1. The short circuits were produced using brass screws through the substrates to make the contact between the baseplate and the strip.

| | Cavity M1 | Cavity M2 | Cavity M4 |
|--|-----------|-----------|-----------|
| Input terminal | 1A | 2A | 4A |
| Output terminal | 1B | 3B | 5B |
| Physical Length (DC) | 155 mm | 73 mm | 73 mm |
| Predicted f_{cav} (assuming $\epsilon_{eff} = 3.17$) | 272 MHz | 577 MHz | 577 MHz |
| $A = \frac{DP}{DC}$ | 0.1 | 0.1 | 0.1 |

TABLE 3.1

3.3.2 Tests on cavities M2 and M4

Test 3A: Cavity M2 was fed through a variable capacitor connected to input terminal 2A as shown in Figure 3.12. The output coupling was a copper wire soldered between the cavity and the microstrip connected to output terminal 3B. The value of C_s was the minimum obtainable on the variable capacitor used and was measured as 3 pF. The swept frequency response is shown in Figure 3.13.

Test 3B: The above test was repeated on cavity M4 to investigate the effect of the type of probe connection (cavity M4 has a 50- Ω microstrip probe). The response is shown in Figure 3.14 which shows that the resonant peaks are at the same frequencies as for cavity M2 but the high-frequency transmission of the system is better for cavity M4.

Test 3C: The value of the capacitor C_s was changed to 5 pF to obtain a different response and the procedure of test 3A was repeated. The response has the first resonance at 430 MHz and is shown in Figure 3.15.

Test 3D: Cavity M2 was fed via C_s but the output was taken from a position which was 0.2 of the cavity length from the short-circuited end. The output was taken via a copper wire link to the 50- Ω microstrip connected to point 4B. The value of C_s was adjusted to give a maximum height first resonance and the response was as shown in Figure 3.16 with the resonance at 460 MHz.

3.3.3 Tests on cavity M1

Test 3E: Cavity M1 was fed via a variable capacitor C_s connected at input 1A and the output was connected to 1B via a direct copper wire link to a point 0.1 times the cavity length from the s/c end of the cavity. It was found that the maximum value of C_s gave a low amplitude resonance at 202 MHz and the minimum value of C_s also gave a small first resonance but at 255 MHz. The response for minimum C_s is given in Figure 3.17. The value of θ_0 was estimated to be 84° .

Test 3F: This was similar to the previous test but with C_s adjusted to give a maximum amplitude first resonance, see Figure 3.18. The value of θ_0 for this was estimated to be 78° .

3.3.4 Summary

It was found that the microstrip probe was more effective than the copper wire probe connection at the higher frequencies. This is shown clearly by comparing Figure 3.13 with 3.14.

The correlation between practical results and theoretical results can be seen by comparing Figure 2.6 with Figure 3.17. It is not as good as for the coaxial cavity but this could be due to the difficulty of providing a tuning capacitor which does not disturb the transmission. A fixed-value chip capacitor could be used but this would not provide the adjustability required. The practical results show a loss compared with the theoretical results of about 2.5 dB for cavity M1 and 1.7 dB for cavity M2.

3.4 Conclusion

The practical results obtained for the cavities are in close agreement with the theoretical results predicted in Chapter 2. This is shown in Figures 3.5 and 3.6 for cavity C1 and in the comparison of Figures 2.6 and 3.17 for cavity M1.

The results for the practical coaxial cavity show that at the resonance the voltage response is about 10% below the theoretical voltage response; this is a difference of less than 1 dB. It is probably due to the losses in the connectors and, to a smaller extent, the losses in the cavity.

The correlation between practical results and theoretical results for the microstrip cavity was not as good as for the coaxial cavity. There was a difference of at least 1.7 dB which could be due to connector loss, cavity loss and radiation loss.

The construction of the coaxial cavity requires careful design of the input capacitance and the probe connection. The microstrip cavity was more easily manufactured but there was a difficulty in designing the input tuning capacitor. The constructional details for each type of cavity are given in sections 3.2.1 and 3.3.1.

Sketch 1: CAVITY

Scale: FULL SIZE

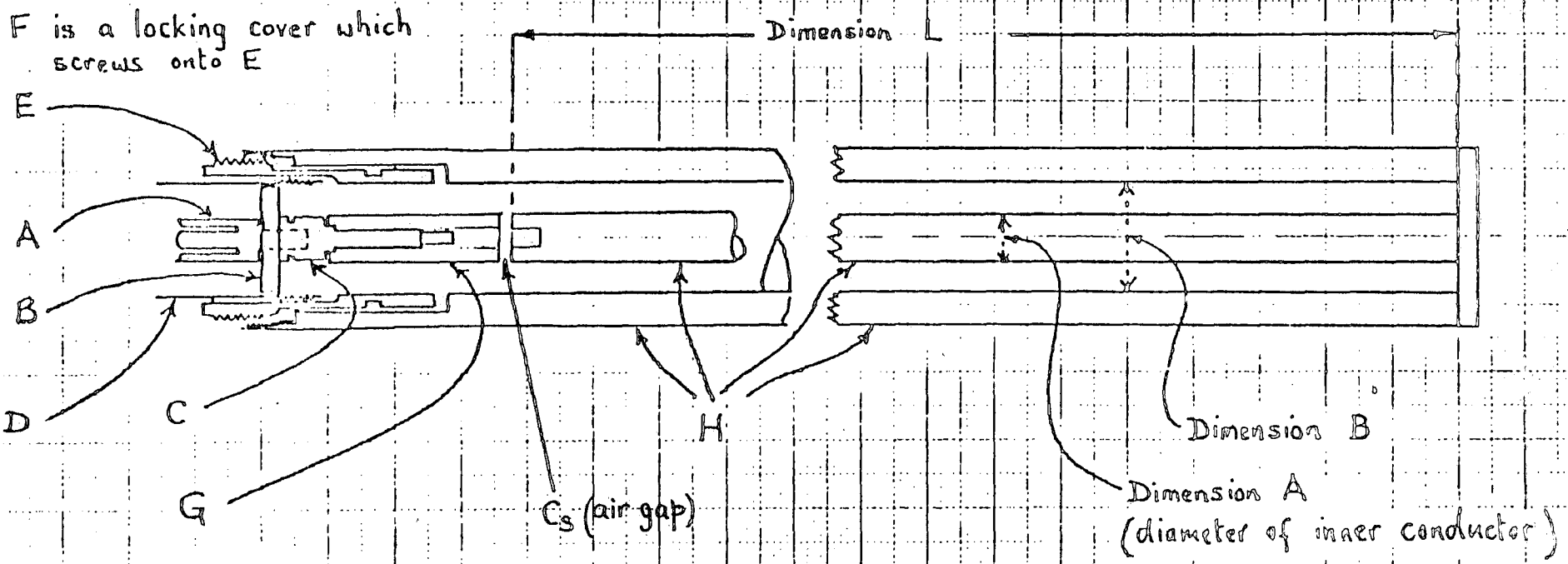


Figure 3.1
Coaxial Cavity C1

Parts J and I are not shown on this drawing. They retain the assembly ABCG in firm contact with D and E as shown on sketch 3.

Sketch 2

CAVITY: Parts C and G.

Scale: 4 x FULL SIZE

Part G to be a close fit onto part C, and to be pinned to it using hole x

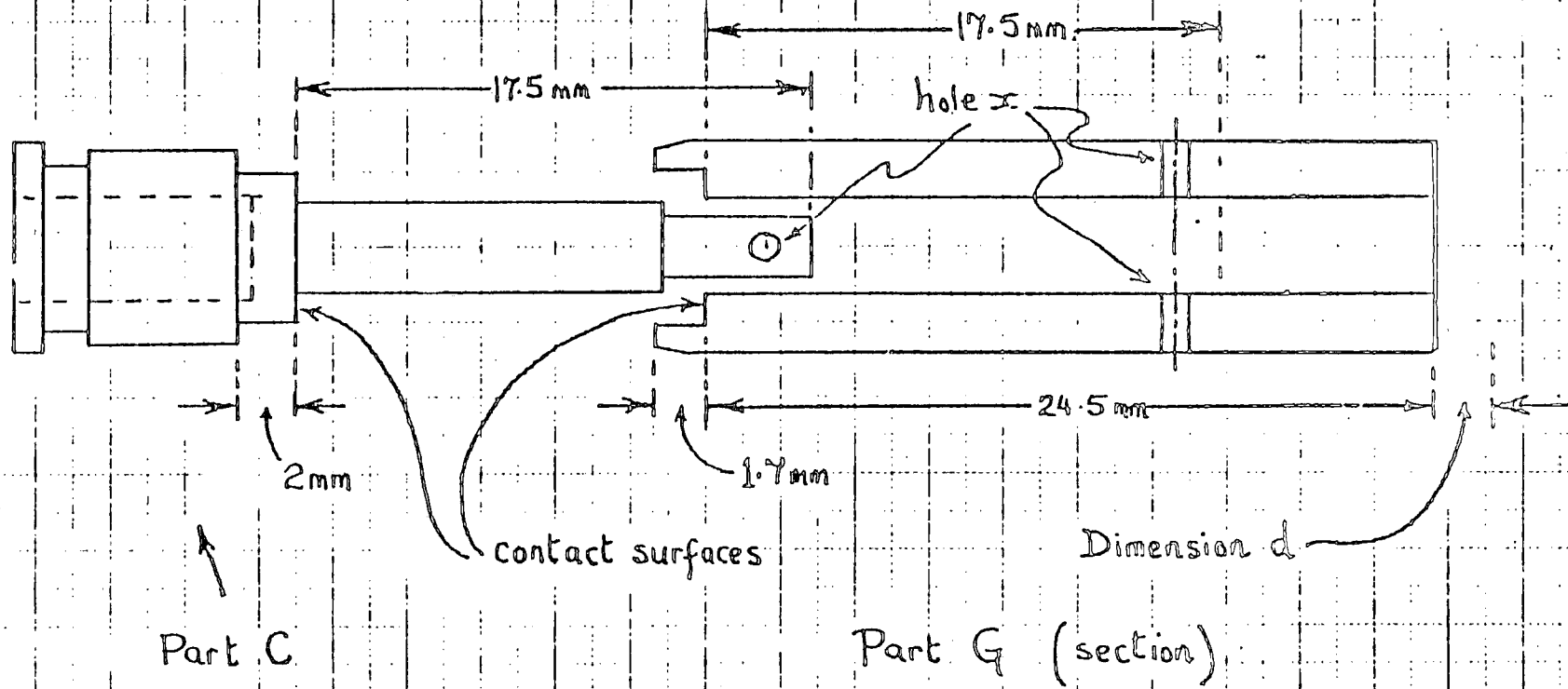


Figure 3.2

Scale: 4 x FULL SIZE.

Sketch 3: CAVITY : Parts H, J and I.

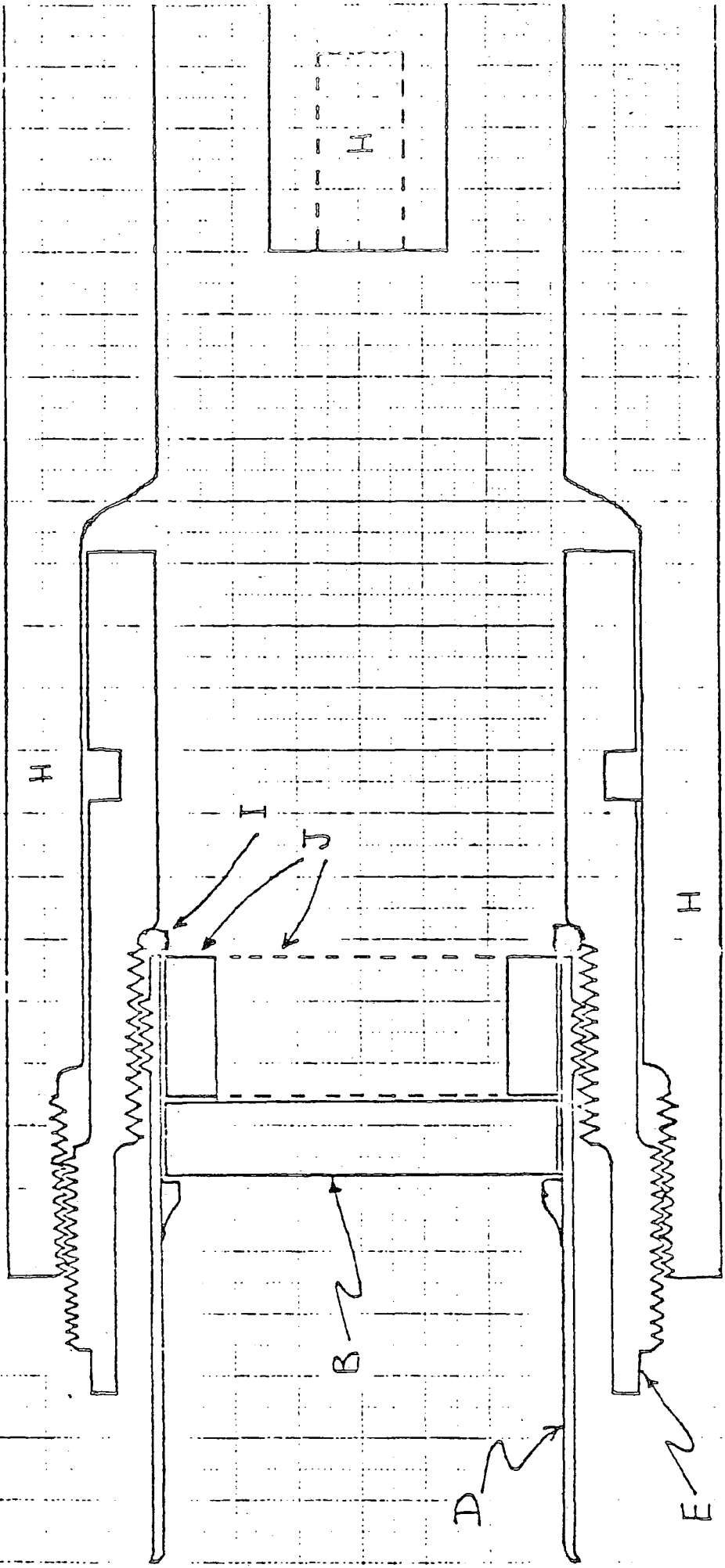
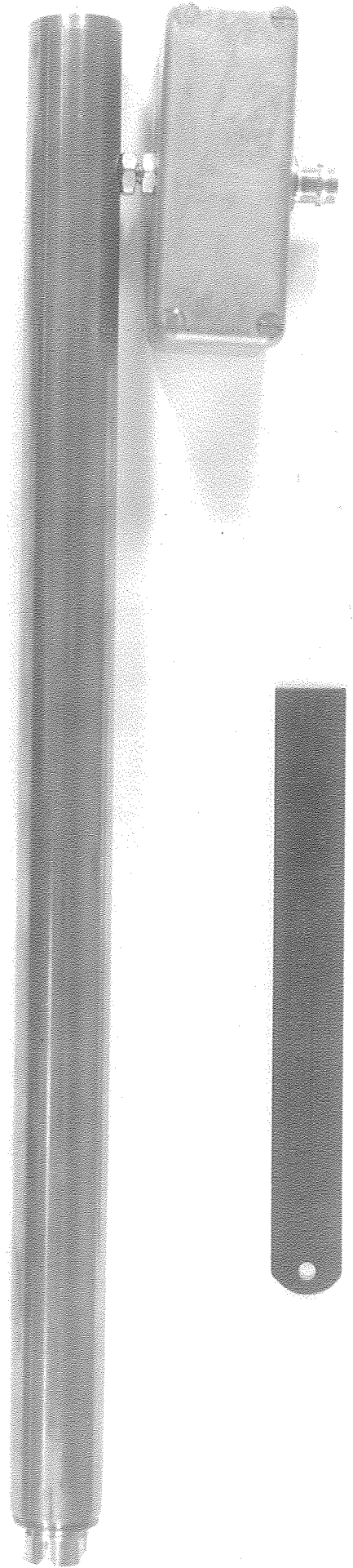


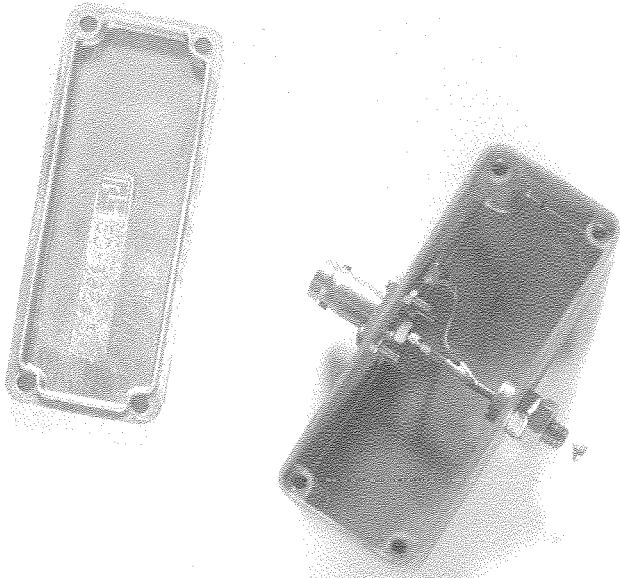
Figure 3.3

OUTPUT PROBE



INPUT CONNECTOR

FIGURE 3.4 COAXIAL CAVITY



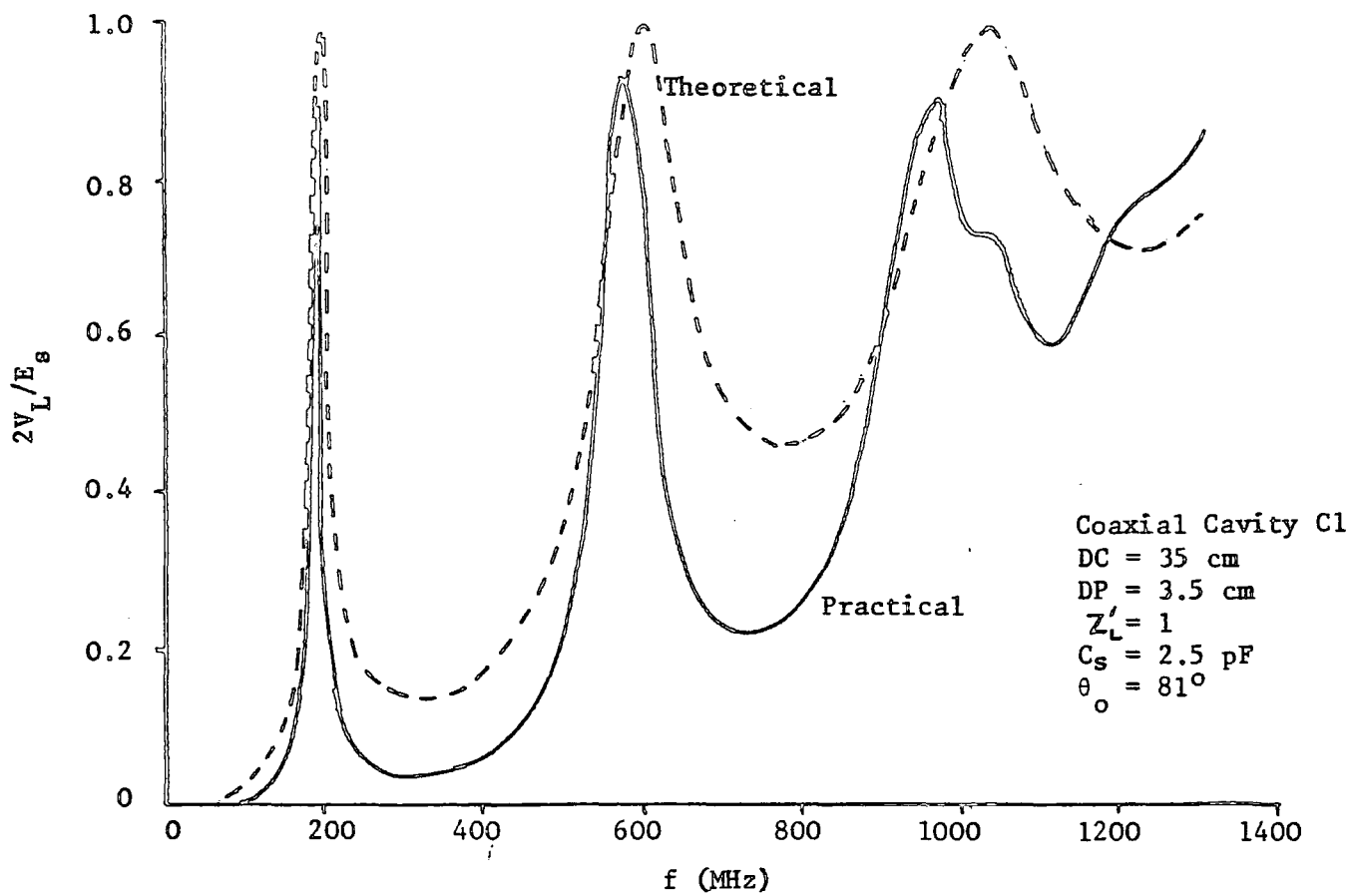


Figure 3.5
Test 2A

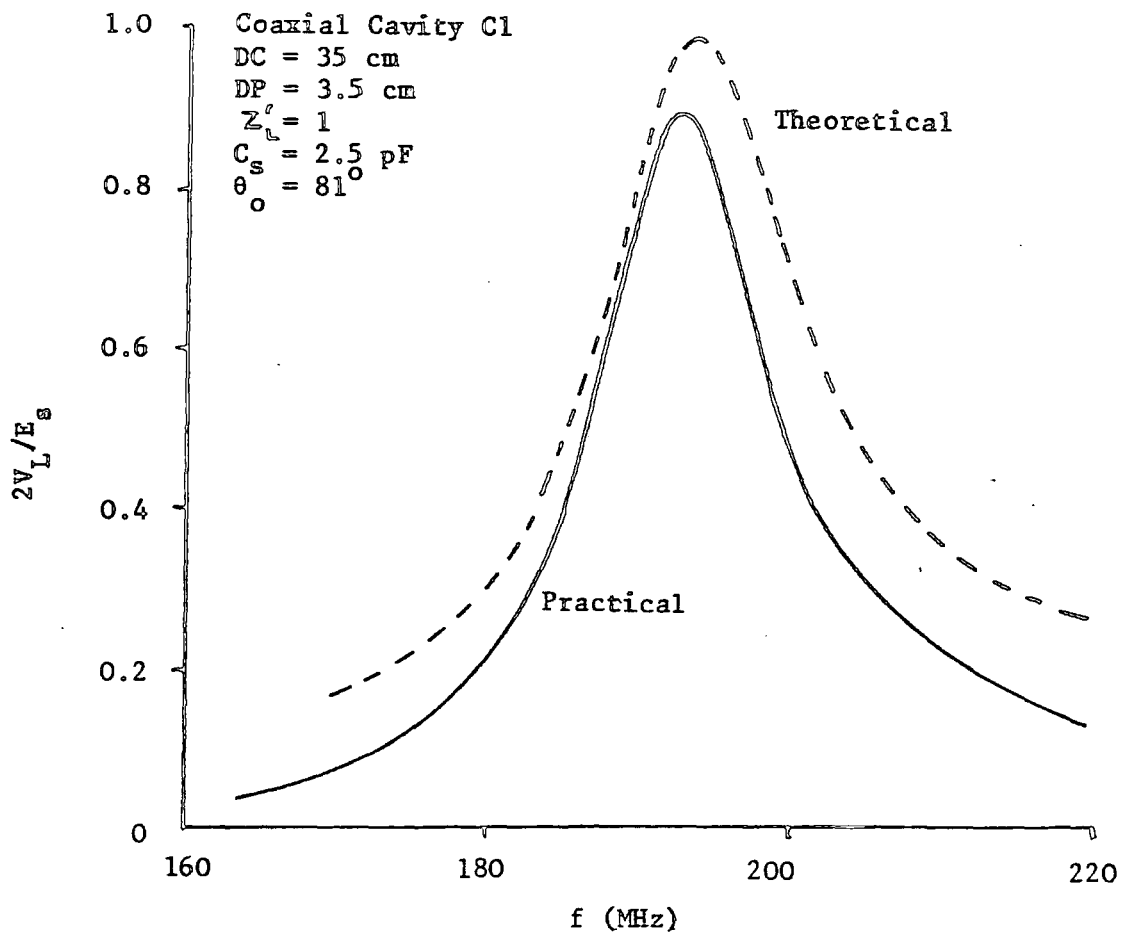


Figure 3.6
Test 2A

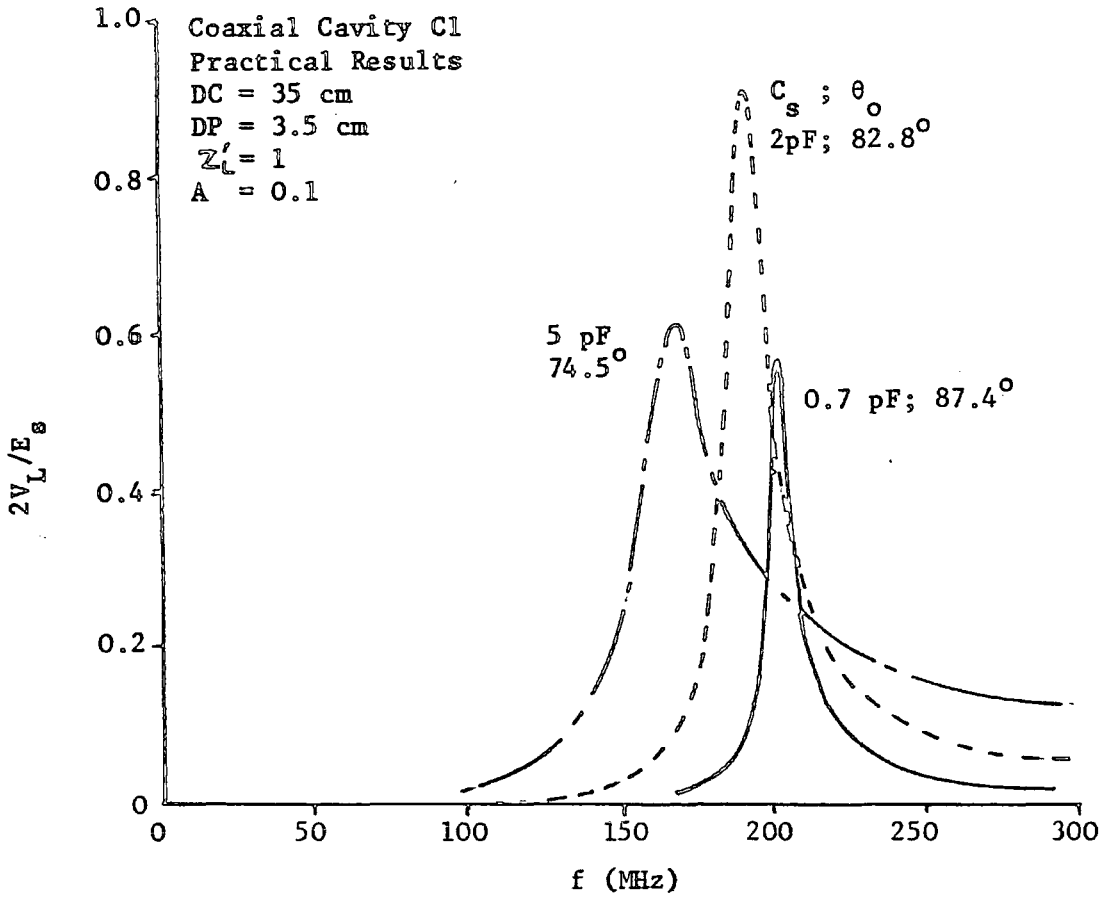


Figure 3.7
Test 2B

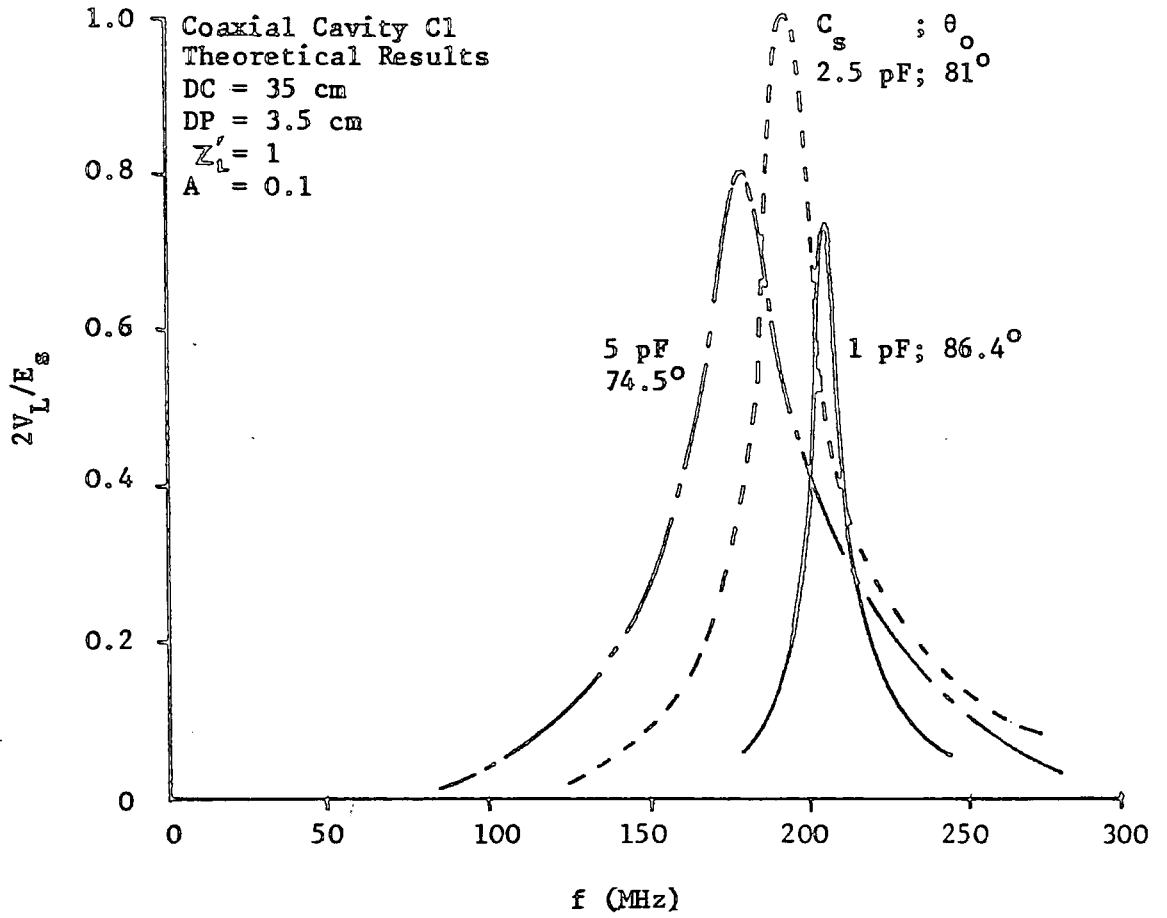


Figure 3.8
Test 2B

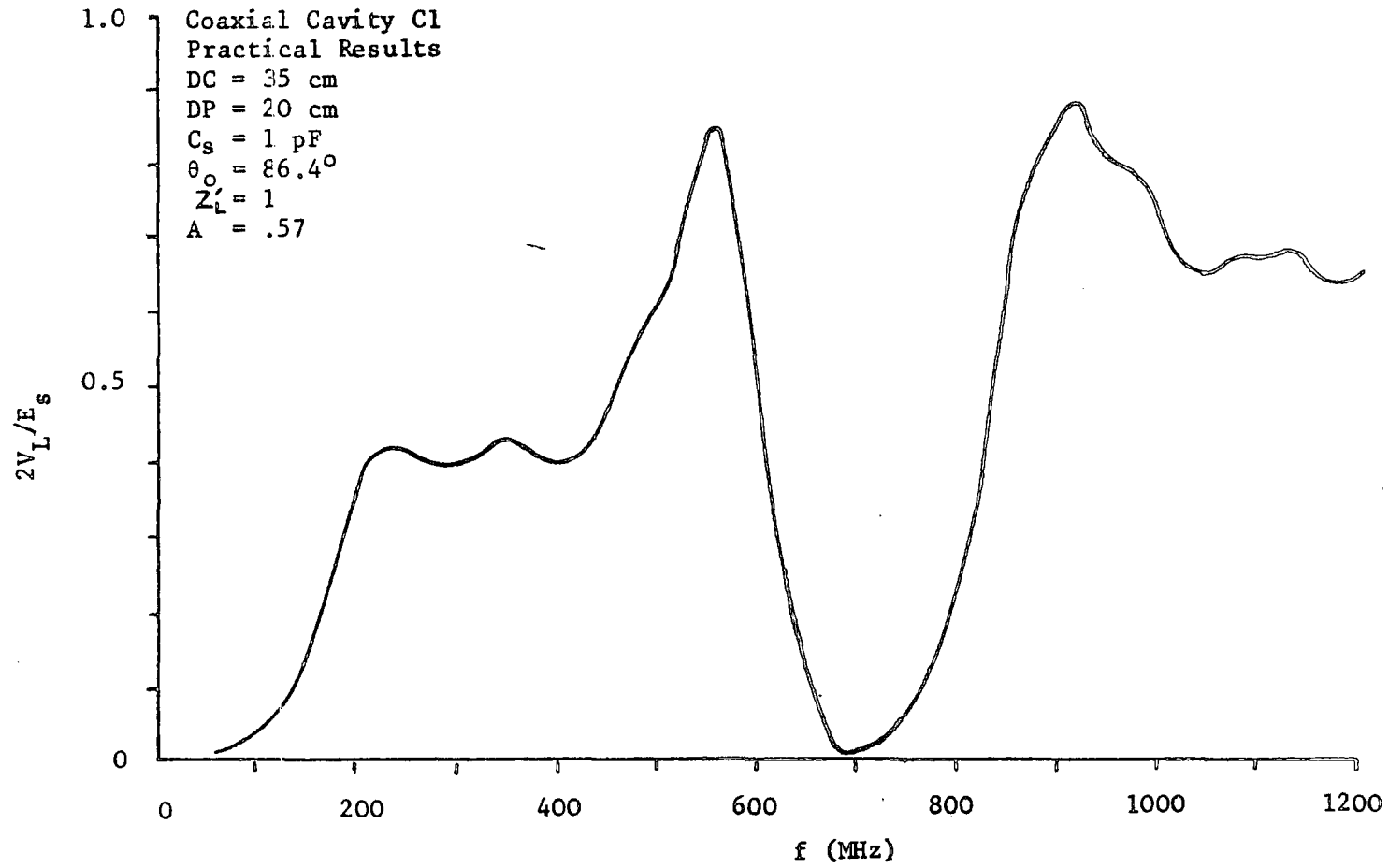


Figure 3.9
Test 2C

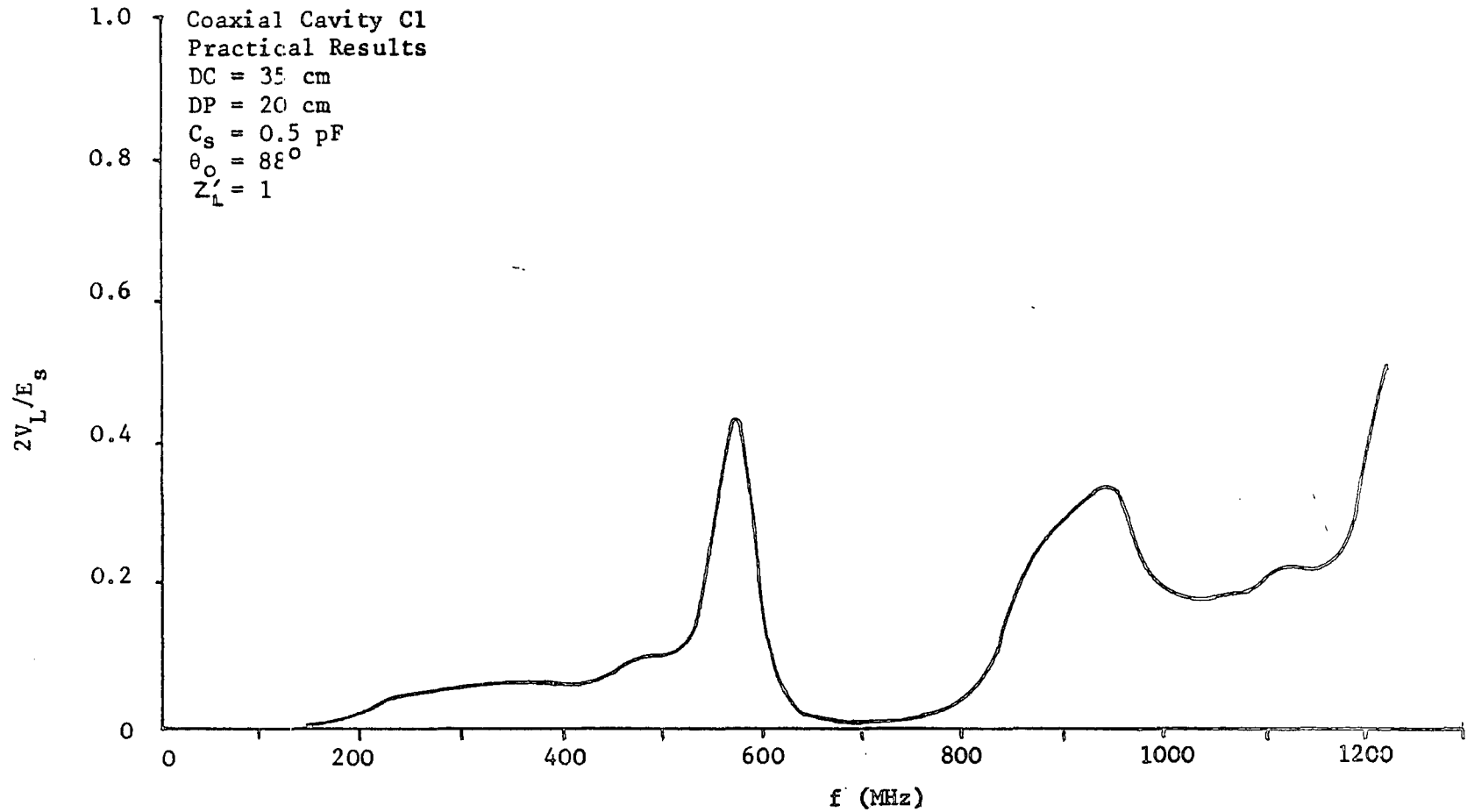


Figure 3.10
Test 2D

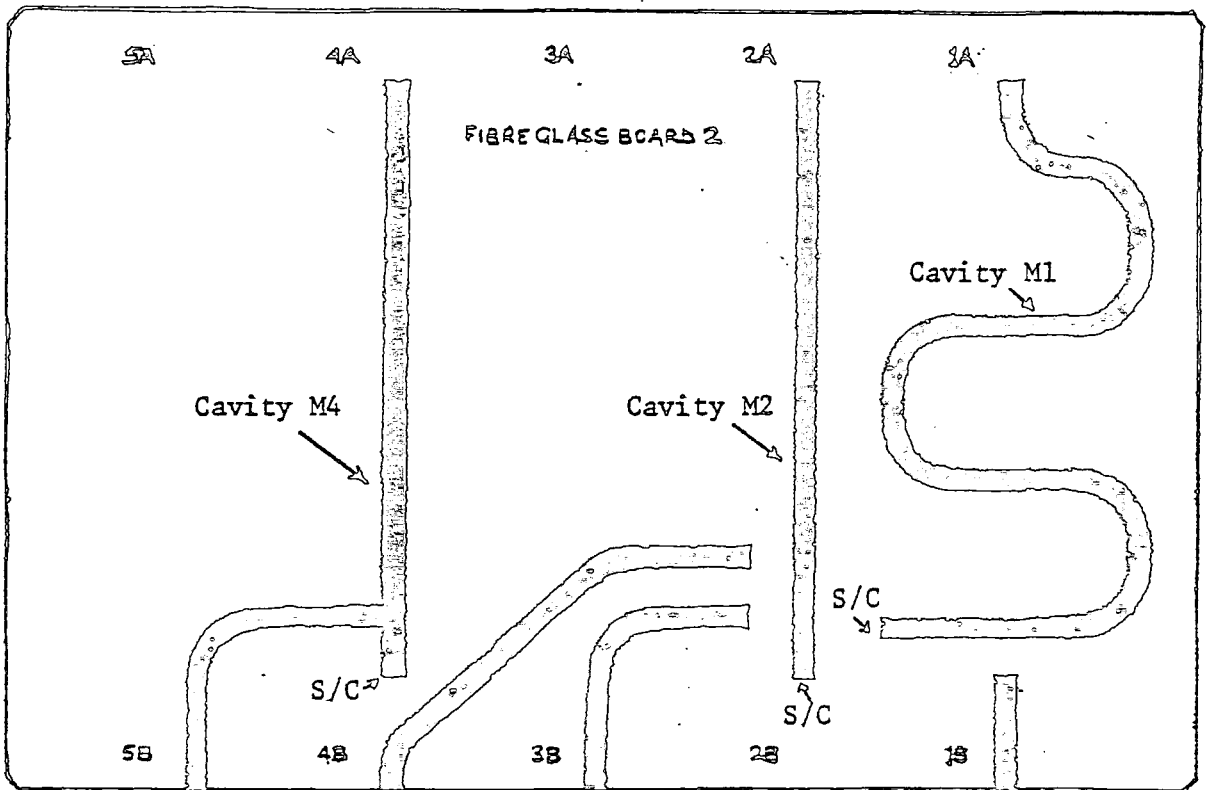


Figure 3.11
Microstrip cavities
(Full size drawing)

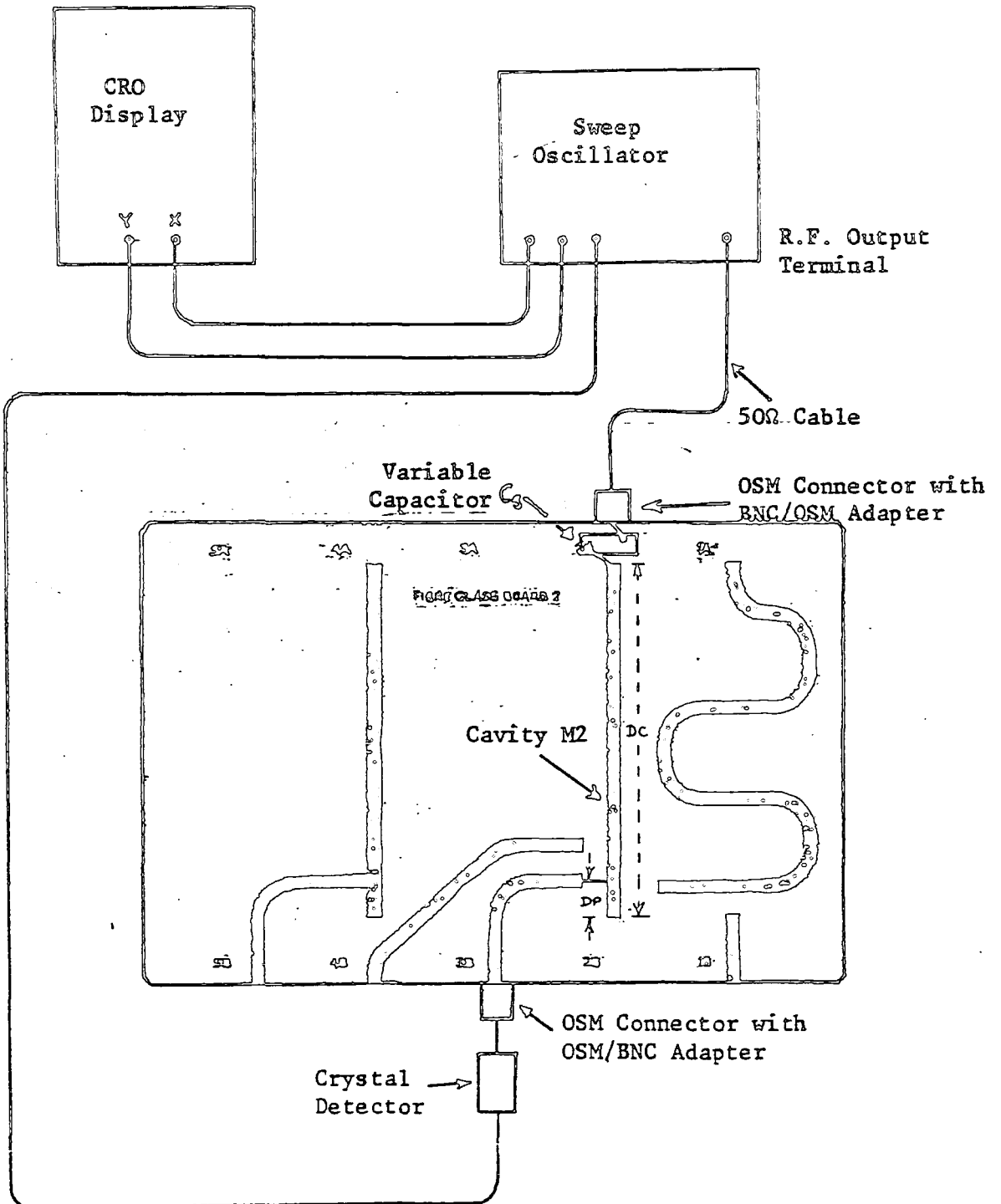


Figure 3.12
Test 3A: circuit diagram

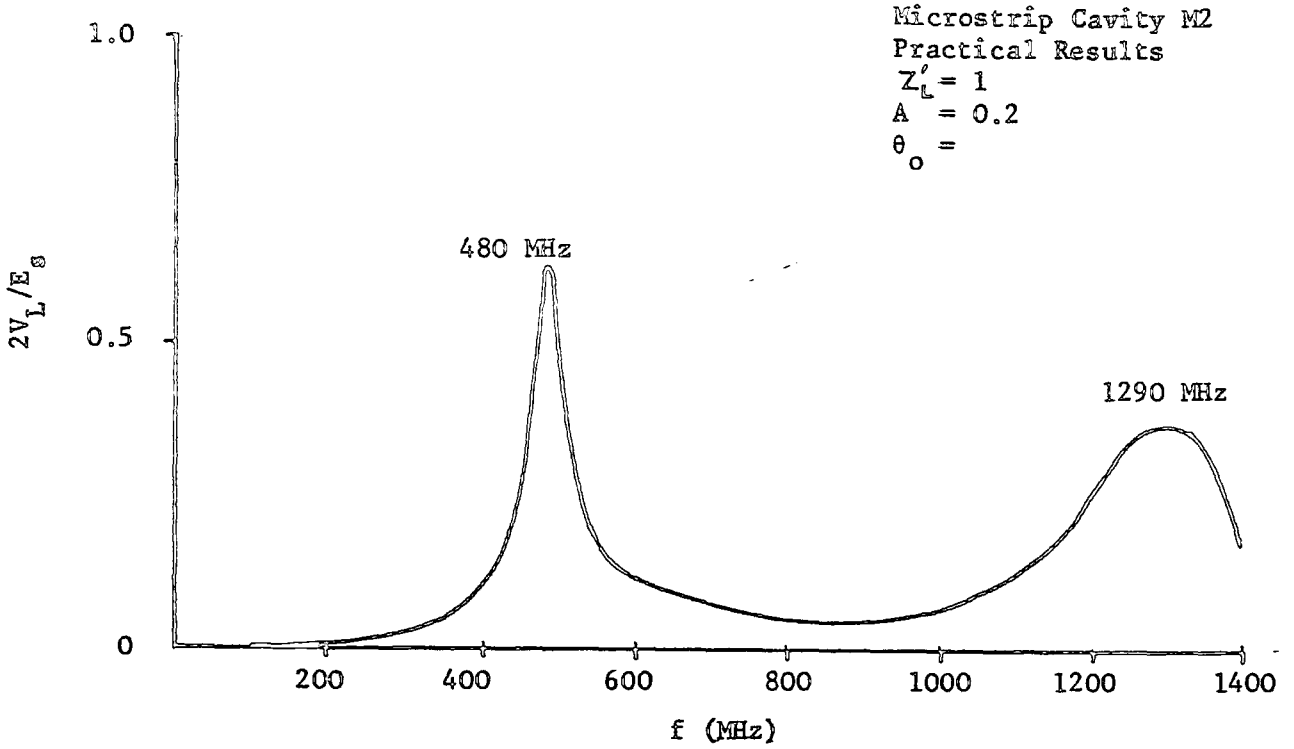


Figure 3.13
Test 3A

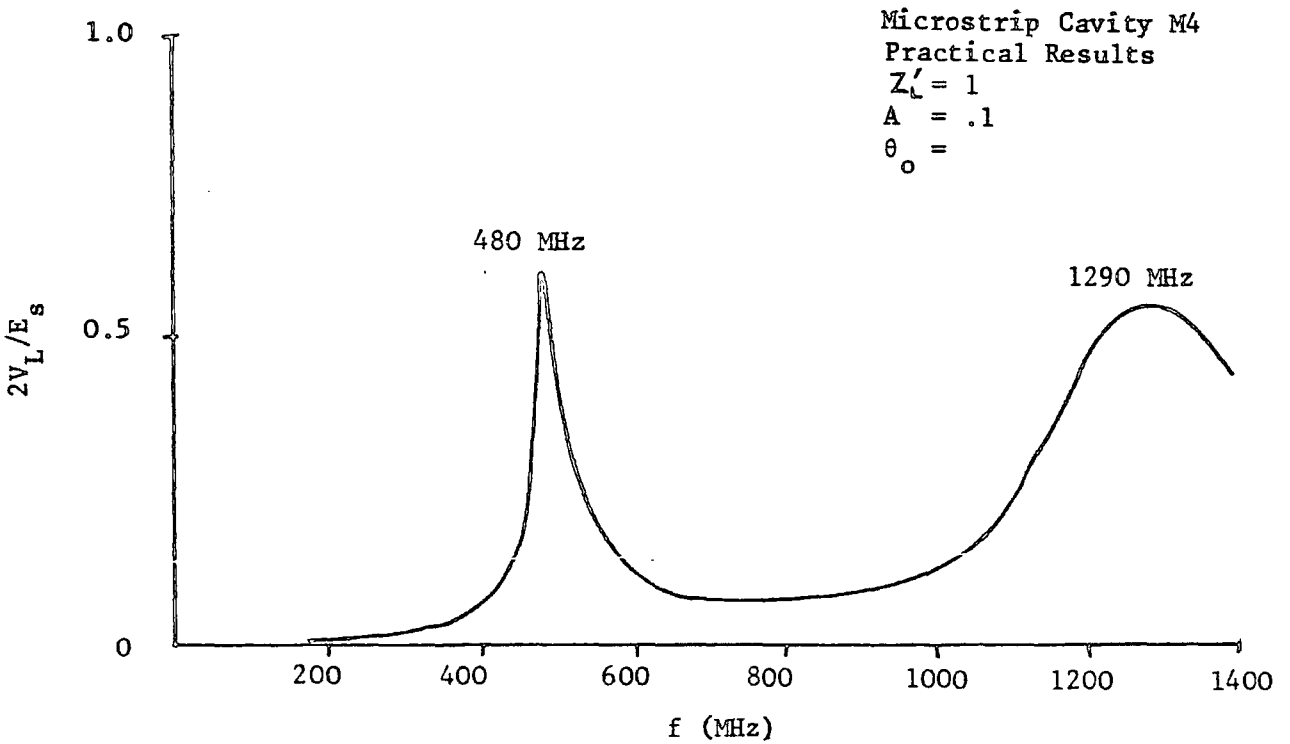


Figure 3.14
Test 3B

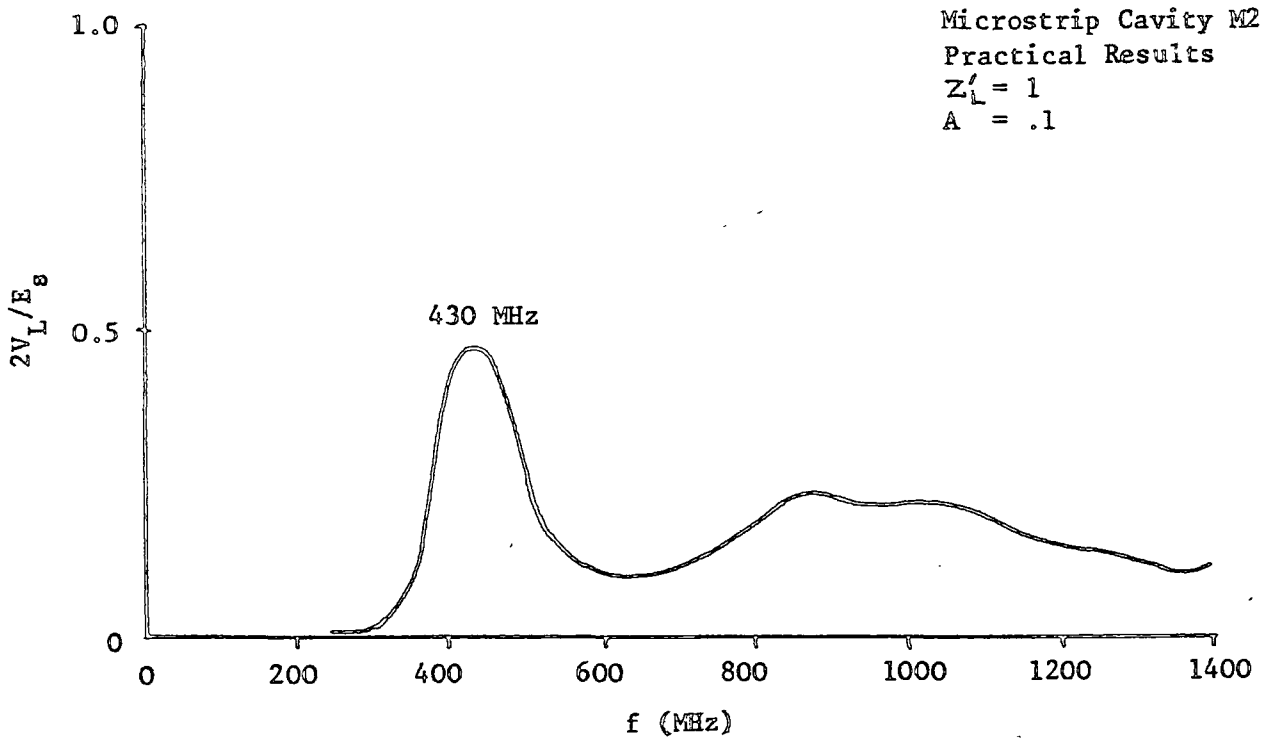


Figure 3.15
Test 3C

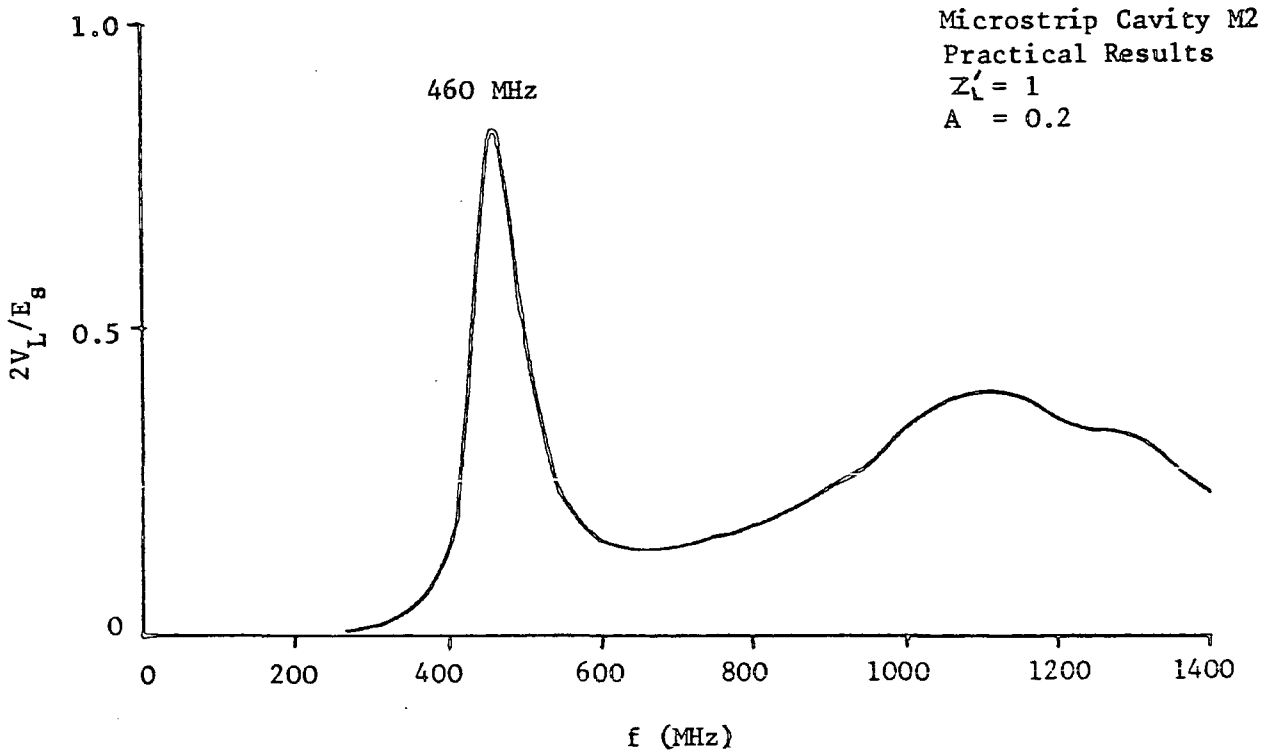


Figure 3.16
Test 3D

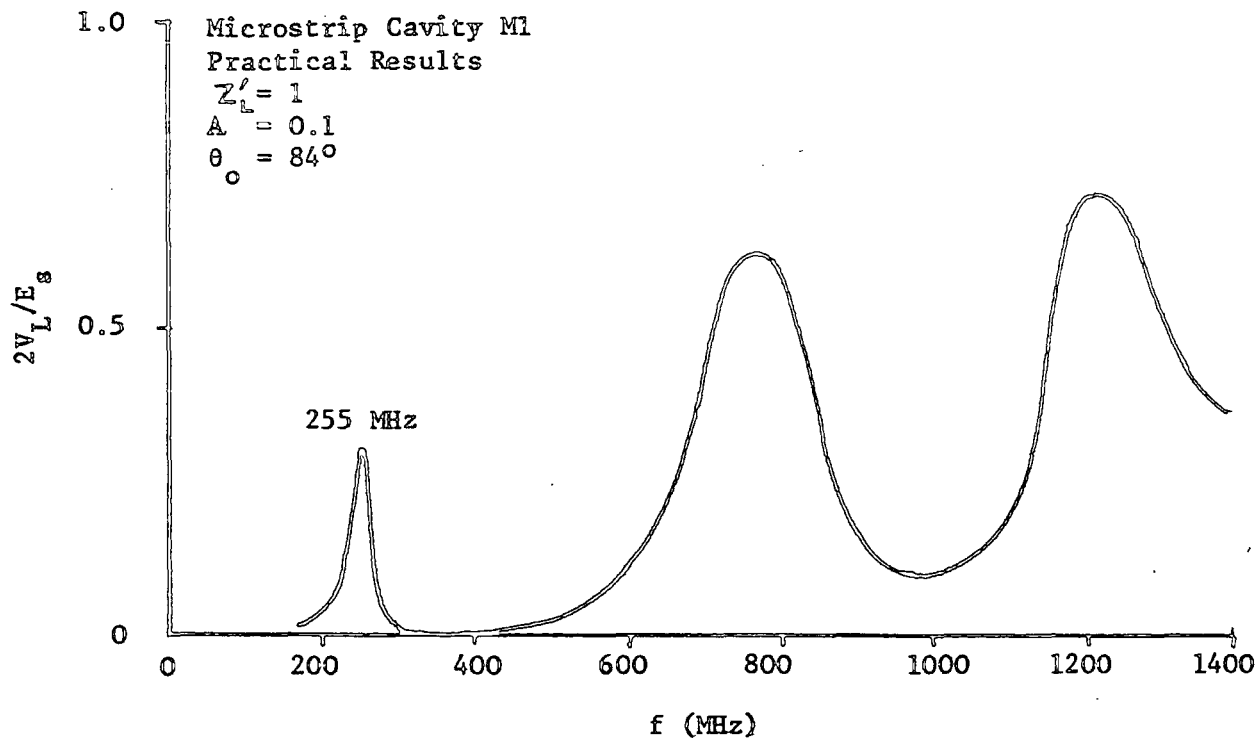


Figure 3.17
Test 3E

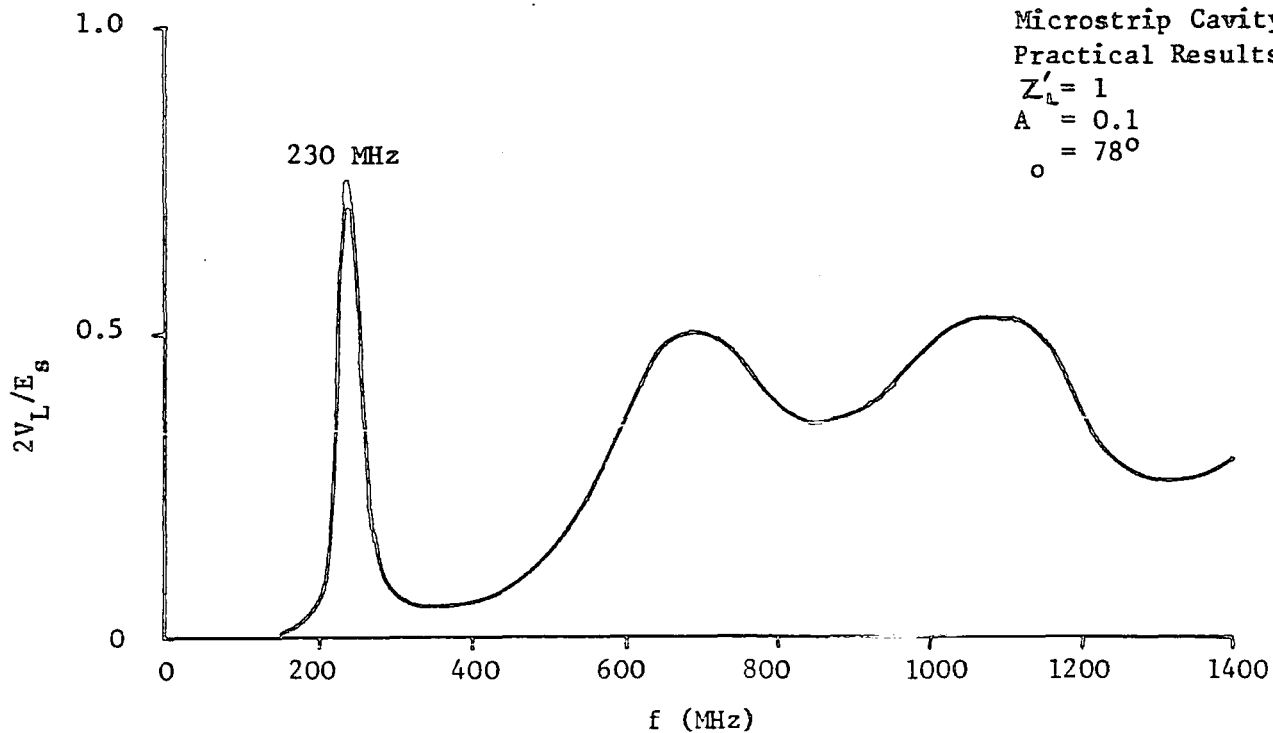


Figure 3.18
Test 3F

CHAPTER 4A METHOD OF ANALYSING DIODE MULTIPLIER
CIRCUITS AND ITS APPLICATION TO THE
SHUNT-DIODE DOUBLER

| | <u>Page</u> |
|---|-------------|
| 4.1 Introduction | 75 |
| 4.2 A Method of Analysis for Multiplier Circuits in Terms of Varactor Spectral Data. | 76 |
| 4.3 Shunt-Diode Doubler Analysis | 84 |
| 4.3.1 Two-term approximation to the diode characteristic | 84 |
| 4.3.2 Three-term approximation to the diode characteristic | 95 |
| 4.3.3 Four-term approximation to the diode characteristic | 99 |
| 4.4 Conclusion | 104 |

4.1 Introduction

This chapter develops a method of analysing frequency multiplier circuits and uses it to obtain expressions for the performance of the shunt-diode doubler circuit. Diode tripler circuits, with and without idlers, are dealt with by the same method in Chapter 5.

The method of analysis is explained in Section 4.2 and can be used for either shunt-connected or series-connected diodes. It assumes that the diode is tested with a cosinusoidal drive of charge in the shunt case or voltage in the series case and the resulting spectra of voltage and charge, respectively, are used to specify the non-linear characteristic of the diode. The performance of the multiplier circuit is then obtained in terms of the magnitudes of the components of the test spectrum.

The performance of a shunt-connected varactor-diode doubler is investigated in Section 4.3 and expressions are found for the maximum output power, the drive levels and load resistance values for which the analysis is valid. The capacitance presented by the diode to the input circuit, and the output capacitance of the diode operating in the second harmonic output circuit are also obtained. These expressions are initially found by an approximate analysis used because of its relative simplicity; the approximation is that the diode does not generate harmonics higher than the second when tested with the cosinusoidal drive. The modifications required when the third and fourth harmonics are taken into account are then investigated in Sections 4.3.2 and 4.3.3 and further insight is gained into the operation of the circuit. A large amount of algebra involved in obtaining these solutions has been put into appendices, and a summary of the results of the analysis is given in Section 4.4.

4.2 A Method of Analysis for Multiplier Circuits in Terms of Varactor Spectral Data

Early work on varactor harmonic generators assumed that operation was constrained so that the voltage across the diode never exceeded the reverse breakdown voltage in one direction and the contact potential of the junction in the other direction. In practice, especially where automatic bias is used for the varactor, harmonic generators are usually driven so that the contact potential is exceeded in the forward direction which results in a short pulse of forward current. This type of operation produces an increased output power and efficiency and is the basis of the switching multipliers which use the step recovery diode (reference 09). The analysis used in this chapter assumes that forward conduction does not occur so that it will not strictly apply to step recovery diode multipliers, although it is hoped that it may be adapted to this case in the future. However, the method is of considerable interest as it gives closed-form solutions which are not restricted to small signals as was the case with the early analyses (reference 17). The method is an adaptation of that proposed by R. ARMSTRONG (reference 02).

Many papers on varactor multipliers have used the relationship between the voltage across the varactor junction V_a and the incremental capacitance C_i as

$$\left. \begin{aligned}
 C_i(V_a) &= \frac{C_o^r}{\left(1 - \frac{V_a}{\phi}\right)^\gamma} \quad \text{when } V_a < \phi \\
 C_i(V_a) &= \infty \quad \text{when } V_a = \phi
 \end{aligned} \right\} \quad (4.1)$$

where ϕ is the contact potential. The measurement of the characteristic of the varactor has also been the subject of several investigations for example, SMITH and BRAMER (reference 37, 1972) and NUYTS and VAN OVERSTRAETEN (reference 26, 1969). Here the varactor Q/V_a relationship will be taken as the sum of Chebyshev Polynomials as shown in equation (4.2) for the series diode case and equation (4.3) for the diode in the shunt connection.

$$Q = \sum_{n=0}^{\infty} Q_{no} T_n(v) \quad (4.2)$$

$$V = \sum_{n=0}^{\infty} V_{no} T_n(q) \quad (4.3)$$

In the above relationships the coefficients Q_{no} are the open circuit harmonic charges developed in the diode when it is driven by a cosinusoidal voltage, the coefficients V_{no} are the open circuit harmonic voltages developed across the diode when it is driven by a cosinusoidal charge, and v and q are normalised quantities which are explained in equations (4.12) and (4.4) in the subsequent text.

(i) The shunt diode

The diode in the shunt connection will now be considered in detail so that equation (4.3) can be fully explained.

The characteristics for the diode are shown in Figure 4.1 where,

C_i = incremental capacitance

Q_d = total charge on p-side of junction

Q_i = injected charge

V_a = applied voltage

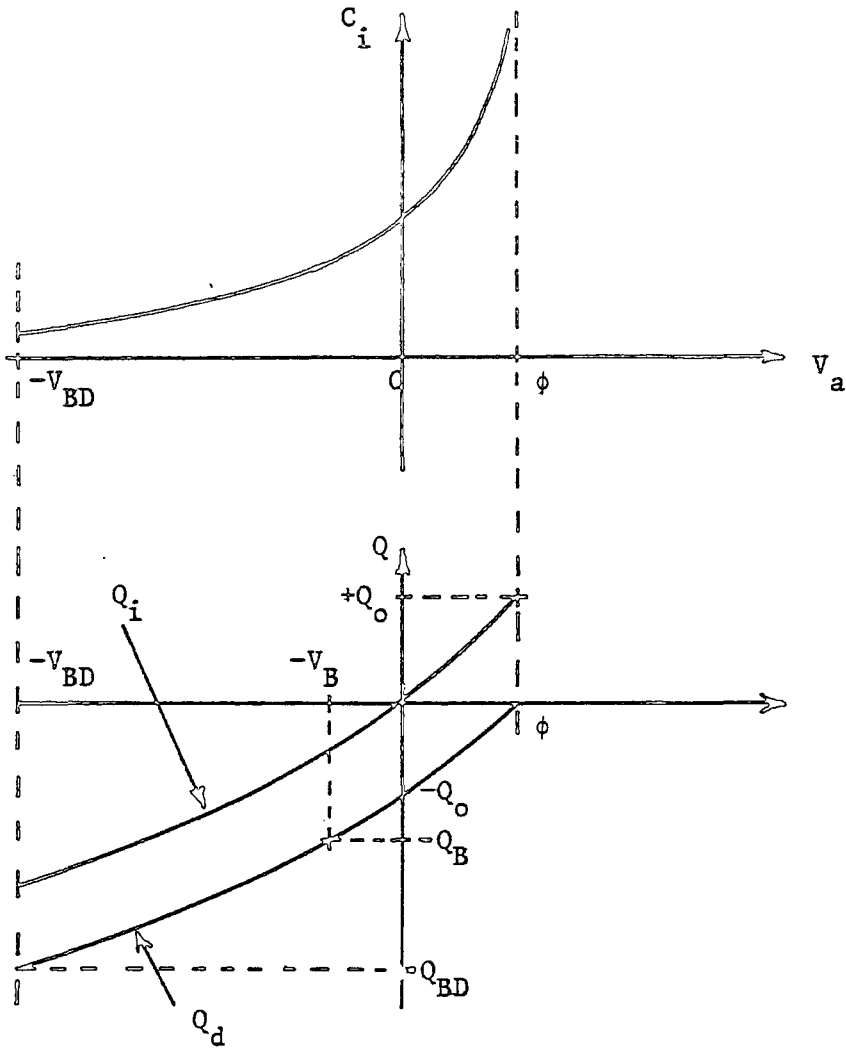


Figure 4.1
C-V and Q-V Characteristics

With reference to Figure 4.1 the diode will be used at a bias of $-V_B$ such that the value of $Q_B = \frac{1}{2} Q_{BD}$; this will enable the charge to be varied between $-Q_{BD}$ and zero. The diode will be tested by varying the charge Q_d by $\hat{Q}_{10} \cos \omega t$ about the bias value $-Q_B$ and \hat{Q}_{10} will be $Q_B = \frac{1}{2} Q_{BD}$. A normalised variable may be defined as the fractional variation in charge, i.e.

$$q = \frac{Q_d - (-Q_B)}{\hat{Q}_{10}} \quad (4.4)$$

where

$$-1 \leq q \leq +1 \quad (4.5)$$

Consequently the value of q in the test can be written as

$$q_0 = \frac{\hat{Q}_{10} \cos \omega t}{\hat{Q}_{10}} = \cos \omega t = \cos \theta \quad (4.6)$$

To apply the cosinusoidal drive to the charge, the diode must be supplied with a sinusoidal current; an expression for this is obtained by differentiating Q_d with respect to time, i.e.

$$\begin{aligned} i_0 &= \frac{d}{dt} (Q_d) = \frac{d}{dt} (q\hat{Q}_{10} + Q_B) \\ &= -\omega\hat{Q}_{10} \sin \omega t \end{aligned} \quad (4.7)$$

When the diode is tested with the cosinusoidal drive of equation (4.6), a spectrum of voltages will be generated which will contain only cosine terms as shown in equation (4.8). The test circuit is shown in Figure 4.2; in practice this test may prove difficult to do as a very high impedance instrument would be needed to find the voltage spectrum.

$$V_0 = V_{00} + \hat{V}_{10} \cos \omega t + \hat{V}_{20} \cos 2\omega t + \hat{V}_{30} \cos 3\omega t + \dots \text{etc} \quad (4.8)$$

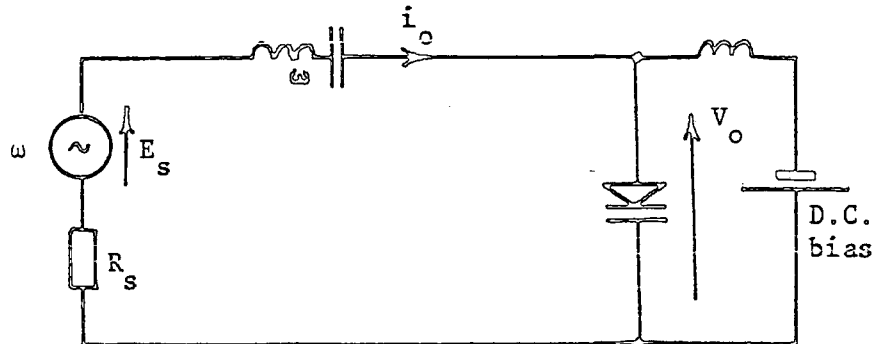


Figure 4.2
Theoretical Test Circuit

The variation of charge can be measured from the bias point and the voltage about the bias point $-V_B$; in effect the Q_d, V_a curve is then translated so that $(-Q_B, -V_B)$ is now the origin, and the new variables are Q and V .

The amplitudes of the components of the spectrum in equation (4.8) can now be used as the coefficients in the characteristic of the diode as expressed by

$$V = V_{00} + \sum_{n=1}^{\infty} \hat{V}_{no} T_n(q) \quad (4.9)$$

where V = voltage deviation from bias value

q = normalised charge deviation given by equation (4.4).

and $T_n(q)$ is the Chebyshev Polynomial of order n .

The justification for writing equation (4.9) is given in Appendix 4(i).

When the diode is used in a shunt multiplier circuit it is driven by the sum of two current components, one of the input frequency and the other of the required output frequency as shown in Figure 4.3. The spectrum of voltages produced is thus different from that produced under no-load conditions. The objective of the analysis is to find the spectrum of voltages produced in the multiplier in terms of the spectrum produced under no-load conditions.

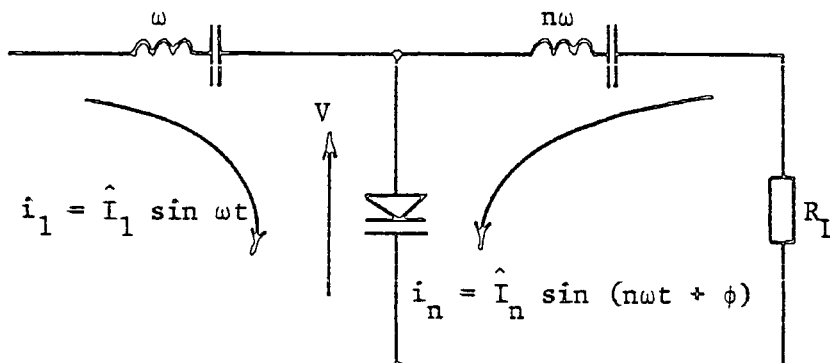


Figure 4.3
Shunt-connected multiplier circuit

The charge variation on the diode in the multiplier circuit is permitted to have two sinusoidal components of input and output frequencies but the total variation must not exceed the variation caused under no-load conditions: for this reason the fundamental frequency charge amplitude is assumed to be $a\hat{Q}_{10}$ where 'a' is a constant which is less than unity and the nth harmonic charge amplitude is $b\hat{Q}_{10}$ where 'b' is a constant also less than unity. This composite charge variation is substituted into equation (4.3) in order to determine the required voltage spectrum. This method of analysis is used in the later sections dealing with shunt multiplier circuits.

(ii) The series diode

In this case the diode must be biased to the mid-point of its total voltage swing which is $(\phi + V_{BD})$ as shown in Figure 4.1, giving finally

$$-V_B = \frac{-V_{BD} + \phi}{2} \quad (4.10)$$

The diode will be tested by varying the voltage V_a about the bias value $-V_B$ by $\hat{V}_{10} \cos \omega t$

$$\hat{V}_{10} = \frac{V_{BD} + \phi}{2} \quad (4.11)$$

A normalised variable v may be defined as the fractional variation in voltage relative to \hat{V}_{10} , i.e.

$$v = \frac{V_a - (-V_B)}{\hat{V}_{10}} \quad (4.12)$$

where

$$-1 \leq v \leq +1 \quad (4.13)$$

The diode will be tested by applying a cosinusoidal voltage and under no-load conditions the normalised test voltage is

$$v_o = 1 \cos \omega t = \cos \theta \quad (4.14)$$

The test circuit is shown in Figure 4.4 and the spectrum of charge which is generated is given by equation (4.15).

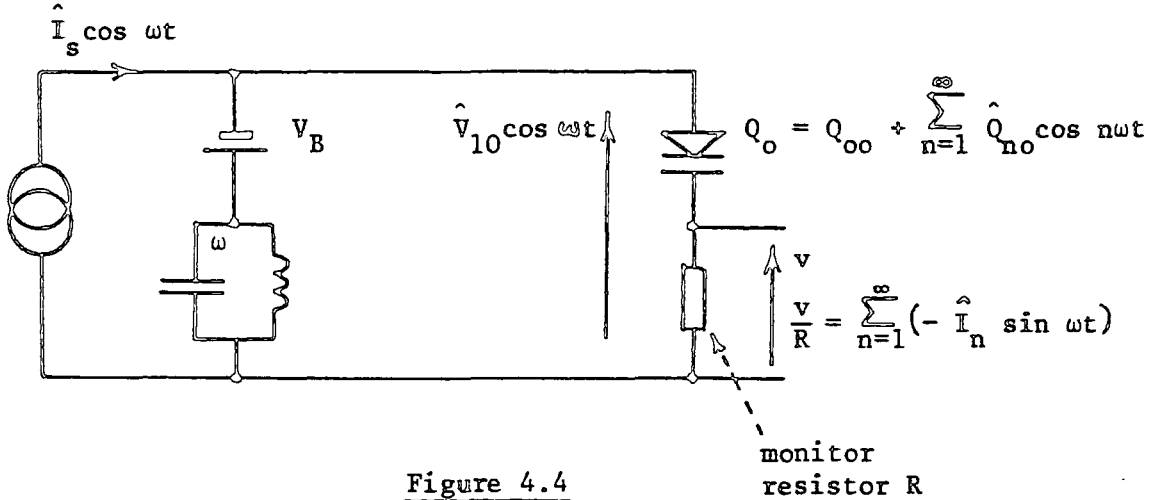


Figure 4.4
No-load Test Circuit

$$Q_o = Q_{00} + \sum_{n=1}^{\infty} \hat{Q}_{no} \cos n\omega t \quad (4.15)$$

It is assumed that variations in voltage and charge occur about the bias point which is the "new origin" for the non-linear Q/V relationship. The test spectrum amplitudes given in equation (4.15) can be used as coefficients in the Chebyshev expansion which represents the diode characteristic as in equation (4.2) which is repeated

$$Q = Q_{00} + \sum_{n=1}^{\infty} \hat{Q}_{no} T_n(v) \quad (4.16)$$

where Q = charge deviation from bias value

and v = normalised voltage deviation from bias voltage.

The justification for writing equation (4.16) is given in Appendix 4(i).

When the diode is used in a series multiplier circuit as shown in Figure 4,5 the voltage variation across the diode consists of two components, one at input frequency and the other at output frequency.

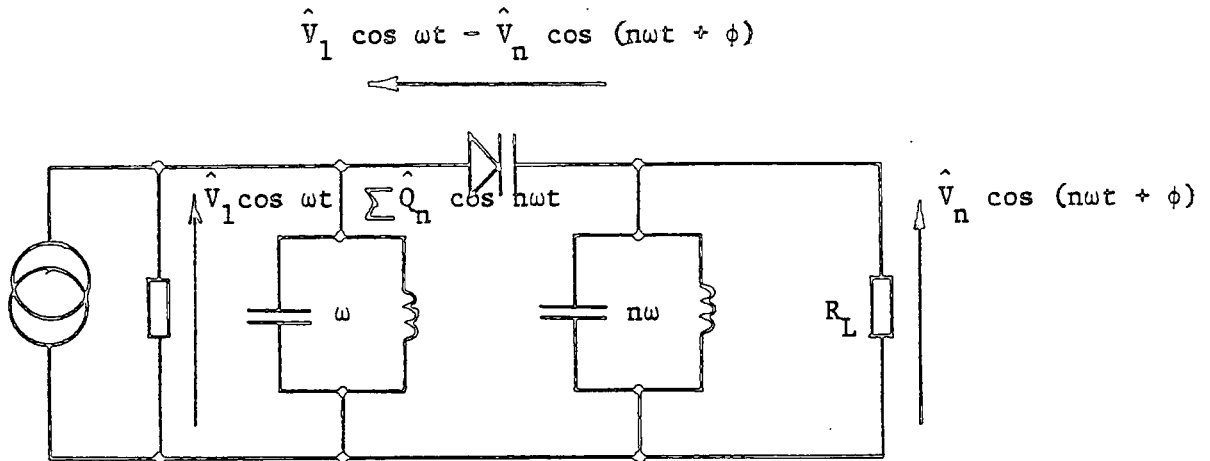


Figure 4.5
Series-connected Multiplier Circuit

The voltage variation must not exceed the variation used in finding the test spectrum and for this reason the drive must be reduced to $a\hat{V}_{10} \cos \omega t$ where 'a' is a constant which is less than 1. The composite voltage variation is substituted into equation (4.16) so that the required charge spectrum is obtained. This method of analysis would be used to deal with series multiplier circuits.

4.3 Shunt-Diode Doubler Analysis

4.3.1 Two-term approximation to the diode characteristic

In this approximate analysis the voltage spectrum obtained for the diode under test assumes that harmonics of higher order than the second are negligible. Thus the test spectrum in this case is,

$$V_0 = V_{00} + \hat{V}_{10} \cos \omega t + \hat{V}_{20} \cos 2\omega t \quad (4.17)$$

and the diode characteristic can be expressed as

$$V = V_{00} + \hat{V}_{10} T_1(q) + \hat{V}_{20} T_2(q) \quad (4.18)$$

The normalised charge variation used in the test is cosinusoidal,

i.e.

$$q = \frac{q_0}{\hat{Q}_{10}} = \frac{\hat{Q}_{10} \cos \omega t}{\hat{Q}_{10}} = \cos \omega t \quad (4.19)$$

When the diode is used in the shunt-connected doubler circuit the charge variation is due to the flow of the two currents shown in the diagram of Figure 4.6. These currents and the current in the diode are given in the equations below.

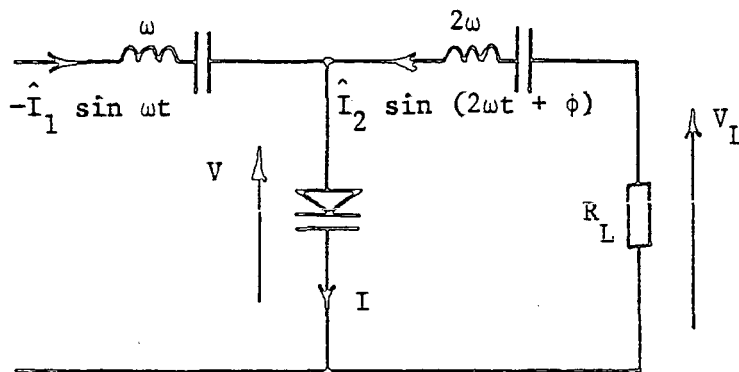


Figure 4.6
Shunt diode doubler

$$q = a \cos \omega t - b \cos (2\omega t + \phi) \quad (4.20)$$

$$I = -a\omega\hat{Q}_{10} \sin \omega t + b2\omega\hat{Q}_{10} \sin (2\omega t + \phi) \quad (4.21)$$

As stated in Section 4.2, the charge variation must not exceed that used in the test so that the following approximate conditions should hold:-

$$-1 \leq a \leq +1$$

$$-1 \leq b \leq +1 \quad (4.22)$$

$$-1 \leq a+b \leq +1$$

The voltage spectrum generated in the diode can be found by substituting (4.20) into (4.18) resulting in

$$\begin{aligned} V = V_{00} + \hat{V}_{10} T_1 \{a \cos \omega t - b \cos (2\omega t + \phi)\} \\ + \hat{V}_{20} T_2 \{a \cos \omega t - b \cos (2\omega t + \phi)\} \end{aligned} \quad (4.23)$$

Substituting for T_1 and T_2 yields

$$\begin{aligned} V = V_{00} - \hat{V}_{20} + a^2 \hat{V}_{20} + b^2 \hat{V}_{20} \\ + \hat{V}_{10} a \cos \omega t - \hat{V}_{20} 2ab \cos (\omega t + \phi) \\ - \hat{V}_{10} b \cos (2\omega t + \phi) + \hat{V}_{20} a^2 \cos 2\omega t \\ - \hat{V}_{20} 2ab \cos (3\omega t + \phi) \\ + \hat{V}_{20} b^2 \cos (4\omega t + 2\phi) \end{aligned} \quad (4.24)$$

Now consider the fundamental and second harmonic components of the voltage across the diode with " $-\sin \omega t$ " and " $-\sin 2\omega t$ " taken as the reference phasors.

Then

$$V = \hat{V}_1 + \hat{V}_2$$

where

$$\hat{V}_1 = -ja\hat{V}_{10} + j2ab\hat{V}_{20} \angle \phi \quad (4.25)$$

and

$$\hat{V}_2 = +jb\hat{V}_{10} \angle \phi - ja^2\hat{V}_{20} \quad (4.26)$$

The currents may be written in similar form as,

$$\hat{I}_1 = a\omega\hat{Q}_{10} \quad (4.27)$$

$$\hat{I}_2 = -2b\omega\hat{Q}_{10} \angle \phi \quad (4.28)$$

The peak value phasor for the voltage across the load resistor is

$$V_L = 2b\omega\hat{Q}_{10} R_L \angle \phi \quad (4.29)$$

The output equivalent circuit

The output circuit may be represented by an equivalent circuit as in Figure 4.7.

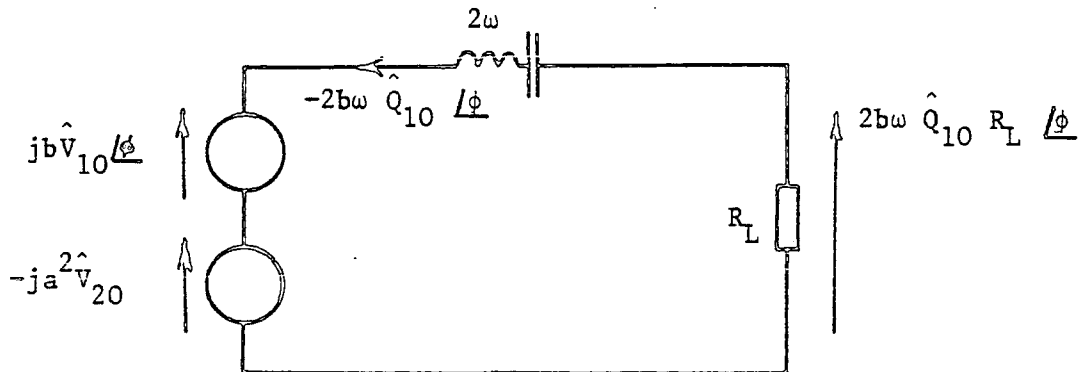


Figure 4.7

One of the voltages in the "diode circuit" is in quadrature with the current and may be replaced in Figure 4.7 by a capacitor which represents the output capacitance of the diode. This capacitance C_o is shown in Figure 4.8 and because it would de-tune the second harmonic filter it must be 'balanced' by the inclusion of an inductive reactance shown as X_L .

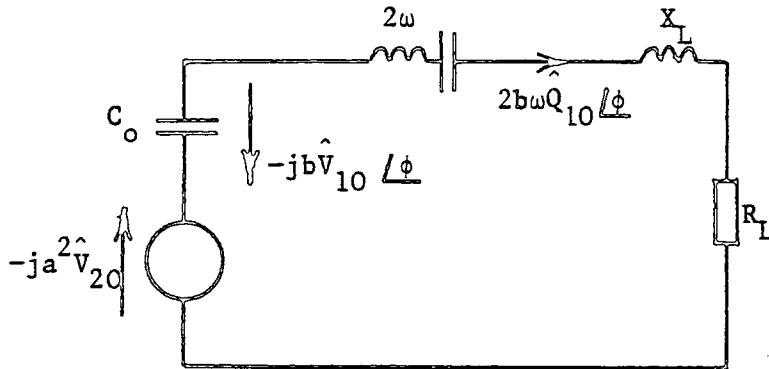


Figure 4.8

It can be deduced that the current must be in phase with the emf generated by the diode and the value of ϕ must be -90° .

The value of C_o is given by,

$$jb\hat{V}_{10} \angle \phi = (-2b\omega\hat{Q}_{10} \angle -90^\circ) \left(-j \frac{1}{2\omega C_o}\right)$$

from which

$$C_o = \frac{\hat{Q}_{10}}{\hat{V}_{10}} \tag{4.30}$$

The inductive reactance X_L required to maintain the tuning of the filter in the output circuit is shown to be

$$X_L = \frac{1}{2\omega C_o} = \frac{\hat{V}_{10}}{2\omega\hat{Q}_{10}} \tag{4.31}$$

The final output equivalent circuit is shown in Figure 4.9.

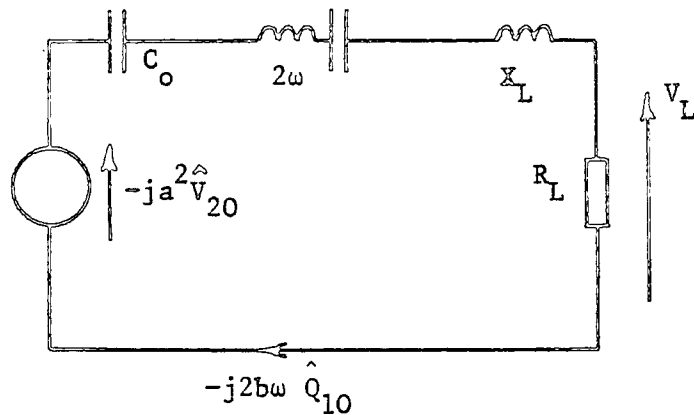


Figure 4.9

Then, equating emf to current times load resistance, gives

$$-ja^2 \hat{V}_{20} = -j2b\omega \hat{Q}_{10} R_L$$

and finally

$$\frac{a^2}{b} = \frac{2\omega \hat{Q}_{10} R_L}{\hat{V}_{20}} = \frac{2\hat{I}_{10} R_L}{\hat{V}_{20}} \quad (4.32)$$

Equation (4.32) is an important relationship between a and b and R_L .

The input equivalent circuit

The input equivalent circuit may be derived by considering equations (4.25) and (4.27) and using the value for ϕ which has been recently determined.

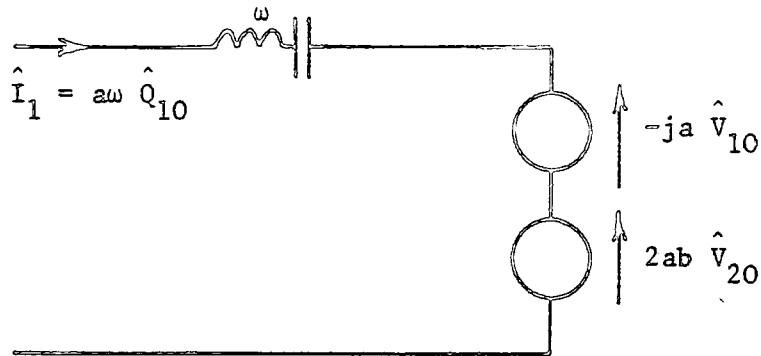


Figure 4.10
Input Equivalent Circuit

One of these voltage components lags by 90° on the input current and this is due to the input capacitance C_{IN} . The other component represents the resistance reflected into the input circuit due to the dissipation of load power. The source impedance must be assumed to have an inductive component X_1 so that the input filter is not de-tuned. The input equivalent circuit has the final version as shown in Figure 4.11

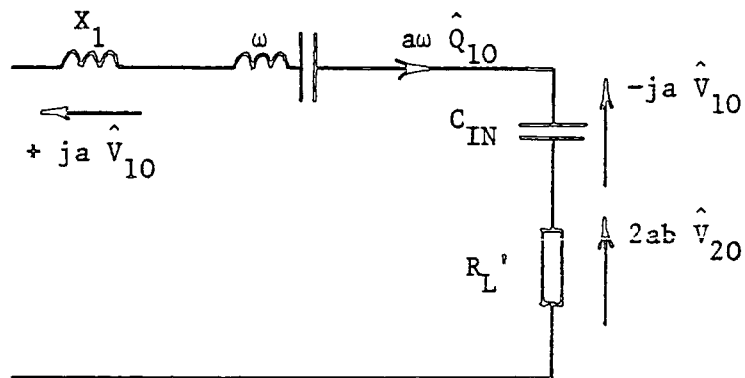


Figure 4.11
Input Equivalent Circuit-final version

The input capacitance and reflected resistance are given below.

$$-ja\hat{V}_{10} = a\omega\hat{Q}_{10} \left(-j \frac{1}{\omega C_{IN}}\right)$$

$$\therefore C_{IN} = \frac{\hat{Q}_{10}}{\hat{V}_{10}} \quad (4.33)$$

$$R_L' = \frac{2ab\hat{V}_{20}}{a\omega\hat{Q}_{10}} = \frac{2b\hat{V}_{20}}{\hat{I}_{10}} \quad (4.34)$$

Substituting from (4.32) into (4.34) results in

$$R_L' = 2b \frac{2bR_L}{a^2} = \frac{4b^2R_L}{a^2} \quad (4.35)$$

The power relationships

The power in the output circuit may be written, using the diagram of Figure 4.9, as

$$P_L = \left[\frac{a^2\hat{V}_{20}}{\sqrt{2}} \right]^2 \frac{1}{R_L} = \frac{a^4\hat{V}_{20}^2}{2R_L} \quad (4.36)$$

or

$$P_L = \left(\frac{a^2\hat{V}_{20}}{\sqrt{2}} \right) \left(\frac{2b\omega\hat{Q}_{10}}{\sqrt{2}} \right) = \omega a^2 b \hat{Q}_{10} \hat{V}_{20} \quad (4.37)$$

or

$$P_L = \left[\frac{2b\omega\hat{Q}_{10}}{\sqrt{2}} \right]^2 R_L = 2b^2\omega^2\hat{Q}_{10}^2 R_L \quad (4.38)$$

The power in the input circuit can be expressed in terms of the reflected load R_L' and as the diode is assumed loss-free the formulae derived in this way should be identical with those given in (4.36), (4.37) and (4.38): this is shown below

$$P_{IN} = \left[\frac{a\omega\hat{Q}_{10}}{\sqrt{2}} \right]^2 R_L' = \frac{a^2\omega^2\hat{Q}_{10}^2}{2} \frac{4b^2R_L}{a^2} = 2b^2\omega^2\hat{Q}_{10}^2 R_L \quad (4.39)$$

$$P_{IN} = \left(\frac{a\omega\hat{Q}_{10}}{\sqrt{2}} \right) \left(\frac{2ab\hat{V}_{20}}{\sqrt{2}} \right) = a^2 b \omega \hat{Q}_{10} \hat{V}_{20} \quad (4.40)$$

and

$$P_{IN} = \left[\frac{2ab\hat{V}_{20}}{\sqrt{2}} \right]^2 \frac{1}{R_L'} = 2a^2 b^2 \hat{V}_{20}^2 \frac{a^2}{4b^2 R_L} = \frac{a^4 \hat{V}_{20}^2}{2R_L} \quad (4.41)$$

Variations of 'a' and 'b' with R_L , R_S and E_S

It is important to be able to find values for 'a' and 'b' when the signal source is applied to the multiplier circuit.

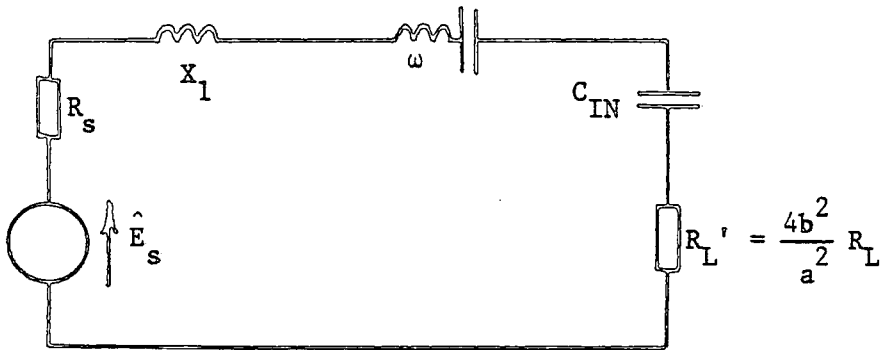


Figure 4.12

Consider the circuit of Figure 4.12.

The input current for the doubler will be,

$$\hat{I}_1 = \frac{\hat{E}_S}{R_S + R_L'} = a\omega\hat{Q}_{10} \quad (4.42)$$

Substituting from (4.35) for R_L' ,

$$\hat{E}_S = a\omega\hat{Q}_{10} \left(R_S + \frac{4b^2 R_L}{a^2} \right) \quad (4.43)$$

A further relationship exists between 'a' and 'b' namely (4.32),

repeated below,

$$b = \frac{a^2 \hat{V}_{20}}{2\omega\hat{Q}_{10} R_L} \quad (4.44)$$

If 'b' is eliminated from the equations (4.43) and (4.44) taken simultaneously, equation (4.45) is obtained.

$$\hat{E}_S = a\omega\hat{Q}_{10} R_S + \frac{4R_L \omega\hat{Q}_{10}}{a} \left(\frac{a^2 \hat{V}_{20}}{2\omega\hat{Q}_{10} R_L} \right)^2 \quad (4.45)$$

This cubic equation in 'a' can be put in the form,

$$a^3 = - \left\{ \frac{\omega^2 \hat{Q}_{10}^2 R_S R_L}{\hat{V}_{20}^2} \right\} a + \left\{ \frac{\hat{E}_S R_L \omega\hat{Q}_{10}}{\hat{V}_{20}^2} \right\} \quad (4.46)$$

A graphical solution may be obtained for 'a' as the intersection of graphs of the functions $F_1(a)$ and $F_2(a)$ shown in Figure 4.13.

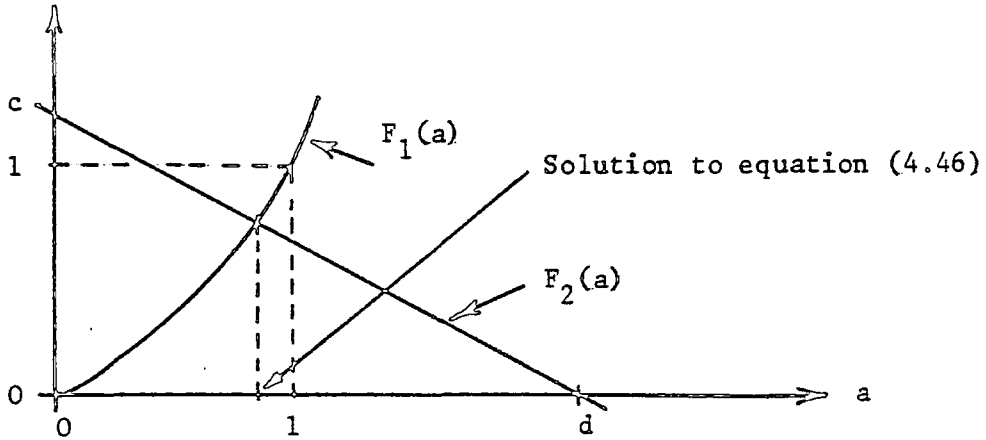


Figure 4.13

where

$$F_1(a) = a^3 \quad (4.47)$$

and

$$F_2(a) = - \left\{ \frac{\omega^2 \hat{Q}_{10}^2 R_S R_L}{\hat{V}_{20}^2} \right\} a + \left\{ \frac{\hat{E}_S R_L \omega\hat{Q}_{10}}{\hat{V}_{20}^2} \right\} \quad (4.48)$$

Noting that,

$$\omega\hat{Q}_{10} = \hat{I}_{10} \quad (4.49)$$

The intercepts 'c' and 'd' in Figure 4.13 are

$$c = \frac{\hat{E}_S \hat{I}_{10} R_L}{\hat{V}_{20}^2} \quad (4.50)$$

$$d = \frac{\hat{E}_S}{\hat{I}_{10} R_S} \quad (4.51)$$

Values of 'a' and 'b' required to give maximum P_L

An expression for 'normalised' power can be derived from (4.37)

as

$$P_N = \frac{P_L}{\hat{I}_{10} \hat{V}_{20}} = a^2 b \quad (4.52)$$

Obviously the load power increases as both 'a' and 'b' increase and these are always related through equation (4.44). However, the restriction given in equation (4.22) must apply even when P_N is a maximum. Thus, for maximum swing on the characteristic, $a + b = 1$ may be substituted into (4.52) giving

$$P_N(\text{with max. signals}) = a^2 (1 - a) \quad (4.53)$$

Equation (4.53) is plotted on Figure 4.18 (page number 102) and is found to have the following maximum value

$$P_N(\text{max}) = 0.148 \quad (4.54)$$

and this occurs when

$$\left. \begin{array}{l} a = 0.667 \\ b = 0.333 \end{array} \right\} \quad (4.55)$$

Then,

$$\left. \begin{array}{l} P_L(\text{max}) = 0.148 \hat{I}_{10} \hat{V}_{20} \\ \text{or} = 0.148 \omega \hat{Q}_{10} \hat{V}_{20} \end{array} \right\} \quad (4.56)$$

Values of drive and load required for maximum power

The intercepts 'c' and 'd' on Figure 4.13 depend upon R_L , R_S and E_S . If any of these quantities change then either c or d changes or perhaps both c and d change. However, for maximum power $a = 0.667$ and $a^3 = .3$ (approx) and by considering the graph of $F_2(a)$, the ratio

$$\frac{d}{c} = \frac{d - 0.667}{0.3} \quad (4.57)$$

By substituting (4.50) and (4.51) into (4.57) the following relationship is obtained between the drive conditions and the load for maximum power,

$$\frac{\hat{E}_S R_L}{R_{20} \hat{I}_{10}^2} - 0.667 \frac{R_L R_S}{R_{20}^2} - 0.3 = 0 \quad (4.58)$$

where

$$R_{20} = \frac{\hat{V}_{20}}{\hat{I}_{10}} \quad (4.59)$$

Summary

- (a) The maximum second harmonic power which can be extracted from the shunt diode doubler circuit is given by equation (4.56).
- (b) The maximum power is extracted when E_S , R_S and R_L obey the relationship given in result (4.58).
- (c) Only certain values of E_S , R_S and R_L are permitted for this analysis to be valid. They must produce a value of 'a' in the graphical solution of Figure 4.13 which does not exceed unity and which gives a value of 'b' from equation (4.44) such that the restrictions of equation (4.22) are maintained.

(d) The input capacitance of the diode is given by equation (4.33). This suggests that the input capacitance presented by the diode is independent of the magnitude of the drive and the load but this is modified when a third harmonic voltage is assumed to be generated by the diode.

(e) The output capacitance of the diode is given by equation (4.30) and is the same result as for the input capacitance, namely,

$$C_o = \frac{\hat{Q}_{10}}{\hat{V}_{10}} = C_{IN}$$

This formula is modified when a third harmonic voltage is assumed to be generated by the diode.

4.3.2 Three-term approximation to the diode characteristic

This analysis is similar to that carried out in Section 4.3.1 but in this case the third harmonic of the test spectrum will be taken into account.

The test spectrum is

$$V_o = V_{00} + \hat{V}_{10} \cos \omega t + \hat{V}_{20} \cos 2\omega t + \hat{V}_{30} \cos 3\omega t \quad (4.60)$$

and the diode characteristic can be expressed as

$$V = V_{00} + \hat{V}_{10} T_1(q) + \hat{V}_{20} T_2(q) + \hat{V}_{30} T_3(q) \quad (4.61)$$

The normalised charge variation in the test is cosinusoidal, i.e.

$$q = \frac{\hat{Q}_{10} \cos \omega t}{\hat{Q}_{10}} = \cos \omega t \quad (4.62)$$

The doubler circuit is shown in Figure 4.6, and the charge on the diode has a second harmonic component as shown in

$$q = a \cos \omega t - b \cos (2\omega t + \phi) \quad (4.63)$$

The current into the diode is therefore as shown in Figure 4.6 and is

$$I = - a\omega\hat{Q}_{10} \sin \omega t + b2\omega\hat{Q}_{10} \sin (2\omega t + \phi) \quad (4.64)$$

The analysis will differ from the previous because more terms will be generated in the voltage, i.e.

$$\begin{aligned} V = V_{00} + \hat{V}_{10}T_1 \{a \cos \omega t - b \cos (2\omega t + \phi)\} \\ + \hat{V}_{20}T_2 \{a \cos \omega t - b \cos (2\omega t + \phi)\} \\ + \hat{V}_{30}T_3 \{a \cos \omega t - b \cos (2\omega t + \phi)\} \end{aligned} \quad (4.65)$$

which should be compared with equation (4.23).

Equation (4.65) can be expanded, as shown in Appendix 4(iii), resulting in

$$\begin{aligned} V = V_{00} - \hat{V}_{20} + a^2\hat{V}_{20} + b^2\hat{V}_{20} - \hat{V}_{30}3a^2b \cos \phi \\ + \hat{V}_{10}a \cos \omega t - \hat{V}_{20}2ab \cos (\omega t + \phi) + \hat{V}_{30}3a^3 \cos \omega t \\ - \hat{V}_{30}3a \cos \omega t - \hat{V}_{30}6ab^2 \cos \omega t \\ - \hat{V}_{10}b \cos (2\omega t + \phi) + \hat{V}_{20}a^2 \cos 2\omega t + \hat{V}_{30}3b \cos (2\omega t + \phi) \\ - \hat{V}_{30}6a^2b \cos (2\omega t + \phi) - \hat{V}_{30}3b^3 \cos (2\omega t + \phi) \\ - \hat{V}_{20}2ab \cos (3\omega t + \phi) + \hat{V}_{30}a^3 \cos 3\omega t + \hat{V}_{30}3ab^2 \cos (3\omega t + 2\phi) \\ + \hat{V}_{20}b^2 \cos (4\omega t + 2\phi) - \hat{V}_{30}3a^2b \cos (4\omega t + \phi) \\ + \hat{V}_{30}3ab^2 \cos (5\omega t + 2\phi) \\ - \hat{V}_{30}b^3 \cos (6\omega t + 3\phi) \end{aligned} \quad (4.66)$$

The terms at fundamental frequency and second harmonic frequency shown in equations (4.25) and (4.26) are thus modified to include terms dependent upon \hat{V}_{30} , i.e.

$$\hat{V}_1 = -ja\hat{V}_{10} + j2ab\hat{V}_{20} \underline{\phi} - j3a^3\hat{V}_{30} - j6ab^2\hat{V}_{30} + j3a\hat{V}_{30} \quad (4.67)$$

$$\hat{V}_2 = +jb\hat{V}_{10} \underline{\phi} - ja^2\hat{V}_{20} + j6a^2b\hat{V}_{30} \underline{\phi} + j3b^3\hat{V}_{30} \underline{\phi} - j3b\hat{V}_{30} \underline{\phi} \quad (4.68)$$

The fundamental and second harmonic currents are as in Figure 4.6 and are given by equations (4.27) and (4.28). The output equivalent circuit is thus modified due to the three extra terms in (4.68).

The output equivalent circuit

The output equivalent circuit of Figure 4.7 is modified to satisfy equation (4.68) and is shown in Figure 4.14.

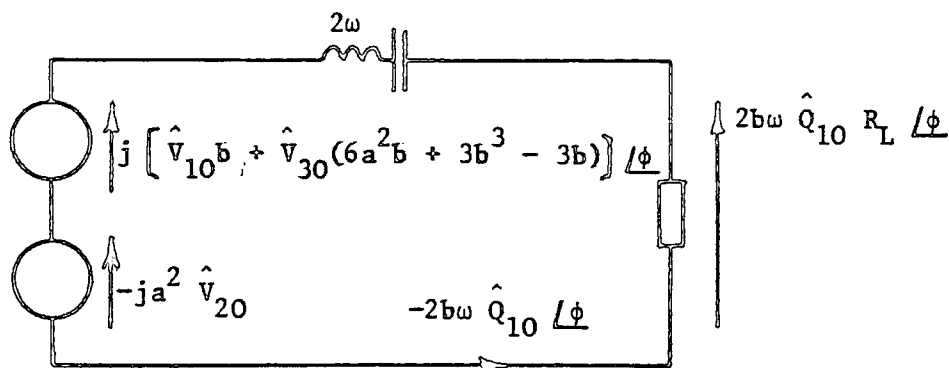


Figure 4.14

The value of C_o given previously by result (4.30) must now change because the voltage across it has been modified. A formula for C_o can be obtained by equating voltage to current times reactance

$$j(\hat{V}_{10}b + \hat{V}_{30}\{6a^2b + 3b^3 - 3b\})\underline{\phi} = (-2b \hat{Q}_{10} \underline{\phi}) \left(-j \frac{1}{2\omega C_o}\right)$$

hence,

$$C_o = \frac{\hat{Q}_{10}}{\hat{V}_{10} + \hat{V}_{30} (6a^2 + 3b^2 - 3)} \quad (4.69)$$

The relationship between 'a' and 'b' given in result (4.32) is not affected by the "third harmonic terms" in (4.68).

The input equivalent circuit

The circuit of Figure 4.10 which was derived in the previous analysis must be modified due to the extra terms in result (4.67). Thus Figure 4.10 could be redrawn as in Figure 4.15, the angle ϕ taking the value -90° as in the previous case.

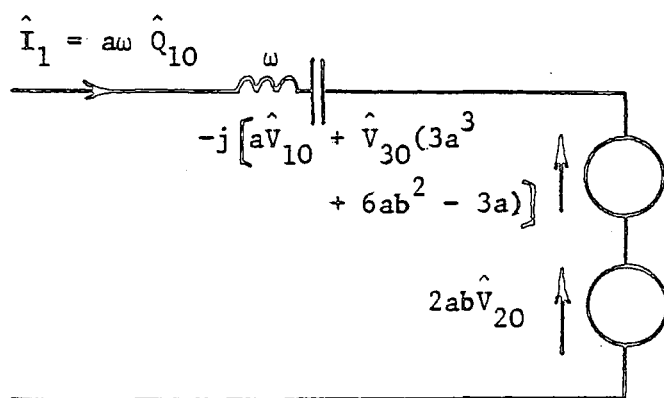


Figure 4.15

The terms in \hat{V}_{30} in result (4.67) do not affect the reflected resistance R_L' and results (4.34) and (4.35) are unchanged. The input capacitance C_{IN} is modified, i.e.

$$-j \{a\hat{V}_{10} + \hat{V}_{30} (3a^3 + 6ab^2 - 3a)\} = a\omega\hat{Q}_{10} \left(-j\frac{1}{\omega C_{IN}}\right)$$

hence

$$C_{IN} = \frac{\hat{Q}_{10}}{\hat{V}_{10} + \hat{V}_{30} (3a^2 + 6b^2 - 3)} \quad (4.70)$$

From this point the analysis is no different from that in section 4.3.1. The power relationships of equations (4.36) to (4.41) again apply and the values of 'a' and 'b' are also unchanged.

Summary

- (a) The third order term in the characteristic does not make any difference to the output power generated at this 2nd harmonic or to the required values of R_S , R_L and E_S for any required output power.
- (b) The only effects are on the input and output capacitances of the diode. These are given by equations (4.69) and (4.70) which are repeated below:-

$$(4.69) \quad C_o = \frac{\hat{Q}_{10}}{\hat{V}_{10} + \hat{V}_{30} (6a^2 + 3b^2 - 3)}$$

$$(4.70) \quad C_{IN} = \frac{\hat{Q}_{10}}{\hat{V}_{10} + \hat{V}_{30} (3a^2 + 6b^2 - 3)}$$

4.3.3 Four-term approximation to the diode characteristic

The analysis for this case is shown in Appendix 4(v) and it leads to the following results.

The output equivalent circuit

The equivalent circuits of Figures 4.7 and 4.14 will need to be modified to that shown in Figure 4.16.

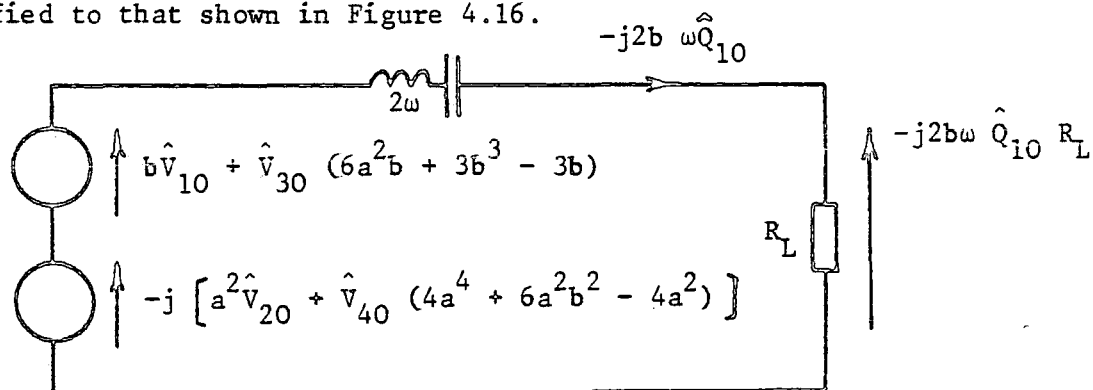


Figure 4.16

The output capacitance, C_o , will be as predicted in Figure 4.14 and given by equations (4.69).

However, the relationship between 'a' and 'b' developed in equation (4.32) will be modified, as,

$$-j \{ a^2 \hat{V}_{20} + \hat{V}_{40} (4a^4 + 6a^2b^2 - 4a^2) \} = -j 2b\omega \hat{Q}_{10} R_L$$

$$\therefore R_L = \frac{a^2 \hat{V}_{20} + \hat{V}_{40} (4a^4 + 6a^2b^2 - 4a^2)}{2b\omega \hat{Q}_{10}} \quad (4.71)$$

The input equivalent circuit

The equivalent circuits of Figures 4.10 and 4.15 require modification due to extra terms appearing in the voltage generators; Figure 4.17 shows all the terms at frequency ω from equation (8) in Appendix 4(v).

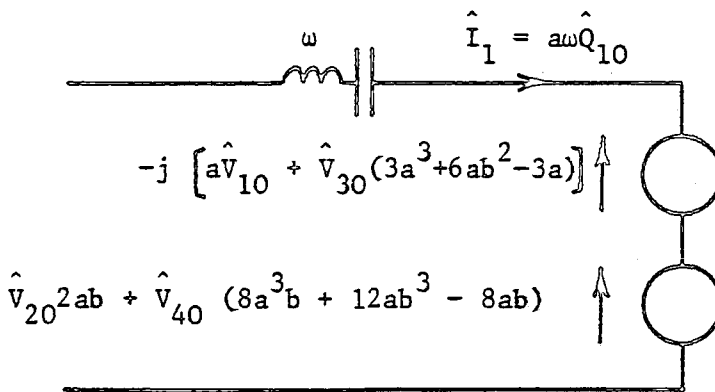


Figure 4.17

The input capacitance will be as given in (4.70) as it is not dependent upon \hat{V}_{40} . However, the reflected resistance R_L' will be modified from the value given in (4.34).

$$R_L' = \frac{\hat{V}_{20} 2ab + \hat{V}_{40} \{8a^3b + 12ab^3 - 8ab\}}{a\omega\hat{Q}_{10}} \quad (4.72)$$

If equation (4.72) is divided by equation (4.71) then,

$$\frac{R_L'}{R_L} = \frac{2ab[\hat{V}_{20} + \hat{V}_{40}(4a^2 + 6b^2 - 4)]}{a\omega\hat{Q}_{10}} \frac{2b\omega\hat{Q}_{10}}{a^2[\hat{V}_{20} + \hat{V}_{40}(4a^2 + 6b^2 - 4)]}$$

or

$$\frac{R_L'}{R_L} = \frac{4b^2}{a^2} \quad (4.73)$$

Hence (4.73) shows the expected relationship between R_L' and R_L .

The power relationships

The load power P_L will contain the extra terms in \hat{V}_{40} compared with (4.37),

$$P_L = \frac{1}{\sqrt{2}} \{a^2\hat{V}_{20} + \hat{V}_{40}(4a^4 + 6a^2b^2 - 4a^2)\} \frac{2b\omega\hat{Q}_{10}}{2}$$

or

$$P_L = \hat{V}_{20}\hat{I}_{10}a^2b + \hat{V}_{40}\hat{I}_{10}a^2b(4a^2 + 6b^2 - 4) \quad (4.74)$$

Variations of 'a' and 'b' with R_L , R_S and E_S

The equation (4.42) still applies to the analysis and if the substitution is made for R_L' from equation (4.73) then

$$E_S = a\omega\hat{Q}_{10}\left(R_S + \frac{4b^2}{a^2}R_L\right) \quad (4.75)$$

Now 'b' can be eliminated by taking (4.75) and (4.71) simultaneously to obtain an equation relating 'a', E_S , R_S and R_L which requires a numerical solution by computer.

Variation of P_L with 'a' and 'b'

As in section 4.3.1 it can be assumed that the following approximate relationship will hold if the charge variation is not to exceed the test condition,

$$a + b = 1$$



The equation (4.76) may be substituted into the load power equation (4.74) to obtain P_L as a function of "a",

$$P_L = \hat{V}_{20} \hat{I}_{10} a^2 (1 - a) + \hat{V}_{40} \hat{I}_{10} a^2 (1 - a) [4a^2 + 6(1 - a)^2 - 4] \quad (4.77)$$

Hence

$$P_L = \hat{V}_{20} \hat{I}_{10} F_3(a) + \hat{V}_{40} \hat{I}_{10} F_4(a) \quad (4.78)$$

where

$$F_3(a) = a^2 - a^3 \quad (4.79)$$

and

$$F_4(a) = -10a^5 + 22a^4 - 14a^3 + 2a^2 \quad (4.80)$$

The functions $F_3(a)$ and $F_4(a)$ are plotted on Figure 4.18. As the function $F_4(a)$ is negative in most of the range $0 \leq a \leq 1$ it is apparent that the load power is reduced by the fourth harmonic term in the diode spectrum. The value of $F_4(a)$ at $a = .667$ is -0.23 .

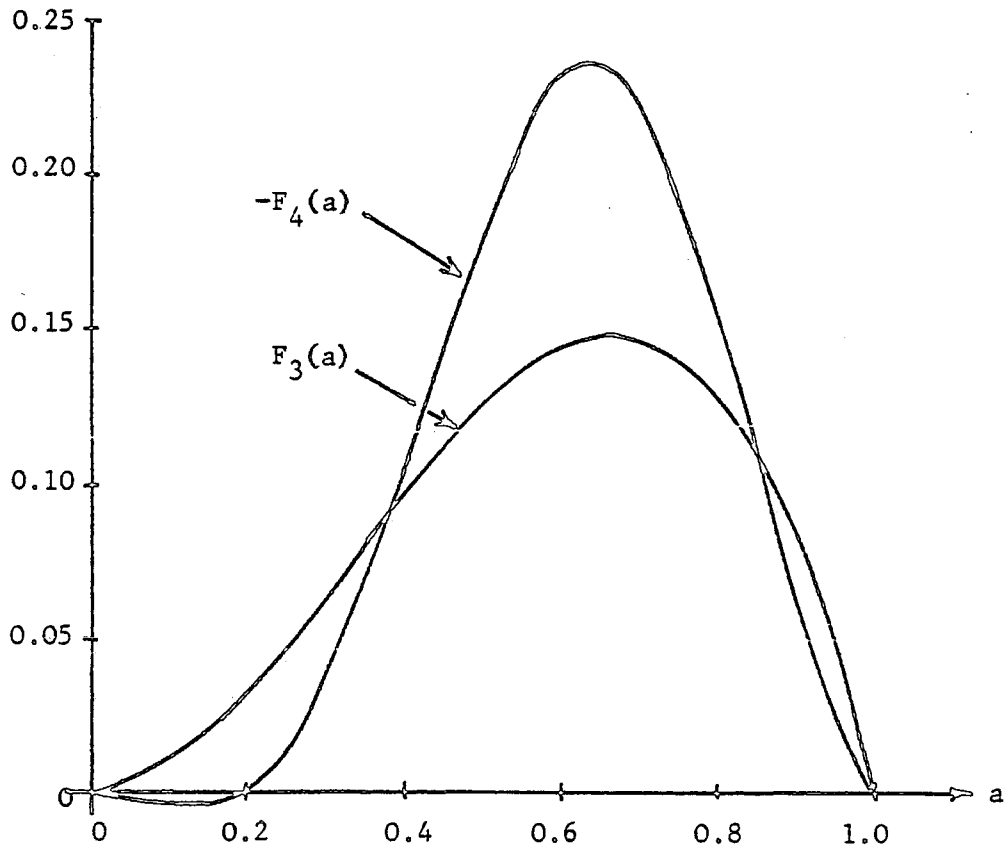


Figure 4.18
Graphs of $F_3(a)$ and $F_4(a)$

Summary

The inclusion of the fourth harmonic term in the diode test spectrum has the following effects:-

- (a) The load power is reduced as shown by result (4.76).
- (b) If E_S and R_S are adjusted so that $a = .667$ then the load power is given by,

$$P_L = 0.148 \hat{V}_{20} \hat{I}_{10} - 0.23 \hat{V}_{40} \hat{I}_{10} \quad (4.81)$$

- (c) The values of 'a' and 'b' may be found by the simultaneous solution of equations (4.71) and (4.75).

4.4 Conclusion

The analysis has produced some interesting results for the shunt-diode doubler which are summarised below:-

- (a) The reflected load resistance R_L' due to a load R_L on the output circuit is given by,

$$(4.73) \quad R_L' = \frac{4b^2}{a} R_L$$

The values of 'a' and 'b' depend upon the load and the drive, i.e. R_L , R_S and E_S . Approximate values for 'a' and 'b' can be found using the graphical solution in Figure 4.13 of the equation (4.46). A more accurate solution for 'a' and 'b' requires that equations (4.71) and (4.75), repeated below, be solved simultaneously,

$$(4.71) \quad 2b\hat{I}_{10}R_L = a^2\hat{V}_{20} + \hat{V}_{40}(4a^4 + 6a^2b^2 - 4a^2)$$

$$(4.75) \quad E_S = a\hat{I}_{10} \left(R_S + \frac{4b^2R_L}{a} \right)$$

- (b) There is a maximum value of power which can be extracted at second harmonic without over-driving the circuit. This occurs when the approximate values of 'a' and 'b' are 0.667 and 0.333 and the load power is then given by (4.81), repeated below,

$$(4.81) \quad P_L(\max) = 0.148 \hat{V}_{20}\hat{I}_{10} - 0.23 \hat{V}_{40}\hat{I}_{10}$$

- (c) The diode presents a capacitance C_{IN} to the input circuit at fundamental frequency which varies with load and drive, and therefore with 'a' and 'b'. If a third harmonic term is included in the diode spectrum C_{IN} varies with drive as expressed by equation (4.70) repeated below,

$$(4.70) \quad C_{IN} = \frac{\hat{Q}_{10}}{\hat{V}_{10} + \hat{V}_{30}(3a^2 + 6b^2 - 3)}$$

The no-load value of C_{IN} may be written as,

$$C_{IN} \text{ (no load)} = \frac{\hat{Q}_{10}}{\hat{V}_{10}} = C_{10} \quad (4.82)$$

As the output power is increased from zero the input capacitance increases and reaches a maximum value at maximum power of,

$$C_{IN} \text{ (max } P_L) = \frac{\hat{Q}_{10}}{\hat{V}_{10} - \hat{V}_{30}} \quad (4.83)$$

(d) The output capacitance of the diode C_o is given by,

$$(4.69) \quad C_o = \frac{\hat{Q}_{10}}{\hat{V}_{10} + \hat{V}_{30} (6a^2 + 3b^2 - 3)}$$

and this has a no-load value of,

$$C_o \text{ (no load)} = \frac{\hat{Q}_{10}}{\hat{V}_{10} + 3\hat{V}_{30}} \quad (4.84)$$

As the load on the multiplier circuit increases the value of C_o increases and at maximum output power it has the value C_{10} ,

$$C_o \text{ (max } P_L) = \frac{\hat{Q}_{10}}{\hat{V}_{10}} = C_{10} \quad (4.85)$$

(e) An expression can be derived for the output resistance of the circuit in terms of the multiplier circuit parameters 'a' and 'b' and the derivation is shown in Appendix 4(vi). The output resistance R_o shown to be,

$$R_o = \left\{ \frac{1 - a^2}{2b} \right\} \frac{\hat{V}_{20}}{\hat{I}_{10}} \quad (4.86)$$

and at maximum output power R_o is therefore

$$R_o \text{ (opt)} = \frac{5}{6} \frac{\hat{V}_{20}}{\hat{I}_{10}} \quad (4.87)$$

This value of the output resistance can be matched in the output circuit to the load resistance R_L by the use of an impedance-transforming technique, and the maximum possible output power is then obtained. The source should then be chosen to have values of E_s and R_s which produce the required values of 'a' and 'b' of $2/3$ and $1/3$ respectively. The source e.m.f. and internal resistance should satisfy the condition,

$$\hat{E}_s = \frac{2}{3} \hat{I}_{10} R_s + \frac{5}{9} \hat{V}_{20} \quad (4.88)$$

The effective source resistance could be reduced by transformation to as low a value as possible so that less power would be lost in the source.

CHAPTER 5ANALYSIS OF THE SHUNT-DIODE TRIPLER

| | <u>Page</u> |
|--|-------------|
| 5.1 Introduction | 108 |
| 5.2 Shunt Diode Tripler Without Idler | 109 |
| 5.2.1 Two-term approximation to the diode characteristic | 109 |
| 5.2.2 Three-term approximation to the diode characteristic | 111 |
| 5.2.3 Four-term approximation to the diode characteristic | 117 |
| 5.3 Shunt Diode Tripler With Idler | 118 |
| 5.3.1 Two-term approximation to the diode characteristic | 118 |
| 5.3.2 Three-term approximation to the diode characteristic | 121 |
| 5.3.3 Four-term approximation to the diode characteristic | 127 |
| 5.4 Conclusion | 129 |

5.1 Introduction

This chapter uses the method of analysis developed in Chapter 4 to predict the performance of varactor diode tripler circuits. The shunt-diode tripler without idler is analysed in section 5.2 and the tripler with idler is dealt with in section 5.3. The basic circuits are shown in Figures 5.1 and 5.4 respectively.

Each analysis is carried out initially for a diode having a test spectrum which contains only d.c., fundamental frequency and second harmonic frequency terms. Then the test spectrum is extended to third and fourth harmonic terms so that the effect of these terms can be evaluated.

In section 5.4 the results are tabulated with results for the shunt-diode doubler so that it is easy to compare the three circuits considered.

5.2 Shunt-Diode Tripler Without Idler

5.2.1 Two-term approximation to the diode characteristic

This analysis is similar to that followed in section 4.3.1 except that the charge variation in the diode will be permitted at fundamental frequency and third harmonic frequency only. The diode characteristic is

$$V = V_{00} + \hat{V}_{10} T_1(q) + \hat{V}_{20} T_2(q) \quad (5.1)$$

When the diode is used in the shunt-connected tripler circuit of Figure 5.1 the charge variation is

$$q = a \cos \omega t - b \cos (3 \omega t + \phi) \quad (5.2)$$

The diode current can be obtained by differentiating the actual charge; hence

$$I = -a\omega\hat{Q}_{10} \sin \omega t + b 3\omega\hat{Q}_{10} \sin (3 \omega t + \phi) \quad (5.3)$$

As before, the charge variation in the tripler circuit must not exceed that for the diode under test conditions so that the following conditions must be observed

$$\begin{aligned} -1 &\leq a \leq +1 \\ -1 &\leq b \leq +1 \\ -1 &\leq a + b \leq +1 \end{aligned} \quad (5.4)$$

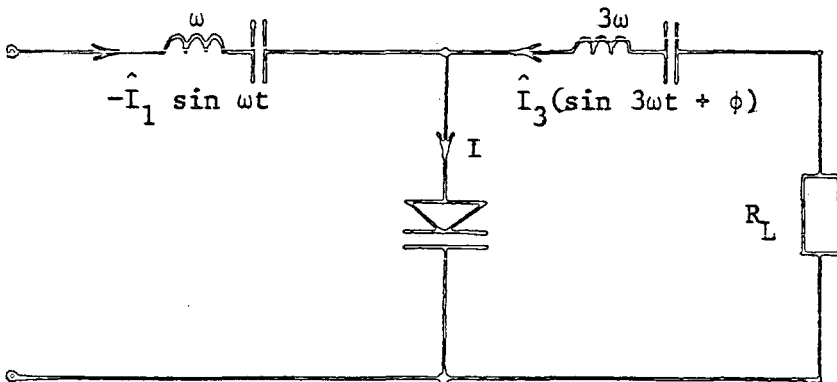


Figure 5.1
Shunt-diode tripler circuit

The voltage spectrum generated in the circuit is

$$V = V_{00} + \hat{V}_{10} T_1 \{a \cos \omega t - b \cos (3\omega t + \phi)\} \quad (5.5)$$

$$+ \hat{V}_{20} T_2 \{a \cos \omega t - b \cos (3\omega t + \phi)\}$$

and this can be expanded to

$$V = V_{00} - \hat{V}_{20} + \hat{V}_{20} a^2 + \hat{V}_{20} b^2$$

$$+ \hat{V}_{10} a \cos \omega t$$

$$+ \hat{V}_{20} a^2 \cos 2 \omega t + \hat{V}_{20} 2ab \cos (2\omega t + \phi)$$

$$- \hat{V}_{10} b \cos (3\omega t + \phi)$$

$$- \hat{V}_{20} 2ab \cos (4\omega t + \phi)$$

$$+ \hat{V}_{20} b^2 \cos (6\omega t + 2\phi) \quad (5.6)$$

The voltage components at 1st and 3rd harmonic frequencies in (5.6) can be written in phasor form, taking $-\sin \omega t$ as the reference phasor,

$$\hat{V}_1 = -j a \hat{V}_{10} \quad (5.7)$$

$$\hat{V}_3 = +j b \hat{V}_{10} \angle \phi \quad (5.8)$$

$$\hat{I}_1 = a \omega \hat{Q}_{10} = a \hat{I}_{10} \quad (5.9)$$

$$\hat{I}_3 = -3 b \omega \hat{Q}_{10} \angle \phi = -3 b \hat{I}_{10} \angle \phi \quad (5.10)$$

From the expressions for the input and output currents and voltages it can be deduced that no power is absorbed at the input because the voltage \hat{V}_1 and the input current \hat{I}_1 are in quadrature. Similarly the output e.m.f. \hat{V}_3 is in quadrature with I_3 and cannot deliver power to R_L .

Summary:

When the diode does not generate a third harmonic under test conditions it cannot be used in this particular circuit as a tripler.

5.2.2 Three-term approximation to the diode characteristic

The diode characteristic is

$$V = V_{00} + \hat{V}_{10} T_1(q) + \hat{V}_{20} T_2(q) + \hat{V}_{30} T_3(q) \quad (5.11)$$

The charge variation when the diode is connected in the circuit of Figure 5.1 is given by

$$q = a \cos \omega t - b \cos (3\omega t + \phi) \quad (5.12)$$

and the diode current is

$$I = -a \omega \hat{Q}_{10} \sin \omega t + 3b \omega \hat{Q}_{10} \sin (3\omega t + \phi) \quad (5.13)$$

or

$$I = -a \hat{I}_{10} \sin \omega t + 3b \hat{I}_{10} \sin (3\omega t + \phi)$$

The voltage spectrum generated in the circuit is

$$\begin{aligned} V = & V_{00} + \hat{V}_{10} T_1 \{a \cos \omega t - b \cos (3\omega t + \phi)\} \\ & + \hat{V}_{20} T_2 \{a \cos \omega t - b \cos (3\omega t + \phi)\} \\ & + \hat{V}_{30} T_3 \{a \cos \omega t - b \cos (3\omega t + \phi)\} \end{aligned} \quad (5.14)$$

The voltage spectrum of expression (5.14) can be expanded into the equation containing 22 terms shown in Appendix 5(i). The fundamental and third harmonic terms are

$$\begin{aligned}
V = & \hat{V}_{10} a \cos \omega t - \hat{V}_{30} \cos \omega t (3a - 6ab^2 - 3a^3) \\
& - \hat{V}_{30} 3a^2 b \cos (\omega t + \phi) \\
& + \hat{V}_{30} a^3 \cos 3 \omega t - \hat{V}_{10} b \cos (3\omega t + \phi) \\
& + \hat{V}_{30} \cos (3\omega t + \phi) (3b - 6a^2 b - 3b^3)
\end{aligned} \tag{5.15}$$

The voltage components at 1st and 3rd harmonic frequencies in (5.15) can be written in phasor form, taking $-\sin \omega t$ as the reference phasor, as

$$\hat{V}_1 = -ja \hat{V}_{10} - ja 3\hat{V}_{30} (a^2 + 2b^2 - 1) + j \hat{V}_{30} 3a^2 b \angle \phi \tag{5.16}$$

and

$$\hat{V}_3 = +jb \hat{V}_{10} \angle \phi - ja^3 \hat{V}_{30} + j \hat{V}_{30} 3b (b^2 + 2a^2 - 1) \angle \phi \tag{5.17}$$

where

$$\hat{I}_1 = a\omega \hat{Q}_{10} \tag{5.18}$$

and

$$\hat{I}_3 = -3b\omega \hat{Q}_{10} \angle \phi \tag{5.19}$$

The input and output equivalent circuits are developed in Appendix 5(ii).

The phase angle ϕ is again shown to be -90° and third harmonic terms appear in the expressions for C_o and C_{IN}

$$C_o = \frac{\hat{Q}_{10}}{\hat{V}_{10} + \hat{V}_{30} (6a + 3b^2 - 3)} \tag{5.20}$$

$$C_{IN} = \frac{\hat{Q}_{10}}{\hat{V}_{10} + \hat{V}_{30} (3a^2 + 6b^2 - 3)} \tag{5.21}$$

The equivalent input and output circuits are shown in Figure 5.2.

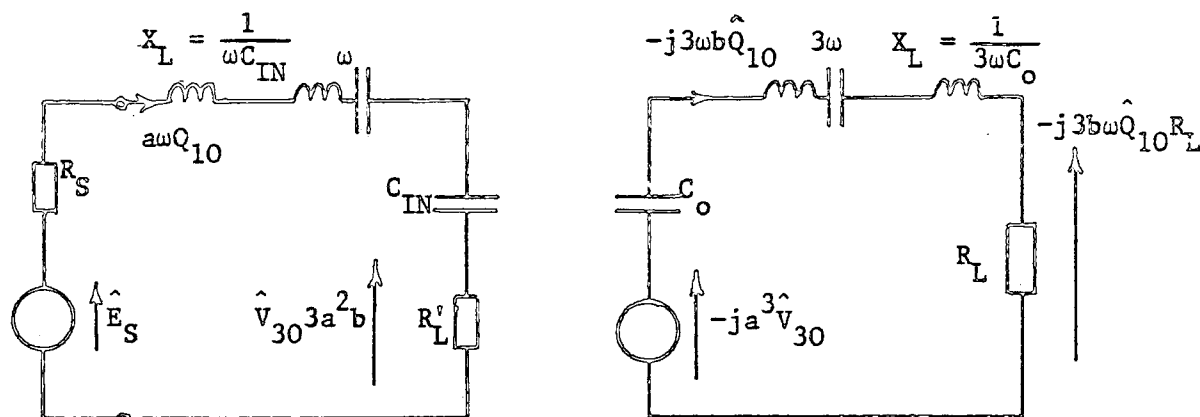


Figure 5.2
Equivalent circuit of tripler

Variation of 'a' and 'b' with R_L , R_s and E_s

One relationship between 'a' and 'b' can be obtained from the output circuit in which

$$-j a^3 \hat{V}_{30} = -j 3b \omega \hat{Q}_{10} R_L$$

hence

$$a^3 = \frac{3\omega \hat{Q}_{10} R_L b}{\hat{V}_{30}} \quad (5.22)$$

The other relationship comes from the input circuit where

$$\hat{E}_s = a\omega \hat{Q}_{10} R_s + \hat{V}_{30} 3a^2 b \quad (5.23)$$

Eliminating 'b' from equations (5.22) and (5.23) produces

$$a^5 = - \left\{ \frac{\omega^2 \hat{Q}_{10}^2 R_s R_L}{\hat{V}_{30}^2} \right\} a + \left\{ \frac{\hat{E}_s R_L \omega \hat{Q}_{10}}{\hat{V}_{30}^2} \right\} \quad (5.24)$$

It is instructive to compare this equation with the similar one obtained in the shunt-diode analysis, namely equation (4.46).

A graphical solution can be obtained for equation (5.24) as shown in Figure 5.3 where

$$F_5(a) = a^5 \quad (5.25)$$

$$F_6(a) = - \left\{ \frac{\omega^2 \hat{Q}_{10}^2 R_s R_L}{\hat{V}_{30}^2} \right\} a + \left\{ \frac{\hat{E}_s R_L \omega \hat{Q}_{10}}{\hat{V}_{30}^2} \right\} \quad (5.26)$$

$$c = \frac{E_s \hat{I}_{10} R_L}{\hat{V}_{30}^2} \quad (5.27)$$

and

$$d = \frac{E_s}{\hat{I}_{10} R_s} \quad (5.28)$$

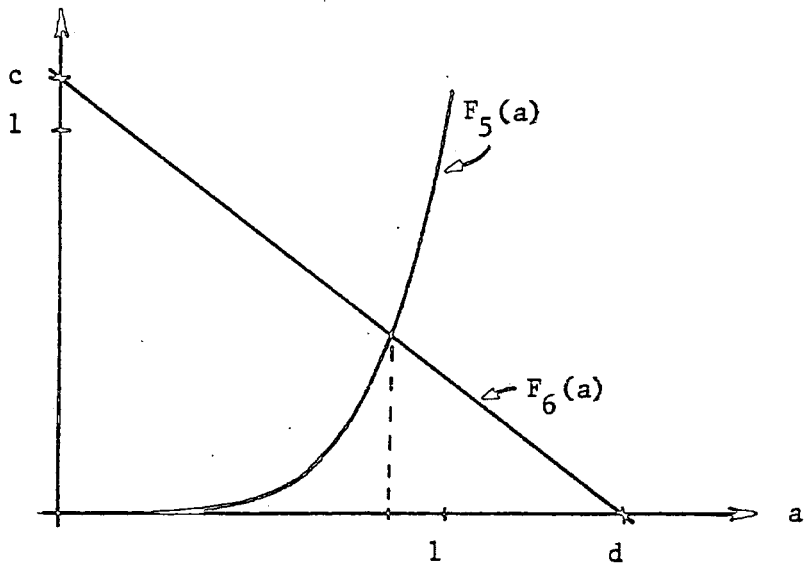


Figure 5.3

Values of 'a' and 'b' for maximum load power

The expression for load power given in equation (5.29) can be obtained by inspection of Figure 5.2

$$P_L = \left(\frac{a^3 \hat{V}_{30}}{\sqrt{2}} \right) \left(\frac{3\omega b \hat{Q}_{10}}{\sqrt{2}} \right) = \frac{3}{2} a^3 b \hat{V}_{30} \hat{I}_{10} \quad (5.29)$$

Using the condition specified in equation (5.4) the load power may also be written as

$$P_L = \hat{V}_{30} \hat{I}_{10} 1.5 a^3 (1 - a) \quad (5.30)$$

or

$$P_L = \hat{V}_{30} \hat{I}_{10} F_7 \quad (a) \quad (5.31)$$

The function $F_7(a) = 1.5a^3(1-a)$ has a maximum of 0.158 when 'a' = 0.75 and 'b' = 0.25.

Hence the maximum load power is

$$P_L (\text{max}) = 0.158 \hat{V}_{30} \hat{I}_{10} \quad (5.32)$$

Values of E_s , R_s , R_L to give maximum load power

The point (0.75, 0.237), i.e. (0.75, 0.237) must lie on the straight line graph of Figure 5.3, therefore

$$0.237 = -0.75 \left\{ \frac{\hat{I}_{10}^2 R_s R_L}{\hat{V}_{30}^2} \right\} + \left\{ \frac{E_s R_L \hat{I}_{10}}{\hat{V}_{30}^2} \right\} \quad (5.33)$$

Re-arranging equation (5.33), the maximum load power occurs when

$$E_s = \hat{V}_{30} \left\{ 0.237 \frac{R_{30}}{R_L} + 0.75 \frac{R_s}{R_{30}} \right\} \quad (5.34)$$

where

$$R_{30} = \frac{\hat{V}_{30}}{\hat{I}_{10}} \quad (5.35)$$

Equation (5.34) can be compared directly with (4.58); the equations are similar in form although the constants are different.

Summary

- (a) The maximum third harmonic power which can be extracted from the shunt diode tripler is given by equation (5.32) repeated below,

$$(5.32) \quad P_L (\text{max}) = 0.158 \hat{V}_{30} \hat{I}_{10}$$

- (b) The maximum power is extracted when E_s , R_s and R_L satisfy the relationship given in (5.34) repeated below,

$$(5.34) \quad E_s = \hat{V}_{30} \left\{ 0.237 \frac{R_{30}}{R_L} + 0.75 \frac{R_s}{R_{30}} \right\}$$

where

$$(5.35) \quad R_{30} = \frac{\hat{V}_{30}}{\hat{I}_{10}}$$

Note that there is a restriction on the value of R_L if $d > 1$ in Figure 5.3.

- (c) Only certain values of E_s , R_s and R_L are permitted. They must produce values of 'a' and 'b' which satisfy the conditions of equation (5.4).

- (d) The input capacitance of the diode is given by equation (5.21) repeated below,

$$(5.21) \quad C_{IN} = \frac{\hat{Q}_{10}}{\hat{V}_{10} + \hat{V}_{30} (3a^2 + 6b^2 - 3)}$$

- (e) The output capacitance of the diode C_o is given by equation (5.20) repeated below

$$(5.20) \quad C_o = \frac{\hat{Q}_{10}}{\hat{V}_{10} + \hat{V}_{30} (6a^2 + 3b^2 - 3)}$$

5.2.3 Four-term approximation to the diode characteristic

The diode characteristic is

$$V = V_{00} + \hat{V}_{10} T_1(q) + \hat{V}_{20} T_2(q) + \hat{V}_{30} T_3(q) + \hat{V}_{40} T_4(q) \quad (5.36)$$

The voltage spectrum generated in the circuit of Figure 5.1 is

$$\begin{aligned} V = & V_{00} + \hat{V}_{10} T_1 \{a \cos \omega t - b \cos (3\omega t + \phi)\} \\ & + \hat{V}_{20} T_2 \{a \cos \omega t - b \cos (3\omega t + \phi)\} \\ & + \hat{V}_{30} T_3 \{a \cos \omega t - b \cos (3\omega t + \phi)\} \\ & + \hat{V}_{40} T_4 \{a \cos \omega t - b \cos (3\omega t + \phi)\} \end{aligned} \quad (5.37)$$

The voltage spectrum of equation (5.37) can be expanded into the equation containing 48 terms shown in Appendix 5(iii); the fundamental and third harmonic terms are found to be no different from those given in equation (5.15) of the analysis in section 5.2.2. Thus the extra term taken in the diode test spectrum does not affect the 3rd harmonic output from the circuit, or the input and output capacitances of the diode.

Summary

The amplitude of the fourth harmonic generated in the spectrum when the diode is tested does not appear to affect the operation of the tripler circuit in any way. It is noted that many extra terms appear in the voltage spectrum at 2nd and 4th harmonic.

5.3 Shunt-Diode Tripler with Idler

5.3.1 Two-term approximation to the diode characteristic

The circuit will permit second and third harmonic currents to flow in the diode in addition to the fundamental current. The basic circuit is shown in Figure 5.4.

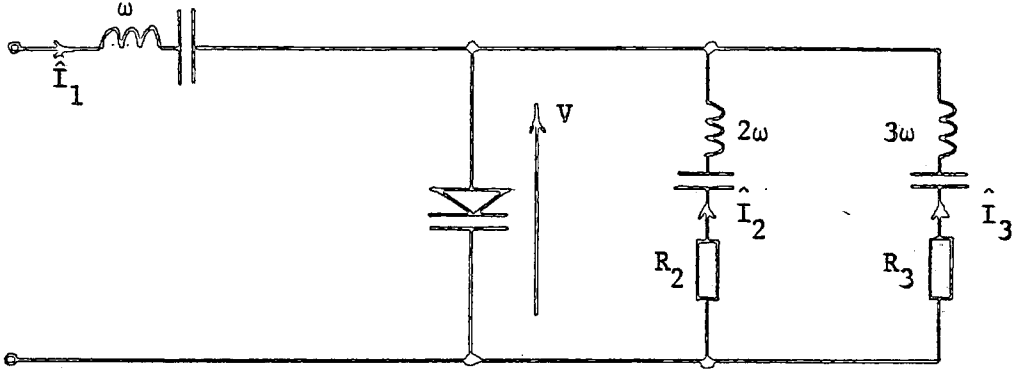


Figure 5.4
Shunt diode circuit with idler

In the first instance it will be assumed that the diode characteristic generates only first and second harmonics when tested with a sinusoidal charge variation

$$q_o = \frac{\hat{Q}_{10} \cos \omega t}{\hat{Q}_{10}} = \cos \omega t \quad (5.38)$$

The diode characteristic can be written as

$$V = V_{00} + \hat{V}_{10} T_1(q) + \hat{V}_{20} T_2(q) \quad (5.39)$$

As second and third harmonic currents are permitted to flow, the charge variation on the diode will be

$$Q = a\hat{Q}_{10} \cos \omega t - b\hat{Q}_{10} \cos (2\omega t + \phi_2) - c\hat{Q}_{10} \cos (3\omega t + \phi_3) \quad (5.40)$$

and the normalised charge will therefore be

$$q = a \cos \omega t - b \cos (2\omega t + \phi_2) - c \cos (3\omega t + \phi_3) \quad (5.41)$$

or

$$q = a \cos \theta - b \cos (2\theta + \phi_2) - c \cos (3\theta + \phi_3) \quad (5.42)$$

The charge variation on the diode in the multiplier circuit must not exceed the test level hence the following conditions apply to the values of a, b and c

$$-1 \leq a \sin \theta - b \cos (2\theta + \phi_2) - c \cos (3\theta + \phi_3) \leq +1 \quad (5.43)$$

An approximate limitation on a, b and c may be taken as

$$-1 \leq a, b, c \leq +1$$

$$-1 \leq a + b + c \leq +1 \quad (5.44)$$

The voltage spectrum generated in the diode can be obtained by substituting the expression for q of equation (5.42) into the diode characteristic of equation (5.39). This is detailed in Appendix 5(v) and the terms of frequency ω , 2ω and 3ω and given in equations (5.45) (5.46) and (5.47), using complex notation to indicate the phase of the components with $-\sin \omega t$ being the reference phase

$$\hat{V}_1 = -ja \hat{V}_{10} - jbc \hat{V}_{20} \angle \phi_3 - \phi_2 + j ab \hat{V}_{20} \angle \phi_2 \quad (5.45)$$

$$\hat{V}_2 = +jb \hat{V}_{10} \angle \phi_2 + jac \hat{V}_{20} \angle \phi_3 - ja^2 \hat{V}_{20} \quad (5.46)$$

$$\hat{V}_3 = +jc \hat{V}_{10} \angle \phi_3 + j ab \hat{V}_{20} \angle \phi_2 \quad (5.47)$$

The currents in the three branches are obtained by differentiating equation (5.40) with respect to time giving the following expressions

$$i_1 = - a\omega \hat{Q}_{10} \sin \omega t$$

hence

$$\hat{I}_1 = a\omega \hat{Q}_{10} \quad (5.48)$$

and

$$i_2 = + b 2\omega \hat{Q}_{10} \sin (2\omega t + \phi_2)$$

hence

$$\hat{I}_2 = - b 2\omega \hat{Q}_{10} \angle \phi_2 \quad (5.49)$$

and

$$i_3 = + c 3\omega \hat{Q}_{10} \sin (3\omega t + \phi_3)$$

hence

$$\hat{I}_3 = - c 3\omega \hat{Q}_{10} \angle \phi_3 \quad (5.50)$$

The third harmonic output circuit may be drawn as in Figure 5.5

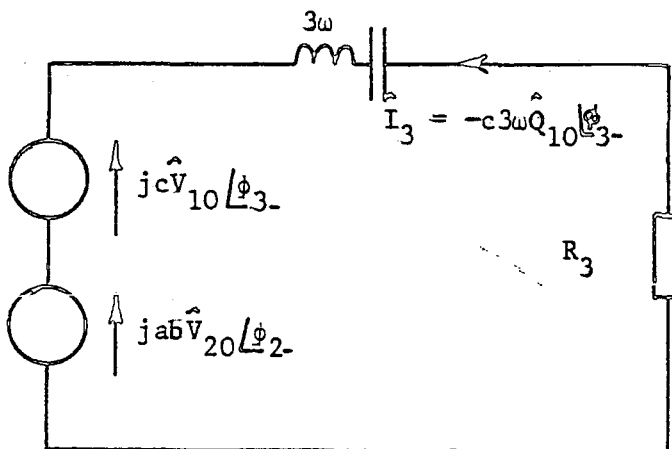


Figure 5.5

Whatever the value of ϕ_3 , the voltage generator $j\omega \hat{V}_{10} \angle\phi_3$ is always in quadrature with the current and hence can deliver no power; it is in the correct phase to represent the voltage across the output capacitance of the diode, C_{03} . If the values of ϕ_2 and ϕ_3 are taken as $-\pi/2$ (as in previous cases) the circuit of Figure 5.5 produces no output power and cannot obey circuit analysis laws. A possible solution would be for the component R_3 to be a pure inductance but this would de-tune the third harmonic filter. It is proposed to repeat the analysis with a third and fourth harmonic term in the diode characteristic.

5.3.2 Three-term approximation to the diode characteristic

The diode characteristic is

$$V = V_{00} + \hat{V}_{10} T_1(q) + \hat{V}_{20} T_2(q) + \hat{V}_{30} T_3(q) \quad (5.51)$$

When the normalised charge variation of equation (5.52) is substituted into (5.51), extra terms are generated in the voltage spectrum as detailed in Appendix 5(vi) and listed in equations (5.53), (5.54) and (5.55) below.

$$\begin{aligned} \hat{V}_1 = & -ja \hat{V}_{10} - j2bc \hat{V}_{20} \angle\phi_3 - \phi_2 + j2ab \hat{V}_{20} \angle\phi_2 \\ & + \hat{V}_{30} \left[+j3a - j3a^3 - j6ab^2 - j6ac^2 + j3a^2c \angle\phi_3 + j3b^2c \angle 2\phi_2 - \phi_3 \right] \end{aligned} \quad (5.53)$$

$$\begin{aligned} \hat{V}_2 = & jb \hat{V}_{10} \angle\phi_2 + j2ac \hat{V}_{20} \angle\phi_3 - ja^2 \hat{V}_{20} + \hat{V}_{30} \left[-j3b \angle\phi_2 \right. \\ & \left. + j3b^3 \angle\phi_2 + j6a^2b \angle\phi_2 + j6bc^2 \angle\phi_2 - j6abc \angle\phi_3 - \phi_2 \right] \end{aligned} \quad (5.54)$$

$$\begin{aligned} \hat{V}_3 = & jc \hat{V}_{10} \angle \phi_3 + j2ab \hat{V}_{20} \angle \phi_2 + \hat{V}_{30} \left[-ja^3 - j3c \angle \phi_3 \right. \\ & \left. + j3c^3 \angle \phi_3 + j6a^2c \angle \phi_3 - j3ab^2 \angle 2\phi_2 + j6b^2c \angle \phi_3 \right] \end{aligned} \quad (5.55)$$

The equation (5.55) may be used to re-draw the equivalent third harmonic circuit of Figure 5.5. Assuming, as in previous cases, that ϕ_2 and ϕ_3 are both $-\pi/2$ then the equivalent circuit is as shown in Figure 5.6

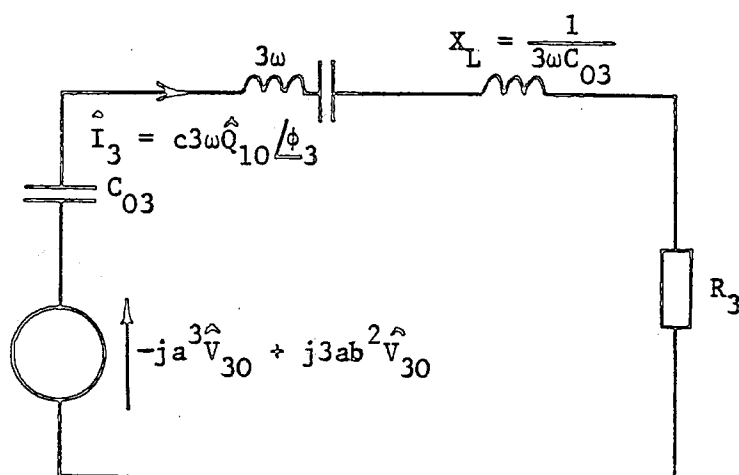


Figure 5.6
Third harmonic output circuit

From equations (5.55) and (5.50)

$$\frac{1}{3\omega C_{03}} = \frac{c\hat{V}_{10} + 2ab \hat{V}_{20} + \hat{V}_{30} \left[3c^3 - 3c + 6a^2c + 6b^2c \right]}{c3\omega \hat{Q}_{10}}$$

hence

$$C_{03} = \frac{\hat{Q}_{10}}{\hat{V}_{10} + \frac{2ab}{c} \hat{V}_{20} + \hat{V}_{30} \left[6a^2 + 6b^2 + 3c^2 - 3 \right]} \quad (5.56)$$

The equivalent circuit at second harmonic frequency can be derived from equations (5.54) and (5.49) and is shown in Figure 5.7

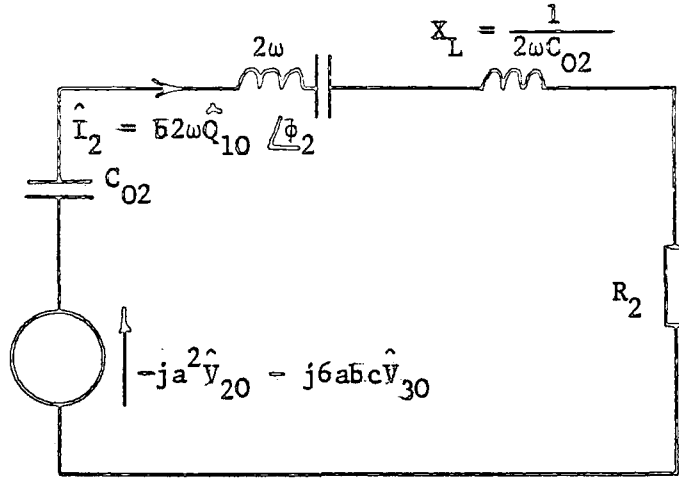


Figure 5.7
Second harmonic output circuit

The capacitance C_{02} is given by

$$\frac{1}{2\omega C_{02}} = \frac{b\hat{V}_{10} + 2ac\hat{V}_{20} + \hat{V}_{30} [3b^3 + 6a^2b + 6bc^2 - 3b]}{b2\omega \hat{Q}_{10}}$$

hence

$$C_{02} = \frac{\hat{Q}_{10}}{\hat{V}_{10} + \frac{2ac}{b}\hat{V}_{20} + \hat{V}_{30} [6a^2 + 6c^2 + 3b^2 - 3]} \quad (5.57)$$

Power at second and third harmonic

From Figures 5.6 and 5.7, the second harmonic load power is

$$P_2 = \frac{(a^2 \hat{V}_{20} + 6abc \hat{V}_{30}) (2b \hat{I}_{10})}{\sqrt{2} \sqrt{2}}$$

or

$$P_2 = a^2 b \hat{V}_{20} \hat{I}_{10} + 6ab^2 c \hat{V}_{30} \hat{I}_{10} \quad (5.58)$$

and the third harmonic load power is

$$P_3 = \frac{(a^3 \hat{V}_{30} - 3ab^2 \hat{V}_{30}) (3c \hat{I}_{10})}{\sqrt{2} \sqrt{2}}$$

or

$$P_3 = \frac{3}{2} ac (a^2 - 3b^2) \hat{V}_{30} \hat{I}_{10} \quad (5.59)$$

The input equivalent circuit

An equivalent input circuit may be derived from equations (5.53) and (5.48); it is drawn in Figure 5.8.

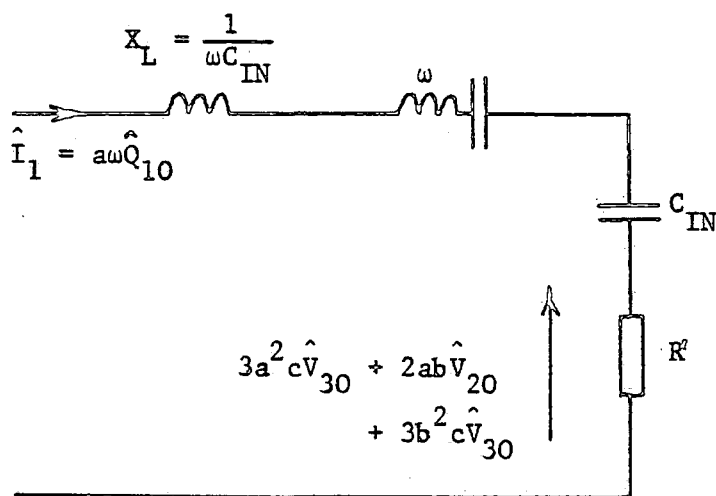


Figure 5.8
Input equivalent circuit

From the equations (5.53) and (5.48) the reflected resistance is

$$R' = \frac{2ab \hat{V}_{20} + \hat{V}_{30} 3c (a^2 + b^2)}{a\omega \hat{Q}_{10}}$$

or

$$R' = 2b \frac{\hat{V}_{20}}{\hat{I}_{10}} + \frac{3c}{a} (a^2 + b^2) \frac{\hat{V}_{30}}{\hat{I}_{10}} \quad (5.60)$$

The input capacitance of the diode is given by

$$\frac{1}{\omega C_{IN}} = \frac{a\hat{V}_{10} + 2bc\hat{V}_{20} + \hat{V}_{30} [3a^3 + 6ab^2 + 6ac^2 - 3a]}{a\omega \hat{Q}_{10}}$$

hence

$$C_{IN} = \frac{\hat{Q}_{10}}{\hat{V}_{10} + \frac{2bc}{a}\hat{V}_{20} + \hat{V}_{30} [3a^2 + 6b^2 + 6c^2 - 3]} \quad (5.61)$$

Variation of 'a', 'b' and 'c' with R_2 , R_3 , R_s and E_s

Applying Kirchhoffs Laws to the three equivalent circuits provides three equations in 'a' 'b' and 'c'

$$\hat{E}_s - a\hat{I}_{10} R_s = 2ab\hat{V}_{20} + 3a^2c\hat{V}_{30} + 3b^2c\hat{V}_{30} \quad (5.62)$$

$$a^2\hat{V}_{20} + 6abc\hat{V}_{30} = 2b\hat{I}_{10} R_2 \quad (5.63)$$

$$a^3\hat{V}_{30} - 3ab^2\hat{V}_{30} = 3c\hat{I}_{10} R_s \quad (5.64)$$

Simultaneous solution of the three equations will produce values of 'a' 'b' and 'c' which must obey the restrictions of equation (5.44).

Variation of second and third harmonic powers with 'a', 'b' and 'c'

Equations (5.58) and (5.59) are repeated below

$$(5.58) \quad P_2 = a^2b\hat{V}_{20}\hat{I}_{10} + 6ab^2c\hat{V}_{30}\hat{I}_{10}$$

$$(5.59) \quad P_3 = \hat{V}_{30}\hat{I}_{10} \left(\frac{3}{2}ac^3 - \frac{9}{2}ab^2c \right)$$

If a certain relationship exists between 'a' and 'b' then P_3 will be zero for any value of c. From (5.59) this relationship is

$$a^2 = 3b^2$$

or

$$a = 1.732 b$$

If the third harmonic power is zero the question arises whether the second harmonic power is then at a maximum. This depends upon the relative values of \hat{V}_{30} , \hat{I}_{10} and \hat{V}_{20} , \hat{I}_{10} and if these are of the same order then it is possible that the value of P_2 given by (5.58) can exceed the value of P_2 given by equation (4.90). The latter equation has a negative fourth harmonic contribution and this requires investigation in the case where an idler is included and the four-term approximation is used for the diode characteristic.

Summary

- (a) There is no easy approximate solution to the problem of finding the currents in the three branches in this case. A numerical solution of equations (5.62) (5.63) and (5.64) is apparently required.
- (b) If values of 'a', 'b' and 'c' can be found by a numerical solution then the power in each circuit can be calculated using (5.58) and (5.59).
- (c) The third harmonic power is reduced by the flow of second harmonic current and the second harmonic power can be increased if the term \hat{V}_{30} is comparable to \hat{V}_{20} .

- (d) The input capacitance C_{IN} is affected by both second and third harmonic currents and is given in equation (5.61). The output capacitances of the diode at second and third harmonic, C_{O2} and C_{O3} , are given in equations (5.57) and (5.56) respectively.

5.3.3 Four-term approximation to the diode characteristic

The details of this analysis are given in Appendix 5(vii) where it is shown that the equivalent circuit given in Figure 5.9 can be derived.

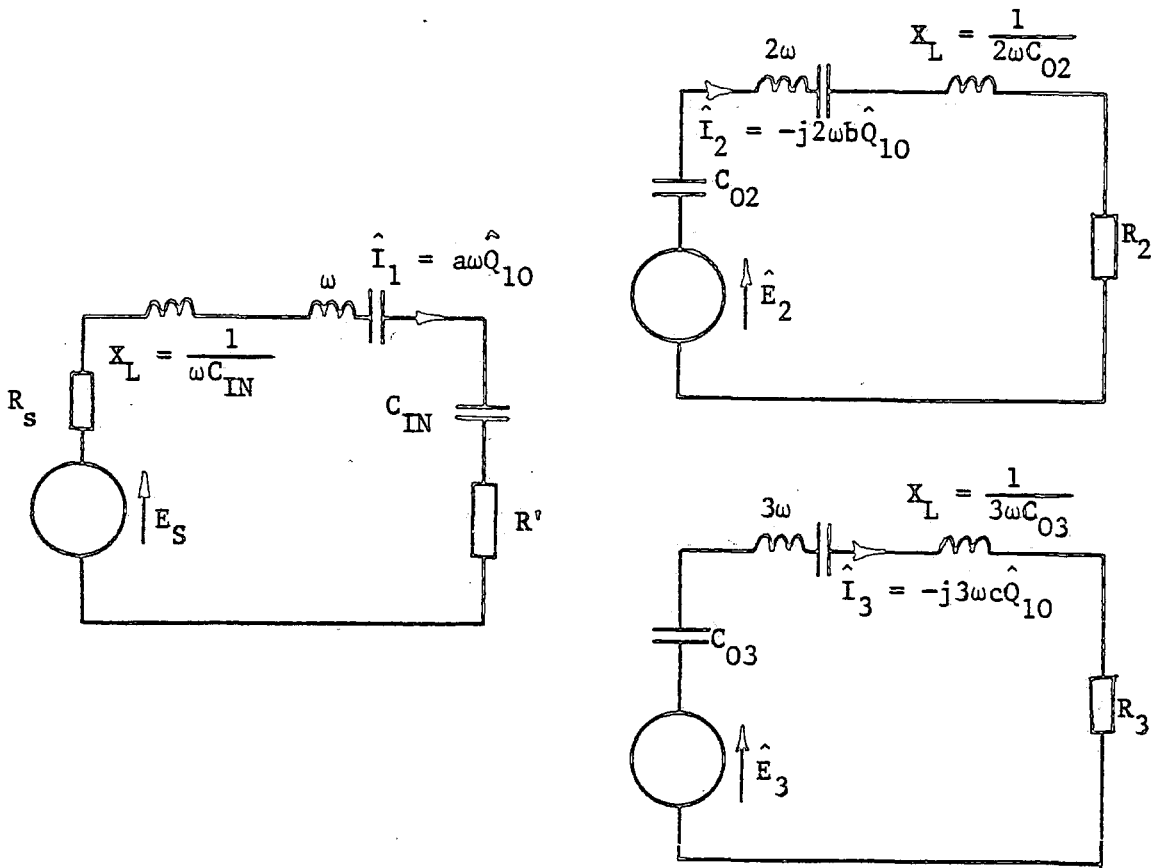


Figure 5.9
Full equivalent circuit

The following expressions relate to the quantities shown in Figure 5.9:

$$\hat{E}_2 = \hat{V}_{20} a^2 + \hat{V}_{30} 6abc + \hat{V}_{40} (4a^4 - 6a^2b^2 + 12a^2c^2 + 6b^2c^2 - 4a^2) \quad (5.66)$$

$$\hat{E}_3 = \hat{V}_{30} (a^3 - 3ab^2) + \hat{V}_{40} (-4b^3c) \quad (5.67)$$

$$R_L = \frac{\hat{V}_{20}}{\hat{I}_{10}} 2b + \frac{\hat{V}_{30}}{\hat{I}_{10}} \frac{3c}{a} (a^2 + b^2) + \frac{\hat{V}_{40}}{\hat{I}_{10}} 4b (2a^2 + 3b^2 + 6c^2 - 2) \quad (5.68)$$

$$C_{IN} = \frac{\hat{Q}_{10}}{\hat{V}_{10} + \frac{2bc}{a} \hat{V}_{20} + \hat{V}_{30} [f_5(a,b,c)] + \hat{V}_{40} [f_6(a,b,c)]} \quad (5.69)$$

where

$$f_5(a,b,c) = 6b^2 + 6c^2 + 3a^2 - 3 \quad (5.70)$$

and

$$f_6(a,b,c) = \frac{4bc}{a} (3b^2 + 3c^2 + 9a^2 - 2) \quad (5.71)$$

Expressions for the second and third harmonic outputs powers may be derived as

$$P_2 = \hat{V}_{20} \hat{I}_{10} (a^2b) + \hat{V}_{30} \hat{I}_{10} (6ab^2c) + \hat{V}_{40} \hat{I}_{10} (4a^4b + 6a^2b^3 + 12a^2bc^2 + 6b^3c^2 - 4a^2b) \quad (5.72)$$

$$P_3 = \hat{V}_{30} \hat{I}_{10} \left(\frac{3}{2} a^3c - \frac{9}{2} ab^2c \right) + \hat{V}_{40} \hat{I}_{10} (-6b^3c^2) \quad (5.73)$$

and the input power (at fundamental frequency) is given by

$$P_1 = \hat{V}_{20} \hat{I}_{10} (a^2b) + \hat{V}_{30} \hat{I}_{10} \left(\frac{3ac}{2} [a^2 + b^2] \right) + \hat{V}_{40} \hat{I}_{10} (2a^2b [2a^2 + 3b^2 + 6c^2 - 2]) \quad (5.74)$$

Hence, as expected,

$$P_1 = P_2 + P_3 \quad (5.75)$$

5.4 Conclusion

The analysis for the tripler circuit without idler gives results which have similarities with those for the doubler circuit.

The ratios of the peak values of second harmonic current to fundamental current to fundamental test current are $b:a:1$ where the values of 'a' and 'b' may be obtained by solution of the equation (5.24). The approximate values may be found by a graphical method shown in Figure 5.3.

The maximum third harmonic power is given by the result (5.32).

The output (third harmonic) power only depends upon the magnitude of the third harmonic generated in the test spectrum, the magnitudes of fundamental, second and fourth harmonics do not directly affect the output power, see result (5.29).

The input and output capacitances are dependent upon the fundamental and third harmonic amplitudes generated in the test spectrum, see results (5.20) and (5.21).

When an idler circuit is used the analysis appears to show that the third harmonic power P_3 is reduced by the flow of second harmonic current. However, the second harmonic power P_2 can be increased as indicated in equation (5.72) which compares with (4.83). When an idler is used the third harmonic term \hat{V}_{30} contributes to P_2 .

The input and output capacitances of the diode, which cause detuning of the filter circuits, are also dependent upon \hat{V}_{10} , \hat{V}_{20} , \hat{V}_{30} and \hat{V}_{40} when an idler circuit is used whereas with no idler circuit they only depend upon \hat{V}_{10} and \hat{V}_{30} .

The values of 'a' 'b' and 'c' require the solution of three simultaneous equations, (5.62) (5.63) and (5.64), which should be done using numerical methods.

Table 5.1 compares the results obtained for the three circuits considered in Chapters 4 and 5.

| | Shunt-diode doubler | Shunt-diode tripler |
|-------------------------------------|--|--|
| Output power P_L | $P_2 = \hat{V}_{20} \hat{I}_{10} a^2 b$ $+ \hat{V}_{40} \hat{I}_{10} \{a^2 b(4a^2 + 6b^2 - 4)\}$ | $P_3 = \hat{V}_{30} \hat{I}_{10} \frac{3}{2} a^3 c$ |
| C_{IN} | $\frac{\hat{Q}_{10}}{\hat{V}_{10} + \hat{V}_{30} (3a^2 + 6b^2 - 3)}$ | $\frac{\hat{Q}_{10}}{\hat{V}_{10} + \hat{V}_{30} (3a^2 + 6c^2 - 3)}$ |
| C_{OUT} | $\frac{\hat{Q}_{10}}{\hat{V}_{10} + \hat{V}_{30} (6a^2 + 3b^2 - 3)}$ | $\frac{\hat{Q}_{10}}{\hat{V}_{10} + \hat{V}_{30} (6a^2 + 3c^2 - 3)}$ |
| $R'_L (= R_{IN})$ | $\frac{\hat{V}_{20}}{\hat{I}_{10}} 2b + \frac{\hat{V}_{40}}{\hat{I}_{10}} 4b (2a^2 + 3b^2 - 2)$ $= 4 \frac{b^2}{a^2} R_L$ | $\frac{\hat{V}_{30}}{\hat{I}_{10}} 3ac = \frac{9c^2}{a^2} R_L$ |
| Simultaneous Equations for a, b, c. | $\hat{V}_{20} a^2 + \hat{V}_{40} (4a^4 + 6a^2 b^2 - 4a^2) - 2b \hat{I}_{10} R_L = 0$ $E_s - a \hat{I}_{10} R_s - \frac{4b^2 R_L}{a} \hat{I}_{10} = 0$ | $a^3 \hat{V}_{30} - 3c \hat{I}_{10} R_L = 0$ $E_s - a \hat{I}_{10} R_s - \hat{V}_{30} 3a^2 c = 0$ |
| approx a, b, c for P_L (max) | $a = 0.667$ $b = 0.333$ | $a = 0.75$ $c = 0.25$ |
| Estimated P_L (max) | $0.148 \hat{V}_{20} \hat{I}_{10} - 0.23 \hat{V}_{40} \hat{I}_{10}$ | $0.158 \hat{V}_{30} \hat{I}_{10}$ |

TABLE 5.1

Shunt-diode tripler with second-harmonic idler

2nd harmonic

$$P_2 = \hat{V}_{20} \hat{I}_{10} a^2 b + \hat{V}_{30} \hat{I}_{10} 6ab^2 c \\ + \hat{V}_{40} \hat{I}_{10} \{a^2 b (4a^2 + 6b^2 + 12c^2 \\ - 4) + 6b^3 c^2\}$$

3rd harmonic

$$P_3 = \hat{V}_{30} \hat{I}_{10} \left(\frac{3}{2} a^3 c - \frac{9}{2} ab^2 c \right) \\ + \hat{V}_{40} \hat{I}_{10} (-6b^3 c^2)$$

$$\frac{\hat{Q}_{10}}{\hat{V}_{10} + \hat{V}_{20} \frac{2bc}{a} + \hat{V}_{30} \{3a^2 + 6b^2 + 6c^2 - 3\} + \hat{V}_{40} \frac{4bc}{a} \{9a^2 + 3b^2 + 3c^2 - 2\}}$$

$$C_{02} = \frac{\hat{Q}_{10}}{\hat{V}_{10} + \hat{V}_{20} \frac{2ac}{b} + \hat{V}_{30} \{6a^2 + 3b^2 + 6c^2 - 3\} + \hat{V}_{40} \frac{4ac}{b} \{3a^2 + 9b^2 + 3c^2 - 2\}}$$

$$C_{03} = \frac{\hat{Q}_{10}}{\hat{V}_{10} + \hat{V}_{20} \frac{2ab}{c} + \hat{V}_{30} \{6a^2 + 6b^2 + 3c^2 - 3\} + \hat{V}_{40} \frac{4ab}{c} \{3a^2 + 3b^2 + 9c^2 - 2\}}$$

$$\frac{\hat{V}_{20}}{\hat{I}_{10}} 2b + \frac{\hat{V}_{30}}{\hat{I}_{10}} \left(3ac + \frac{3cb^2}{a} \right) + \frac{\hat{V}_{40}}{\hat{I}_{10}} 4b \{2a^2 + 3b^2 + 6c^2 - 2\} \\ = \frac{4b^2}{a^2} R_2 + \frac{9c^2}{a^2} R_3$$

$$a^2 \hat{V}_{20} + \hat{V}_{30} 6abc - 2b \hat{I}_{10} R_2 = 0$$

$$a^3 \hat{V}_{30} - \hat{V}_{30} 3ab^2 - 3c \hat{I}_{10} R_3 = 0$$

$$E_s - a \hat{I}_{10} R_s - \hat{V}_{20} 2ab - \hat{V}_{30} 3a^2 c - \hat{V}_{30} 3b^2 c = 0$$

requires numerical solution

requires numerical solution

CHAPTER 6PERFORMANCE OF PRACTICAL MULTIPLIER CIRCUITS

| | <u>Page</u> |
|-----------------------------------|-------------|
| 6.1 Introduction | 133 |
| 6.2 General Test Procedure | 135 |
| 6.3 Microstrip Cavity Multipliers | 137 |
| 6.3.1 Design details | 137 |
| 6.3.2 Practical results | 138 |
| 6.3.3 Summary | 143 |
| 6.4 Coaxial Cavity Multipliers | 144 |
| 6.4.1 Introduction | 144 |
| 6.4.2 Design details | 144 |
| 6.5 Conclusion | 146 |

6.1 Introduction

The design, construction and testing of practical frequency multiplier circuits are described in this chapter. The multipliers were designed as frequency doublers with the diode in the shunt connection as shown in the basic circuit of Figure 6.1, and the input and output filters were required to have low impedance at fundamental and second harmonic frequencies respectively.

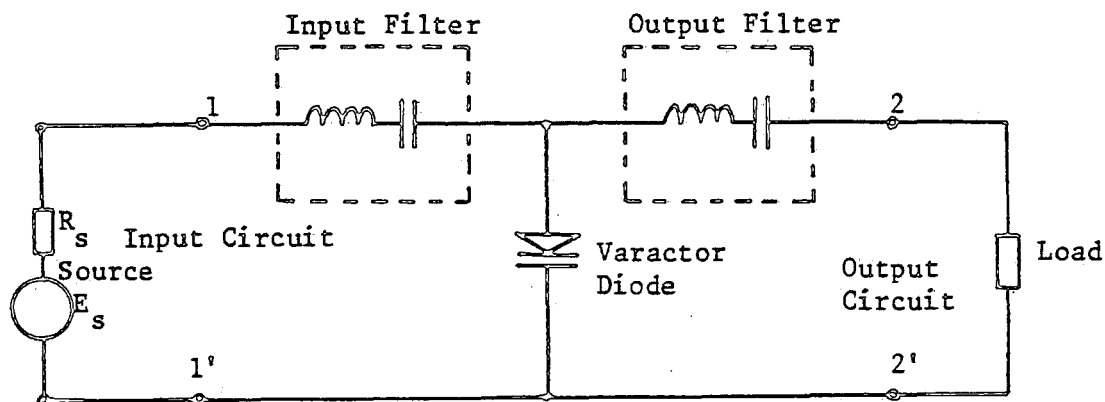


Figure 6.1

One objective of the investigation was the assessment of the merits of the series-tuned cavity as a component in frequency multiplier circuits. This form of filter was therefore used in the multiplier circuit as represented in Figure 6.2. Each cavity consisted of a length of short-circuited transmission line with a series tuning capacitor at the input and an output tapping near the short-circuited end. In Figure 6.2, C_{S1} and C_{S2} are the series tuning capacitors of the input and output cavities respectively.

6.2 General Test Procedure

When a multiplier was connected between a signal source and a load, as represented in the circuits of Figures 6.1 and 6.2, the variables external to the multiplier were the e.m.f. and internal resistance of the source and the load resistance. The input fundamental current was assumed to be a fraction "a" of \hat{I}_{10} , where the latter was defined as the amplitude of the fundamental current supplied to the diode under the spectrum test conditions. The second harmonic current delivered to the load, and, incidently, also passing through the diode, was assumed to be $2b\hat{I}_{10}$ where the parameter "b" was actually the ratio of the second harmonic charge variation to the fundamental charge variation during the spectrum test as defined in equation (4.20). The total current flowing in the diode was assumed to cause a variation in charge not greater than that in the spectrum test, and was expressed as,

$$I = -a\hat{I}_{10} \sin \omega t + 2b\hat{I}_{10} \sin (2\omega t - \pi/2) \quad (6.1)$$

as derived in section 4.3.1.

The parameters "a" and "b" could be called the "multiplier circuit parameters" and they were shown to play an important role in the operation of the multiplier. The second harmonic load power P_L had been shown in the theoretical analysis to depend upon these parameters as,

$$P_L = a^2 b \hat{I}_{10} \hat{V}_{20} \quad (6.2)$$

where \hat{V}_{20} was the amplitude of the second harmonic of the voltage spectrum generated in the diode under test conditions in which the diode current is $-\hat{I}_{10} \sin \omega t$.

The values of the multiplier circuit parameters depend upon the source and load and they can be found using the graphical method of Figure 4.13. The maximum load power P_L (max) was predicted to occur at a particular pair of values of "a" and "b" given by,

$$a = 0.667 \quad (6.3)$$

$$b = 0.333 \quad (6.4)$$

$$P_L \text{ (max)} = 0.148 \hat{I}_{10} \hat{V}_{20} \quad (6.5)$$

The practical tests on the multipliers were required to show that the values of the multiplier circuit parameters varied in accordance with the predictions given by the graphical solution to the equations relating "a" and "b" to \hat{E}_s , R_s and R_L . It was difficult at the frequencies used to provide source and load resistances of any value other than 50Ω except by incorporating impedance-matching circuits within the multiplier. Thus all the series-tuned cavities were designed with $50\text{-}\Omega$ transmission lines and impedance transformation was used between the cavities and the diode. With the effective values of \hat{E}_s and R_s remaining constant, the value of "a" was expected to decrease from unity as R_L was reduced from infinity, i.e. as the loading was increased. The value of "b" was given by,

$$b = \frac{\hat{V}_{20} a^2}{2 \hat{I}_{10} R_L} \quad (6.6)$$

and this was expected to increase as the value of R_L was reduced. The quantity which could be measured was, of course, the load power which was given by equation (6.2). At a particular value of R_L the load power was expected to reach a maximum value.

6.3 Microstrip Cavity Multipliers

6.3.1 Design details

Several experimental shunt-diode frequency doublers were designed and tested with input cavities tuned to 1.56 GHz at which frequency a 2W solid-state laboratory source was available. The connection of the diode in parallel with the microstripline can be seen in the photograph of Figure 6.1. The diode was rigidly clamped in position by a fibreglass strip and the cavity tuning was achieved by adjustable parallel-plate capacitors with dielectric consisting of MYLAR sheet of thickness $50 \cdot 10^{-6}$ m.

The development of the multiplier design is indicated in Figure 6.2 to 6.7 which show the negatives used for the microstrip circuits.

The particular features of each circuit were:

- (i) Doubler No. 11A, Figure 6.2.

Doubler with no impedance matching.

- (ii) Doubler No. 12, Figure 6.3.

Doubler with impedance matching for 25Ω in the output circuit by means of a quarter-wavelength transformer. Extra connections have been provided at input and output so that the input and output cavities could be independently tuned.

- (iii) Doubler No. 13, Figure 6.4.

Doubler with impedance matching to present 25Ω to the diode in both input and output circuits by means of quarter-wavelength transformers. Input and output cavities could be independently tuned before connection to the diode.

- (iv) Doubler No. 14, Figure 6.5.

Doubler with impedance matching to present 20Ω to the diode in both input and output circuits by means of quarter-wavelength

transformers. Input and output cavities could be independently tuned before connection to the diode but the output cavity was, in fact, connected in the wrong direction.

(v) Doubler No. 14A, Figure 6.6.

Doubler with 20Ω values for R_L and R_S similar to design No. 14 but with output cavity in correct direction.

(vi) Doubler No. 15, Figure 6.7.

Doubler arranged so that single-stub matching may be used for impedance matching in the input and output circuits. Input and output cavities could be independently tuned before connection to the diode. All microstriplines have characteristic impedance of 50Ω .

6.3.2 Practical results

The results of measurements made on the doublers are shown in Table 6.1. Test 1 in the table gives the output powers with the cavities separately tuned to the input and output frequencies of 1.56 GHz and 3.12 GHz respectively, and test 2 was with the tuning capacitors adjusted for maximum second harmonic output power. Further tests were carried out for some of the doubler circuits in order to assess the effects of the settings of the tuning capacitors. The circuits were fed from the 2W solid-state source through an attenuator and the output power was measured using the attenuator on the spectrum analyser.

| | | Doublers Test Circuit Number | | | | |
|-----------|------------------------|------------------------------|------|-------|------|-------|
| | | 11A | 12 | 13 | 14A | 15 |
| TEST 1 | Input at f_o (dBm) | +27 | +30 | +30 | +30 | +30 |
| | Output at $2f_o$ (dBm) | -10 | 0 | +9 | +7 | -7 |
| | Output at f_o (dBm) | -3 | -5 | +4 | +1 | +1 |
| | C_{IN} (divisions) | +2 | -2 | +1.75 | +2.1 | +2.75 |
| | C_o (divisions) | 0 | +3.5 | -1.5 | -2 | -3 |
| TEST 2 | Input at f_o (dBm) | +27 | +30 | | +30 | +30 |
| | Output at $2f_o$ (dBm) | -8 | 8 | | +15 | +12 |
| | Output at f_o (dBm) | -5 | 12 | | +13 | +29 |
| | C_{IN} (divisions) | +1.5 | +0.7 | | -1.6 | 0 |
| | C_o (divisions) | +1 | +2 | | -1.1 | 0 |
| TEST 3 | Input at f_o (dBm) | +27 | | | +30 | |
| | Output at $2f_o$ (dBm) | +7 | | | +13 | |
| | Output at f_o (dBm) | +4 | | | +23 | |
| | C_{IN} (divisions) | +1.5 | | | +2.1 | |
| | C_o (divisions) | +1 | | | -1.1 | |
| TEST 4 | Input at f_o (dBm) | +33 | | | | |
| | Output at $2f_o$ (dBm) | -7 | | | | |
| | Output at f_o (dBm) | +4 | | | | |
| | C_{IN} (divisions) | +1.5 | | | | |
| | C_o (divisions) | +1 | | | | |

Table 6.1

Comments:

(i) Doubler No. 11A.

The lengths of the cavities were found to be incorrect on this design which was the first circuit to use 1.56 GHz as the input frequency. The microstrip width was, by mistake, not increased to that needed for the Duroid substrate which was used in place of the fibreglass previously employed at lower frequencies.

The input and output cavities were separately tuned by cutting gaps in the copper striplines with a sharp blade and using silver conducting paint to make necessary connections; the swept-frequency responses are shown in Figures 6.8 and 6.9.

The second harmonic output power was very small presumably because there was no impedance matching in the circuit. There was a relatively large output component at f_0 due to the poor performance of the cavity filters which are not working between 50Ω impedances. This circuit had microstriplines of characteristic impedance 65Ω .

(ii) Doubler No. 12.

The results were improved relative to those of doubler No. 11 but the output power was much lower than required.

(iii) Doubler No. 13.

The quarter-wavelength transformers were designed to match from 50Ω to 25Ω , and the results showed some improvement but the second harmonic output was not sufficiently large. Later tests on doubler 14A showed that very fine tuning adjustment was required in order to obtain the best output, and it was possible that larger output powers were available from this circuit.

(iv) Doubler No. 14.

This was designed but not completed as the output cavity was in the wrong direction.

(v) Doubler No. 14A.

This was the re-design of doubler No. 14 with impedance matching of 50Ω to 20Ω . The diode was mounted in the 20Ω microstripline. A standing wave test was carried out on this doubler using the circuit represented in Figure 6.10 and the standing wave patterns were as shown in Figure 6.11.

It was found that careful adjustment of the tuning capacitors could produce an output of +15 dBm which was greater than previously obtained. As the output power was increased the SWR measured on the slotted line decreased as expected.

(vi) Doubler No. 15.

This doubler was designed with all microstriplines having 50Ω characteristic impedance. Tests 1 and 2 were then made in the usual manner except that the SWRs were also measured, giving results of 36 and 15 respectively.

An open-circuit stub was then painted onto the circuit using silver conducting paint to provide impedance matching using the "single stub matching" technique.

The $50\text{-}\Omega$ stub was at a position 1.3 cm from the diode on the output side and a stub length of 0.55 cm gave maximum output at $2f_0$. However, the output obtained was only -5 dBm and the SWR was 30.

Test 2 showed that the cavities could be tuned so that a second harmonic output power of +12 dBm could be obtained but this was not valid as the filters were also allowing the fundamental frequency input power to appear at the output. As the input power contains +10 dBm of second harmonic, the output power should be considerably higher than this, for example, in the range 20 dBm to 30 dBm.

The stub matching was not successful in this case; the length of stub required might be expected to be more than a quarter-wavelength whereas it appeared to require a very short stub to improve the output power. Stub matching should be possible but apparently not by the technique used here.

6.3.3 Summary

(i) It was found that the cavity tuning capacitors required adjustment from their initial settings when each doubler circuit was tested. This was expected as the diode acts as a capacitance in both the input and the output circuits.

(ii) The second harmonic output power P_2 was measured for the following transformed values of R_L and R_s :

$$R_L = 20\Omega, R_s = 20\Omega; P_2 = +15 \text{ dBm}$$

$$R_L = 25\Omega, R_s = 25\Omega; P_2 = +9 \text{ dBm}$$

$$R_L = 50\Omega, R_s = 50\Omega; P_2 < 0 \text{ dBm}$$

These figures show that changes in R_L and R_s with E_s constant produce changes in the multiplier parameters "a" and "b" which are measured as changes in P_2 . Obviously, more extensive testing is required to verify the theory of Chapter 4.

(iii) Stub-matching technique requires further investigation as a method of impedance matching to produce a good transfer of power from the source to the load.

6.4 Coaxial Cavity Multipliers

6.4.1 Introduction

The design of coaxial cavity multipliers has been detailed in various technical application notes from manufacturers such as Motorola Semiconductor Products Incorporated and Hewlett Packard Ltd (references 10 and 26). These designs have used the transmission-line cavity as a tapped parallel-tuned circuit with input and output tapings as shown in Figure 6.12 so that filtering and impedance transformation are achieved together.

An objective of this project was the investigation of the use of series-tuned coaxial cavities in frequency multipliers, and a preliminary design is discussed in the next section of this report. Series-tuned cavities had been used successfully in coaxial multipliers by KULESZA (Reference 17, 1967) who reported an efficient multiplier chain giving multiplication by a factor of 144. The matching between the diode and coaxial cavities in his circuits was implemented where possible by capacitative transformers and this gave an overall efficiency of 2.5% which at the time was an excellent performance for such a high multiplication factor. In view of this previous work, this thesis has concentrated upon implementing the series cavity circuits in microstripline.

6.4.2 Design details

A preliminary design for a coaxial multiplier is shown in the photograph of Figure 6.13. The input and output cavities were designed to have series resonant frequency of 1 GHz and 2 GHz respectively, and the outer conductors were of square cross-section which is the usual practice. The diode was situated in a hole through the piece of white insulator (P.T.F.E.) in Figure 6.13 to connect between the outer of the cavity and a brass disc inner conductor which was set into the middle

of the insulator. Probes connected the N-type input and output sockets to the centre threaded conductors of the cavities by means of springy strips of brass. The threaded centre conductors form tuning capacitances with the disc in the white insulator and the capacitances are held at fixed values by tightening the knurled lock nuts.

When the diode was replaced by a direct connection so that each cavity could be separately tuned to the desired frequencies, it was found that a cavity could only be tuned when the inner conductor of the other had been almost completely removed. Thus this particular design was abandoned.

It was obvious that the two cavities should be completely screened from each other by the insertion of an earthed plate in the position occupied by the diode in Figure 6.13. The cavities might be more easily designed if positioned side-by-side rather than back-to-back and a proposed design is shown in Figure 6.14. However, this design was not produced because experimental microstripline circuits were far easier, cheaper and quicker to produce and therefore the microstrip designs were pursued with the greater vigour.

6.4 Conclusion

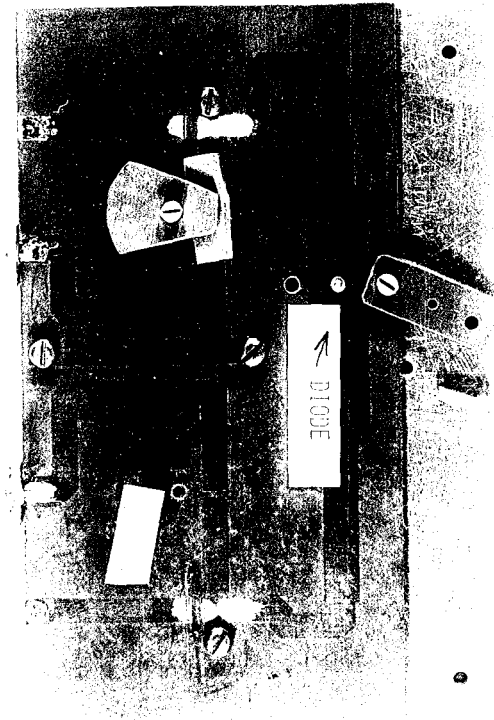
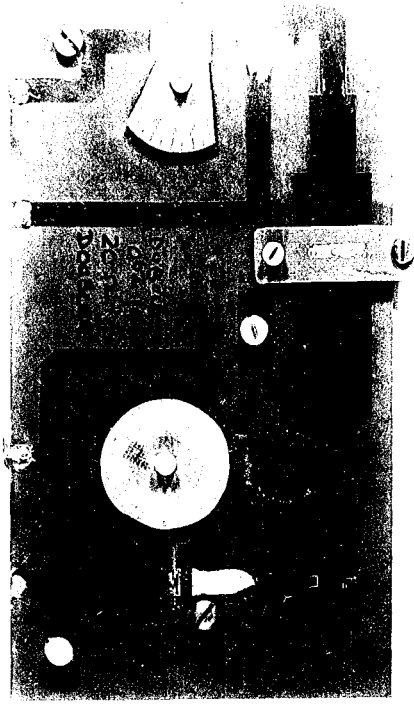
Frequency doublers using varactor diodes in microstripline circuits with series-tuned cavities have been designed, constructed, and tested with the objective of verifying the multiplier theory developed in Chapters 4 and 5. This type of multiplier circuit, i.e. microstripline, was investigated because the development of experimental circuits was much easier, quicker and cheaper than designs which use coaxial transmission lines.

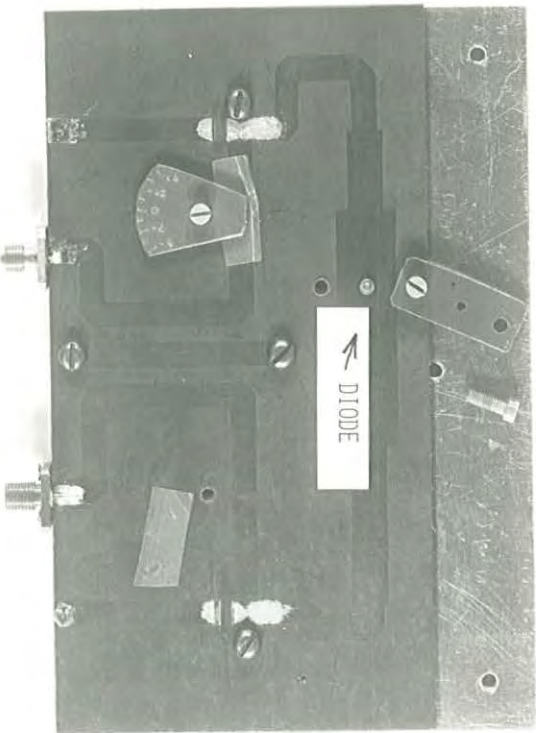
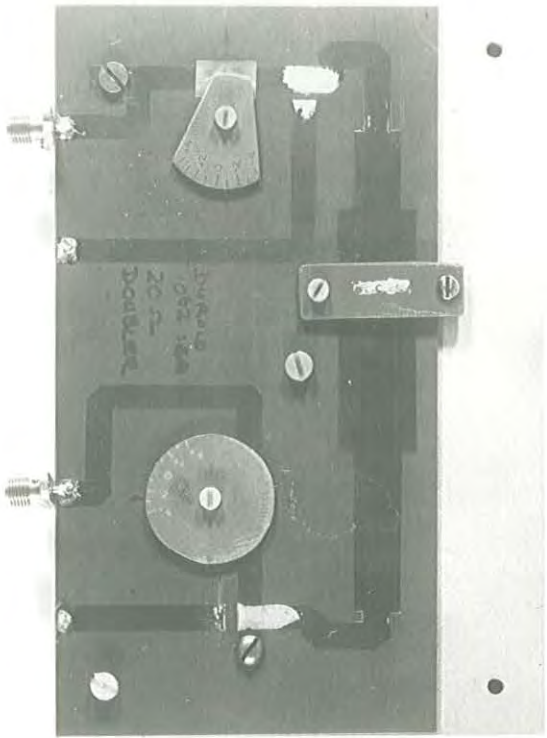
The tests were required to show that the multiplier circuit parameters "a" and "b", and hence the second harmonic output power were dependent upon the source e.m.f. E_s , the source resistance R_s and the load resistance R_L in the manner stated in the conclusions of Chapter 4. The actual values required for R_s and R_L for maximum output power were not found from spectral tests on the varactor diodes because this was too large a project. It was suspected, however, that the values needed for R_s and R_L would be less than 10Ω because impedance matching of this order has always been used in varactor diode multiplier circuits. The source and load resistances R_s and R_L were transformed to several different values by means of quarter-wavelength transformers and the second harmonic output power was measured for each case. The results are summarised in section 6.3.3 and it can be seen that increasing the transformation ratios N_1 and N_2 (where source resistance is transformed to R_s/N_1^2 and load resistance to R_L/N_2^2) produced an increase in output power. The values of N_1 and N_2 should have been increased until a decrease in the output power was observed as this situation is predicted by the theory of Chapter 4. However, the highest value which was used for both N_1 and N_2 was 1.58 and higher values than this become difficult as the stripline width increases.

When the diode was connected in parallel between a wide strip conductor and the earth plane it was not at all certain that the travelling wave could be assumed to arrive correctly at the diode. In one case the effect of connecting three diodes in parallel was investigated but no obvious advantage was noted.

The maximum second harmonic power obtained from the microstrip doubler was +15 dBm at 3.12 GHz when the effective source and load resistances were both 20Ω . The actual input power in this case was not measured but the available power from the source was +30 dBm. It is thought that more output power would have been obtained with the "correct" matching, and that very careful tuning would also produce a greater output. Although it cannot be claimed that the theory of Chapter 4 has been verified, much useful experience on the design of microstrip doublers has been obtained.

A future investigation might make more use of the impedance-transforming properties of the series-tuned cavity. All the computer studies in Chapter 2 were made for a load resistance of 50Ω because microwave power measurements are usually made in a 50Ω load. However, it is possible for impedance transformation to be achieved in the series-tuned cavity and higher transformation ratios might be obtained compared with those in quarter wavelength transformer designs.





TUNING CAPACITOR

FIGURE 6.1 MICROSTRIPLINE DOUBLERS

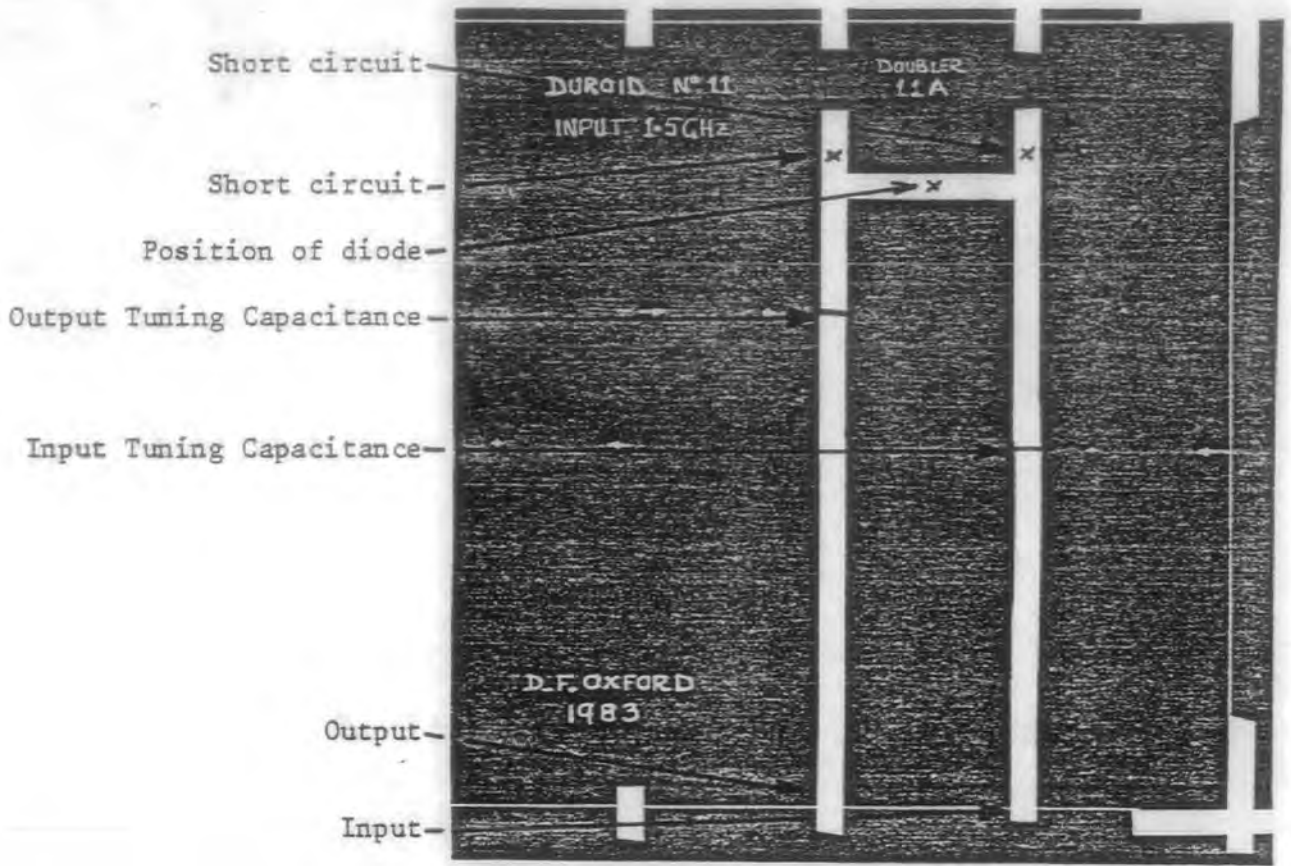


Figure 6.2
Doubler No. 11A

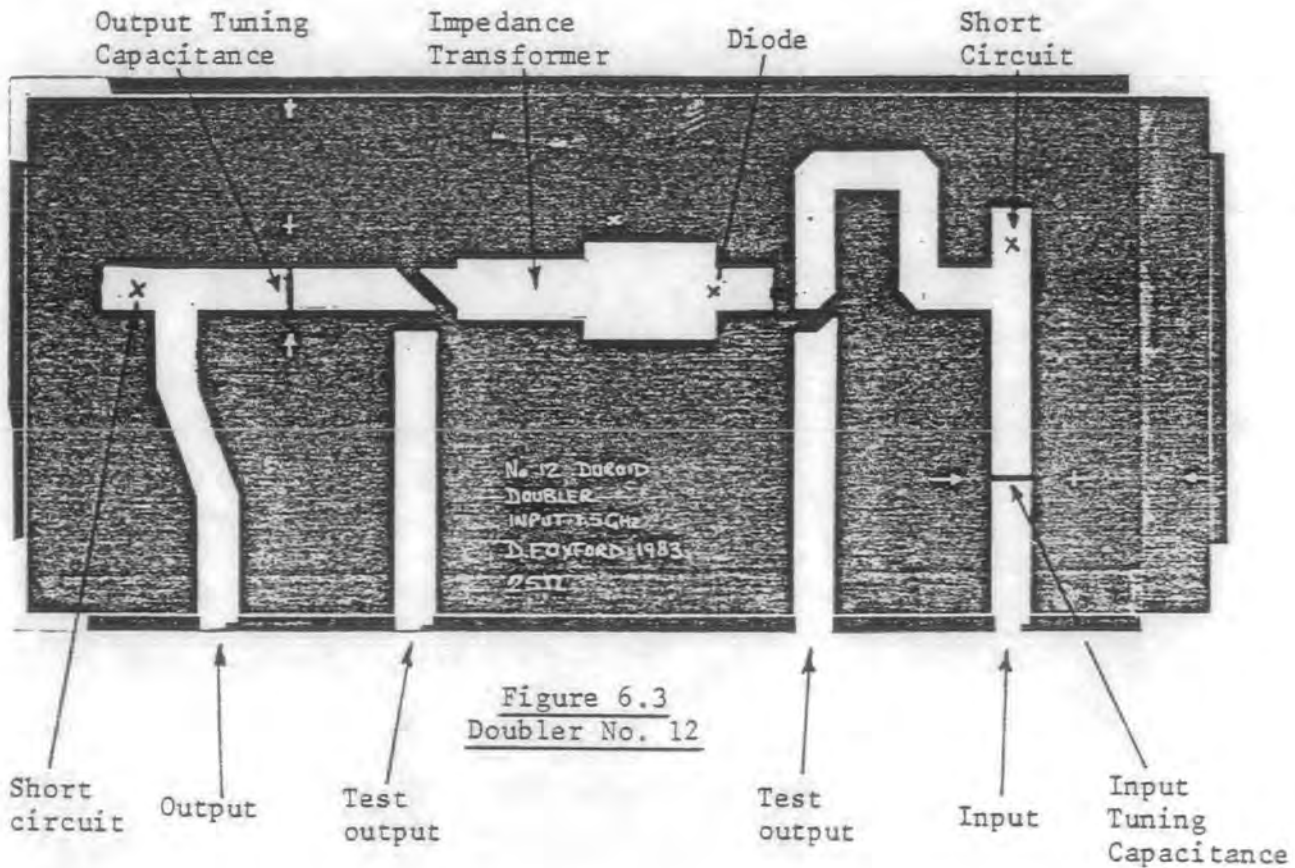


Figure 6.3
Doubler No. 12

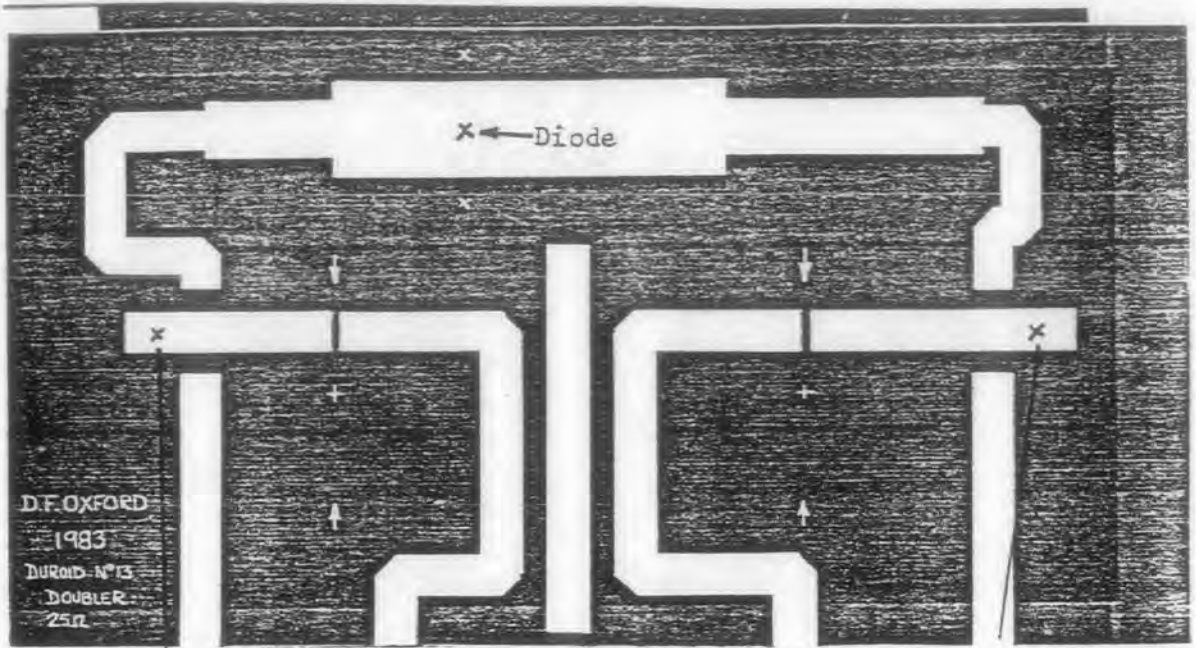


Figure 6.4
Doubler No. 13

Short circuit output Input Short circuit

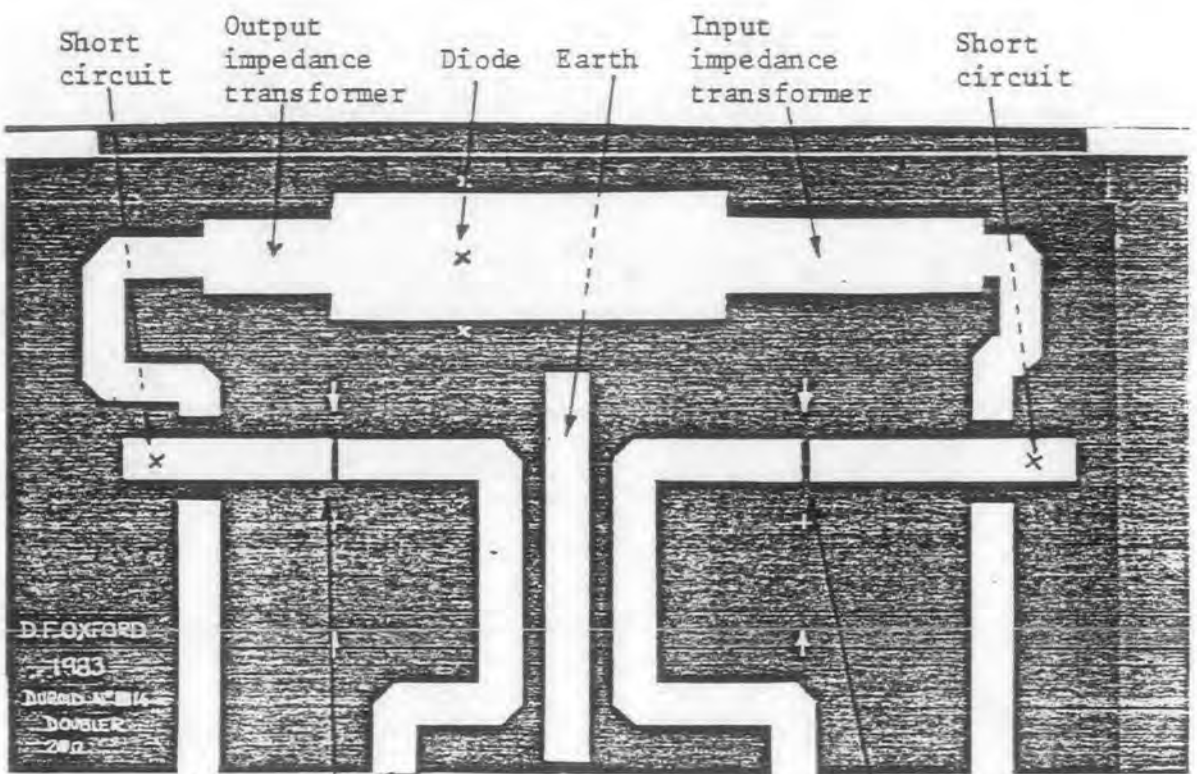
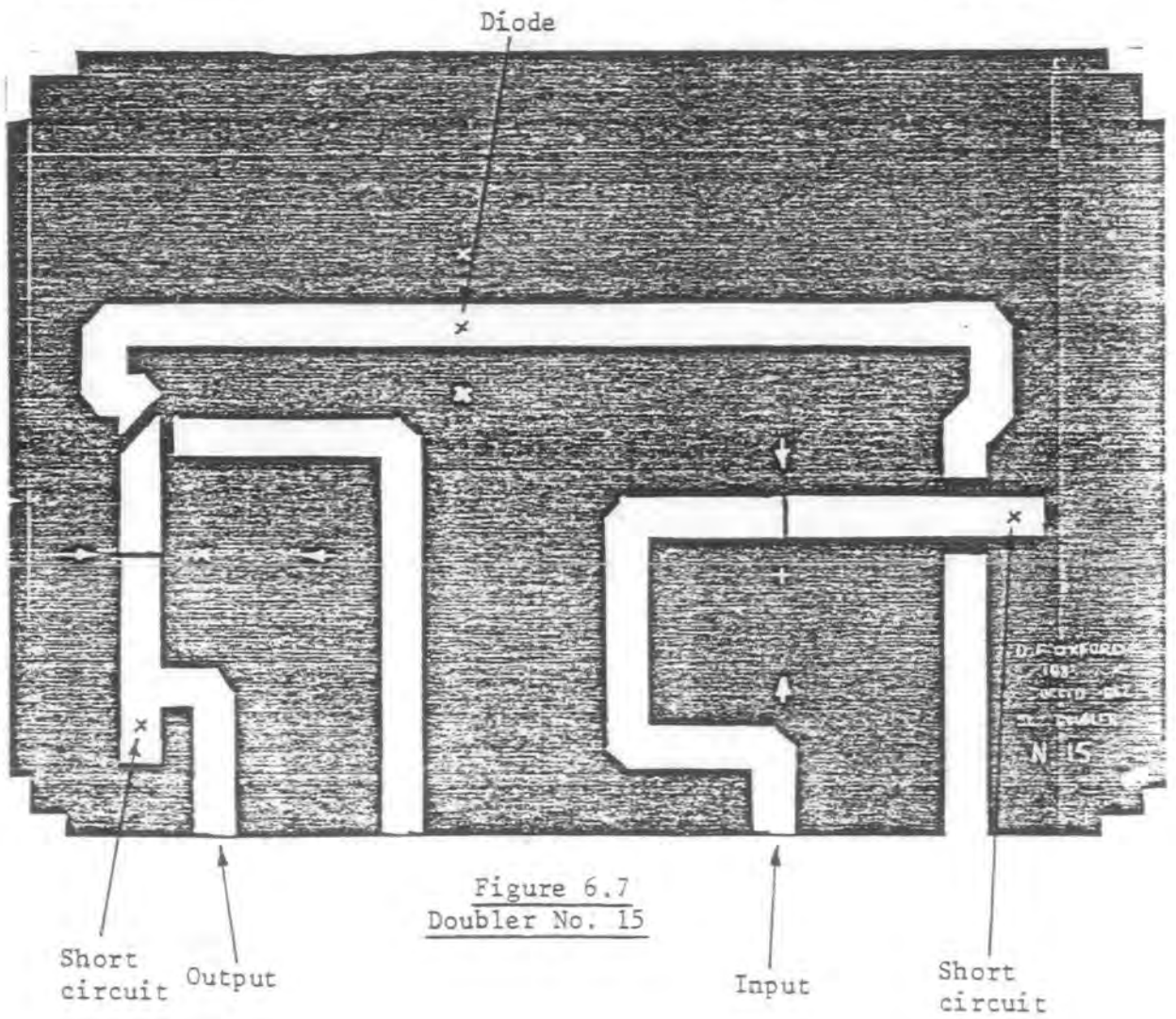
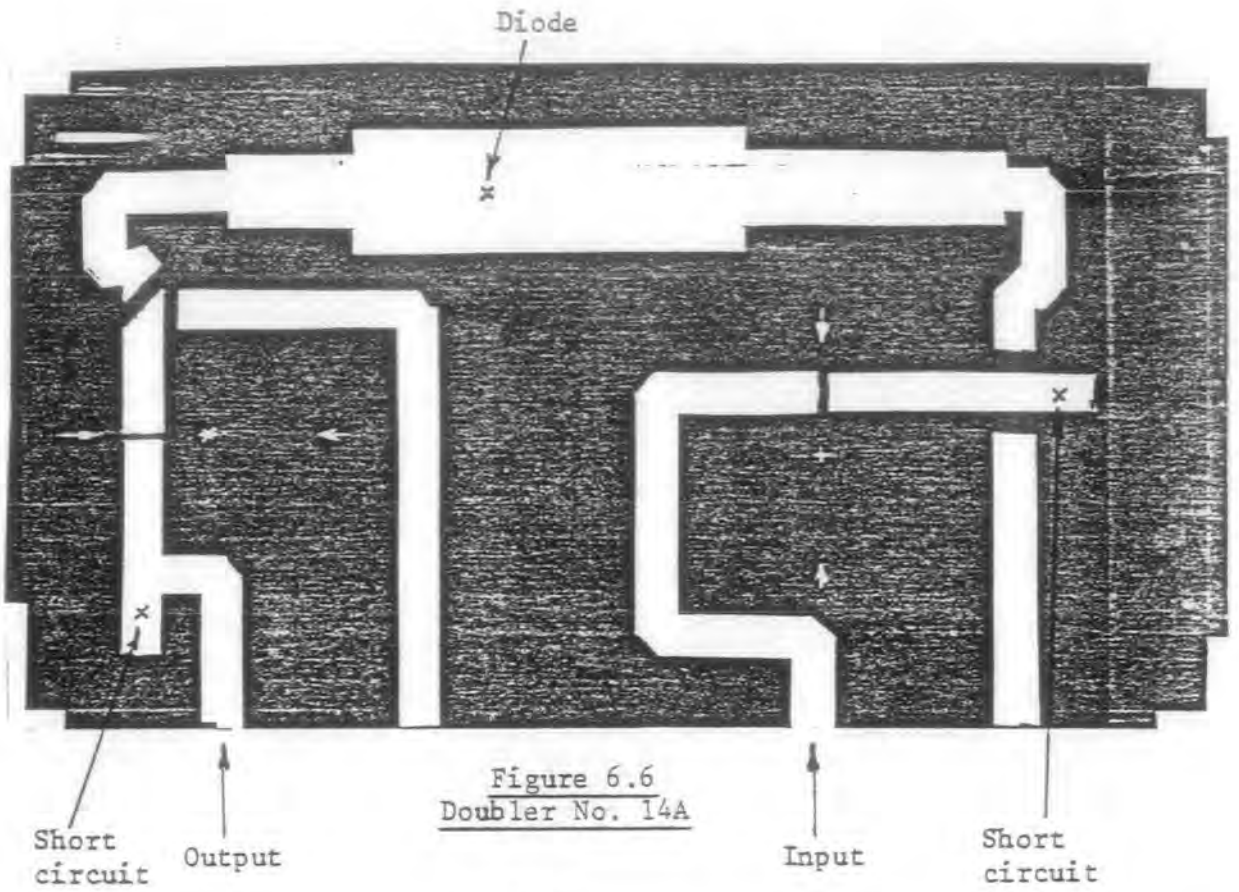


Figure 6.5
Doubler No. 14

Output test connection Output tuning capacitance Input Input tuning capacitance Input test connection



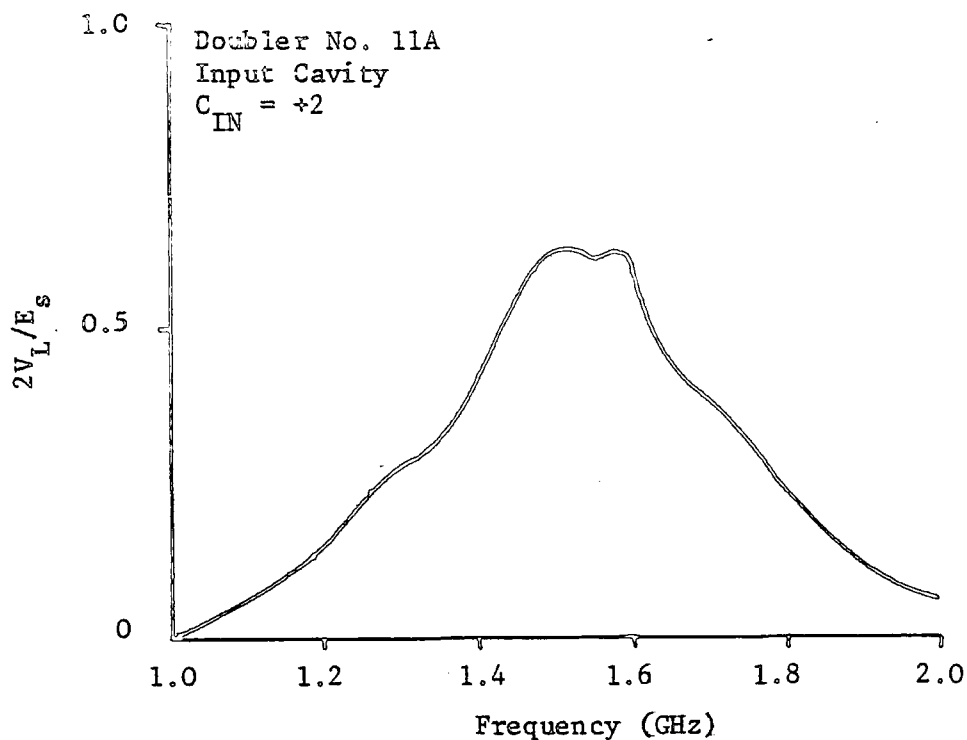


Figure 6.8

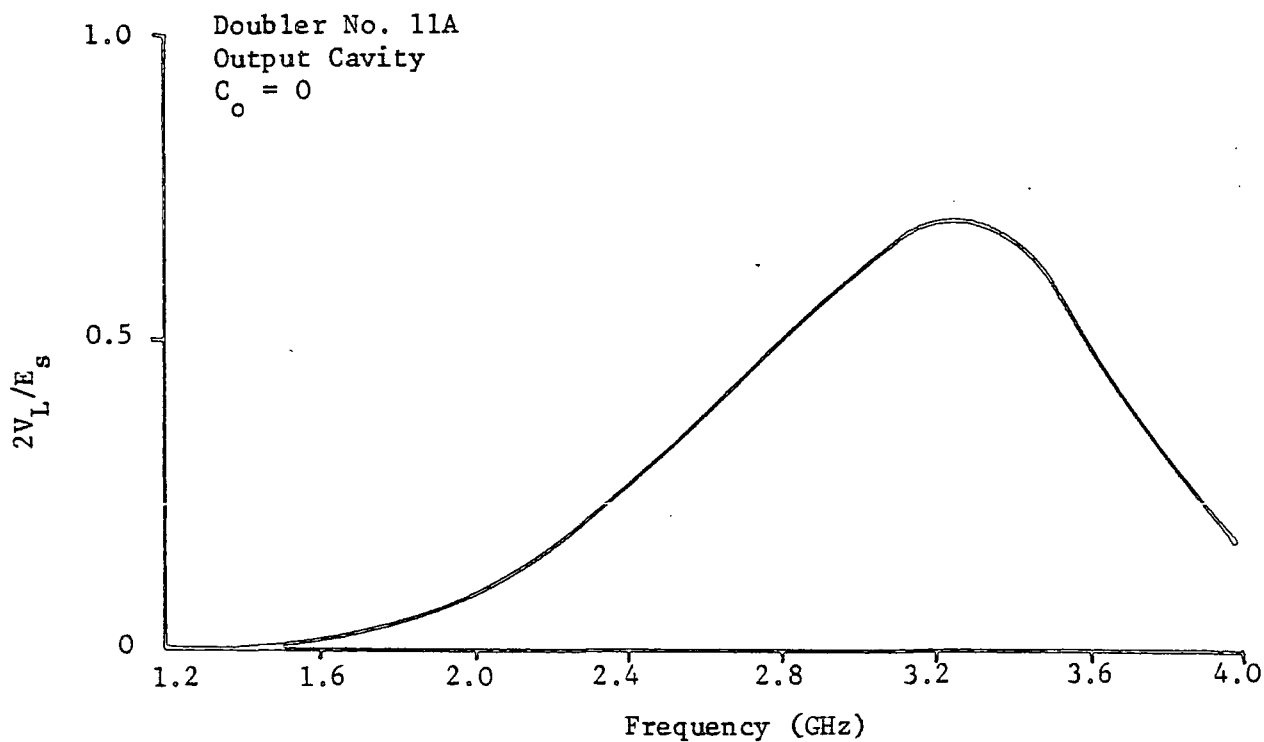


Figure 6.9

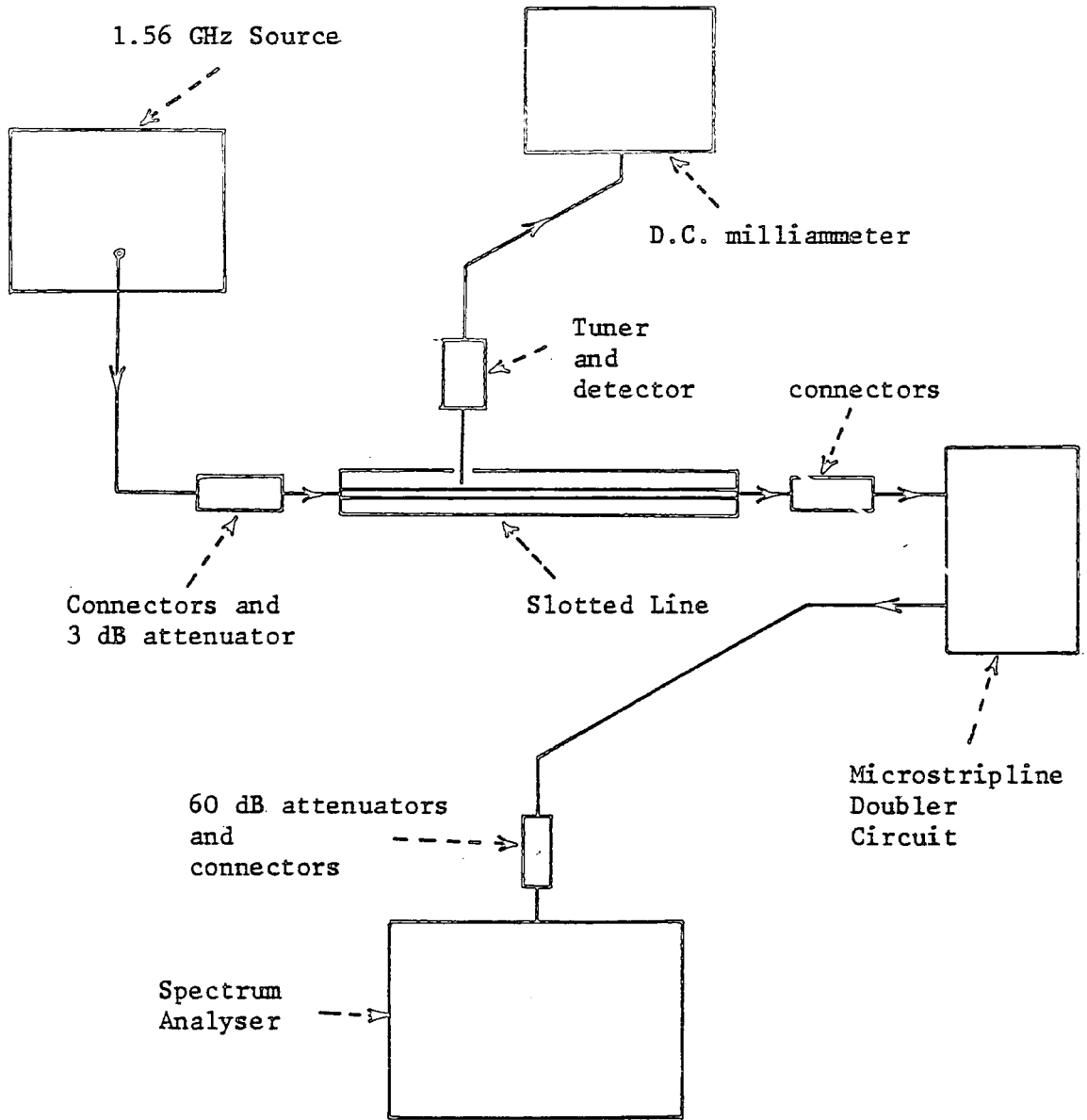


Figure 6.10

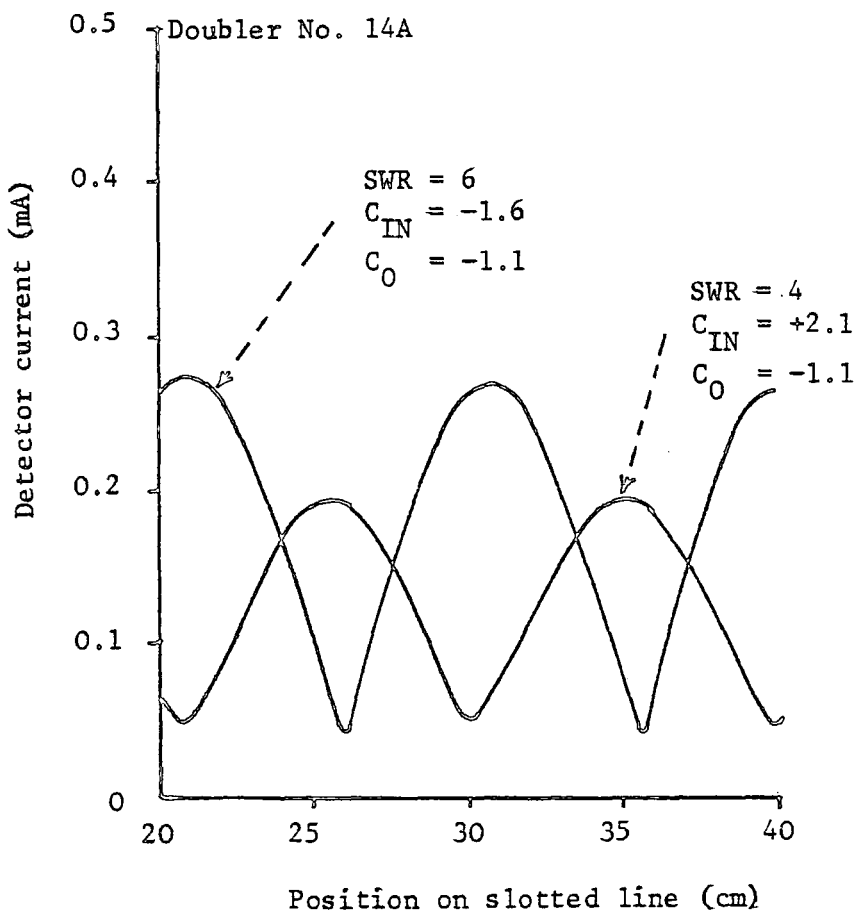


Figure 6.11

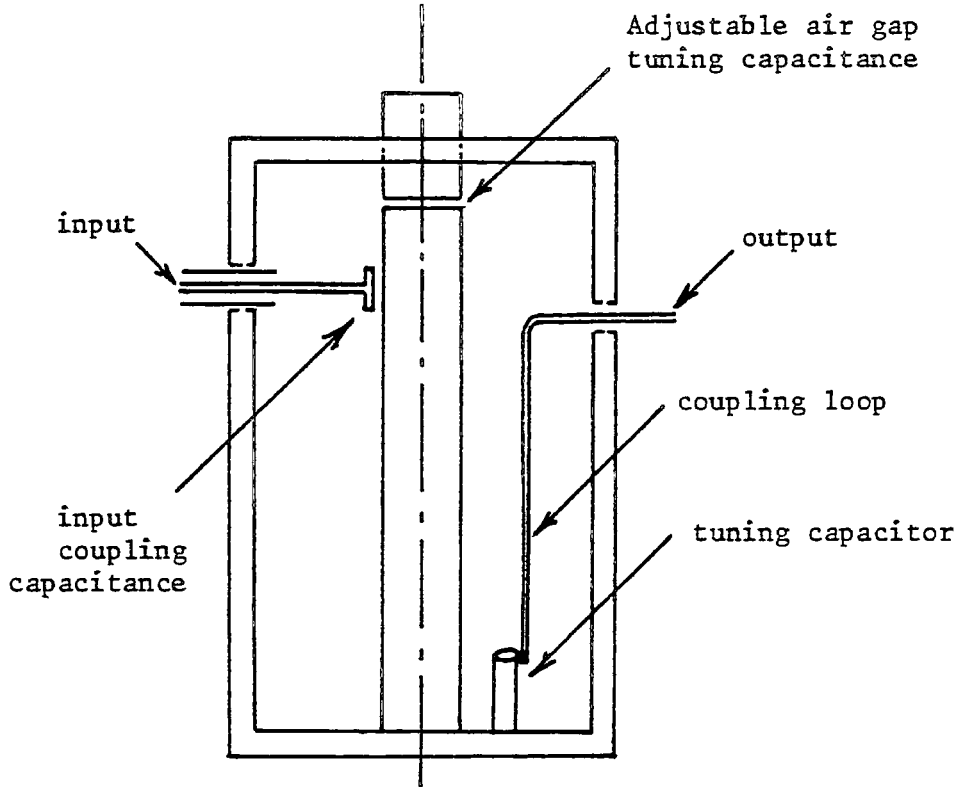


Figure 6.12

Schematic Diagram of
Parallel-tuned Coaxial Cavity

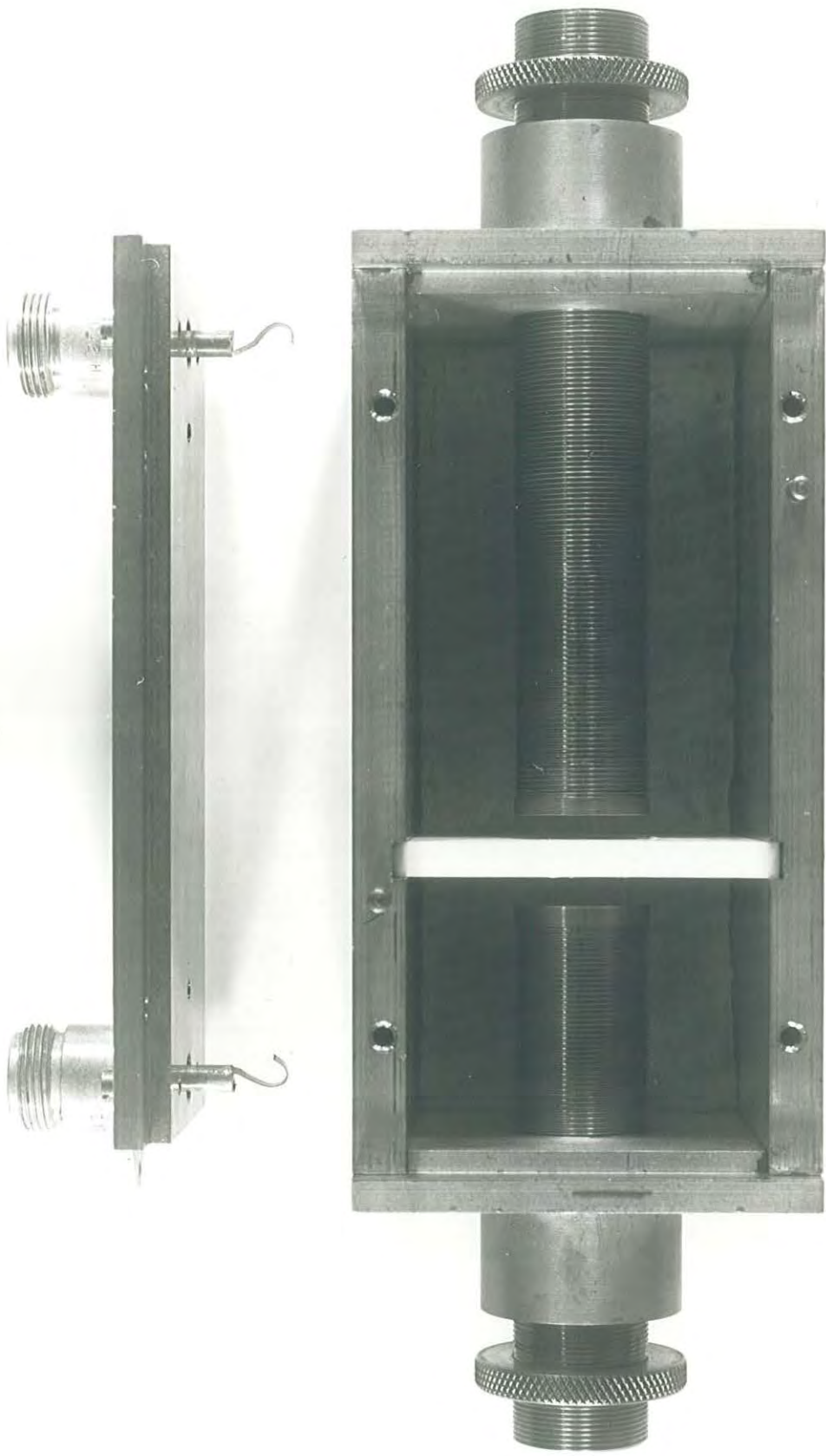


FIGURE 6.13 COAXIAL DOUBLER

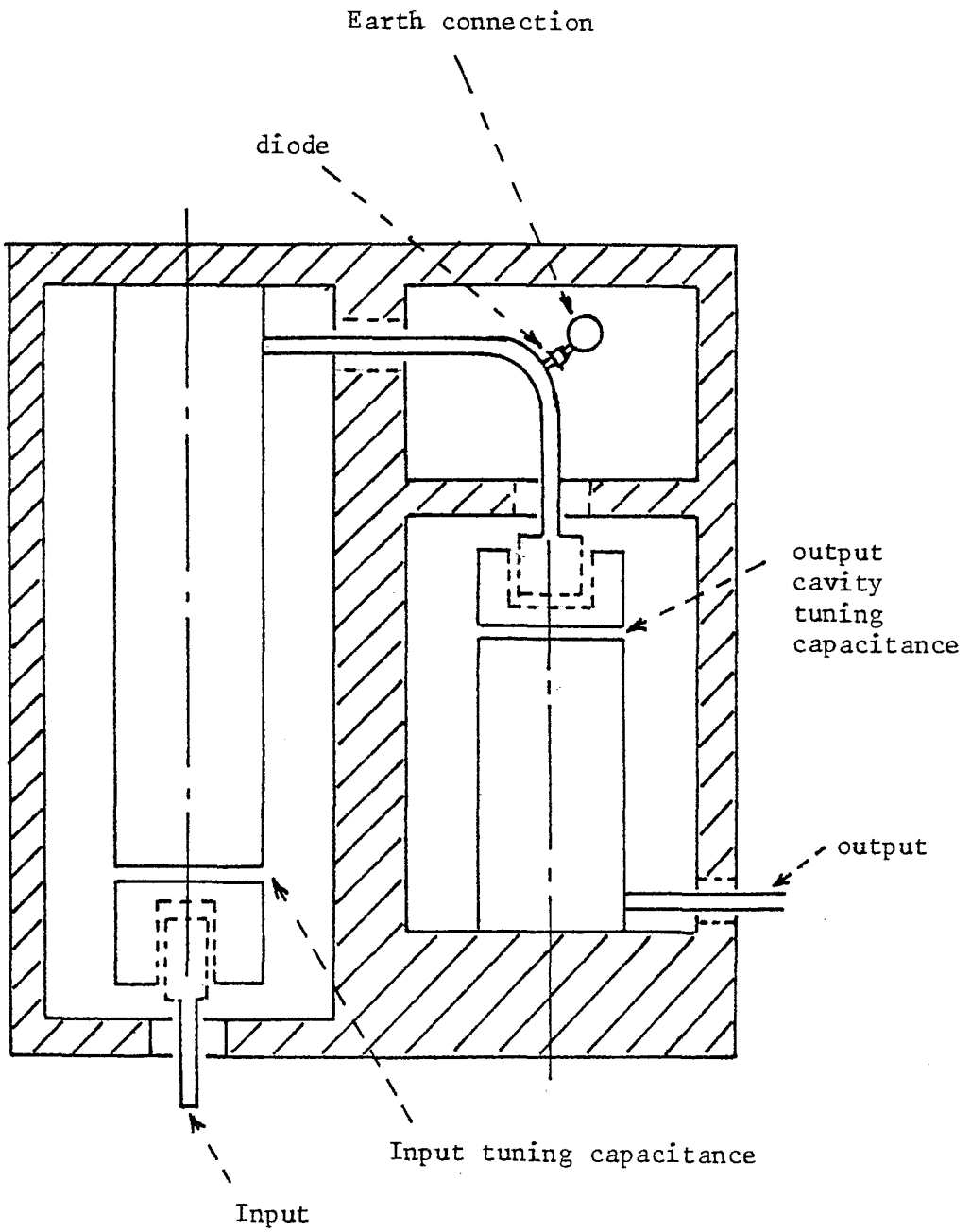


Figure 6.14

CHAPTER 7

CONCLUSION

| | <u>Page</u> |
|--|-------------|
| 7.1 The Analysis of the Multiplier Circuit | 159 |
| 7.2 Practical Multiplier Circuits | 164 |
| 7.3 Future Developments | 167 |

7.1 The Analysis of the Multiplier Circuit

The predictions of the performance of the shunt-diode doubler and tripler which materialize from the analyses are summarized in Table 5.1 in the conclusion to Chapter 5. Formulae are given for the maximum load power from the multipliers in terms of parameters obtained from a spectral test on the diode over a specified part of its characteristic; the measurement of these parameters is a separate problem which is discussed later. The results show that there are definite limits to the amounts of power which can be converted to second and third harmonic output power and that these are dependent upon the parameters \hat{V}_{20} and \hat{V}_{30} . These parameters are the amplitudes of the second and third harmonic voltages generated by the diode when it is excited by a specified amplitude sinusoidal charge variation at fundamental frequency, and they are dependent upon the degree of non-linearity of the diode characteristic. Other researchers have stated that all the input power may be converted to output power (assuming zero losses) if a complex conjugate impedance match is used at the input (reference 18). However, this last statement does not mean that the available power from the source can all be converted to a particular harmonic power.

The second harmonic output power from a doubler is theoretically diminished by the presence of a fourth harmonic in the diode test spectrum and it is probable that similar results would be obtained for a tripler circuit in which the third harmonic output power would be decreased by any sixth harmonic appearing in the diode spectrum. This reduction in output power due to higher harmonic terms in the test spectrum is caused by the production of an output e.m.f. which is in antiphase with the "principal" output e.m.f. Hence the analysis predicts

that a "basic" doubler would produce more output power if the test spectrum of its diode did not contain fourth harmonic.

Note that this assumes that a fourth harmonic current is not allowed to flow anywhere in the circuit.

A number of other researchers (e.g. reference 16) mention that only the second harmonic is present if the diode characteristic has the parameter $\gamma = \frac{1}{2}$, and this agrees with one of the conclusions of Chapter 5 which predicts that a "basic" tripler circuit will produce zero output if its diode test spectrum has no harmonics higher than the second. When an idler is used with the shunt-diode tripler the analysis of Chapter 5 indicates that the third harmonic power may be less than for the basic tripler circuit. It also proposes that the second harmonic output power can be greater when a third harmonic idler is used than for a basic doubler circuit. Results from other researchers have always indicated that the output power is always increased by the use of idlers in that the currents of the two frequencies are said to mix in the non-linear characteristic and produce power at the required sum or difference frequency. The present analysis shows that this may not always be the case and further investigation is required.

The effects of the diode capacitance on the de-tuning of the filters in the input and output circuits are included in the analysis. To a first approximation the input and output capacitances are both equal to the ratio of the test charge amplitude \hat{Q}_{10} to the fundamental component of the voltage generated during the spectrum test, \hat{V}_{10} . This value, symbol C_{10} , is also the output capacitance on no-load when terms up to the fourth harmonic are included in the diode test spectrum. However, for such a test spectrum the input and output capacitances of the diode will

vary as the multiplier output power changes. As the output power is increased from zero (i.e. no load) the input capacitance increases from C_{10} and reaches a maximum value at maximum output power. The output capacitance has a no-load value which is lower than C_{10} and it increases as the output power is increased until it reaches the value C_{10} at maximum output power. The results imply that the output filter would require no re-tuning if the multiplier were required to operate on maximum output power. It is noted that the input and output capacitances depend only upon the fundamental and third harmonic terms in the diode test spectrum in the basic doubler and tripler circuits. In the case of the tripler with second-harmonic idler all the harmonic terms of the diode test spectrum appear in the formulae for input and output capacitance (see Table 5.1).

The results predicted for multiplier operation by the analysis are difficult to prove due to the practical problems involved in finding the test spectrum for the shunt-connected diode. It is possible to measure the spectrum of currents for a reverse-biased diode driven by a sinusoidal voltage and this would give the parameters required for use in the analysis of the series-diode multiplier. If the C_1 -V characteristic of the diode could be calculated from the data in the "series spectrum" then it should be possible to generate the "shunt spectrum" for the diode by a mathematical method. This has not yet been attempted and might form part of a future investigation.

The multiplier circuits analysed in this report have been circuits in which very little forward current is allowed to flow in the diode. Hence the "overdriven case" has not been considered and this is unfortunate in that it generally gives higher output power and efficiency

compared with multipliers which generate harmonics due to the non-linearity of the reverse-biased part of the diode characteristic. In the analysis given by Hamilton and Hall (reference 09) the varactor diode is used as a narrow-pulse generator which gives an output rich in high-order harmonics of the input frequency. In order to apply the present method of analysis the diode would require a spectrum test under conditions in which step-recovery action occurs. In this case the spectrum would probably contain sine and cosine terms and thus the phase of each component would require to be measured. These terms would complicate the analysis as they would give rise to Chebyshev Polynomials of the second kind in the diode characteristic. The first kind and second kind polynomials are defined as $T_n(\theta) = \cos(n \cos^{-1} \theta)$ and $U_n(\theta) = \sin(n \cos^{-1} \theta)$ respectively and their inclusion in the characteristic will lead to many other terms in the multiplier circuit equations. Thus the results might be too complex for interpretation and it might be necessary to evaluate them using the computer in which case the method would have no advantage when compared with a numerical analysis which starts from the diode characteristic.

In all the theoretical work in this report the series resistance of the varactor diode and the losses in the filter circuits have been ignored. This has been done to simplify the analysis so that the important problem of impedance matching would not be obscured. Obviously the usual requirement in diode multipliers is for maximum output power when driven from a specific source, and the main achievement of the present analysis is that a method is proposed by which this can be accomplished. The output resistance R_o has been shown in Chapter 4 to depend upon the multiplier circuit parameters 'a' and 'b' and the ratio $\hat{V}_{20}/\hat{I}_{10}$. When the circuit operates at maximum

power the output resistance has its optimum value, $R_o(\text{opt})$, and this has been evaluated at $0.833 \hat{V}_{20} / \hat{I}_{10}$. For operation at maximum output power the load resistance R_L should be matched to $R_o(\text{opt})$ by impedance transformation and the source e.m.f. and internal resistance should then be chosen to give the required values of the multiplier circuit parameters "a" and "b". The value of source resistance R_s can be transformed to match the input resistance of the circuit and the value of E_s must then be adjusted to obtain the correct values of "a" and "b".

7.2 Practical Multiplier Circuits

The design of the practical multiplier circuits shown in Chapter 6 was developed using the series-tuned cavity as the basic filter circuit. The computer-plotted graphs of the performance of the cavity had been plotted for operation between a source of 50Ω and a load of 50Ω , and thus in the multiplier circuit the cavity was again expected to work between 50Ω resistances, and impedance transforming circuits were inserted between the cavities and the diode. The shunt-connected diode multiplier was chosen because it was easier to mount in the microstrip-line circuit.

Two types of impedance transforming circuit were investigated in the multiplier circuits, namely, the quarter-wavelength transformer and single stub matching. Of the two the former appeared to be the more promising and it was also easier to design. The variables in single stub matching are the position and length of the stub and it was impossible to calculate the required values of these on both input and output sides of the diode. It was also very difficult to adjust the four variables by "trial and error" to attempt to obtain efficient harmonic generation. The quarter-wavelength transformers were much simpler to design as they consisted of a length of line of characteristic impedance Z_{12} which could be found from $\sqrt{Z_1 \cdot Z_2}$ where Z_1 and Z_2 were the impedances which were to be matched. The lengths of these sections were required to be a quarter-wavelength at the relevant frequency i.e. 3.12 GHz in the output circuit and 1.56 GHz in the input circuit.

Several impedance transformations were made using the quarter-wavelength transformer technique and the output powers obtained from the circuits showed an increase as the transformation ratio increased.

The maximum transformation used was from 20Ω to 50Ω with the diode in the $20\text{-}\Omega$ microstripline. Any further decrease in the impedance of the line containing the diode was not carried out as the width of the line was becoming excessive. It was considered that a single diode of the "pill" form might not be properly fed from a wide microstripline and this needed further investigation which was curtailed due to lack of time. One technique which was tested involved the connection of three varactor diodes in parallel across the wide $20\text{-}\Omega$ microstripline but this appeared to make no improvement. A method is perhaps required by which the output circuit transformation ratio is continuously variable and the values of \hat{E}_s and R_s are also separately variable; in the tests carried out here the effective values of \hat{E}_s and R_s were both dependent upon the transformation ratio N_1 . A particular fixed source having emf and internal resistance \hat{E}_s and R_s respectively becomes an effective source of emf \hat{E}_s/N_1 and resistance R_s/N_1^2 and has the same available power. One method of changing the available power would be to use attenuators between the source and the multiplier circuit and it would also be possible to use a microstrip power splitter to drive two doubler circuits in parallel, or push-pull.

One difficulty that was noticed with the circuit used here was the poor selectivity apparently achieved by the output cavity. When the output cavity was separately tuned to the second harmonic frequency of 3.12 GHz (i.e. before connection in the multiplier circuit) the multiplier output at fundamental frequency was usually at least 6 dB below the second harmonic output, but when the cavities were re-tuned for maximum second harmonic output the fundamental output was also considerably increased. It must be concluded that the

series-tuned cavity is a difficult component to use in the multiplier circuit due to the fact that the impedance presented to the cavity by the diode is a value which can change considerably if the circuit conditions vary. This variation in impedance would also, of course, degrade the performance of most other filter circuits.

There were considerable difficulties in converting the theoretical multiplier circuit into a practical design but the experience gained during the project is invaluable and it is felt that the foundations have been laid for the design of microstrip series-tuned cavity multipliers. However, if high output power is the main consideration then the step-recovery type of multiplier could need to be given more attention, and the microstrip parallel-tuned cavity should also be investigated.

7.3 Future Developments

An important investigation which was not made due to lack of time was the measurement of the parameters \hat{V}_{10} , \hat{V}_{20} , \hat{V}_{30} etc for the diode. One method of finding these parameters which may be used in the future would involve the multiple reflections which occur when the diode terminates a slotted line which also has a mismatch at the generator end. In this case standing waves exist on the slotted line at fundamental and harmonic frequencies and from their measurement the spectrum generated in the diode may be calculated. This method could be used to check the measurement of the spectrum of the series-connected diode which can be obtained by more conventional means.

It would be useful to investigate the performance of the series-tuned cavity with load resistances having various values in the range 1Ω to 20Ω . This would entail computer calculations which would give the filter frequency response of the cavity when matching the $50\text{-}\Omega$ source or load to the diode impedance.

Other practical objectives which should be pursued include the verification of the results predicted for the operation of the multiplier with idler. This might be rather easier than the verification of the basic multiplier circuit operation as the second harmonic output could be observed, for example, as the third harmonic load was varied.

Further theoretical work would also be useful on the subjects covered in this project. One such topic is the connection between the "series spectrum" and the "shunt spectrum" of a diode, as mentioned in section 7.1, which would be useful for deriving the latter from the former which happens to be much more easily measured.

The application of the method of analysis to the "overdriven case", which has also been discussed in section 7.1, might, if successful, yield useful results on the impedance matching which is needed in step-recovery multiplier circuits. Another application for the analysis is the multiplier circuit which uses either the silicon or gallium arsenide avalanche diode, a relatively recent circuit which is used for multiplication in the range 10 GHz to 100 GHz. When multipliers are used in chains the load presented by the second stage on the first stage obviously affects the operating conditions of that stage and vice versa. The problem here is to operate both stages in the best conditions so that the final output power reaches the desired level. The interdependence of the two stages could be responsible for the generation of spurious frequency components and an investigation might discover the mechanism by which they occur. Thus the analysis could produce some very useful results but the full verification of doubler operation should first be made.

REFERENCES

01. ACCATINO, L., and ANGELUCCI, A.
"A Ku-Band Times Six Microstrip SRD Multiplier" CSELT Rapporti
Tecnici, Vo. VII, No. 2, Giugno 1979.
02. ARMSTRONG, R.
"Spectral Identification of Non Linear Devices"
PhD Thesis, University of Durham, 1983.
03. BENEDEK, R., and SILVESTER, P.
"Equivalent Capacitances for Microstrip Gaps and Steps"
IEEE Trans on Microwave Theory and Techniques, Vol. MTT-20,
No. 11, November 1972, pp. 29-733.
04. BURCKHARDT, C.B.
"Analysis of Varactor Frequency Multipliers for Arbitrary
Capacitance Variation and Drive Level", BELL SYSTEM TECH J.
Vol. 44, p. 75, 1965.
05. CRISTAL, R.G.
"Coupled Circular Cylindrical Rods Between Parallel Ground Planes"
I.E.E.E. Trans on Microwave Theory & Techniques, Vol. MTT-12,
pp. 428, July 1964.
06. EMMETT, J.R.
"Microwave Lattice Mixers at 4.5 GHz"
PhD Thesis, University of Durham, 1974.
07. FLEMING, M.A.
"Microstrip Circuits and Filters on Printed Circuit Board Substrates"
Report, Ukaea, Harwell, Oxon, England, August 1979, available from
HMSO, London, England.
08. GARDINER, J.G., and WAGIEALLA, W.Z.
"The Step-Recovery Diode in Series Mode Harmonic Generation"
University of Bradford, Post Graduate School of Electrical and
Electronic Engineering, Report No. 44, 1973.

09. HAMILTON, S., and HALL, R.
"Shunt-Mode Harmonic Generation using The Step Recovery Diode"
Microwave Journal, pp. 69-78, April 1967.
10. HEWLETT PACKARD
Application Note 928 "Ku-Band Step Recovery Multipliers".
11. HEWLETT PACKARD
"A Frequency Doubler with High Output Power from 18 to 26.5 GHz"
H.P. Journal, Volume 33, No. 2, February 1982.
12. KELLEY, D. et al
"Microstrip Filters and Couplers"
IEEE Trans. on Microwave Theory and Techniques, August 1968,
pp. 560-562.
13. KOMPA, G., and MEHRAN, R.
"Planar Waveguide Model for Calculating Microstrip Components"
Electron-Letters, 1975, Vol. 11, pp. 459-460.
14. KOTZEBUE, K.L.
"A Circuit Model of the Step-Recovery Diode"
Proc. IEEE, Correspondence, December 1965, pp. 2119-2120.
15. KRAMER, B.M., DERYCKE, A.C., FARRAYRE, A., and MASSE, C.F.
"High-Efficiency Frequency Multiplication with GaAs Avalanche Diodes"
IEEE Trans. on Microwave Theory & Techniques, November 1976, pp. 861-863.
16. KULESZA, B.L.J.
"Highly Efficient Harmonic Generation using Varactors with Hyper-
Abrupt Junctions"
Electronic Communicator, Vol. 1, No. 4, July/August 1966, p. 10.
17. KULESZA, B.L.J.
"Efficient Harmonic Generation and Frequency Changing using
Semiconductor Devices"
PhD Thesis, University of Birmingham, October 1967.

18. LEESON, D.B. and WEINREB, S.
"Frequency Multiplication with Non-Linear Capacitors - A Circuit Analysis" Proc. Inst. Radio Engineers, Vol. 46, pp. 2076-2084, December 1959.
19. MAKIMOTE, M. and YAMASHITA, S.
"Bandpass Filters using Parallel Stepped Impedance Resonators" IEEE Trans on Microwave Theory and Techniques, Vol. MTT-28, No. 12, December 1980, pp. 1413-1417.
20. MANLEY, J.M, and ROWE, H.E.
"Some General Properties of Non Linear Elements - Part I General Energy Relations"
Proc. IRE. Vol. 44, pp. 904-913, July 1956.
21. MATTHAEI, G.L.
"Interdigital Band-Pass Filters"
IEEE Trans. on Microwave Theory and Techniques, Vol. MTT-10, pp. 479-491, November 1962.
22. MATTHAEI, G.L.
"Comb-Line Band-Pass Filters of Narrow or Moderate Bandwidth"
Microwave Journal, Vol. 6, pp. 82-96, August 1963.
23. MATTHAEI, G.L., YOUNG, L., and JONES, E.M.T.
Book, "Microwave Filters, Impedance Matching Networks and Coupling Structures"
McGraw-Hill, 1964.
24. MOLL, J.L., KRAKAUER, S., and SHEN, R.
"P-N Junction Charge-Storage Diodes"
Proc. IRE, January 1962, pp. 43-53.
25. MONTGOMERY, C.G., RICKIE, R.H., and PURCELL, E.M.
Book, "Principles of Microwave Circuits"
pp. 208-239, Radiation Laboratory Series, McGraw-Hill, 1948.

26. MOTOROLA
Schaffner, G. (Editor)
"Design Tips for Coaxial-Cavity Varactor Multipliers"
Application Note AN-159
Motorola Semiconductor Products Inc.
27. NUYTS, W., and VAN OVERSTRAETEN, R.J.
"Numerical Calculations of the Capacitance of Linearly Graded
Si P-N Junctions"
Electronic Letters 5, pp. 54-55, 6th February 1969.
28. PAGE, C.H.
"Harmonic Generation with Ideal Rectifiers",
Proc. IRE, Vol. 46, pp. 1738-1740, October 1958.
29. PENFIELD, P., and RAFUSE, R.P.
Book, "Varactor Applications"
M.I.T. 1962.
30. PETROV, B.Y.
"Stability of Steady States of Varactor Frequency Multipliers"
Radio Engineers and Electronic Physics, Vol. 21, Part 6,
pp. 81-89, 1976.
31. ROLLAND, P.A., SALMER, G., DERYCKE, A., and MICHEL, J.
"Very-High-Rank Avalanche Diode Frequency Multiplier"
Proc. IEEE, December 1973, pp. 1757-1758.
32. SAUL, P.H.
"Evaluation of a Step-Recovery Diode in a Broad-Band Frequency
Multiplier"
PhD Thesis, University of Durham, 1974.
33. SCANLAN, J.O., and LAYBOURN, P.J.R.
"Large Signal Analysis of Varactor Harmonic Generators without
Idlers"
Proc. IEE, 1965, Vol. 112, pp. 1515-1520.

34. SCANLAN, J.O., and LAYBOURN, P.J.R.
"Analysis of Varactor Multipliers with Idlers"
The Radio and Electronic Engineer, Vol. 31, No. 6, pp. 35 -367,
June 1966.
35. SCANLAN, J.O., and LAYBOURN, P.J.R.
"Analysis of Varactor Harmonic Generators with Arbitrary Drive
Levels"
Proc. IEEE, Vol. 14, No. 11, pp. 1598-1604, November 1967.
36. SCHNEIDER, M.V.
"Microstrip Lines for Microwave Integrated Circuits"
B.S.T.J. May-June 1969, pp. 1421-1444.
37. SCHNEIDER, M.V.
"Microstrip Dispersion"
Proc. IEEE, 1972, Vol. 60, pp. 144-146.
38. SMITH, R.B., and BRAMER, B.
"Measurement of Varactor Capacitance Parameters"
The Radio and Electronic Engineer, Vol. 42, No. 8, pp. 381-387,
August 1972.
39. STINEHELFER, H.E.
"An Accurate Calculation of Uniform Microstrip Transmission Lines"
IEEE Trans on Microwave Theory & Techniques, Vol. MTT-16, No. 7,
1968, pp. 439-444.
40. TANG, C.C.H.
"An Exact Analysis of Varactor Frequency Multipliers"
IEEE Trans. on Microwave Theory and Techniques, Vol. MTT-14,
pp. 210-212, April 1966.
41. UHLIR, A.
"The Potential of Semiconductor Diodes in High-Frequency Communications"
Proc. IRE. Vol. 46, pp. 1099-1115, June 1958.

42. WHEELER, H.A.

"Transmission-Line Properties of Parallel Strips Separated by
a Dielectric Sheet"

IEEE. Trans. on Microwave Theory & Techniques, Vol. MTT-13,
1965, pp. 172-185.

(A1)

APPENDICES TO CHAPTER 2

Page

2(i) List of symbols

A2

Appendix 2(i)List of Symbols

Note that in a few cases a symbol has been used for more than one parameter, but this does not cause confusion as it is always clear which parameter is meant from the context in which it is found.

- | | | |
|--------|----------|---|
| 1. | A | Ratio of DP to DC |
| 2. | A_c | Plate area of tuning capacitor for coaxial cavity |
| 3(i). | a | Radius of inner conductor in coaxial transmission line |
| 3(ii). | a | Ratio of the fundamental charge variation in the diode in a shunt multiplier circuit to the fundamental charge variation used in finding the test spectrum of the diode |
| 4(i). | b | Radius of outer conductor in coaxial transmission line |
| 4(ii). | b | Ratio of the second harmonic charge variation in the diode in a shunt multiplier circuit to the fundamental charge variation used when finding the test spectrum of the diode |
| 5. | C_{IN} | Input capacitance |
| 6. | C_i | Incremental capacitance of varactor diode |
| 7. | C_m | Capacitance per unit length of transmission line |
| 8. | C_o | Output capacitance |
| 9. | C_o^v | Incremental capacitance of diode at $V_a = \text{zero}$ |
| 10. | C_{O2} | Output capacitance at 2nd harmonic frequency |

11. C_{03} Output capacitance at 3rd harmonic frequency
12. C_S Capacitance of series tuning capacitor at input of short-circuited transmission line cavity
13. C_{SN} Value of C_S which produces series resonance with the unloaded cavity when θ has a specific value θ_0
- 14(i). c Velocity of e.m. waves in vacuum
- 14(ii). c Ratio of the third harmonic charge variation in the diode in a shunt multiplier circuit to the fundamental charge variation used when finding the test spectrum of the diode
15. DC Length of short-circuited transmission line cavity
16. DP Distance between position of probe and short-circuit end of cavity
17. d_c Distance between plates of tuning capacitor for coaxial cavity
18. E_S E.m.f. of signal source
19. E_2 E.m.f. at second harmonic frequency
20. E_3 E.m.f. at third harmonic frequency
21. $F_1(a)$ Function used in multiplier analysis
to $F_7(a)$
22. f Frequency
23. f' Normalised frequency: ratio of f to f_{cav}
24. f_{CAV} Frequency at which cavity is a quarter wavelength long
25. f_0 Series resonant frequency of the unloaded cavity when value of C_S is C_{SN} and value of θ is θ_0

| | | |
|-----|-------------|--|
| 26. | f_o | Normalised value of f_o ; ratio of f_o to f_{CAV} |
| 27. | G | Available power gain; ratio of P_L to P_A |
| 28. | G_m | Shunt conductance per metre length of transmission line |
| 29. | h | Thickness of dielectric in microstrip line |
| 30. | \hat{I}_n | Amplitude of current of harmonic frequency of order n |
| 31. | i_o | Input current producing cosinusoidal charge variation for generation of diode voltage spectrum |
| 32. | L | Insertion loss in dB |
| 33. | L_m | Inductance per unit length of transmission line |
| 34. | log | Logarithm to the base 10 |
| 35. | ln | Natural logarithm to the base "e" |
| 36. | P_A | Power available from the signal source |
| 37. | P_L | Load power |
| 38. | P_1 | Input power at fundamental frequency |
| 39. | P_2 | Load power at second harmonic frequency |
| 40. | P_3 | Load power at third harmonic frequency |
| 41. | Q | Charge |
| 42. | Q_B | Bias charge on varactor |
| 43. | Q_{BD} | Charge on varactor diode at breakdown voltage |
| 44. | Q_d | Total charge on the p-side of diode junction |

| | | |
|-----|-------------|--|
| 45. | Q_i | Charge injected into diode |
| 46. | \hat{Q}_n | Amplitude of charge of harmonic frequency of order n |
| 47. | Q_{no} | Open-circuit harmonic charges developed on the varactor diode when driven by the test voltage of cosinusoidal form |
| 48. | q | Normalised charge variation on varactor diode |
| 49. | $R_{i/p}$ | Resistive part of Z_{IN} |
| 50. | $R_{i/p}^v$ | Real part of Z_{IN}^v ; ratio of $R_{i/p}$ to Z_o |
| 51. | R_L | Load resistance |
| 52. | R_L^v | Reflected load resistance in the equivalent input circuit of the diode multiplier |
| 53. | R_m | Series resistance per metre length of transmission line |
| 54. | R_S | Resistance of signal source |
| 55. | R_2 | Load resistance at second harmonic frequency |
| 56. | R_3 | Load resistance at third harmonic frequency |
| 57. | R_{30} | Ratio of \hat{V}_{30} to \hat{I}_{10} |
| 58. | $T_n(\)$ | Chebyshev polynomial of order n |
| 59. | τ | Thickness of conductor in microstrip line |
| 60. | V | Voltage |
| 61. | V_a | Voltage across the varactor diode |
| 62. | V_B | Bias voltage on the varactor |
| 63. | V_{BD} | Breakdown voltage of the varactor diode |

| | | |
|-----|-------------|---|
| 64. | V_L | Voltage across the load impedance Z_L |
| 65. | V_O | Voltage spectrum produced by varactor diode driven by cosinusoidal charge variation |
| 66. | V_{OC} | E.m.f. of Thévenin equivalent circuit |
| 67. | V_{OC}' | Ratio of V_{OC} to E_S |
| 68. | \hat{V}_n | Amplitude of voltage of harmonic frequency of order n |
| 69. | V_{no} | Open-circuit harmonic voltages developed in the varactor diode when driven with a cosinusoidal charge variation |
| 70. | v | Normalised voltage generated in the varactor diode |
| 71. | w | Width of conductor in microstrip line |
| 72. | $X_{i/p}$ | Reactive part of Z_{IN} |
| 73. | $X_{i/p}'$ | Imaginary part of Z_{IN}' ; ratio of $X_{i/p}$ to Z_0 |
| 74. | X_L | Inductive reactance used to re-tune the output circuit of the multiplier |
| 75. | X_I | Inductive reactance used to re-tune the input circuit of the multiplier |
| 76. | Z_{IN} | Input impedance of the loaded cavity including the tuning capacitor C_S |
| 77. | Z_{IN}' | Normalised value of Z_{IN} ; ratio of Z_{IN} to Z_0 |
| 78. | Z_{in} | Input impedance |
| 79. | $Z_{i/p}$ | Input impedance of the loaded cavity, not including tuning capacitor C_S |
| 80. | Z_L | Load impedance |
| 81. | Z_L' | Normalised load impedance; ratio of Z_L to Z_0 |

| | | |
|---------|------------------------|--|
| 82. | Z_0 | Characteristic impedance of transmission line |
| 83. | Z_{0A} | Characteristic impedance of microstrip assuming relative permittivity of dielectric is 1 |
| 84. | $Z_{o/p}$ | Output impedance of Thevenin equivalent circuit |
| 85. | $Z_{o/p}'$ | Ratio of $Z_{o/p}$ to Z_0 |
| 86. | Z_{SC} | Input impedance of transmission line terminated in a short circuit |
| 87. | Z_T | Terminating impedance |
| 88. | β | Phase change constant per unit length of transmission line |
| 89(i). | γ | Propagation constant per unit length of transmission line |
| 89(ii). | γ | Constant in varactor diode characteristic |
| 90. | ϵ_{eff} | Effective relative permittivity in microstrip line |
| 91. | ϵ_0 | Permittivity of free space |
| 92. | ϵ_r | Relative permittivity of the dielectric of a transmission line |
| 93. | λ | Wavelength |
| 94. | λ_G, λ_m | Wavelength in microstrip line |
| 95. | λ_0 | Free-space wavelength |
| 96(i). | θ | Electrical length of cavity in radians |
| 96(ii). | θ | Used as wt |
| 97. | θ_0 | Value of θ for the cavity at the frequency f_0 |

- 98(i). ϕ Electrical length in radians equivalent to the distance $D\beta$
- 98(ii). ϕ Work function, used in varactor diode characteristic
- 98(iii). ϕ Phase angle
99. μ_0 Permeability of free space
100. μ_r Relative permeability of the dielectric of a transmission line
101. ω Angular frequency

APPENDICES TO CHAPTER 4

| | <u>Page</u> |
|---|-------------|
| 4(i) To show that the coefficients of the Chebyshev Expansion representing a non-linear characteristic are the magnitudes of the harmonics obtained by driving the non-linear characteristic with a cosinusoidal drive. | A10 |
| 4(ii) Derivation of equation (4.24) from equation (4.23). | A14 |
| 4(iii) Derivation of equation (4.66) from equation (4.65). | A15 |
| 4(iv) Extra terms due to inclusion of terms $\hat{V}_{40} T_4(q)$ in the diode characteristic. | A16 |
| 4(v) Four-term Approximation to the Diode Characteristic. | A18 |
| 4(vi) The derivation of a formula for the output resistance of the diode at the harmonic output frequency. | A21 |

Appendix 4 (i)

To show that the coefficients of the Chebyshev Expansion representing a non-linear characteristic are the magnitudes of the harmonics obtained by driving the non-linear characteristic with a cosinusoidal drive.

Equation (4.9) expresses the characteristic of the diode,

$$V = f(Q)$$

in the form of the sum of Chebyshev Polynomials $T_n(q)$ where q is the normalised charge deviation from the bias value. In the proof given below, the variable q is replaced by x and the variable V is replaced by y .

Equation (4.16) expresses the characteristic of the diode,

$$Q = f(v)$$

in the form of the sum of Chebyshev Polynomials $T_n(v)$ where v is the normalised voltage deviation from the bias value. In the proof given below, the variable v is replaced by x and the variable Q is replaced by y .

Proof:

Let the non-linear characteristic be given by the power expansion given in equation (1) and the sum of the Chebyshev Polynomials in equation (2).

$$y = a_0 + a_1x + a_2x^2 + a_3x^3 + \dots \quad (1)$$

$$y = c_0 + c_1T_1(x) + c_2T_2(x) + c_3T_3(x) \dots \quad (2)$$

Note that the Chebyshev Polynomials are defined as in (3) below,

$$T_n(x) = \cos(n \cos^{-1} x) \quad (3)$$

If we make x vary with time, i.e. apply a drive to the characteristic (2) given by equation (4) below then result (5) would be obtained.

$$x = \cos \omega t = \cos \theta \quad (4)$$

Substitute (4) into (2),

$$y = c_0 + c_1 T(\cos \theta) + c_2 T_2(\cos \theta) + c_3 T_3(\cos \theta) \dots$$

$$\therefore y = c_0 + c_1 \cos(\cos^{-1} \cos \theta) + c_2 \cos(2 \cos^{-1} \cos \theta) \\ + c_3 \cos(3 \cos^{-1} \cos \theta) + \dots$$

$$\therefore y = c_0 + c_1 \cos \theta + c_2 \cos 2\theta + c_3 \cos 3\theta + \dots \quad (5)$$

The equation (5) shows that the amplitudes of the harmonics generated when the non-linear characteristic given in (1) and (2) is driven by the sinusoidal function given in (4) are the coefficients of the Chebyshev terms used in the characteristic in (2).

Thus it can be concluded that the diode characteristic may be written as either equation (4.9) or equation (4.16)

It is useful to see how the 'c' coefficients are related to the 'a' coefficients used in (1). The Chebyshev Polynomials are given below in equations (6) to (11).

$$T_0(x) = 1 \quad (6)$$

$$T_1(x) = x \quad (7)$$

$$T_2(x) = 2x^2 - 1 \quad (8)$$

$$T_3(x) = 4x^3 - 3x \quad (9)$$

$$T_4(x) = 8x^4 - 8x^2 + 1 \quad (10)$$

$$T_5(x) = 16x^5 - 20x^3 + 5x \quad (11)$$

Substituting these into (2),

$$y = c_0 + c_1x + c_2(2x^2 - 1) + c_3(4x^3 - 3x) + c_4(8x^4 - 8x^2 + 1) \\ + c_5(16x^5 - 20x^3 + 5x) \quad (12)$$

Equating coefficients of powers of x in equations (1) and (12)

we can obtain the following results:-

$$a_0 = c_0 - c_2 + c_4 \dots \quad (13)$$

$$a_1 = c_1 - 3c_3 + 5c_5 \dots \quad (14)$$

$$a_2 = 2c_2 - 8c_4 + \dots \quad (15)$$

$$a_3 = 4c_3 - 20c_5 + \dots \quad (16)$$

$$a_4 = 8c_4 - \dots \quad (17)$$

$$a_5 = 16c_5 - \dots \quad (18)$$

The advantage of the Chebyshev representation for the non-linear characteristic is that each term in the series improves the approximation of the law.

It can similarly be shown that,

$$c_0 = a_0 + \frac{1}{2}a_2 + \frac{3}{8}a_4 + \dots \quad (19)$$

$$c_1 = a_1 + \frac{3}{4}a_3 + \frac{5}{8}a_5 + \dots \quad (20)$$

$$c_2 = \frac{1}{2}a_2 + \frac{1}{4}a_4 + \dots \quad (21)$$

$$c_3 = \frac{1}{4}a_3 + \frac{5}{16}a_5 + \dots \quad (22)$$

(A13)

$$c_4 = \frac{1}{8} a_4 + \dots \quad (23)$$

$$c_5 = \frac{1}{16} a_5 + \dots \quad (24)$$

Appendix 4(ii)

Derivation of equation (4.24) from equation (4.23).

(4.23) may be written as,

$$\begin{aligned}
 V &= V_{00} + \hat{V}_{10} \{a \cos \theta - b \cos (2\theta + \phi)\} \\
 &\quad + \hat{V}_{20} 2\{a \cos \theta - b \cos (2\theta + \phi)\}^2 - 1 \\
 &= V_{00} - \hat{V}_{20} \\
 &\quad + a\hat{V}_{10} \cos \theta - b\hat{V}_{10} \cos (2\theta + \phi) \\
 &\quad + 2\hat{V}_{20}a^2 \cos^2 \theta + 2\hat{V}_{20}b^2 \cos^2 (2\theta + \phi) \\
 &\quad - 4\hat{V}_{20}ab \cos \theta \cos (2\theta + \phi) \\
 &= V_{00} - \hat{V}_{20} \\
 &\quad + a\hat{V}_{10} \cos \theta - b\hat{V}_{10} \cos (2\theta + \phi) \\
 &\quad + 2\hat{V}_{20}a^2 \left(\frac{1}{2} + \frac{1}{2} \cos 2\theta\right) + 2\hat{V}_{20}b^2 \left\{\frac{1}{2} + \frac{1}{2} \cos (4\theta + 2\phi)\right\} \\
 &\quad - 4\hat{V}_{20}ab \left\{\frac{1}{2} \cos (3\theta + \phi) + \frac{1}{2} \cos (\theta + \phi)\right\} \\
 &= V_{00} - \hat{V}_{20} + a^2\hat{V}_{20} + b^2\hat{V}_{20} \\
 &\quad + a\hat{V}_{10} \cos \theta - 2ab\hat{V}_{20} \cos (\theta + \phi) \\
 &\quad + a^2\hat{V}_{20} \cos 2\theta - \hat{V}_{10}b \cos (2\theta + \phi) \\
 &\quad - \hat{V}_{20}2ab \cos (3\theta + \phi) \\
 &\quad + \hat{V}_{20}b^2 \cos (4\theta + 2\phi)
 \end{aligned} \tag{4.24}$$

Appendix 4(iii)

Derivation of equation (4.66) from equation (4.65).

$$\begin{aligned}
 V &= V_{00} + \hat{V}_{10} T_1 \{a \cos \theta - b \cos (2\theta + \phi)\} \\
 &+ \hat{V}_{20} T_2 \{a \cos \theta - b \cos (2\theta + \phi)\} \\
 &+ \hat{V}_{30} T_3 \{a \cos \theta - b \cos (2\theta + \phi)\} \qquad (4.65)
 \end{aligned}$$

= The 10 terms given in result (4.24) which are obtained from the first 3 terms of (4.65)

$$\begin{aligned}
 &+ \hat{V}_{30} \{4\{a \cos \theta - b \cos (2\theta + \phi)\}^3 - 3\{a \cos \theta \\
 &\quad - b \cos (2\theta + \phi)\}
 \end{aligned}$$

= The 10 terms of result (4.24)

$$\begin{aligned}
 &+ \hat{V}_{30} 4a^3 \cos^3 \theta - 12\hat{V}_{30} a^2 \cos^2 \theta b \cos (2\theta + \phi) \\
 &+ 12\hat{V}_{30} a \cos \theta b^2 \cos^2 (2\theta + \phi) - 4\hat{V}_{30} b^3 \cos^3 (2\theta + \phi) \\
 &- 3\hat{V}_{30} a \cos \theta + 3b\hat{V}_{30} \cos (2\theta + \phi)
 \end{aligned}$$

= The 10 terms of result (4.24)

$$\begin{aligned}
 &+ \hat{V}_{30} 4a^3 \left(\frac{3}{4} \cos \theta + \frac{1}{4} \cos 3\theta\right) \\
 &- \hat{V}_{30} 12a^2 b \left(\frac{1}{2} + \frac{1}{2} \cos 2\theta\right) \cos (2\theta + \phi) \\
 &+ \hat{V}_{30} 12ab^2 \cos \theta \left[\frac{1}{2} + \frac{1}{2} \cos (4\theta + 2\phi)\right] \\
 &- \hat{V}_{30} 4b^3 \left[\frac{3}{4} \cos (2\theta + \phi) + \frac{1}{4} \cos (6\theta + 3\phi)\right] \\
 &- \hat{V}_{30} 3a \cos \theta + \hat{V}_{30} 3b \cos (2\theta + \phi)
 \end{aligned}$$

Appendix 4(iv)

Extra terms due to inclusion of term $\hat{V}_{40}T_4(q)$ in the diode characteristic.

The extra terms, V_{EX} , are

$$\begin{aligned}
 V_{EX} &= \hat{V}_{40}T_4 \{a \cos \theta - b \cos (2\theta + \phi)\} \\
 &= \hat{V}_{40} \left[8 \{a \cos \theta - b \cos (2\theta + \phi)\}^4 - 8 \{a \cos \theta - b \cos (2\theta + \phi)\}^2 + 1 \right] \\
 &= \hat{V}_{40} \{3a^4 + 3b^4 + 12a^2b^2 - 4a^2 - 4b^2 + 1\} \\
 &\quad + \hat{V}_{40} \cos (\theta + \phi) \{8ab - 12ab^3 - 12a^3b\} \\
 &\quad + \hat{V}_{40} \cos (\theta - \phi) \{-4a^3b\} \\
 &\quad + \hat{V}_{40} \cos 2\theta \{4a^4 + 12a^2b^2 - 4a^2\} \\
 &\quad + \hat{V}_{40} \cos (2\theta + 2\phi) \{6a^2b^2\} \\
 &\quad + \hat{V}_{40} \cos (3\theta + \phi) \{8ab - 12a^3b - 12ab^3\} \\
 &\quad + \hat{V}_{40} \cos 4\theta \{a^4\} \\
 &\quad + \hat{V}_{40} \cos (4\theta + 2\phi) \{4b^4 + 12a^2b^2 - 4b^2\} \\
 &\quad + \hat{V}_{40} \cos (5\theta + \phi) \{-4a^3b\} \\
 &\quad + \hat{V}_{40} \cos (5\theta + 3\phi) \{-4ab^3\} \\
 &\quad + \hat{V}_{40} \cos (6\theta + 2\phi) \{6a^2b^2\} \\
 &\quad + \hat{V}_{40} \cos (7\theta + 3\phi) \{-4ab^3\} \\
 &\quad + \hat{V}_{40} \cos (8\theta + 4\phi) \{b^4\}
 \end{aligned}$$

= 10 terms of result (4.24)

$$\begin{aligned}
 & - \hat{V}_{30} 3a^2 b \cos \phi \\
 & + \hat{V}_{30} 3a^3 \cos \theta + \hat{V}_{30} 6ab^2 \cos \theta - \hat{V}_{30} 3a \cos \theta \\
 & - \hat{V}_{30} 6a^2 b \cos (2\theta + \phi) - \hat{V}_{30} 3b^3 \cos (2\theta + \phi) \\
 & \quad + \hat{V}_{30} 3b \cos (2\theta + \phi) \\
 & + \hat{V}_{30} a^3 \cos 3\theta + \hat{V}_{30} 3ab^2 \cos (2\theta + 2\phi) \\
 & - \hat{V}_{30} 3a^2 b \cos (4\theta + \phi) \\
 & + \hat{V}_{30} 3ab^2 \cos (5\theta + 2\phi) \\
 & - \hat{V}_{30} b^3 \cos (6\theta + 3\phi)
 \end{aligned}$$

$$\begin{aligned}
 = & v_{00} - \hat{V}_{20} + a^2 \hat{V}_{20} + b^2 \hat{V}_{20} - \hat{V}_{30} 3a^2 b \cos \phi \\
 & + \hat{V}_{10} a \cos \theta - \hat{V}_{20} 2ab \cos (\theta + \phi) + \hat{V}_{30} 3a^3 \cos \theta \\
 & + \hat{V}_{30} 6ab^2 \cos \theta - \hat{V}_{30} 3a \cos \theta \\
 & - \hat{V}_{10} b \cos (2\theta + \phi) + \hat{V}_{20} a^2 \cos 2\theta - \hat{V}_{30} 6a^2 b \cos (2\theta + \phi) \\
 & - \hat{V}_{30} 3b^3 \cos (2\theta + \phi) + \hat{V}_{30} 3b \cos (2\theta + \phi) \\
 & - \hat{V}_{20} 2ab \cos (3\theta + \phi) + \hat{V}_{30} a^3 \cos 3\theta + \hat{V}_{30} 3ab^2 \cos (3\theta + 2\phi) \\
 & + \hat{V}_{20} b^2 \cos (4\theta + 2\phi) - \hat{V}_{30} 3a^2 b \cos (4\theta + \phi) \\
 & + \hat{V}_{30} 3ab^2 \cos (5\theta + 2\phi) \\
 & - \hat{V}_{30} b^3 \cos (6\theta + 3\phi) \tag{4.66}
 \end{aligned}$$

Appendix 4(v)

The Analysis of the Shunt Diode Multiplier using the Four-Term Approximation to the Diode Characteristic.

This analysis is similar to that carried out in sections 4.3.1 and 4.3.2 but in this case the fourth harmonic of the test spectrum will be taken into account.

The test spectrum will be assumed to be that given by equation (1) and the diode characteristic will be expressed as equation (2)

$$V_0 = V_{00} + \hat{V}_{10} \cos \omega t + \hat{V}_{20} \cos 2\omega t + \hat{V}_{30} \cos 3\omega t + \hat{V}_{40} \cos 4\omega t \quad (1)$$

$$V = V_{00} + \hat{V}_{10} T_1(q) + \hat{V}_{20} T_2(q) + \hat{V}_{30} T_3(q) + \hat{V}_{40} T_4(q) \quad (2)$$

The normalised charge variation in the test is cosinusoidal as in equation (3)

$$q = \frac{\hat{Q}_{10} \cos \omega t}{\hat{Q}_{10}} = \cos \omega t = \cos \theta \quad (3)$$

The shunt-diode doubler circuit is as shown in Figure 4.6 and the charge on the diode then has a second harmonic component. The fundamental charge variation is assumed to be reduced to a fraction 'a' of its test value and the second harmonic charge variation is 'b' times the test value where 'b' is also a fraction. The conditions given in (4.22) must hold for the values of 'a' and 'b' for this analysis to remain appropriate.

Thus the normalised diode charge q is given by (4) and the current by (5) after differentiating the expression for charge.

$$q = a \cos \omega t - b \cos (2\omega t + \phi) \quad (4)$$

$$I = -a\omega\hat{Q}_{10} \sin \omega t + b2\omega\hat{Q}_{10} \sin (2\omega t + \phi) \quad (5)$$

The expression for q in (4) is then substituted into the characteristic equation (2) with θ in place of ωt

$$\begin{aligned} V = V_{00} &+ \hat{V}_{10}T_1 \{a \cos \theta - b \cos (2\theta + \phi)\} \\ &+ \hat{V}_{20}T_2 \{a \cos \theta - b \cos (2\theta + \phi)\} \\ &+ \hat{V}_{30}T_3 \{a \cos \theta - b \cos (2\theta + \phi)\} \\ &+ \hat{V}_{40}T_4 \{a \cos \theta - b \cos (2\theta + \phi)\} \end{aligned} \quad (6)$$

Twenty-six extra terms are generated in the voltage due to the inclusion of the term $\hat{V}_{40}T_4(q)$ in equation (4.72). All the extra terms are given in appendix 4(iv) and those at frequencies ω and 2ω only are shown in equation (7) below.

$$\begin{aligned} V(\text{extra terms}) = &\hat{V}_{40}8ab \cos (\theta + \phi) - \hat{V}_{40}12a^3b \cos (\theta + \phi) \\ &- \hat{V}_{40}12ab^3 \cos (\theta + \phi) - \hat{V}_{40}4a^3b \cos (\theta - \phi) \\ &+ \hat{V}_{40}4a^4 \cos 2\theta + \hat{V}_{40}12a^2b^2 \cos 2\theta \\ &+ \hat{V}_{40}6a^2b^2 \cos (2\theta + 2\phi) - \hat{V}_{40}4a^2 \cos 2\theta \end{aligned} \quad (7)$$

The equations (5) and (6) will now require to be modified to include all the terms in (4.67) and (4.68) plus terms due to equation (7); the revised equations are shown below in (8) and (9).

$$\begin{aligned} \hat{V}_1 = &\hat{V}_{10}(-ja) + \hat{V}_{20}(j2ab\phi) + \hat{V}_{30}(-j3a^3 - j6ab^2 + j3a) \\ &+ \hat{V}_{40}\{-j8ab\phi + j12a^3b\phi + j12ab^3\phi + j4a^3b\phi\} \end{aligned}$$

and inserting $\phi = -\pi/2$

$$\begin{aligned}\hat{V}_1 &= \hat{V}_{10}(-ja) + \hat{V}_{20}(2ab) + \hat{V}_{30}(-j3a^3 - j6ab^2 + j3a) \\ &\quad + \hat{V}_{40}(-8ab + 12a^3b + 12ab^3 - 4a^3b)\end{aligned}$$

or

$$\begin{aligned}\hat{V}_1 &= \hat{V}_{10}(-ja) + \hat{V}_{20}(2ab) + \hat{V}_{30}(-j3a^3 - j6ab^2 + j3a) \\ &\quad + \hat{V}_{40}(8a^3b + 12ab^3 - 8ab)\end{aligned}\tag{8}$$

and

$$\begin{aligned}\hat{V}_2 &= \hat{V}_{10}(b) + \hat{V}_{20}(-ja^2) + \hat{V}_{30}(6a^2b + 3b^3 - 3b) \\ &\quad + \hat{V}_{40}(-j4a^4 - j12a^2b^2 + j4a^2 + j6a^2b^2)\end{aligned}$$

or

$$\begin{aligned}\hat{V}_2 &= \hat{V}_{10}(b) + \hat{V}_{20}(-ja^2) + \hat{V}_{30}(6a^2b + 3b^3 - 3b) \\ &\quad + \hat{V}_{40}(-j4a^4 - j6a^2b^2 + j4a^2)\end{aligned}\tag{9}$$

The output equivalent circuit can be found for this case by considering equation (9) above and Figure 4.14 is shown to be modified to Figure 4.16 which is given in section 4.3.3.

Appendix 4(vi)

The derivation of a formula for the output resistance of the diode at the harmonic output frequency.

An output equivalent circuit (see Figure 4.10) is shown below.

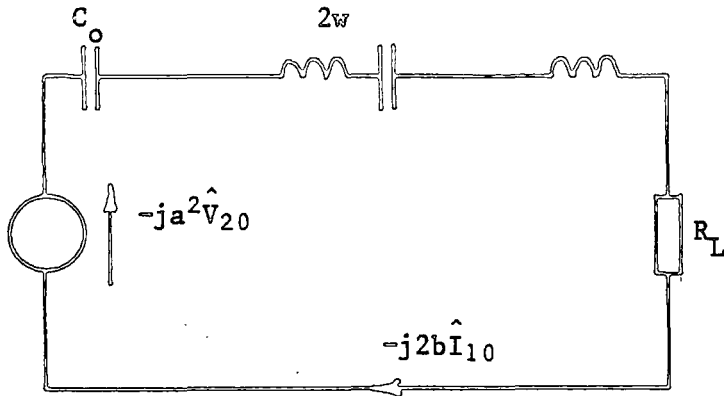


Figure 1

The reduction in the second harmonic e.m.f. from $-j \hat{V}_{20}$ to $-ja^2 \hat{V}_{20}$ could be due to the internal resistance of the source, R_o . Thus Figure 1 could be re-drawn to include a source resistance,

$$R_o = \left[\frac{1 - a^2}{2b} \right] \frac{\hat{V}_{20}}{\hat{I}_{10}} \quad (1)$$

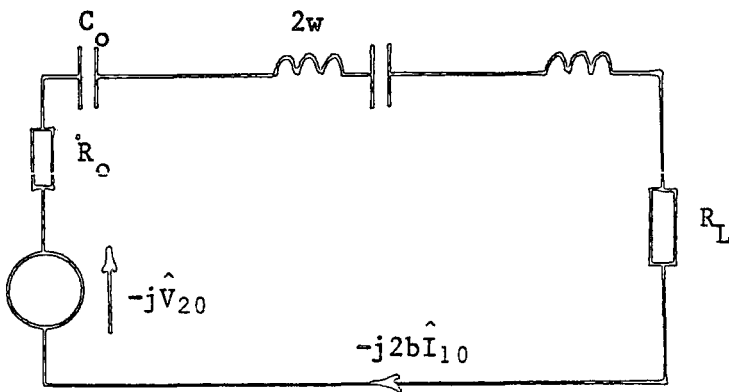


Figure 2

The output equivalent circuit of Figure 2 is at the frequency 2ω .

The maximum output power is obtained when the load resistance R_L is matched to R_o and then the values of 'a' and 'b' will be $2/3$ and $1/3$ respectively.

$$\text{Let } R_o = R_o \text{ (opt) when } a = 2/3, b = 1/3 \quad (2)$$

Hence,

$$R_o \text{ (opt)} = \frac{5}{6} \frac{\hat{V}_{20}}{\hat{I}_{10}} \quad (3)$$

The max output power may then be calculated as

$$P_L \text{ (max)} = \frac{\left(\frac{\hat{V}_{20}}{\sqrt{2}}\right)^2}{4 R_o \text{ (opt)}} = \frac{3}{20} \hat{V}_{20} \hat{I}_{10} \quad (4)$$

and this agrees with the previous calculation shown in equation (4.56).

Circuit operation at maximum output power:

The load resistance R_L should be matched to R_o (opt) by impedance transformation. The source should then be chosen to have values of E_s and R_s (which give the required values of 'a' and 'b') which satisfy the condition

$$\hat{E}_s = \frac{2}{3} \hat{I}_{10} R_s + \frac{5}{9} \hat{V}_{20} \quad (5)$$

The source impedance could be reduced by transformation to as low a value as possible so that less power would be lost in R_s .

APPENDICES TO CHAPTER 5

| | | |
|--------|---|-----|
| 5(i) | The full expansion of equation (5.14) | A24 |
| 5(ii) | Development of the equivalent circuit of Figure 5.1 in section 5.2.2. | A25 |
| 5(iii) | The full expansion of equation (5.37) | A28 |
| 5(iv) | Identities needed in 5.3.2. | A31 |
| 5(v) | Analysis of section 5.3.1. | A32 |
| 5(vi) | Analysis of section 5.3.2. | A34 |
| 5(vii) | Analysis of section 5.3.3. | A37 |

Appendix 5(i)

The full expansion of equation (5.14)

The equation (5.14) can be expanded using equations (6) to (9) in Appendix 4(i). The following result may then be obtained:

$$\begin{aligned}
 V = & V_{00} - \hat{V}_{20} + \hat{V}_{20} a^2 + \hat{V}_{20} b^2 \\
 & + \hat{V}_{10} a \cos \theta - \hat{V}_{30} 3a \cos \theta + \hat{V}_{30} 3a^3 \cos \theta + \hat{V}_{30} 6ab^2 \cos \theta \\
 & - \hat{V}_{30} 3a^2 b \cos (\theta + \phi) \\
 & + \hat{V}_{20} a^2 \cos 2\theta + \hat{V}_{20} 2ab \cos (2\theta + \phi) \\
 & - \hat{V}_{10} b \cos (3\theta + \phi) + \hat{V}_{30} 3b \cos (3\theta + \phi) + \hat{V}_{30} a^3 \cos 3\theta \\
 & \qquad \qquad \qquad - \hat{V}_{30} 3b^3 \cos (3\theta + \phi) \\
 & - \hat{V}_{30} 6a^2 b \cos (3\theta + \phi) \\
 & - \hat{V}_{20} 2ab \cos (4\theta + \phi) \\
 & - \hat{V}_{30} 3a^2 b \cos (5\theta + \phi) + \hat{V}_{30} 3ab^2 \cos (5\theta + 2\phi) \\
 & + \hat{V}_{20} b^2 \cos (6\theta + 2\phi) \\
 & + \hat{V}_{30} 3ab^2 \cos (7\theta + 2\phi) \\
 & - \hat{V}_{30} b^3 \cos (9\theta + 3\phi)
 \end{aligned} \tag{1}$$

where the substitution

$$\theta = \omega t \tag{1a}$$

has been used as an abbreviation.

Appendix 5(ii)

Development of the equivalent circuit of Figure 5.1 in section 5.2.2.

An equivalent output circuit may be drawn using equations (5.17) and (5.19) as shown in Figure 1 below.

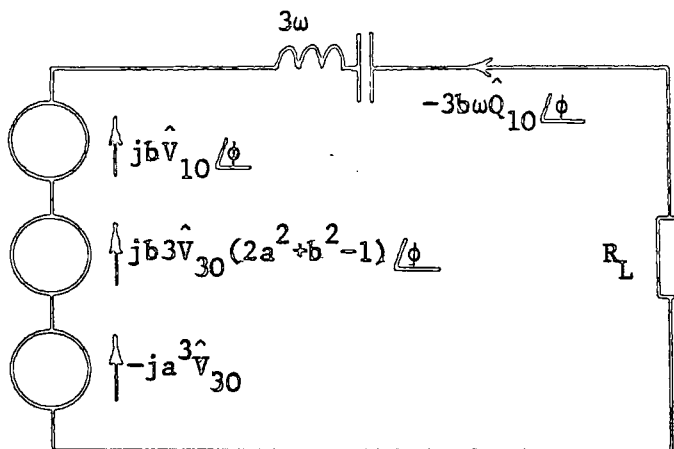


Figure 1

Two of the voltage generators in Figure 1 are lagging the current by 90° and may be considered as the output capacitance C_o of the diode.

The reactance of C_o can be written as

$$\frac{1}{3\omega C_o} = \frac{b \hat{V}_{10} + \hat{V}_{30} (3b^3 + 6a^2b - 3b)}{3b\omega \hat{Q}_{10}}$$

or

$$C_o = \frac{\hat{Q}_{10}}{\hat{V}_{10} + \hat{V}_{30} (6a^2 + 3b^2 - 3)} \quad (1)$$

The output capacitance causes de-tuning of the output circuit filter but this must be assumed to be corrected so that only 3rd harmonic current flows in the load. The load current must be in phase with the generator e.m.f. and thus the value of ϕ must be -90° .

Then,

$$-j a^3 \hat{V}_{30} = -j R_L 3b\omega \hat{Q}_{10}$$

and

$$a^3 = \frac{3\omega \hat{Q}_{10} R_L b}{\hat{V}_{30}} \quad (2)$$

Equation (2) is an important relationship between 'a' and 'b' and becomes equation (5.22) in section 5.2.2.

An equivalent circuit at the input frequency may be obtained using equations (5.16) and (5.18) and it is shown in Figure 2 below

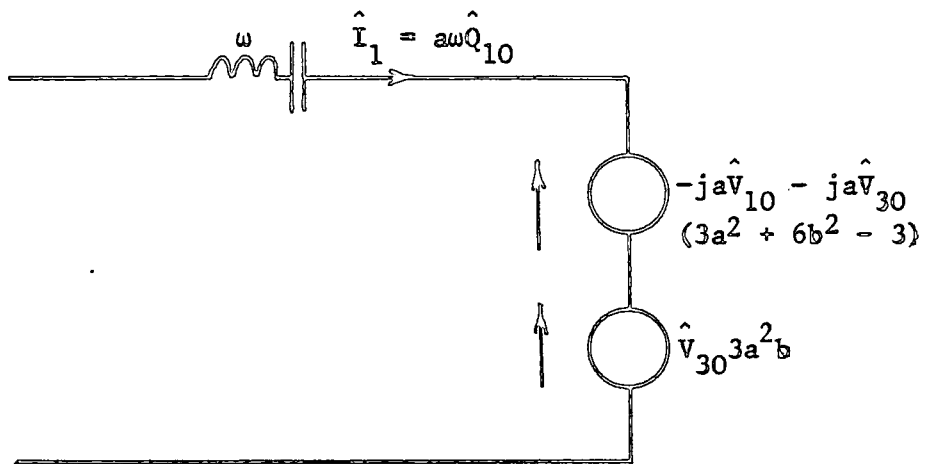


Figure 2

One voltage generator may be replaced by the input capacitance C_{IN} as shown in Figure 5.2. A compensating inductance must also be shown to prevent de-tuning of the input filter. The value of C_{IN} is derived from,

$$\frac{1}{\omega C_{IN}} = \frac{a \hat{V}_{10} + a \hat{V}_{30} (3a^2 + 6b^2 - 3)}{a\omega \hat{Q}_{10}}$$

from which

$$C_{IN} = \frac{\hat{Q}_{10}}{\hat{V}_{10} + \hat{V}_{30} (3a^2 + 6b^2 - 3)} \quad (3)$$

The other voltage generator in the circuit of Figure 2 represents the load resistance reflected into the input circuit, R_L^0 .

Hence

$$R_L^v = \frac{\hat{V}_{30} 3a^2 b}{a\omega \hat{Q}_{10}} \quad (4)$$

If (2) and (4) are combined then result (5) is easily obtained,

$$R_L^v = 9 \frac{b^2}{a} R_L \quad (5)$$

Appendix 5(iii)

The full expansion of equation (5.37).

When equation (5.37) is expanded it will contain the 22 terms of equation (1) in Appendix 5(i), plus extra terms due to the fourth harmonic term:

Hence

$$V = 22 \text{ terms} + \text{extra terms} \quad (1)$$

$$\begin{aligned} \text{where extra terms} &= \hat{V}_{40} T_4 \{a \cos \theta - b \cos (3\theta + \phi)\} \\ &= \hat{V}_{40} \left[8 \{a \cos \theta - b \cos (3\theta + \phi)\}^4 - 8 \{a \cos \theta - b \cos (3\theta + \phi)\}^2 + 1 \right] \\ &= \hat{V}_{40} \left[8a^4 \cos^4 \theta - 32 a^3 b \cos^3 \theta \cos (3\theta + \phi) \right. \\ &\quad + 48 a^2 b^2 \cos^2 \theta \cos^2 (3\theta + \phi) - 32 ab^3 \cos \theta \cos^3 (3\theta + \phi) \\ &\quad + 8b^4 \cos^4 (3\theta + \phi) - 8a^2 \cos^2 \theta \\ &\quad \left. + 16 ab \cos \theta \cos (3\theta + \phi) - 8b^2 \cos^2 (3\theta + \phi) + 1 \right] \end{aligned} \quad (2)$$

The terms in equation (2) can now be expanded using the useful identities given in equations (3) to (11):

$$\cos^2 A = \frac{1}{2} + \frac{1}{2} \cos 2A \quad (3)$$

$$\cos^3 A = \frac{3}{4} \cos A + \frac{1}{4} \cos 3A \quad (4)$$

$$\cos^4 A = \frac{5}{8} + \frac{1}{2} \cos 2A + \frac{1}{8} \cos 4A \quad (5)$$

$$\cos A \cos B = \frac{1}{2} \cos (A + B) + \frac{1}{2} \cos (A - B) \quad (6)$$

$$\cos^2 A \cos B = \frac{1}{2} \cos B + \frac{1}{4} \cos (2A + B) + \frac{1}{4} \cos (2A - B) \quad (7)$$

$$\cos^3 A \cos B = \frac{3}{8} \cos (A + B) + \frac{3}{8} \cos (B - A) + \frac{1}{8} \cos (3A - B) + \frac{1}{8} \cos (3A + B) \quad (8)$$

$$\cos^2 A \cos^2 B = \frac{1}{4} + \frac{1}{4} \cos 2A + \frac{1}{4} \cos 2B + \frac{1}{8} \cos (2A + 2B) + \frac{1}{8} \cos (2A - 2B) \quad (9)$$

$$(A - B)^3 = A^3 - 3A^2B + 3AB^2 - B^3 \quad (10)$$

$$(A - B)^4 = A^4 - 4A^3B + 6A^2B^2 - 4AB^3 + B^4 \quad (11)$$

$$\begin{aligned} \text{Extra terms} &= \hat{V}_{40} \left[8a^4 \left(\frac{3}{8} + \frac{1}{2} \cos 2\theta + \frac{1}{8} \cos 4\theta \right) \right. \\ &\quad - 32a^3b \left(\frac{3}{8} \cos (4\theta + \phi) + \frac{3}{8} \cos (2\theta + \phi) \right. \\ &\quad \left. \left. + \frac{1}{8} \cos (-\phi) + \frac{1}{8} \cos (6\theta + \phi) \right) \right. \\ &\quad + 48a^2b^2 \left\{ \frac{1}{2} + \frac{1}{4} \cos 2\theta + \frac{1}{4} \cos (6\theta + 2\phi) + \frac{1}{8} \cos (8\theta + 2\phi) + \frac{1}{8} \cos (4\theta + \right. \\ &\quad \left. - 32ab^3 \left\{ \frac{3}{8} \cos (4\theta + \phi) + \frac{3}{8} \cos (2\theta + \phi) + \frac{1}{8} \cos (8\theta + 3\phi) + \frac{3}{8} \cos (10\theta + 3\phi) \right\} \right. \\ &\quad \left. + 8b^4 \left\{ \frac{3}{8} + \frac{1}{2} \cos (6\theta + 2\phi) + \frac{1}{8} \cos (12\theta + 4\phi) \right\} \right. \\ &\quad - 8a^2 \left\{ \frac{1}{2} + \frac{1}{2} \cos 2\theta \right\} \\ &\quad - 16ab \left\{ \frac{1}{2} \cos (4\theta + \phi) + \frac{1}{2} \cos (2\theta + \phi) \right\} \\ &\quad \left. - 8b^2 \left\{ \frac{1}{2} + \frac{1}{2} \cos (6\theta + 2\phi) \right\} + 1 \right] \end{aligned}$$

$$\begin{aligned}
= \hat{V}_{40} & \left[1 + 5a^4 - 4a^3b \cos \phi + 12a^2b^2 + 5b^4 - 4a^2 - 4b^2 \right. \\
& + 4a^4 \cos 2\theta - 12a^3b \cos (2\theta + \phi) + 12a^2b^2 \cos 2\theta \\
& - 12ab^3 \cos (2\theta + \phi) - 4a^2 \cos 2\theta + 8ab \cos (2\theta + \phi) \\
& + a^4 \cos 4\theta - 12a^3b \cos (4\theta + \phi) + 6a^2b^2 \cos (4\theta + 2\phi) \\
& - 12ab^3 \cos (4\theta + \phi) + 8ab \cos (4\theta + \phi) \\
& - 4a^3b \cos (6\theta + \phi) + 12a^2b^2 \cos (6\theta + 2\phi) + 4b^4 \cos (6\theta + 2\phi) \\
& \quad - 4b^2 \cos (6\theta + 2\phi) \\
& + 6a^2b^2 \cos (8\theta + 2\phi) - 4ab^3 \cos (8\theta + 3\phi) \\
& - 4ab^3 \cos (10\theta + 3\phi) \\
& \left. + b^4 \cos (12\theta + 4\phi) \right] \tag{12}
\end{aligned}$$

The extra terms given in equation (12) do not include any of frequency ω or 3ω . The terms in (5.37) at these frequencies are as given in equation (5.15) of section 5.2.2.

Appendix 5(iv)

Identities needed in 5.3.2.

$$\begin{aligned}
 (A - B - C)^3 &= A^3 - B^3 - C^3 - 3A^2B - 3A^2C + 3AB^2 \\
 &\quad + 3AC^2 + 6ABC - 3B^2C - 3BC^2
 \end{aligned} \tag{1}$$

$$\begin{aligned}
 \cos A \cos B \cos C &= \frac{1}{4} \cos (A + B + C) + \frac{1}{4} \cos (A - B - C) \\
 &\quad + \frac{1}{4} \cos (A + B - C) + \frac{1}{4} \cos (A - B + C)
 \end{aligned} \tag{2}$$

$$\begin{aligned}
 (A - B - C)^4 &= A^4 + B^4 + C^4 + 6A^2B^2 + 6A^2C^2 + 6B^2C^2 \\
 &\quad - 4A^3B - 4AB^3 - 4AC^3 - 4A^3C + 4B^3C \\
 &\quad + 4BC^3 + 12A^2BC - 12AB^2C - 12ABC^2
 \end{aligned} \tag{3}$$

Appendix 5(v)

Analysis of section 5.3.1.

$$V = V_{00} + \hat{V}_{10} [A - B - C] + \hat{V}_{20} [2 \{A - B - C\}^2 - 1] \quad (1)$$

$$\text{where } A - B - C = a \cos \theta - b \cos (2\theta + \phi_2) - c \cos (3\theta + \phi_3) \quad (2)$$

$$\therefore V = V_{00} + \hat{V}_{10} [A - B - C] + \hat{V}_{20} [2A^2 + 2B^2 + 2C^2 + 4BC - 4BC - 4AC - 1] \quad (3)$$

$$\begin{aligned} &= V_{00} - \hat{V}_{20} + \hat{V}_{10} a \cos \theta - \hat{V}_{10} b \cos (2\theta + \phi_2) - \hat{V}_{10} c \cos (3\theta + \phi_3) \\ &+ \hat{V}_{20} [2a^2 \cos^2 \theta + 2b^2 \cos^2 (2\theta + \phi_2) + 2c^2 \cos^2 (3\theta + \phi_3) \\ &\quad + 4bc \cos (2\theta + \phi_2) \cos (3\theta + \phi_3) \\ &\quad - 4ab \cos (2\theta + \phi_2) \cos \theta \\ &\quad - 4ac \cos (3\theta + \phi_3) \cos \theta] \quad (4) \end{aligned}$$

$$\begin{aligned} &= V_{00} - \hat{V}_{20} + \hat{V}_{10} a \cos \theta - \hat{V}_{10} b \cos (2\theta + \phi_2) \\ &\quad - \hat{V}_{10} c \cos (3\theta + \phi_3) \\ &\quad + \hat{V}_{20} 2a^2 \left(\frac{1}{2} + \frac{1}{2} \cos 2\theta \right) \\ &\quad + \hat{V}_{20} 2b^2 \left[\frac{1}{2} + \frac{1}{2} \cos (4\theta + 2\phi_2) \right] \\ &\quad + \hat{V}_{20} 2c^2 \left[\frac{1}{2} + \frac{1}{2} \cos (6\theta + 2\phi_3) \right] \\ &\quad + \hat{V}_{20} 4bc \left[\frac{1}{2} \cos (5\theta + \phi_2 + \phi_3) + \frac{1}{2} \cos (\theta + \phi_3 - \phi_2) \right] \\ &\quad - \hat{V}_{20} 4ab \left[\frac{1}{2} \cos (3\theta + \phi_2) + \frac{1}{2} \cos (\theta + \phi_2) \right] \\ &\quad - \hat{V}_{20} 4ac \left[\frac{1}{2} \cos (4\theta + \phi_3) + \frac{1}{2} \cos (2\theta + \phi_3) \right] \quad (5) \end{aligned}$$

$$\begin{aligned}
\therefore V &= V_{CO} - \hat{V}_{20} + a^2 \hat{V}_{20} + b^2 \hat{V}_{20} + c^2 \hat{V}_{20} \\
&+ \hat{V}_{10} a \cos \theta + \hat{V}_{20} 2bc \cos (\theta + \phi_3 - \phi_2) \\
&- \hat{V}_{20} 2ab \cos (\theta + \phi_2) \\
&- \hat{V}_{10} b \cos (2\theta + \phi_2) + \hat{V}_{20} a^2 \cos 2\theta - \hat{V}_{20} 2ac \cos (2\theta + \phi_3) \\
&- \hat{V}_{10} c \cos (3\theta + \phi_3) - \hat{V}_{20} 2ab \cos (3\theta + \phi_2) \\
&+ \hat{V}_{20} b^2 \cos (4\theta + 2\phi_2) - \hat{V}_{20} 2ac \cos (4\theta + \phi_3) \\
&+ \hat{V}_{20} 2bc \cos (5\theta + \phi_2 + \phi_3) \\
&+ \hat{V}_{20} c^2 \cos (6\theta + 2\phi_3) \tag{6}
\end{aligned}$$

$$\therefore \hat{V}_1 = -ja \hat{V}_{10} - j 2bc \hat{V}_{20} \underline{\angle \phi_3 - \phi_2} + j 2ab \hat{V}_{20} \underline{\angle \phi_2} \tag{7}$$

$$\hat{V}_2 = +jb \hat{V}_{10} \underline{\angle \phi_2} + j 2ac \hat{V}_{20} \underline{\angle \phi_3} - ja^2 \hat{V}_{20} \tag{8}$$

$$\hat{V}_3 = +jc \hat{V}_{10} \underline{\angle \phi_3} + j 2ab \hat{V}_{20} \underline{\angle \phi_2} \tag{9}$$

Appendix 5(vi)

Analysis of section 5.3.2

The extra terms generated in the spectrum are,

$$\hat{V}_{EX} = \hat{V}_{30} \left[\{4A - B - C\}^3 - 3\{A - B - C\} \right] \quad (1)$$

where

$$A = a \cos \theta \quad (2)$$

$$B = b \cos (2\theta + \phi_2) \quad (3)$$

$$C = c \cos (3\theta + \phi_3) \quad (4)$$

$$\begin{aligned} \therefore \hat{V}_{EX} &= \hat{V}_{30} \left[4A^3 - 4B^3 - 4C^3 - 12A^2B - 12A^2C + 12AB^2 \right. \\ &\quad + 12AC^2 + 24ABC - 12B^2C - 12BC^2 \\ &\quad \left. - 3A + 3B + 3C \right] \\ &= \hat{V}_{30} \left[4a^3 \cos^3 \theta \right. \\ &\quad - 4b^3 \cos^3 (2\theta + \phi_2) \\ &\quad - 4c^3 \cos^3 (3\theta + \phi_3) \\ &\quad - 12a^2b \cos^2 \theta \cos (2\theta + \phi_2) \\ &\quad - 12a^2c \cos^2 \theta \cos (3\theta + \phi_3) \\ &\quad + 12ab^2 \cos^2 (2\theta + \phi_2) \cos \theta \\ &\quad + 12ac^2 \cos^2 (3\theta + \phi_3) \cos \theta \\ &\quad - 12b^2c \cos^2 (2\theta + \phi_2) \cos (3\theta + \phi_3) \\ &\quad - 12bc^2 \cos^2 (3\theta + \phi_3) \cos (2\theta + \phi_2) \\ &\quad + 24abc \cos (3\theta + \phi_3) \cos (2\theta + \phi_2) \cos \theta \\ &\quad \left. - 3a \cos \theta + 3b \cos (2\theta + \phi_2) + 3c \cos (3\theta + \phi_3) \right] \end{aligned}$$

$$\begin{aligned}
\hat{V}_{EX} &= \hat{V}_{30} \left[4a^3 \left\{ \frac{3}{8} \cos \theta + \frac{1}{8} \cos 3\theta \right\} \right. \\
&\quad - 4b^3 \left\{ \frac{3}{8} \cos (2\theta + \phi_2) + \frac{1}{8} \cos (6\theta + 3\phi_2) \right\} \\
&\quad - 4c^2 \left\{ \frac{3}{8} \cos (3\theta + \phi_3) + \frac{1}{8} \cos (9\theta + 3\phi_3) \right\} \\
&\quad - 12a^2b \left\{ \frac{1}{2} \cos (2\theta + \phi_2) + \frac{1}{8} \cos (4\theta + \phi_2) + \frac{1}{8} \cos (-\phi_2) \right\} \\
&\quad - 12a^2c \left\{ \frac{1}{2} \cos (3\theta + \phi_3) + \frac{1}{8} \cos (5\theta + \phi_3) + \frac{1}{8} \cos (-\theta - \phi_3) \right\} \\
&\quad + 12ab^2 \left\{ \frac{1}{2} \cos \theta + \frac{1}{8} \cos (5\theta + 2\phi_2) + \frac{1}{8} \cos (3\theta + 2\phi_2) \right\} \\
&\quad + 12ac^2 \left\{ \frac{1}{2} \cos \theta + \frac{1}{8} \cos (7\theta + 2\phi_3) + \frac{1}{8} \cos (5\theta + 2\phi_3) \right\} \\
&\quad - 12b^2c \left\{ \frac{1}{2} \cos (3\theta + \phi_3) + \frac{1}{8} \cos (7\theta + \phi_2 + \phi_3) + \frac{1}{8} \cos (\theta + 2\phi_2 - \phi_3) \right\} \\
&\quad - 12bc^2 \left\{ \frac{1}{2} \cos (2\theta + \phi_2) + \frac{1}{8} \cos (8\theta + 2\phi_3 + \phi_2) + \frac{1}{8} \cos (4\theta + 2\phi_3 - \phi_2) \right\} \\
&\quad + 24abc \left\{ \frac{1}{8} \cos (6\theta + \phi_3 + \phi_2) + \frac{1}{8} \cos (\phi_3 - \phi_2) \right. \\
&\quad \quad \left. + \frac{1}{8} \cos (4\theta + \phi_3 + \phi_2) + \frac{1}{8} \cos (2\theta + \phi_3 - \phi_2) \right\} \\
&\quad \left. - 3a \cos \theta + 3b \cos (2\theta + \phi_2) + 3c \cos (3\theta + \phi_3) \right] \\
\therefore \hat{V}_{EX} &= \hat{V}_{30} \left[-3a^2b \cos \phi_2 + 6abc \cos (\phi_3 - \phi_2) \right. \\
&\quad - 3a \cos \theta + 3a^3 \cos \theta - 3a^2c \cos (\theta + \phi_3) \\
&\quad + 6ab^2 \cos \theta + 6ac^2 \cos \theta - 3b^2c \cos (\theta + 2\phi_2 - \phi_3) \\
&\quad + 3b \cos (2\theta + \phi_2) - 3b^3 \cos (2\theta + \phi_2) - 6a^2b \cos (2\theta + \phi_2) \\
&\quad - 6bc^2 \cos (2\theta + \phi_2) + 6abc \cos (2\theta + \phi_3 - \phi_2) \\
&\quad + 3c \cos (3\theta + \phi_3) + a^3 \cos 3\theta - 3c^3 \cos (3\theta + \phi_3) \\
&\quad \left. - 6a^2c \cos (3\theta + \phi_3) + 3ab^2 \cos (3\theta + 2\phi_2) - 6b^2c \cos (3\theta + \phi_3) \right]
\end{aligned}$$

$$\begin{aligned}
& - 3ab^2 \cos (4\theta + \phi_2) - 3b^2c \cos (4\theta + 2\phi_3 - \phi_2) + 6abc \cos (4\theta + \phi_3 + \phi_2) \\
& - 3a^2c \cos (5\theta + \phi_3) + 3ab^2 \cos (5\theta + 2\phi_2) + 3ac^2 \cos (5\theta + 2\phi_3) \\
& - b^3 \cos (6\theta + 3\phi_2) + 6abc \cos (6\theta + \phi_3 + \phi_2) \\
& + 3ac^2 \cos (7\theta + 2\phi_3) - 3b^2c \cos (7\theta + \phi_2 + \phi_3) \\
& - 3bc^2 \cos (8\theta + 2\phi_3 + \phi_2) \\
& - c^3 \cos (9\theta + 3\phi_3)]
\end{aligned}$$

The extra terms generated at ω , 2ω and 3ω are shown in equations (5) (6) and (7) with $-\sin \theta$ taken as reference phasor.

$$\begin{aligned}
\hat{V}_1(\text{ex}) = \hat{V}_{30} \left[+ j3a - j3a^3 + j3a^2c \angle \phi_3 \right. \\
\left. - j6ab^2 - j6ac^2 + j3b^2c \angle 2\phi_2 - \phi_3 \right] \quad (5)
\end{aligned}$$

$$\begin{aligned}
\hat{V}_2(\text{ex}) = \hat{V}_{30} \left[-j3b \angle \phi_2 + j3b^3 \angle \phi_2 + j6a^2b \angle \phi_2 \right. \\
\left. + j6bc^2 \angle \phi_2 - j6abc \angle \phi_3 - \phi_2 \right] \quad (6)
\end{aligned}$$

$$\begin{aligned}
\hat{V}_3(\text{ex}) = \hat{V}_{30} \left[-ja^3 - j3c \angle \phi_3 + j3c^3 \angle \phi_3 \right. \\
\left. + j6a^2c \angle \phi_3 - j3ab^2 \angle 2\phi_2 + j6b^2c \angle \phi_3 \right] \quad (7)
\end{aligned}$$

Appendix 5(vii)

Analysis of section 5.3.3.

Extra terms due to the 4th harmonic:

$$\hat{V}_{EX} = \hat{V}_{40} [8\{A - B - C\}^4 - 8\{A - B - C\}^2 + 1] \quad (1)$$

where $A - B - C = a \cos \theta - b \cos (2\theta + \phi_2) - c \cos (3\theta + \phi_3)$

$$\begin{aligned} \therefore \hat{V}_{EX} = \hat{V}_{40} [& 8\{A^4 + B^4 + C^4 + 6A^2B^2 + 6A^2C^2 + 6B^2C^2 - 4A^3B \\ & - 4AB^3 - 4AC^3 - 4A^3C + 4B^3C + 4BC^3 + 12A^2BC \\ & - 12AB^2C - 12ABC^2\} - 8\{A^2 + B^2 + C^2 - 2AB \\ & - 2AC + 2BC\} + 1] \quad (2) \end{aligned}$$

$$\begin{aligned} = \hat{V}_{40} [& 8a^4 \cos^4 \theta \\ & - 8b^4 \cos^4 (2\theta + \phi_2) \\ & - 8c^4 \cos^4 (3\theta + \phi_3) \\ & + 48a^2b^2 \cos^2 \theta \cos^2 (2\theta + \phi_2) \\ & + 48a^2c^2 \cos^2 \theta \cos^2 (3\theta + \phi_3) \\ & + 48b^2c^2 \cos^2 (2\theta + \phi_2) \cos^2 (3\theta + \phi_3) \\ & - 32a^3b \cos^3 \theta \cos (2\theta + \phi_2) \\ & - 32ab^3 \cos \theta \cos^3 (2\theta + \phi_2) \\ & - 32ac^3 \cos \theta \cos^3 (3\theta + \phi_3) \\ & + 32b^3c \cos^3 (2\theta + \phi_2) \cos (3\theta + \phi_3) \\ & + 32bc^3 \cos (2\theta + \phi_2) \cos^3 (3\theta + \phi_3) \\ & - 32a^3c \cos^3 \theta \cos (3\theta + \phi_3) \end{aligned}$$

$$\begin{aligned}
& + 96a^2bc \cos^2 \theta \cos (2\theta + \phi_2) \cos (3\theta + \phi_3) \\
& - 96ab^2c \cos \theta \cos^2 (2\theta + \phi_2) \cos (3\theta + \phi_3) \\
& - 96abc^2 \cos \theta \cos (2\theta + \phi_2) \cos^2 (3\theta + \phi_3) \\
& - 8a^2 \cos^2 \theta - 8b^2 \cos^2 (2\theta + \phi_2) - 8c^2 \cos^2 (3\theta + \phi_3) \\
& + 16ab \cos \theta \cos (2\theta + \phi_2) \\
& + 16ac \cos \theta \cos (3\theta + \phi_3) \\
& - 16bc \cos (2\theta + \phi_2) \cos (3\theta + \phi_3) \\
& + 1] \tag{3}
\end{aligned}$$

$$\begin{aligned}
= \hat{V}_{40} & \left[1 + 8a^4 \left\{ \frac{3}{8} + \frac{1}{2} \cos 2\theta + \frac{1}{8} \cos 4\theta \right\} \right. \\
& - 8b^4 \left\{ \frac{3}{8} + \frac{1}{2} \cos (4\theta + 2\phi_2) + \frac{1}{8} \cos (8\theta + 4\phi_3) \right\} \\
& - 8c^4 \left\{ \frac{3}{8} + \frac{1}{2} \cos (6\theta + 2\phi_3) + \frac{1}{8} \cos (12\theta + 4\phi_3) \right\} \\
& + 48a^2b^2 \left\{ \frac{1}{2} + \frac{1}{2} \cos 2\theta + \frac{1}{2} \cos (4\theta + 2\phi_2) + \frac{1}{8} \cos (6\theta + 2\phi_2) + \frac{1}{8} \right. \\
& \qquad \qquad \qquad \left. \cos (2\theta + 2\phi_2) \right\} \\
& + 48a^2c^2 \left\{ \frac{1}{2} + \frac{1}{2} \cos 2\theta + \frac{1}{2} \cos (6\theta + 2\phi_3) + \frac{1}{8} \cos (8\theta + 2\phi_3) + \frac{1}{8} \right. \\
& \qquad \qquad \qquad \left. \cos (4\theta + 2\phi_3) \right\} \\
& + 48b^2c^2 \left\{ \frac{1}{2} + \frac{1}{2} \cos (4\theta + 2\phi_2) + \frac{1}{2} \cos (6\theta + 2\phi_3) + \frac{1}{8} \cos (10\theta + 2\phi_3 + 2\phi_2) \right. \\
& \qquad \qquad \qquad \left. + \frac{1}{8} \cos (2\theta + 2\phi_3 - 2\phi_2) \right\} \\
& - 32a^3b \left\{ \frac{3}{8} \cos (3\theta + \phi_2) + \frac{3}{8} \cos (\theta + \phi_2) + \frac{1}{8} \cos (\theta - \phi_2) + \frac{1}{8} \cos \right. \\
& \qquad \qquad \qquad \left. (5\theta + \phi_2) \right\} \\
& - 32ab^3 \left\{ \frac{3}{8} \cos (3\theta + \phi_2) + \frac{3}{8} \cos (\theta + \phi_2) + \frac{1}{8} \cos (5\theta + 3\phi_2) + \frac{1}{8} \cos \right. \\
& \qquad \qquad \qquad \left. (7\theta + 3\phi_2) \right\} \\
& - 32ac^3 \left\{ \frac{3}{8} \cos (4\theta + \phi_3) + \frac{3}{8} \cos (2\theta + \phi_3) + \frac{1}{8} \cos (8\theta + 3\phi_3) + \frac{1}{8} \cos \right. \\
& \qquad \qquad \qquad \left. (10\theta + 3\phi_3) \right\} \\
& - 32ac^3 \left\{ \frac{3}{8} \cos (4\theta + \phi_3) + \frac{3}{8} \cos (2\theta + \phi_3) + \frac{1}{8} \cos (\phi_3) + \frac{1}{8} \cos (6\theta + \phi_3) \right\}
\end{aligned}$$

$$\begin{aligned}
& + 32b^3c \left\{ \frac{3}{8} \cos (5\theta + \phi_2 + \phi_3) + \frac{3}{8} \cos (\theta + \phi_3 - \phi_2) + \frac{1}{8} \cos (3\theta + 3\phi_2 - \phi_3) \right. \\
& \qquad \qquad \qquad \left. + \frac{1}{8} \cos (9\theta + 3\phi_2 + \phi_3) \right\} \\
& + 32bc^3 \left\{ \frac{3}{8} \cos (5\theta + \phi_2 + \phi_3) + \frac{3}{8} \cos (\theta + \phi_3 - \phi_2) + \frac{1}{8} \cos (7\theta + 3\phi_3 - \phi_2) \right. \\
& \qquad \qquad \qquad \left. + \frac{1}{8} \cos (11\theta + 3\phi_3 + \phi_2) \right\} \\
& + 96a^2bc \left\{ \left(\frac{1}{2} + \frac{1}{2} \cos 2\theta \right) \left[\frac{1}{2} \cos (5\theta + \phi_2 + \phi_3) + \frac{1}{2} \cos (\theta + \phi_3 - \phi_2) \right] \right\} \\
& - 96ab^2c \left\{ \left[\frac{1}{2} + \frac{1}{2} \cos (4\theta + 2\phi_2) \right] \left[\frac{1}{2} \cos (4\theta + \phi_3) + \frac{1}{2} \cos (2\theta + \phi_3) \right] \right\} \\
& - 96abc^2 \left\{ \left[\frac{1}{2} + \frac{1}{2} \cos (6\theta + 2\phi_2) \right] \left[\frac{1}{2} \cos (3\theta + \phi_2) + \frac{1}{2} \cos (\theta + \phi_2) \right] \right\} \\
& - 8a^2 \left\{ \frac{1}{2} + \frac{1}{2} \cos 2\theta \right\} \\
& - 8b^2 \left\{ \frac{1}{2} + \frac{1}{2} \cos (4\theta + 2\phi_2) \right\} \\
& - 8c^2 \left\{ \frac{1}{2} + \frac{1}{2} \cos (6\theta + 2\phi_3) \right\} \\
& + 16ab \left\{ \frac{1}{2} \cos (3\theta + \phi_2) + \frac{1}{2} \cos (\theta + \phi_2) \right\} \\
& + 16ac \left\{ \frac{1}{2} \cos (4\theta + \phi_3) + \frac{1}{2} \cos (2\theta + \phi_3) \right\} \\
& - 16bc \left\{ \frac{1}{2} \cos (5\theta + \phi_3 + \phi_2) + \frac{1}{2} \cos (\theta + \phi_3 - \phi_2) \right\} \tag{4}
\end{aligned}$$

The terms at fundamental frequency are:

$$\begin{aligned}
\hat{V}_1(\text{ex}) = \hat{V}_{40} \left[-12a^3b \cos (\theta + \phi_2) - 4a^3b \cos (\theta - \phi_2) \right. \\
- 12ab^3 \cos (\theta + \phi_2) + 12b^3c \cos (\theta + \phi_3 - \phi_2) \\
+ 12bc^3 \cos (\theta + \phi_3 - \phi_2) + 8ab \cos (\theta + \phi_2) \\
- 8bc \cos (\theta + \phi_3 - \phi_2) + 24a^2bc \cos (\theta + \phi_3 - \phi_2) \\
\left. + 12a^2bc \cos (\theta - \phi_3 + \phi_2) - 24abc^2 \cos (\theta + \phi_2) \right] \tag{5}
\end{aligned}$$

The terms at second harmonic are:

$$\begin{aligned}
 \hat{V}_2(\text{ex}) = \hat{V}_{40} \left[4a^4 \cos 2\theta + 12a^2b^2 \cos 2\theta \right. \\
 + 6a^2b^2 \cos (2\theta + 2\phi_2) + 12a^2c^2 \cos 2\theta \\
 + 6b^2c^2 \cos (2\theta + 2\phi_3 - 2\phi_2) - 12ac^3 \cos (2\theta + \phi_3) \\
 - 12a^3c \cos (2\theta + \phi_3) - 4a^2 \cos 2\theta \\
 + 8ac \cos (2\theta + \phi_3) - 24ab^2c \cos (2\theta + \phi_3) \\
 \left. - 12ab^2c \cos (2\theta + 2\phi_2 - \phi_3) \right] \quad (6)
 \end{aligned}$$

The terms at third harmonic frequency are:

$$\begin{aligned}
 \hat{V}_3(\text{ex}) = \hat{V}_{40} \left[-12a^3b \cos (3\theta + \phi_2) - 12ab^3 \cos (3\theta + \phi_2) \right. \\
 + 4b^3c \cos (3\theta + 3\phi_2 - \phi_3) + 8ab \cos (3\theta + \phi_2) \\
 + 12a^2bc \cos (3\theta + \phi_2 + \phi_3) + 12a^2bc \cos (3\theta + \phi_3 - \phi_2) \\
 \left. - 24abc^2 \cos (3\theta + \phi_2) - 12abc^2 \cos (3\theta + 2\phi_3 - \phi_2) \right] \quad (7)
 \end{aligned}$$

The reference phasor will be taken as $-\sin$, as previously, and if $\phi_2 = \phi_3 = -\pi/2$ the equations for V_1 , V_2 and V_3 can be written in complex notation as,

$$\begin{aligned}
 \hat{V}_1 = -ja \hat{V}_{10} - j2bc \hat{V}_{20} + 2ab \hat{V}_{20} \\
 + \hat{V}_{30} \left[-j3a^3 + j3a + 3a^2c - j6ab^2 - j6ac^2 + 3b^2c \right] \\
 + \hat{V}_{40} \left[-j12b^3c - j12bc^3 + j8bc - j36a^2bc \right. \\
 \left. + 8a^3b + 12ab^3 - 8ab + 24abc^2 \right] \quad (8)
 \end{aligned}$$

$$\begin{aligned}
\hat{V}_2 &= b \hat{V}_{10} + 2ac \hat{V}_{20} - ja^2 \hat{V}_{20} \\
&+ \hat{V}_{30} [-3b + 3b^3 + 6a^2b + 6bc^2 - j6abc] \\
&+ \hat{V}_{40} [-j4a^4 - j6a^2b^2 - j12a^2c^2 - j6b^2c^2 + j4a^2 \\
&+ 12ac^3 + 12a^3c - 8ac + 36ab^2c] \quad (9)
\end{aligned}$$

$$\begin{aligned}
\hat{V}_3 &= c \hat{V}_{10} + 2ab \hat{V}_{20} \\
&+ \hat{V}_{30} [-3c + 3c^3 + 6a^2c + 6b^2c - ja^3 + j3ab^2] \\
&+ \hat{V}_{40} [+12a^3b + 12ab^3 + 36abc^2 - 8ab + j4b^3c] \quad (10)
\end{aligned}$$

The equations (8), (9) and (10) may be used to modify the equivalent circuits of Figures 5.6, 5.7 and 5.8. The expression for C_{O3} given in equation (5.56) would become,

$$\begin{aligned}
c \ 3\omega \hat{Q}_{10} \frac{1}{3\omega C_{O3}} &= c \hat{V}_{10} + 2ab \hat{V}_{20} + \hat{V}_{30} [3c^3 + 6a^2c + 6b^2c - 3c] \\
&+ \hat{V}_{40} [12a^3b + 12ab^3 + 36abc^2 - 8ab]
\end{aligned}$$

$$\text{Hence } C_{O3} = \frac{1}{\hat{V}_{10} + \frac{2ab}{c} \hat{V}_{20} + \hat{V}_{30} [f_1(abc)] + \hat{V}_{40} [f_2(abc)]} \quad (11)$$

$$\text{where } f_1(abc) = 6a^2 + 6b^2 + 3c^2 - 3 \quad (12)$$

$$f_2(abc) = \frac{4ab}{c} (3a^2 + 3b^2 + 9c^2 - 2) \quad (13)$$

The equation (5.57) must be modified to,

$$\begin{aligned}
\frac{1}{2\omega C_{O2}} b2\omega \hat{Q}_{10} &= b \hat{V}_{10} + 2ac \hat{V}_{20} + \hat{V}_{30} [3b^3 + 6a^2b + 6bc^2 - 3b] \\
&+ \hat{V}_{40} [12a^3c + 12ac^3 + 36ab^2c - 8ac]
\end{aligned}$$

and thus,

$$C_{02} = \frac{\hat{Q}_{10}}{\hat{V}_{10} + \frac{2ac}{b} \hat{V}_{20} + \hat{V}_{30} [f_3(abc)] + \hat{V}_{40} [f_4(abc)]} \quad (14)$$

$$\text{where } f_3(abc) = 6a^2 + 6c^2 + 3b^2 - 3 \quad (15)$$

$$f_4(abc) = \frac{4ac}{b} (3a^2 + 3c^2 + 9b^2 - 2) \quad (16)$$

The second and third harmonic powers given in equations (5.58) and (5.59) must be modified in the following ways:

$$P_2 = \left[a^2 \hat{V}_{20} + 6abc \hat{V}_{30} + \hat{V}_{40} (4a^4 + 6a^2b^2 + 12a^2c^2 + 6b^2c^2 - 4a^2) \right] \\ \cdot \frac{1}{\sqrt{2}} \frac{1}{\sqrt{2}} [2b \hat{I}_{10}]$$

or

$$P_2 = \hat{V}_{20} \hat{I}_{10} (a^2b) + \hat{V}_{30} \hat{I}_{10} (6ab^2c) + \hat{V}_{40} \hat{I}_{10} (4a^4b + 6a^2b^3 + 12a^2bc^2 \\ + 6b^3c^2 - 4a^2b) \quad (17)$$

$$P_3 = \left[a^3 \hat{V}_{30} - 3ab^2 \hat{V}_{30} - 4b^3c \hat{V}_{40} \right] \frac{1}{\sqrt{2}} \frac{1}{\sqrt{2}} [3c \hat{I}_{10}]$$

or

$$P_3 = \hat{V}_{30} \hat{I}_{10} \left(\frac{3}{2} a^3c - \frac{9}{2} ab^2c \right) + \hat{V}_{40} \hat{I}_{10} (-6b^3c^2) \quad (18)$$

The reflected resistance in the input circuit becomes,

$$R' = \frac{2ab \hat{V}_{20} + \hat{V}_{30} (3a^2c + 3b^2c) + \hat{V}_{40} (8a^3b + 12ab^3 + 24abc^2 - 8ab)}{a \hat{I}_{10}}$$

or

$$R' = 2b \frac{\hat{V}_{20}}{\hat{I}_{10}} + \frac{\hat{V}_{30}}{\hat{I}_{10}} \frac{3c}{a} (a^2 + b^2) + \frac{\hat{V}_{40}}{\hat{I}_{10}} 4b (2a^2 + 3b^2 + 6c^2 - 2) \quad (19)$$

The input capacitance C_{IN} previously expressed in equation (5.61) is modified below to include the fourth harmonic term

$$\frac{1}{\omega C_{IN}} a\omega \hat{Q}_{10} = a \hat{V}_{10} + 25c \hat{V}_{20} + \hat{V}_{30} [3a^3 + 6ab^2 + 6ac^2 - 3a] \\ + \hat{V}_{40} [12b^3c + 12bc^3 + 36a^2bc - 8bc]$$

or

$$C_{IN} = \frac{\hat{Q}_{10}}{\hat{V}_{10} + \frac{2bc}{a} \hat{V}_{20} + \hat{V}_{30} [f_5(abc)] + \hat{V}_{40} [f_6(abc)]} \quad (20)$$

$$\text{where } f_5(abc) = (6b^2 + 6c^2 + 3a^2 - 3) \quad (21)$$

$$f_6(abc) = \frac{4bc}{a} (3b^2 + 3c^2 + 9a^2 - 2) \quad (22)$$

The equivalent circuits for fundamental, second and third harmonic frequencies are shown in section 5.3.3.

